Slurry Flow Measurement Using Coriolis Flowmeters

A Thesis Submitted to the University of Kent

For the Degree of Doctor of Philosophy

In Electronic Engineering

By

JINGQIONG ZHANG BEng MSc

October 2020

Abstract

This thesis describes a novel methodology for slurry flow measurement using Coriolis flowmeters incorporating error compensation and structural condition monitoring techniques. This work investigates the influence of entrained solid particles on Coriolis flow metering along with the potential wear problem of Coriolis flowmeters handling such abrasive medium. A review of slurry flow measurement techniques is given, together with the associated technical issues in slurry flow metering using Coriolis flowmeters. The negative impact of the presence of solid particles on Coriolis flow metering is identified through experimental work. A semi-empirical analytical model is proposed to compensate the effect of solid particles on Coriolis flow metering. An in-situ condition monitoring technique is presented for examining the structural health of Coriolis measuring tubes.

A laboratory-scale slurry flow test rig has been designed and constructed to provide the experimental platform for this work. Experimental tests were conducted on the slurry flow test rig with solid fraction up to 4% in volume. Experimental results illustrate that negative measurement errors are produced from the Coriolis flowmeters with dilute slurry flow. A basic analytical model is derived from the existing decoupling effect theory for predicting and correcting the measurement errors of Coriolis flowmeters. According to the actual experimental data, a correction term is introduced into the basic analytical model to improve the predictive performance. After correction, the errors in mass flowrate measurement are reduced to mostly within ±0.2% and remaining errors in density measurement are not beyond ±0.4%. The capability of Coriolis flowmeters can be extended to slurry flow measurement with a semi-empirical analytical model incorporated.

Structural conditions of Coriolis flowmeters are monitored through on-line determination of tube stiffness. In order to give an early warning of tube erosion and reduce the chance of false alarms, factors which can affect stiffness determination are investigated, both theoretically and experimentally. The influence of temperature effect on stiffness determination is evaluated and a compensation scheme is proposed to improve the accuracy of stiffness determination. Erosive tests were performed on the slurry flow test rig to evaluate the feasibility and sensitivity of the condition monitoring technique. Experimental assessment suggests the capability of structural condition monitoring for reporting tube erosion at an early time when a relative change in SRDP (stiffness related diagnostic parameter) reaches −1%.

Acknowledgements

The author wishes to express grateful thanks to the following:

Prof. Yong Yan	My first supervisor, whose advice, encouragement, and contributions made it possible for me to complete this work.
Prof. Tao Wang	My co-supervisor, whose industrial expertise and invaluable research advice drove the project to progress at all times.
Dr. Jinyu Liu	My co-supervisor, whose technical support drove the project to progress and promoted the collaboration with the industrial partner.

School of Engineering and Digital Arts, University of Kent for awarding me the scholarship and the technicians for helping the construction of the test rig.

KROHNE Ltd for providing me the financial support that has allowed this research to be completed as well as in-kind support by supplying the Coriolis flowmeters along with the materials for building the test rig.

Special thanks to a number of students at the University of Kent, for their help during experimental trials, Faisal Abbas, Yueheng Ding, Li Qin, Rui Xu and Shuo Gong. The academic staff in Instrumentation and Control Group for offering me advice and help, Dr. Gang Lu, Dr. Lijuan Wang, Dr. Md. Hossain and Dr. Xinggang Yan. The friends I have known here who kept me going, Kamel Reda, Yonghui Hu, Mengyang Wei, Qi Luo, Wei Hu, Yan Zhang, and Qi Zheng.

This thesis is dedicated to my parents, for their encouragement, help and support throughout the project.

Table of Contents

Nomenclature

A	Cross-sectional area of pipe [m^2]
A_t	Cross-sectional area of Coriolis tube [m^2]
ASY	Asymmetry of Coriolis flowmeters
ASY_N	Normalized asymmetry of Coriolis flowmeters
B	Flux density of magnetic field [T]
C	Constant for mass flow measurement in Coriolis flowmeters
C_E	Thermal change ratio
C_F	Correction coefficient for original decoupling ratio (F)
C_{FCF}	Flow calibration factor for Coriolis flowmeters
C_{MF}	Correction factor for changes in electromagnetic coil temperature
C_f	Correction factor for changes in fluid temperature
C_{SF}	Scale factor between physical frequency response and measured frequency response
c_1	Damping [N/(m/s)]
c_C	Damping related diagnostic parameter
c_l	Speed of sound traveling in liquid [m/s]
c_m	Speed of sound traveling in two-phase mixture [m/s]
c_s	Speed of sound traveling in solid [m/s]
D	Inner diameter of pipe [m]
D_t	Outer diameter of Coriolis tube [m]
d_t	Inner diameter of Coriolis tube [m]
$E_{c,\dot{m}}$	Compressibility error in mass flowrate from modelling [%]
$E_{c,\rho}$	Compressibility error in density from modelling [%]
$E_{d,\dot{m}}$	Decoupling error in mass flowrate from modelling [%]
$E_{d,\rho}$	Decoupling error in density from modelling [%]
$E_{\dot{m}}$	Relative error in mass flowrate [%]

E_ρ	Relative error in density [%]
E_t	Young's modulus of Coriolis tube material [Pa]
F	Original decoupling ratio from modelling
F'	Corrected decoupling ratio
F_1	External force on a spring [N]
F_A	Added mass force [N]
F_B	Buoyancy-like force [N]
F_C	Drive force added in Coriolis flowmeters [N]
F_T	Total force [N]
f_r	Resonant frequency [Hz]
f_{or}	Off-resonant frequency [Hz]
G_{sr}	Location of motion sensors arranged on Coriolis tube
$\dot{H}$	Transfer function
I	Drive current added in Coriolis flowmeters [A]
I_{dr}	Normalized drive level of Coriolis flowmeters [%]
I_t	Moment of inertia of Coriolis tube [kg m^2]
i_l	Instantaneous velocity of liquid phase in the pipe axial direction [m/s]
i_s	Instantaneous velocity of solid phase in the pipe axial direction [m/s]
K_0	Intercept coefficient in linear regression
K_1	Slope coefficient in linear regression
k	Physical stiffness of Coriolis tube [N/m]
k_1	Physical tube stiffness vibrating in the first mode [N/m]
k_C	Stiffness related diagnostic parameter
k_{C0}	Initial value of stiffness related diagnostic parameter, obtained under a reference condition in factory
k_{CI}	Stiffness related diagnostic parameter, acquired by the operator in situ
k_p	Corrected stiffness for changes in fluid temperature

k_{p0}	Initial value of corrected stiffness, obtained under a reference condition in factory
k_R	Reference value of stiffness in simulation
k_S	Stiffness outcomes from simulation
L_{dr}	Effective length of drive coil of Coriolis flowmeters [m]
L_{sr}	Effective length of sensor coil of Coriolis flowmeters [m]
L_t	Effective length of Coriolis tube [m]
m	Mass [kg]
m_1	Effective mass in the first vibrating mode [kg]
m_A, m_W	Mass of the conveying fluid (air or water) in Coriolis tube [kg]
m_a	Actual (true) mass of the conveying fluid in Coriolis tube [kg]
m_C	Mass related diagnostic parameter
m_d	Apparent mass sensed by Coriolis tube according to decoupling model [kg]
m_I	Induced mass related to added mass force (F_A) [kg]
$m_{m,app}$	Apparent (observed) mass reading provided by totalizer of Coriolis flowmeters [kg]
$m_{m,S}$	Total weight of sand-water mixture sample [kg]
m_R	Reference mass (weight) provided by weighing scale [kg]
$m_{s,S}$	Weight of the sand particles in sand-water mixture sample [kg]
m_t	Mass of the empty Coriolis tube [kg]
$m_{w,D}$	Weight of the displaced water [kg]
$\dot{m}_m$	Total mass flowrate of two-phase mixed flow [kg/s]
$\dot{m}_l$	Mass flowrate of liquid phase [kg/s]
$\dot{m}_{m,app}$	Apparent mass flowrate reading from Coriolis flowmeters [kg/s]
$\dot{m}_s$	Mass flowrate of solid phase [kg/s]
N_{Rd}	Relative density (also known as specific gravity)
P_{2P}	2-phase signal level of Coriolis flowmeters [%]
P_d	Damping indicator of Coriolis flowmeters

P_{dN}	Normalized damping indicator of Coriolis flowmeters
Q	Q factor
R^2	R-squared, a goodness-of-fit measure for linear regression
R_{dr}	Drive coil resistance of Coriolis flowmeters [Ω]
R_{dr0}	Initial value of drive coil resistance, obtained under a reference condition in factory [Ω]
r_s	Radius of solid particles [m]
r_t	Inner radius of Coriolis tube [m]
S_A, S_B	Signal level of sensor A & B of Coriolis flowmeters [%]
S_{A0}, S_{B0}	Initial value of signal level of sensor A & B [%]
t	Time [s]
T_{EMC}	Electromagnetic coil temperature [°C]
T_{EMC0}	Initial value of electromagnetic coil temperature, obtained under a reference condition in factory [°C]
T_f	Fluid temperature [°C]
T_{f0}	Initial value of fluid temperature, obtained under a reference condition in factory [°C]
U_s	Vibration amplitude of solid particles [m]
U_t	Vibration amplitude of Coriolis tube [m]
u_s	Velocity of solid particles in the Coriolis oscillation direction [m/s]
u_t	Velocity of Coriolis tube in the Coriolis oscillation direction [m/s]
V_s	Volume of solid particles [m^3]
$V_{s,D}$	Volume of sand particles in water displacement method [m^3]
V_t	Internal volume of Coriolis tube [m^3]
$V_{w,D}$	Volume of displaced water [m^3]
x	Displacement [m]
$\dot{x}$	Velocity [m/s]
X_s	Displacement of solid particles during Coriolis oscillation [m]
X_t	Displacement of Coriolis tube during Coriolis oscillation [m]

z	Relative difference between simulation output and the reference [%]
α_{dr}	Temperature coefficient of drive coil of Coriolis flowmeters
α_e	Thermal expansion coefficient
α_s	Volume fraction of solid particles [%]
$\alpha_{s,app}$	Apparent volume fraction of solid particles, calculated from apparent density reading [%]
$\alpha_{s,R}$	Reference volume fraction of sand in sand-water mixture sample [%]
β_m	Compressibility of two-phase mixture [m^2/N]
β_s	Weight fraction of solid particles [%]
$\beta_{s,R}$	Reference weight fraction of sand in sand-water mixture sample [%]
δ_N	Normalized inverse Stokes number (also known as penetration depth)
ε	Sensor voltage induced in Coriolis flowmeters [V]
θ	Phase shift due to entrained solid particles [rad]
μ_l	Dynamic viscosity of liquid [Pa s]
v_l	Kinematic viscosity of liquid [m^2/s]
ρ	Density [kg/m^3]
ρ_f	Density of the conveying fluid (liquid or gas) in Coriolis tube [kg/m^3]
ρ_l	Liquid density [kg/m^3]
ρ_m	Solid-liquid mixture density [kg/m^3]
$\rho_{m,app}$	Apparent density reading from Coriolis flowmeters [kg/m^3]
$\rho_{m,R}$	Reference density of sand-water mixture sample [kg/m^3]
ρ_R	Reference density obtained from sampling [kg/m^3]
ρ_s	Solid (sand) density [kg/m^3]
ρ_w	Water density [kg/m^3]
$\rho_{w,app}$	Apparent water density reading from Coriolis flowmeters [kg/m^3]
σ	Standard deviation
$\emptyset_l$	Liquid phase void fraction [%]

$\emptyset_s$	Solid phase void fraction [%]
ω	Angular frequency [rad/s]
ω_{or}	Off-resonant angular frequency [rad/s]
ω_r	Resonant angular frequency [rad/s]
ω_{r1}	Resonant angular frequency of the first vibration mode [rad/s]
ω_{rA}, ω_{rW}	Resonant angular frequencies when pure air or water flow through Coriolis tube [rad/s]

List of Abbreviations

CF1	The upstream Coriolis flowmeter under test, with belly up
CF2	The downstream Coriolis flowmeter under test, with belly down
EGM	Entrained Gas Management
EIT	Electrical Impedance Tomography
EMF	Electromagnetic Flowmeter
ERT	Electrical Resistance Tomography
FCF	Flow Calibration Factor
FRF	Frequency Response Function
GVF	Gas Volume fraction
MDOF	Multi-Degree-Of-Freedom
MF	Magnetic Field
OPD	Online Parameter Determination
RTD	Resistance Temperature Detector
SDOF	Single-Degree-Of-Freedom
3DOF	Three-Degree-Of-Freedom
SMV	Smart Meter Verification
SRDP	Stiffness Related Diagnostic Parameter
SVF	Solid Volume fraction
SWF	Solid Weight fraction
TBR	Transient Bubble Remediation
TMR	Transient Mist Remediation

List of Tables

List of Figures

Chapter 1
Technical Requirements for Slurry Flow Measurement

1.1 Introduction

1.1.1 **Slurry Flow Measurement**

Slurry flow is the mixture of solid particles with liquid medium, typically used to convey solids by carrier liquid, such as coal-water slurry, paper pulp, drilling mud and clays [1]. Slurry flow transportation is widely encountered in various industries, for instance, the mining process, the manufacturing process (e.g. the production of cement, brick, mortar, concrete or glass), as well as the petroleum industry which injects the pressurized fluid (mainly containing water with silica sand and chemical additives) for extracting oil or natural gas (this process called “hydraulic fracturing”, “ pressure pumping”, or “well stimulation”) [2], [3]. In some circumstances, the presence of solid particles is unexpected or unintentional, such as the production of sand from sandstone reservoirs during hydrocarbon recovery [4]. In these industrial processes, accurate measurement of solid-liquid two-phase flow is important to realize flow quantification, operation monitoring, process optimization and product quality control.

Moreover, depending on the characteristics of flow mixtures, the delivered slurry could be abrasive and/or corrosive. As a result, the transportation of slurry may cause erosive damages to the piping system (e.g. valves, pipelines), plant equipment (e.g. pumps, feeders), along with measuring instruments (e.g. flowmeters). The complex nature of two-phase flow together with the abrasive property of slurry flow cause difficulties in both flow metering and condition monitoring. In order to seek the solutions to the measurement problems of slurry flow, this research focuses on the accuracy issues in solid-liquid two-phase flow measurement as well as the wear problem of the measuring instruments when applied in such abrasive medium.

In many manufacturing industries where slurry is commonly used to deliver solids as raw materials whilst the liquid medium is served as a carrier, accurate two-phase flow metering is highly desirable to ensure smooth slurry transportation for process control. If solids are delivered under inappropriate conditions (e.g. heavy solid content with improper flow velocity), liquid medium may not be able to carry the solids to move together. Since solid phase is typically denser than liquid, solids would tend to accumulate and settle on the bottom of pipe which can eventually results in poor product quality, pipeline blockage and even facility failure [5]. Among slurry flow characteristics, flowrate (or flow velocity) and solid concentration are of considerable interest to materials balance [6].

In the petroleum industry, hydraulic fracturing has been widely employed as a well stimulation technique since the 1940s. It utilizes the high-pressure injection of fracturing fluid to assist in extracting oil or natural gas from the reservoirs [7], [8]. Fracturing fluid is majorly composed of water (roughly 95% by volume), deliberately added "proppant" (commonly silica sand with volume fraction about 4%) together with a small amount of treatment chemicals (typically less than 1% by volume) [9]. The function of "proppant" is to hold the fractures open, offering adequate pore space for petroleum fluids to flow to a well [10]. In such applications, accurate measurement of flowrate as well as solid concentration is highly desirable to enhance hydrocarbon recovery in terms of the production rates and the yields.

Another typical example in the petroleum industry is the production of solids derived from hydrocarbon recovery. Quite often oil and gas wells also contain water and solid materials (primarily sand). In this case, sand production is unintentional, which commonly appears from the early stage of the well life (clean-up stage), most likely during the end of well life (typically when water breaks through) and occasionally throughout the well life [11]. The poorly-consolidated reservoirs constitute roughly 70% of the world's oil and gas reservoirs [12]. The existence of sand particles can lead to the instability of the production cavities and sometimes the filling of the boreholes. Additionally, it can also result in severe erosive damage to the facilities as well as sand deposition in the separators. Thus, reliable slurry flow measurement is highly advantageous to guarantee the hydrocarbon recovery process and becoming more and more essential to the custody transfer in the oil and gas industry.

The problems of measuring solid-liquid flow mixtures have been of great interest to a wide variety of industrial processes associated with slurry transportation since the 1950s,

particularly in the manufacturing, chemical, mining, oil and gas industries [13]–[15]. Over the past few decades, significant efforts have been devoted to address the challenges of solid-liquid two-phase flow metering. Basically, flowrates (or flow velocities) and phase fractions are the key parameters for slurry flow measurement, which are crucial to realize flow quantification and process control. The traditional approaches by separating or sampling the mixed flow have obvious disadvantages, such as taking up too much space, low efficiency, difficulties in maintenance, and more importantly, significant time delay making them difficult to achieve real-time monitoring and control. One typical solution to solid-liquid two-phase flow characterisation is combining different measurement techniques together owing to the advantages or limitations of each technique. For example, phase fractions are often measured by using techniques such as electrical tomography, gamma ray, X-ray, wave attenuation of microwave or ultrasonic or acoustic methods. Individual phase densities are typically obtained from densitometers (e.g. using gamma ray, ultrasonic or microwave methods) whilst Coriolis flowmeters are likely able to determine the mixture density with proper compensation. Flowrates or flow velocities are commonly determined by employing differential pressure devices, electromagnetic flowmeters, Coriolis flowmeters, ultrasonic, acoustic sensors, or laser doppler instruments [5], [16], [17]. Although the strategy of the combination of different techniques could contribute to characterizing slurry flow, these solutions could have the limitations of measurement accuracy, the difficulties in calibration and maintenance, or the problems of using radioactive sources. It is still challenging to provide stable, continuous and accurate measurement of solid-liquid mixtures so far.

1.1.2 **Coriolis Flowmeters**

Coriolis flowmeters are one of the most accurate single-phase mass flowmeters, with the benefit of offering multiple outputs including mass flowrate, density, temperature and even viscosity in some circumstances [18]. Mass flow metering can be immune to the influence of changes in process or operating conditions (e.g. temperature, pressure) encountered in volumetric flow metering. Nevertheless, the primary limitation is the degradation of measurement accuracy of Coriolis flowmeters when dealing two-phase or multiphase flow.

The potential extension of Coriolis flow metering technology from single-phase flow to two-phase or multiphase flow has received considerable attention over the past few years. Benefitting from the recent advances in flow converters (or called flow transmitters) as

well as signal processing and soft computing techniques, Coriolis flowmeters are becoming a promising tool for two-phase or multiphase flow metering. Extensive theoretical studies have been undertaken to investigate the physical mechanisms leading to measurement errors of Coriolis flowmeters under multiphase flow conditions. Different approaches have been proposed and implemented into Coriolis flowmeters for handling multiphase flow. Here examples are given with the focus on the technical improvements in the commercially available Coriolis flowmeters from several leading manufacturers. Endress+Hauser has offered MFT (Multi-Frequency Technology) to compensate the compressibility effect on Coriolis flow metering due to gas entrained in liquid [19]. KROHNE has introduced EGM (Entrained Gas Management) technology as a solution of gas entrainments for various industrial applications [20]. Micro Motion has proposed TBR (Transient Bubble Remediation) and TMR (Transient Mist Remediation) strategies in order to handle multiphase flow [21]. Moreover, with the rapid development of artificial intelligence and machine learning tools, soft computing techniques have shown the potential to assist with Coriolis flowmeters for providing mass flow measurement with gas present in liquid [22], [23].

One benefit of using Coriolis flowmeters is to obtain mixture mass flowrate and density simultaneously, which can give a better insight into slurry flow characteristics. By introducing appropriate compensation methods (e.g. analytical modelling or soft computing techniques) for reducing the influence of entrained solid particles, Coriolis flow metering technology is a promising candidate which may achieve satisfactory accuracy of the measurement of mass flowrate and density of the solid-liquid mixtures. In addition, in some cases for instance the dilute slurry being transported in homogenous suspension or non-settling flow regime, individual phase fractions can also be estimated from the mixture density, with the prior information of liquid density and solid density (e.g. acquired by sampling). It can be seen that one advantage of applying Coriolis flowmeters into homogeneous and dilute slurry flow is its potential capability to provide measurement of the mixed flow as well as the individual components, without using a second instrument to characterize solid-liquid two-phase flow.

1.2 Technical Challenges

The difficulties in slurry flow measurement mainly arise from the complex nature of the solid-liquid mixtures being metered due to the simultaneous presence of two different

phases together with the potential wear problem of the measuring instruments due to the successive contacts with solids present in liquid. The liquid phase is typically a continuous phase while the solid phase is usually a dispersed phase. The solid-liquid interactions can generally affect the performance of the measuring instruments and such effects are often dependent on the properties of flow mixtures as well as the process or operating conditions (e.g. temperature, pressure) varying from different applications. Besides, because of the abrasiveness of slurry, erosive damages to the measuring instruments would inevitably occur and therefore, careful attention should be given on the structural health of the measuring instruments, particularly in the use of intrusive sensing techniques (e.g. turbine flow metering).

1.2.1 **Challenges in Flow Measurement of Solid-Liquid Mixtures**

In general, a desirable flowmeter for slurry flow metering should be able to offer accurate, stable, continuous and repeatable measurement. Additionally, considerations should also be given on reducing the size, cost, maintenance, and the use of radioactive sources (e.g. gamma ray). The main technical challenges to fulfil the requirements for slurry flow measurement have been identified as follows:

- High accuracy

The required accuracy depends on the specific applications and local conditions. In general, higher accuracy (or lower uncertainty) of flow measurement is often required for the purpose of custody transfer in the oil and gas industry. For the complex industrial processes, a realistic and acceptable measurement uncertainty would be allowed to a wider range, such as ±1% [24]. In the case of single-phase flow, Coriolis flowmeters are capable of delivering highly accurate mass flowrate measurement, typically achieving uncertainty of within ±0.1%. Therefore, the challenge is to extend the ability of the Coriolis flowmeters to maintain such high accuracy when solid-liquid two-phase flow occurs.

- Real-time measurement

Real-time measurement is usually required for the purpose of process monitoring and product quality control. For the complex scenarios, for example, the multiphase flow containing oil, water, solid materials and gas from the wellheads or during well drilling where accurate measurement of each phase is practically difficult to perform, high

sensitivity and fast response in tracking changes of flowrate or phase fraction on a real-time basis can be helpful for reservoir management. Hence, the challenge is to employ on-line flow metering techniques to continuously monitor such flow which are expected to be sensitive and can respond fast to the changes in flow conditions.

- Wide applicability under variable process conditions

The process or operating conditions could likely differ from various applications (e.g. cryogenic temperature, high pressure, viscous flow medium). As a result, technical difficulties exist in reducing the impacts of variations in process conditions (e.g. ambient temperature, pressure) on flow metering. Accordingly, it is challenging to deliver stable and accurate flow measurement under real-world process conditions. Appropriate compensation should be applied to the measurement results in order to keep the accuracy over a wide variety of process conditions.

- Small footprint, cost-effectiveness, low maintenance

In some cases (e.g. off-shore platform, mobile unit, ferries), the installation space is a critical factor which requires a measuring device to be compact. Separation or sampling based methods are less preferable owing to the disadvantages of bulk size and mechanical complexity. Thereby, it is a challenge for a measuring device to serve the application with very limited installation space. Moreover, low cost, ease of use as well as low maintenance are practically beneficial. Although multiphase flowmeters deploying radioactive source own the advantages of high accuracy and good adaptability, which is prevalent in the commercial market of multiphase flowmeters, it is expensive to purchase and operate whilst it often requires frequent maintenance/calibration. Therefore, development of a radiation-free and cost-effective technique to measure slurry flow is another challenge.

1.2.2 **Challenges in Structural Condition Monitoring of the Measuring Instruments in Abrasive Applications**

Due to the abrasive solid particles present in liquid, wear problems may occur on the measuring instruments during slurry flow measurement. The erosive damage can adversely affect the performance of the measuring device whilst excessive erosive can even cause facility failure leading to safety issues. Therefore, how to monitor the structural condition of the measuring device is the second primary concern in this research, which is crucial to

guarantee accurate flow measurement for slurry. The main technical challenges have been identified below:

- Satisfactory sensitivity and reliability

The required sensitivity in reporting erosion is dependent on the specific types of the measuring devices as well as the applications. Higher sensitivity can advise the sign of erosion at an earlier stage. Unfortunately, improperly high sensitivity could increase the occasions of false alarms which would confuse the operator. Nevertheless, seeking a fairly reliable warning of the presence of erosion could to some extent limits the sensitivity. Therefore, one major difficulty lies in the selection of an appropriate threshold, which can report erosion with confidence. Considerations should be given on providing a satisfactory sensitivity for the purpose of early warning as well as a good reliability in diagnostic results with low probability of false alarms.

- In-situ and on-line condition monitoring

Since erosive wear can happen during slurry flow metering, it is essential to provide real-time and on-line condition monitoring of the measuring instruments during the service life. Off-line inspection or recalibration is less preferred because a shutdown or operational disruption to the ongoing flow transportation could negatively impact on the manufacturing processes (e.g. in terms of time, cost). Thus, it is another challenge to develop an in-situ and on-line condition monitoring technique to examine the structural health of a measuring device for abrasive applications.

- Immunity to variable process conditions

In consideration of the complexity of real-world applications, the development of structural condition monitoring of a measuring instrument should take the influences of variations in process or operating conditions into account. One main challenge is that the condition monitoring technique should be capable of indicating the structural changes in the measuring instrument, meanwhile, owning an adequate level of immunity with respect to process effects in situ.

- Compact size, cost-effectiveness

Structural condition monitoring of a measuring instrument can be regarded as a secondary function to check the structural integrity which can be used to assist in delivering accurate measurement in slurry flow. Hence, it is desirable to utilize less supplementary sensors which can be easily installed or operated for implementing condition monitoring into a measuring device on a pipeline. In addition, the cost and size of the monitoring system to be developed should be acceptable.

1.3 Research Objectives

This research programme aims to develop a a methodology for slurry flow measurement using Coriolis flowmeters together with an in-situ condition monitoring technique for ensuring the structural integrity of Coriolis flowmeters. The objectives of the research programme are defined as follows:

- To define the state-of-the-art in the research field. Existing techniques for slurry flow measurement and associated technical issues in slurry flow metering using Coriolis flowmeters will be reviewed whilst gaps that require further research in this field will be identified.
- To experimentally evaluate the influences of entrained solid particles on Coriolis flow metering. A slurry flow test rig will be designed and constructed in order to offer an experimental platform for assessing the performance of Coriolis flowmeters under solid-liquid two-phase conditions in terms of mass flowrate and density measurement. Experimental tests will be carried out on slurry flow test rig with dilute sand-water flow. The measurement uncertainty of Coriolis flowmeters with slurry flow will be examined quantitatively.
- To examine the feasibility and effectiveness of analytical modelling approach for compensating the effect of entrained solids on Coriolis flow metering. Based on the existing theoretical studies revealing the underlying physics causing the measurement errors of Coriolis flowmeters under two-phase flow conditions, a basic analytical model will be established for error prediction and correction. Moreover, according to the differences between the outcomes from model prediction and experimental work, the basic analytical model will be improved to offer better prediction of actual experimental results. As a result, a semi-empirical analytical model will be proposed for compensating the measurement errors of Coriolis flowmeters for slurry flow metering.

- To perform in-situ structural condition monitoring of Coriolis flowmeters through on-line measurement of Coriolis tube stiffness. Stiffness related diagnostic data will be used to track and monitor the structural health of Coriolis flowmeters for reporting the potential erosive wear on Coriolis measuring tubes. The factors which can affect stiffness determination (e.g. damping level, two-phase flow conditions) as well as the influence of changes in temperature (including fluid temperature and electromagnetic coil temperature) on stiffness determination will be identified and analysed, theoretically and experimentally. Accordingly, a compensation method will be proposed against the effect of temperature changes, in order to achieve high accuracy of stiffness determination which equates to high sensitivity in erosion warning. Furthermore, the performance of the structural health monitoring technique will be assessed through erosive testing with dilute sand-water slurry.

1.4 Thesis Outline

The contributions of this thesis to the state-of-the-art in slurry flow metering include (1) experimental investigations into the performance of Coriolis flowmeters under solid-liquid two-phase flow conditions, (2) evaluation of the feasibility and effectiveness of using analytical model for predicting and correcting measurement errors of Coriolis flowmeters for slurry flow metering, (3) use of a stiffness diagnostics based structural health monitoring technique to track erosion on the Coriolis measuring tubes, (4) identification of factors affecting stiffness measurement and compensation of temperature effect for yielding a high sensitivity in erosion warning.

This thesis is organised in six chapters as follows:

- Chapter 1 introduces the importance of slurry flow measurement, and covers the technical challenges in accurate measurement of slurry flow along with effective monitoring of wear problems for abrasive industrial applications, and outlines the proposed objectives of the research programme.
- Chapter 2 reviews the state-of-the-art techniques for slurry flow measurement and associated technical issues in slurry flow measurement using Coriolis flowmeters.
- Chapter 3 gives the detailed descriptions of the design and construction of a slurry flow test rig for covering the experimental tests as required in this work.

- Chapter 4 presents the experimental tests and results for identifying the impact of entrained solid particles on Coriolis flow metering. Moreover, a novel analytical model is derived from the existing theory which explains the physical mechanisms causing the measurement errors of Coriolis flowmeters and then adopted for error prediction as well as correction. A further improvement on the basic analytical model is proposed in order to yield better prediction of actual experimental data.
- Chapter 5 reports the structural condition monitoring of Coriolis flowmeters through stiffness diagnostics. The factors which can affect stiffness determination are analysed through computational simulation and investigated through experimental work, which can help understand the causes of false alarms. Besides, one common and main factor, temperature effect, is discussed and a compensation scheme is proposed so as to reduce the temperature effect on stiffness determination. The performance of the structural condition monitoring technique is assessed by erosive tests with dilute slurry. In addition, the behaviour of eroded Coriolis flowmeters is verified by using clean water.
- Chapter 6 concludes the work presented from this thesis and provides suggestions and recommendations for future work.

Chapter 2

Review of Techniques for Slurry Flow Measurement and Associated Technical Issues

2.1 Introduction

The presence and movement of solid particles in liquid as well as the abrasive nature of solid-liquid mixtures make slurry flow measurement one of the most challenging multiphase flow metering applications. The study of slurry flow measurement has attracted considerable research attention over the past few decades. Significant efforts have been devoted to develop effective techniques or improve the performance of conventional instruments for measuring slurry flow. However, there still exists some limitations to meet all the requirements of slurry flow metering in real-world industrial processes. This literature survey not only provides necessary background knowledge about slurry flow measurement but also assists in demonstrating a clear contribution of this work to the state-of-the-art solutions to slurry flow metering.

This chapter is organised as follows. Firstly, the chapter begins with a brief description of slurry flow characteristics as well as the key parameters in slurry flow measurement. Then, this chapter reviews the existing techniques which can provide direct on-line measurement of slurry flow. This part of review mainly highlights the influence of entrained solid particles on flow measurement accuracy along with the consideration of potential wear problems in contact with solids. Lastly, the chapter focuses on the relevant previous studies on Coriolis flow metering technology in order to identify the associated technical issues and remaining technical challenges of slurry flow measurement using Coriolis flowmeters.

2.2 Slurry Flow Characteristics

Slurry flow is encountered in many industries such as chemical, pharmaceutical, manufacturing, mining processes as well as petroleum industry. Slurry flow is typically used for the hydraulic transportation of solid materials, of which the physical characteristics strongly depend on a range of factors, including the relevant properties of solid phase (e.g. the size, shape, surface roughness, velocity, density, concentration and cross-sectional distribution of solid particles), pipe diameter and orientation, as well as the properties of liquid phase (e.g. velocity, density, temperature and viscosity of the liquid carrier). Among them, some properties can be regarded as the prior information or constants with compensations given according to the process conditions, such as liquid density, solid density, pipe diameter and orientation [25]. The dominant variables are phase fractions and phase flowrates (or phase velocities), which need to be continuously monitored to achieve desirable slurry transportation [6].

The focus of this research is the slurry transportation in horizontal pipelines. According to the behaviours of solid particles suspended in the carrier fluid, slurry flow regime in horizontal pipeline can be basically classified as follows [25], [26]: (1) Non-settling, wherein the solids stay fully suspended in the fluid medium; (2) unhindered-settling, wherein the suspended particles can settle freely under the gravity effect; (3) hindered-settling, wherein the relatively upward motion of liquid phase impedes the downward motion of particles. Alternatively, four flow regimes for suspensions are commonly grouped as follows: homogeneous suspension (or pseudo-homogeneous); heterogeneous suspension; heterogeneous suspension flow with a moving bed, or sometimes “two-layer” flow; saltation flow with a stationary bed, or sometimes “three-layer” flow [25], [27], [28]. Typical slurry flow regimes are shown in Figure 2.1.

1) Homogeneous suspension (or pseudo-homogeneous), in which all solid particles are distributed (nearly) evenly and the concentration is constant across the pipe cross-section;

2) Heterogeneous suspension, in which a concentration gradient exists in the distribution of particles in suspension;

3) Heterogeneous suspension flow with a moving bed, or “two-layer” flow, in which some portion of the particles has accumulated and formed a moving bed that slides

along the bottom of the pipe. The upper part of pipe is occupied by a heterogeneous mixture.

4) Saltation flow with a stationary bed, or sometimes "three-layer" flow, in which a stationary deposit is observed at the pipe bottom. On top of the deposit, particles are sliding as a separate moving bed and the upper layer of the flow is a heterogeneous mixture.

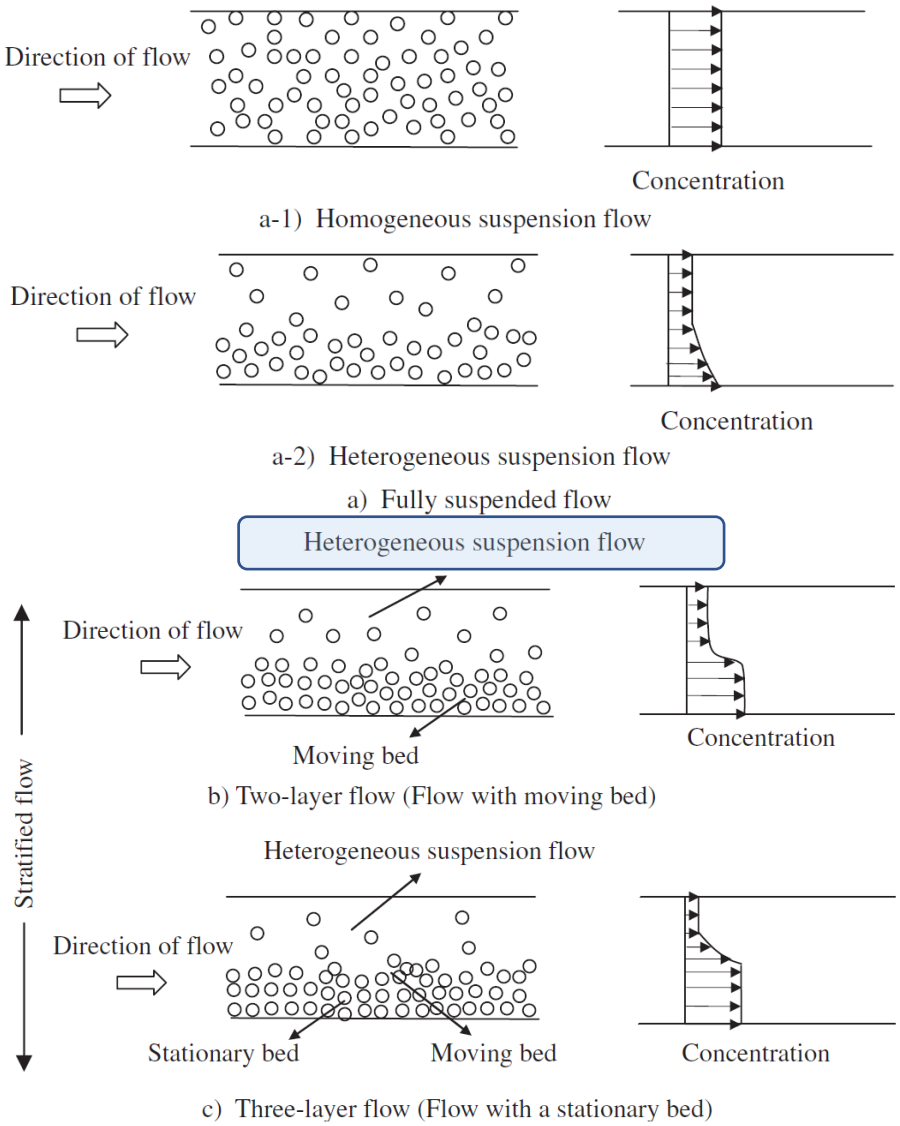

Figure 2.1. Slurry flow regime map in a horizonal pipe [27]

Generally, non-settling or fully-suspended slurry can be subdivided into two flow regimes, homogenous and heterogenous suspension flow [27]. Homogenous suspension is often observed when extremely fine particles (typically in size between 40 μm to 70 μm) with relatively low density are present in the liquid [5]. Examples of homogenous suspension

include coal-water slurry, drilling mud, clays, fine limestone as well as paper pulp [29]. When liquid contains larger and heavier solids (e.g. coarse coal, sand or gravel), the particles can still be suspended but likely the suspension may become heterogenous [25].

It is recommended to deliver slurry as a non-settling flow regime within an appropriate range of liquid velocity and solid concentration. Solid settlement should be prevented as they can lower transportation efficiency, cause unstable flow conditions and even plugged pipeline. In real-world processes, slurry may also hold some gas bubbles or gas slugs. Since gas entrainment is a different topic which can adversely affect the performance of a variety of flow measurement techniques, entrained gas should be carefully avoided throughout the experimental tests in this research. The experimental work will focus on the case of dilute slurry, being delivered in homogenous suspension or non-settling flow regime. Dilute slurry containing a small portion of sand particles along with a large fraction of liquid is a typical example of sand slurry and also widely involved in the petroleum industry.

Furthermore, as solid-liquid two-phase flow is essentially complex usually associated with a certain level of turbulence, the flow characteristics often fluctuates with respect to time and varies from the different locations over the pipe cross-section (e.g. the variations of local phase velocities and phase fractions from the location near the pipe wall to the pipe central line) [6]. Slurry properties are typically measured in terms of the area-averaged mean values which are of considerate importance to control materials balance. It should be noted that the area-averaged mean values are the interest to this research, rather than the local information of slurry flow.

2.3 Slurry Flow Measurement Techniques

Individual phase flowrates or mixture flowrate (volumetric flowrates or mass flowrates), phase fractions (generally volume fractions are better indices than mass fractions [6]) as well as mixture density (closely linked with mixed fluid composition) are usually used to characterise two-phase flow quantitatively [30]. In terms of flowrate measurement, mass flowrate is often favoured over volumetric flowrate due to the immunity to variable process conditions, especially in the highly demanding applications of custody transfer such as oil and gas industry. Thus, the main focus of this research is the mass flowrate measurement of slurry flow.

This section will firstly give a brief overview of current slurry flow measurement techniques. Then, the section will review a number of existing techniques which can offer direct measurement of slurry flow. Here the particular emphasis is the impact of entrained solid particles on the measurement accuracy as well as the potential wear problem resulting from the abrasiveness of slurry flow. Lastly, the measured parameters, advantages together with limitations of the existing techniques for slurry flow metering will be summarized. This review is primarily concentrated on the measurement of individual phase flowrates (alternatively phase velocities), mixture flowrate along with phase fractions of slurry flow, while the research concerned with flow regime identification is beyond the scope of this research programme.

2.3.1 **Overview**

During the past few decades, a vast number of studies have been carried out to develop suitable techniques for slurry flow measurement or improve the performance of conventional instruments for extending the abilities to serve slurry applications. So far it is still challenging to characterise slurry flow due to the complex solid-liquid interactions along with the abrasive nature. Traditional approaches using off-line separation or on-line sampling systems cannot meet the requirements for real-time flow measurement or control, due to the evident drawbacks, such as significant time delay and low efficiency. Hence, the primary interest here will be the on-line and real-time measurement techniques for slurry flow metering, without using separation or sampling systems. As reported in the early research [30], on-line two-phase flow measurement techniques can be generally categorised into two groups, direct and indirect approaches, which will be briefly described below.

2.3.1.1 **Direct Approach**

Direct approach is able to offer direct measurement of the physical properties of two-phase flow. A typical example of direct approach for solid-liquid two-phase flow metering is shown in Figure 2.2. Derived from the measured properties of each individual phase (phase velocity, fraction and density), volumetric flowrate or mass flowrate of each phase can be acquired and the mixed (total) mass flowrate ($\dot{m}$) can be further determined. The relevant calculations are given as follows,

$$\dot{m}_m = \dot{m}_s + \dot{m}_l = A\,(\emptyset_s\, i_s\, \rho_s + \emptyset_l\, i_l\, \rho_l) \qquad (2\text{-}1)$$

$$\emptyset_s + \emptyset_l = 1 \tag{2-2}$$

where $\dot{m}_m$ denotes the mixed mass flowrate; A is the cross-sectional area of the pipe, $\emptyset$ is the phase void fraction; i represents the instantaneous velocity and ρ is the density. Subscripts "s" and "l" refer to solid and liquid phases, respectively.

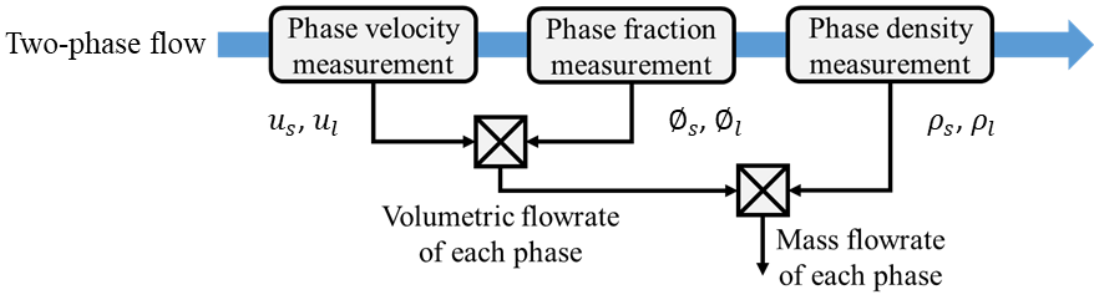

Figure 2.2. Principle of the direct approach to on-line two-phase flow measurement [24]

Flowrates or flow velocities are usually measured using differential pressure devices, electromagnetic flowmeters, Coriolis flowmeters, ultrasonic or acoustic sensors along with cross-correlation techniques. Electrical tomography techniques, gamma energy absorption, ultrasonic or acoustic or microwave attenuation techniques are often deployed to obtain phase fractions of slurry flow. Individual phase densities are typically obtained from densitometers (e.g. based on gamma ray, ultrasonic or microwave methods). For mixture density, Coriolis flowmeters are capable of offering satisfactory density measurement for single-phase flow and have the potential to be extended to determine the mixture density of slurry flow. In consideration of the measured parameters, advantages as well as limitations of each technique, several different measurement techniques can be combined together for slurry two-phase flow metering. However, the combination of multiple sensing systems would increase the size, cost, as well as difficulties in maintenance and calibration of the measuring instruments.

2.3.1.2 **Indirect Approach**

In contrast to the direct approach, an indirect approach is applying models (e.g. empirical models, soft computing models) which are typically established based on experimental data, so as to infer (predict) the physical parameters as required for flow characterisation, as displayed in Figure 2.3. With the tremendous technological progress of artificial intelligence and machine learning, soft computing techniques can be served as alternative

approaches to traditional statistical methods for extending the capabilities of empirical models. An up-to-date review of soft computing techniques for multiphase flow measurement has been presented by Yan et al. [30].

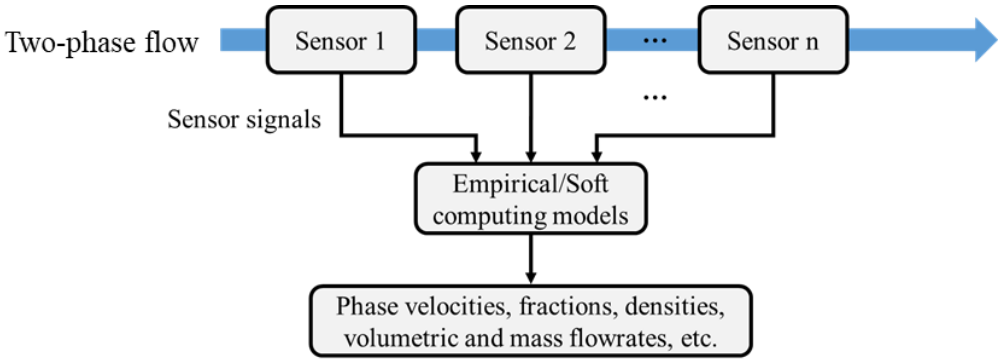

Figure 2.3 Principle of the indirect approach to on-line two-phase flow measurement [31]

There are a number of studies employing the indirect approach into the measurement of phase fractions or phase flowrates of gas-liquid and liquid-liquid flow, whereas very limited work has been published regarding slurry flow measurement [30]. Only several relevant investigations have been undertaken for predicting the pressure drop [32] and critical velocity [33], [34] using the indirect approach, which are concerned with slurry transportation, rather than slurry flow metering. The reason here probably is that the solid-liquid interactions in slurry flow could be less complex than the interactions with gas bubbles, making it possible to employ the direct approach to achieve satisfactory measurement accuracy with slurry flow. With a focus on the direct approach, the existing slurry flow measurement techniques will be reviewed in the following sub-sections.

2.3.2 **Differential Pressure Devices**

As conventional measurement techniques, differential pressure devices (e.g. orifice plate, pitot tubes and venturi tube) incorporating pressure transducers are the most common industrial flowmeters worldwide, from which flow velocity or flowrate can be typically obtained based on the Bernoulli principle, being widely used for single-phase flow (e.g. liquids, gases) measurement [35]. Shook et al. [36] have presented an optimized venturi meter for measuring mixture volumetric flowrate of slurry, suitable for homogeneous flow. It has been identified that the flow regime can affect the behaviour of venturi flowmeters due to the effect of frictions with the wall of the meter. When the flow regime shifted from homogenous to heterogeneous slurry, the discharge coefficient of venturi flowmeters

decreased [37]. In addition, as the discharge coefficient is a function of slurry mixture flowrate and solid volumetric concentration, differential pressure devices can also be utilized to measure solid concentration [38].

However, when differential pressure devices are applied into slurry, erosion can occur on the devices and correspondingly the discharge coefficient will change. As a result, the measurement performance will be degraded owing to erosion. Moreover, since flow velocity dominates the erosion rate, the increased velocity in the constricted area (e.g. the throat of a venturi flowmeter) can accelerate the erosion faster than the damage on pipeline. The previous study [11] investigated the wear of a venturi flowmeter with erosive tests. According to the experimental results, the discharge coefficient drifted into a negative direction resulting from erosion. Through visual inspection, evident damage was noticed downstream of the holes for pressure tapping whilst ripple surface was also observed on the wall of the meter. Moreover, the solid particles could cause the blockage of pressure taps which also limits the use of differential pressure devices for slurry flow metering.

2.3.3 **Electromagnetic Flowmeters**

Electromagnetic Flowmeters (EMF) have been employed to measure the volumetric flowrate or velocity of single-phase liquid in a wide range of industries. With the advantage of the simple structural design without hindering components and no pressure drop, EMF is a popular choice for volumetric flowrate measurement especially for hostile environment (e.g. corrosive or abrasive fluids). However, due to the working principle based on Faraday's Law of electromagnetic induction, EMF is only able to sense electrically conductive fluid medium. For example, when dealing with sand-water mixtures, the reading of EMF is generated from the water phase, whereas the sand particles cannot be sensed. Low conductivities of fluid containing nonconductive materials (e.g. sand, hydrocarbons or gases) would negatively impact on the measurement performance.

Besides, the presence of solid particles would affect the signal derived from slurry flow and lead to the fluctuations in the outputs during slurry flow measurement [39]. When solid particles scratch the electrodes of EMF, the electrical double layers nearby electrodes will be disturbed and a sort of spike-like noise will appear in the slurry flow signal [40], [41]. To solve the problems arising from slurry flow metering, some strategies and techniques have been developed so as to reduce the noise interferences due to the presence

of solids, such as the dual-frequency excitation [42], wavelet processing method incorporating with neural network to predict flowrate [43]. The main drawbacks are that EMF is solely applicable to conductive fluid and only feasible for the measurement of phase flowrate or velocity. In order to fulfill the requirement of slurry flow characterisation, a second flow measurement technique (e.g. electrical resistance tomography [44], [45]) is required to deliver phase fraction information, in combination with EMF.

2.3.4 **Electrical Resistance Tomography Systems**

Electrical tomography techniques can be used to identify flow regime and visualise the phase distribution of slurry flow which are inferred from the electrical properties of the mixed flow being monitored [46]. Several researchers have applied ERT (electrical resistance tomography) [44], [47] or EIT (electrical impedance tomography) [48], [49] techniques to characterise the solid particles suspended in slurry flow. A typical ERT system consists of an ERT sensing unit, a data acquisition system along with an image reconstruction system, as shown in Figure 2.4. The primary advantage of employing tomography techniques is that tomography can yield cross-sectional distribution information, such as local and detailed phase volume fraction. In addition, velocity profile can also be determined through cross-correlation of reconstructed images derived from adjacent electrode rings placed on the pipeline [50].

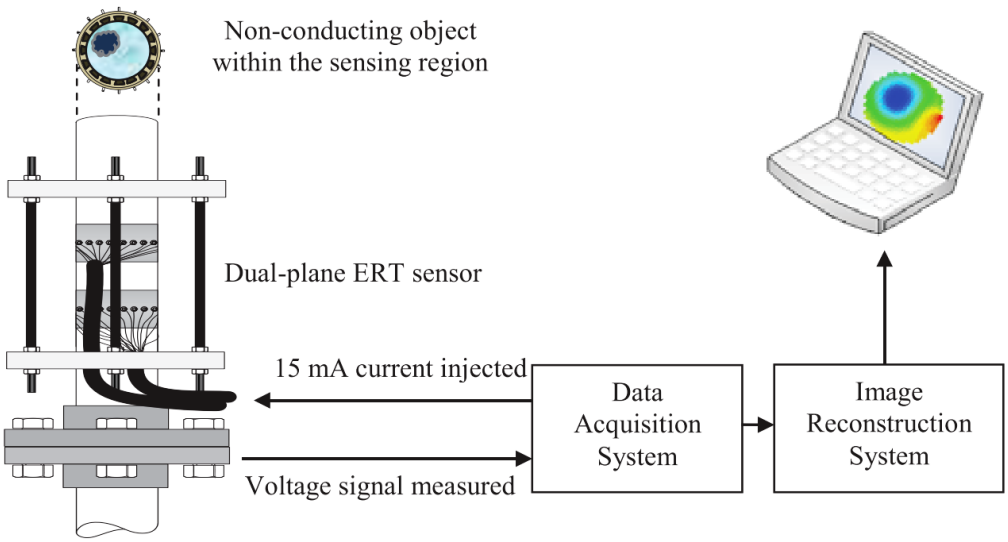

Figure 2.4. Schematic of a typical ERT system [47]

The profile of solid volume fraction as well as solid phase velocity can be acquired by using ERT or EIT systems. Area-averaged mean solid phase volume fraction, mean solid

phase velocity and solid phase volumetric flowrate can be further obtained. However, the major limitation of using ERT or EIT systems for slurry flow metering is that merely the flow information of dispersed phase (solid particles) can be determined while the velocity (or flowrate) of continuous phase (liquid carrier) cannot be measured. In order to determine the liquid phase velocity or flowrate which is fairly crucial to monitor slurry transportation, it is required to deploy a supplementary approach (e.g. EMF [44], [45]). Moreover, attention should also be given on the potential erosion of electrodes when using invasive and intrusive electrical transducers for process tomography. The main disadvantage of electrical tomography methods is that the measured electrical properties are always sensitive to the changes in fluid dielectric properties as well as flow regimes. Frequent on-line calibrations are required in order to offer accurate flow measurement results, which would limit the application of electrical tomography techniques into real-world industrial processes.

2.3.5 **Ultrasonic Sensors**

As a well-developed flow measurement technology, ultrasonic flowmeters have been applied to determine volumetric flowrates by measuring the velocity of fluids flowing in pipe. Compared with traditional flowmeters, such as orifice, vortex or turbine metering, the non-invasive ultrasonic flowmeters can be inline or clamp-on devices to suit some challenging environments for instance corrosive or abrasive chemicals, having the benefit of long service life, no maintenance and no pressure loss. Ultrasonic flowmeters always use either time-of-flight or Doppler techniques to determine the fluid velocity, which classifies the main two types.

One problem is that when an active ultrasonic system is employed into some two-phase cases such as dense bubbly or particulate flow, particularly with the flow regime of clearly-separated phases, the presence and movement of the dense phase could lead to the attenuation or even breakup of the ultrasonic waves. In the situation of some specific gases, such as CO_2, gas phase would significantly absorb the ultrasound wave, making signal processing difficult because of the extremely weak ultrasonic signal. As a result, in contact with solids or bubbles, the interferences (or multiple reflections) can affect the propagation of sound and thereby the measurement of time-of-flight would be less accurate.

Besides, the capability of ultrasonic techniques can be extended to determine solid phase fraction of slurry flow, based on the dependency between the characteristics of sound waves (e.g. acoustic impedance, speed of sound, attenuation of ultrasound) and the properties of slurry flow (e.g. solid concentration) [51]–[53]. Nevertheless, there are still many problems in slurry flow measurement using ultrasonic methods. Although solid concentration can be potentially inferred from the attenuation of ultrasound waves, noticeable attenuation can adversely affect the sound propagation thus degrading the measurement accuracy of solid phase fraction, as well as flow velocity or flowrate. Therefore, it is still challenging to accurately measure the phase velocity and phase fraction simultaneously. The applicable range of using an ultrasonic technology for slurry flow metering would be limited by the content of suspended solids, so as to achieve satisfactory measurement results.

In addition, a range of mechanisms including diffraction, reflection and attenuation of sound waves will alter the characteristics of an ultrasonic wave directed into a slurry mixture. In the meantime, propagation of sound can be impacted by temperature, flow regime, fluid viscosity, suggesting the sensitivity to ambient environment and requirement of on-line calibration. Furthermore, in some circumstances, ultrasonic probes need to be installed in direct contact with the flow being metered because the sound attenuation can be noticeable when pass through the pipe wall, which also increases the risk of probe damage.

2.3.6 **Passive Acoustic Sensors**

In recent years, O'Keefe et al. has proposed a new type of non-invasive sonar flowmeters based on an array of passive acoustic sensors being mounted to the outside wall of pipe [16], [54]. The collected acoustic signal conveys information of the disturbances associated with flow transportation. As explained in [16], these disturbances can be categorised into three groups: disturbances carried by the flow, acoustic waves propagating in the fluid, together with vibrations passing through the pipe wall. With regard to the disturbances carried by the flow, the overall mean velocity of these disturbances travelling along the axial direction of the pipe is equivalent to the mean flow velocity. Therefore, mean flow velocity can be acquired by separating and analysing the signal component induced by the disturbances which are carried by the flow. The basic working principle of this passive

acoustic method for flow velocity (or volumetric flowrate) measurement is illustrated by Figure 2.5.

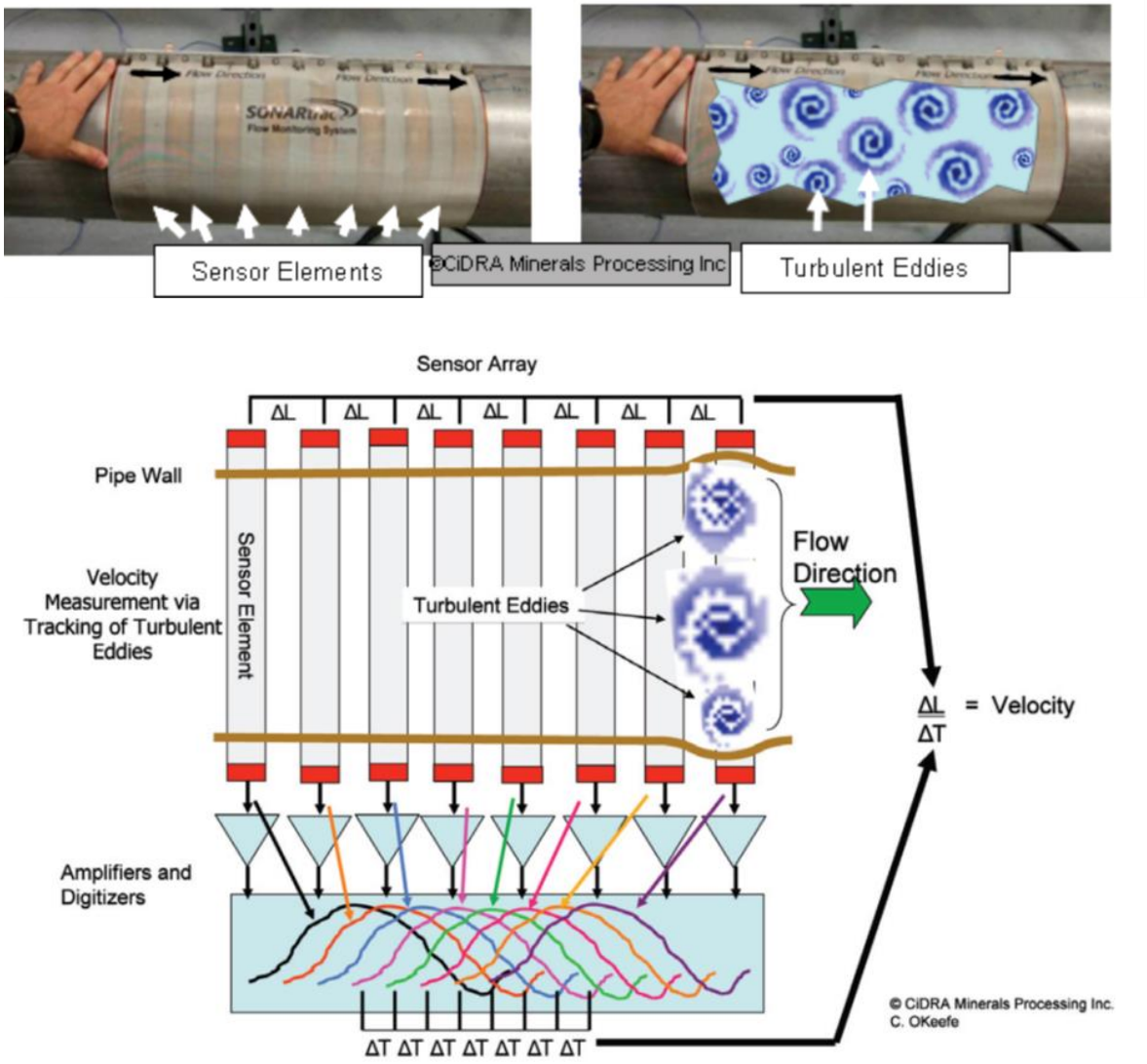

Figure 2.5. Working principle of flow velocity measurement using passive acoustic sensors [16]

In addition to flow velocity measurement, the potential use of this passive acoustic technique for characterising some multiphase cases has also been reported in [16], [54]. Based on the analysis of the signal component generated by acoustic waves propagating in the fluid, the speed of sound travelling in the mixed flow can be obtained. Since the speed of sound is a function of the physical properties of mixture fluid, the fluid composition (phase fraction) can be further inferred. Several cases of the application into multiphase flow can be sourced from [16], [54], including solid concentration measurement with thick slurry, gas fraction measurement with gas entrained into a liquid or slurry.

The major advantage of this proposed passive acoustic method is the capability of handling some harsh industrial environments such as ferromagnetic slurry, dense slurry, abrasive or corrosive applications, along with the non-invasive feature. However, as the typical shortcomings of acoustic methods, the external noises can negatively affect the measurement performance, especially when the interested signal component becomes weak compared with environmental noises. For example, the strong noises from external environment when a large pump or other heavy vibration machine is operated around, or other acoustic signals produced from slurry flow transportation (e.g. solids collisions, solids impingement on pipe wall), can cause several different and large noises being mixed with the interested disturbances conveyed by the flow. As a result, it will become difficult to classify and pick out the interested signal which is related to the flow characteristics. Besides, on-line calibration or some correction is also required for determining volumetric flowrate or fluid composition in the case of multiphase flow.

2.3.7 **Coriolis Flowmeters**

Coriolis flowmeters have been successfully applied into a wide variety of liquid and gas applications for delivering highly accurate single-phase mass flow measurement. Among these measuring instruments as mentioned above, Coriolis flowmeters are the only measuring device offering direct measurement of mass flowrate. Since volumetric flowrate can be sensitive to process conditions, mass flowrate measurement becomes more favoured, particularly in the highly demanding applications such as custody transfer in the oil and gas industry. Apart from mass flowrate, Coriolis flow metering is also able to supply an independent and simultaneous measurement of density, which is beneficial to characterise the flow being metered.

With a symmetrical design, a typical Coriolis measuring system mainly consists of vibrating tube(s) excited by a driving unit located at the centre, together with two motion sensors arranged on the inlet and outlet side respectively, illustrated by Figure 2.6. The basic measuring principle is that the interaction between the moving fluid and its conveying tube(s) creates Coriolis force which is a function of mass flowrate of the fluid. Mass flowrate is obtained from the measurement of time delay (or phase shift) between the signals collected from the two motion sensors, as shown in Figure 2.7. Coriolis flowmeters are driven at a resonant frequency (commonly in its first vibration mode) so as to consume less energy for keeping constant oscillation. By tracking the resonant frequency, the

density of the fluid medium can be determined. Moreover, Coriolis flowmeters also output the process (fluid) temperature with a temperature sensor typically attached to one measuring tube, and even flow viscosity in some circumstances.

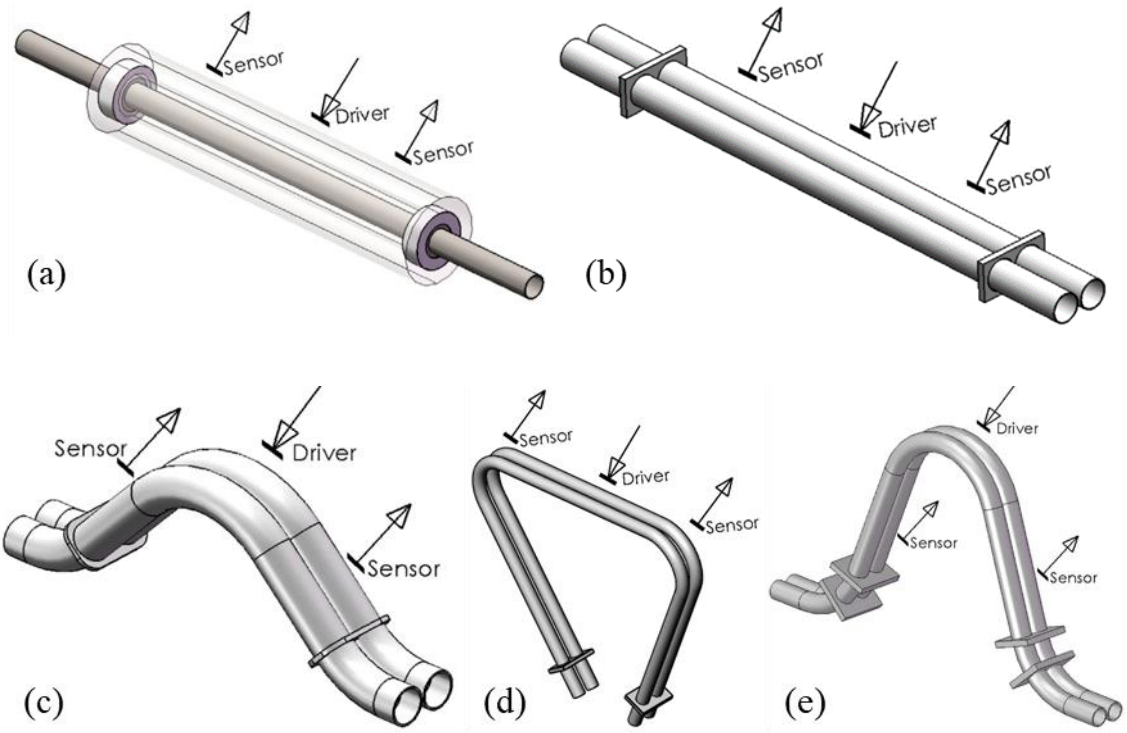

Figure 2.6 Several typical designs of Coriolis flow sensors (a) Single straight-tube flow sensor (b) Twin straight-tube flow sensor (c) Twin bent-tube flow sensor with two shallower V-shaped (d) Twin bent-tube flow sensor with two triangular (or Ω-shaped) tubes (e) Twin bent-tube flow sensor with two deeper V-shaped tubes [18]

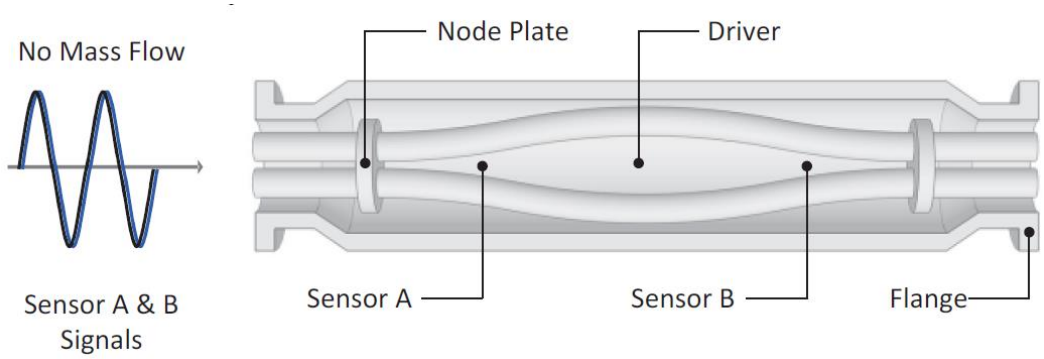

(a) Vibration of Coriolis tubes without flow (exaggerated)

(b) Vibration of Coriolis tubes with flow (exaggerated)

Figure 2.7 Measurement principle of mass flowrate of Coriolis flowmeters [55]

Over the last two decades, significant efforts have been devoted to improve the performance of Coriolis flow metering technology, for instance appropriate compensation on the effects of variable process conditions, optimized meter design, advanced signal processing and control techniques, making Coriolis flowmeters capable of delivering stable, reliable and the most accurate measurement of single-phase flow, which can be immune to changes in fluid temperature, pressure as well as flow viscosity [18], [56]. However, Coriolis flowmeters in general struggle to maintain high measurement accuracy under multiphase flow conditions. There are a number of studies reporting the measurement errors of Coriolis flowmeters with gas entrained into the liquid being metered. Hemp [57] and Basse [58] have proposed the theoretical foundations of the physical mechanisms resulting in measurement errors of Coriolis flowmeters due to the presence of a second phase. Phase decoupling effect and compressibility effect have been recognized as two leading error sources which cause the deviations in the measurement outcomes from the true values. And gas entrainment has been clearly identified as a key factor which can adversely affect the performance of Coriolis flowmeters, attributable to decoupling effect as well as compressibility effect [59], [60]. More importantly, besides the theoretical analysis, extensive experimental work has been undertaken to evaluate the typical behaviour of Coriolis flowmeters under aeration condition, providing the experimental support [22], [23], [31], [55], [59], [61]–[67]. In addition, experimental investigations are helpful to explore the effects of other factors involved in real-world process conditions, for instance, flow regime, fluid viscosity, meter installation orientation, meter tube geometry as well as meter size.

Nevertheless, the influence of the existence of solid particles on Coriolis flow metering is still unclear. Only some theoretical analysis has been carried out [58], [63], [68], [69], while very few experimental investigations and results are available. Without the

experimental evidence, the feasibility and efficiency of using Coriolis flowmeters for slurry flow metering remains doubtful, which motivates this present work to fill in the gaps. The relevant studies on the application of Coriolis flowmeters into slurry will be reviewed in detail in the following section (Section 2.4).

2.3.8 **Summary of Slurry Flow Measurement Techniques**

Table 2.1 summarizes the direct slurry flow measurement techniques reviewed above.

Table 2.1 Direct measurement techniques for slurry flow metering

Measurement Techniques	Measured Parameters	Advantages	Limitations
Differential Pressure Devices [36]–[38]	• Slurry velocity • Solid phase fraction	• Simple • Low cost	• Intrusive • Relatively easily eroded • Discharge coefficient changes due to erosion • Plugged pressure tapping holes
Electromagnetic Flowmeters [39]–[43]	• Liquid phase velocity	• Suitable for abrasive medium • Applicable to highly concentrated slurry	• Only sense electrically conductive liquid • Measurement errors due to entrained solids
ERT or EIT [44]–[49]	• Solid phase fraction • Solid phase velocity	• Visualize phase distribution • Local flow information	• Potential erosion of electrodes • Sensitive to mixture properties and process conditions
Ultrasonic Sensors [51]–[53]	• Slurry velocity • Solid phase fraction	• Non-invasive • Suitable for abrasive medium	• Ultrasonic wave attenuation or even breakup with thick slurry • Solid concentration measurement affected by mixture properties and process conditions
Passive Acoustic Sensors [16], [54]	• Slurry velocity • Solid phase fraction	• Non-invasive • Suitable for abrasive medium • Applicable to thick slurry	• Susceptible to external acoustic and vibration noises • Solid concentration measurement affected by mixture properties and process conditions
Coriolis Flowmeters [58], [63], [69]	• Slurry mixed mass flowrate • Slurry mixture density	• Capable of measuring mass flowrate and density • High accuracy	• Potential erosion of measuring tubes • Measurement errors due to entrained solids

2.4 Technical Issues in Slurry Flow Measurement Using Coriolis Flowmeters

With the drastic improvements in Coriolis flow metering technology, Coriolis flowmeters, as the most accurate single-phase mass flowmeters, are considered to be a promising and suitable candidate for slurry flow measurement. By introducing appropriate compensation methods (e.g. analytical modelling or soft computing techniques) for reducing the influence of entrained solid particles, Coriolis flow metering technology is highly likely able to measure mass flowrate and density of the mixed slurry flow with satisfactory accuracy. In addition, for dilute slurry typically being transported in homogenous suspension or non-settling flow regime, phase volume fraction can also be estimated from the mixture density, with known individual phase density (solid and liquid density).

2.4.1 Influences of Solid Particles on Flow Measurement Accuracy

The behaviour of Coriolis flowmeters under solid-liquid two-phase conditions has not been fully understood so far. As stated above, very limited research has evaluated the influence of entrained solid particles. Moreover, it is worth noting that there are several previous studies [44], [70] which assessed the performance of their proposed measurement techniques against Coriolis flowmeters with slurry flow, without considering the possible measurement errors of Coriolis flowmeters. Due to a lack of experimental investigations into the influence of solid particles, relevant research in which Coriolis flowmeters are served as the reference devices for slurry metering could become less convincing.

Several basic theoretical analyses have been conducted for providing a comparison between the effects of entrained gas and solid particles on Coriolis flow metering [58], [63], [68], [69]. Basse [58] has theoretically examined the measurement errors of Coriolis flowmeters using three typical examples, covering air-water, oil-water and sand-water mixtures. According to the theory of decoupling effect and compressibility effect, compared with gas entrainment, the existence of solids is expected to cause less problems in Coriolis flow metering which is favourable to the application of Coriolis flowmeters into slurry, since both liquid phase and solid phase are relatively incompressible. The existing theoretical studies offer theoretical basis for conducting theoretical analysis of measurement errors of Coriolis flowmeters and analytical modelling for error prediction. However, quite few experimental studies have been undertaken for quantifying the actual

influence of solid particles on Coriolis flow metering, especially for mass flowrate measurement. Relevant experimental reports are only available from Weinstein et al. [63] and Zhu [69].

Weinstein et al. [63] utilized a high speed video camera to track the motion of a solid sphere in an oscillating system. Their results validated the decoupled motion of a solid particle over a wide range of density ratio and inverse Stokes number, which can be applied to analyse the decoupling effect on Coriolis flow metering. Zhu [69] performed a group of static tests for evaluating the effect of solids on the density measurement in Coriolis flowmeters. By using two chains of small beads (glass) and large beads (stone), noticeable negative errors were observed from the density reading provided by a single straight-tube Coriolis flowmeter (Endress+Hauser PROMASS 83I DN25) vertically placed, as shown in Figure 2.8. According to the experimental outcomes, −5.12% and −8.83% errors in density occurred in the Coriolis flowmeter under test, corresponding to the cases of small beads and large beads with solid volume fractions of 10.40% and 17.58%, respectively.

Figure 2.8 Static tests for evaluating the influence of solid particles on density measurement [69]

2.4.2 **Potential Erosion on Coriolis Measuring Tubes**

Apart from the concerns of measurement accuracy affect by entrained solids, the wear problem of meters is also quite important due to the consideration of the abrasive nature of slurry flow. There is a potential to erode the vibrating tubes of Coriolis flowmeters in contact with solids. If a Coriolis tube is eroded, the thickness of tube wall will decrease and the structural property (tube stiffness) will change. Consequently, Coriolis flowmeters can become less accurate whilst serve damage can even lead to meter failure. Wear problems of Coriolis flowmeters is receiving a growing attention in the last decade. Boussouara et al. [11] conducted erosive tests to wear Coriolis flowmeters intentionally and assessed the performance of eroded meters using water (single-phase flow). Their experimental results demonstrated the large measurement errors in both mass flowrate and density readings from the eroded meters. Figure 2.9 displays the excessive erosion observed from the outlet side of Coriolis tubes in [11].

Figure 2.9 Excessive erosion in the outlet side of Coriolis tubes [11]

To reduce the chance of erosion encountered in abrasive or corrosive applications, several suggestions have been provided by the manufacturers [71], including the selection of suitable tube material, flow profile conditioning, preventing solid-liquid separation as well as considerations on straight-tube over bent-tube. More importantly, how to monitor the structural condition of a Coriolis flowmeter during its service life becomes considerably advantageous, in order to guarantee the structural integrity as well as maintaining excellent performance (typically ±0.1% uncertainty of mass flowrate measurement). If an early warning can be given to the operator when the structural property starts drifting, the Coriolis flowmeters in use can be cleaned or recalibrated or replaced promptly (depending on the specific cases).

Regarding the in-situ structural conditions of Coriolis flowmeters, some patented technologies have been reported by three main manufacturers (Micro Motion [72], Endress+Hauser [73], KROHNE [74]) while very limited research work has been published so far. Micro Motion has developed a diagnostic tool SMV (Smart Meter Verification) with a claimed uncertainty of ±4%, which means it can give a warning when the structural change in Coriolis tubes exceeds ±4% [75]. As explained in [76], four additional off-resonant frequencies are applied into the drive signal so as to characterize the Coriolis oscillation behaviour, from which the effective mass, stiffness and damping of the oscillation system can be estimated. But the detailed signal processing along with calculation procedures are not given. Endress+Hauser has proposed a new feature Heartbeat Technology for examining the structural integrity. As described in its patent [73], the meter is excited with one additional frequency higher than the normal working frequency (resonant frequency) in order to identify the changes in the thickness of tube wall.

Besides these recent advances contributed from the manufacturers, there are still many remaining questions in this field which need significant research efforts. The technical details of the methods for monitoring the structural health of a Coriolis flowmeter have not been fully published so far. Moreover, to validate the feasibility of the proposed monitoring techniques, the existing studies utilized an accelerated erosion process (e.g. with high velocity or heavy solid contents or acids) which makes it hard to identify the sensitivity. Instead of using a high erosion rate, a slow erosive test can help give more details about the sensitivity or uncertainty. Furthermore, the exact reasons triggering false alarms have not been fully understood whilst the effect of variable process conditions (e.g. fluid temperature, pressure, the presence of a second phase) is still unclear.

2.5 Summary

This chapter has briefly described slurry flow characteristics and the key parameters of significant interest in slurry flow measurement. The existing direct on-line slurry flow measurement techniques have been reviewed, highlighting the influence of entrained solids on the measurement accuracy as well as the potential wear problem due to the abrasive nature of slurry flow. Moreover, with a focus on the relevant studies on Coriolis flow metering technology, technical issues in slurry flow measurement using Coriolis flowmeters haven been identified.

Complex two-phase flow conditions as well as the hostile working environment cause the technical difficulties in offering a desirable solution to slurry flow measurement in real-world applications. As can be seen from the cited work (Section 2.3), a variety of measurement techniques have been proposed or improved to serve slurry applications. However, due to the limitations of these existing techniques (summarized in Table 2.1), it is still challenging to provide stable, continuous and accurate measurement of slurry flow. The Coriolis flow metering technology is able to deliver superior performance of single-phase mass flow measurement. However, there are many technical issues that remain challenging in applying Coriolis flowmeters into slurry flow, as can be seen from the cited work (Section 2.4).

In this review, gaps that require further research have been identified. Firstly, only theoretical analysis has been conducted for exploring the impact of solid particles on Coriolis flow metering, whereas very few experimental studies have been undertaken. Due to the lack of experimental investigations with slurry flow, the performance of Coriolis flowmeters under solid-liquid two-phase flow conditions is still unclear, which motivates this research programme. Experimental investigations will be carried out in this research to provide experimental evidence of the negative impact of entrained solid particles on Coriolis flow metering, which will be presented in Chapter 4. Secondly, regarding the potential wear problem of Coriolis flowmeters, only few relevant technical reports have been provided by the manufacturers whilst very limited research has been conducted on this topic so far. Based on the review of existing work, how to improve the sensitivity for warning tube erosion and how to avoid false alarms under real-world process conditions will be the key questions to answer and the relevant contents will be presented in Chapter 5.

The literature review has clearly demonstrated that there are certain gaps between the existing techniques for slurry flow measurement and the requirements of real-world industrial applications. Coriolis flowmeters incorporating compensation techniques for reducing the influence of solid particles along with condition monitoring techniques for examining the structural health of measuring tubes are believed to be a promising solution to slurry flow measurement.

Chapter 3
Design and Construction of the Slurry Flow Test Rig

3.1 Introduction

A laboratory-scale slurry flow test rig has been designed and constructed in order to provide the experimental platform for conducting the experimental tests in this work. This chapter primarily presents the design and construction of the slurry flow test rig.

This chapter, firstly, describes the essential functions of the slurry flow test rig. Two main experimental tasks are required to be performed on the test rig, including flow measurement tests for identifying the measurement errors of Coriolis flowmeter under solid-liquid two-phase flow conditions along with erosive tests for creating erosive flow conditions to assess the potential wear problem of Coriolis flowmeters handling slurry applications. Then, the chapter explains the full details of rig design and construction, sharing the practical considerations and the relevant experience from this work. Here the primary focus of the rig design and construction is to offer accurate references to the Coriolis flowmeters under test. It should be noted that a full discussion of various designs of erosive slurry flow test rig or specialized solids-handling equipment are out of the scope of this work. Thirdly, the data acquisition system as well as the operating procedures are presented. Lastly, the advantages and limitations of this slurry flow test rig are briefly discussed.

3.2 Essential Functions of the Test Rig

First of all, it is necessary to state the focus of this research is the measurement of dilute slurry flow. One typical example of dilute slurry flow is the sand-water slurry containing a small portion of sand particles carried by water. In addition, dilute slurry flow is often employed for oil and gas exploration, for instance, the fracturing fluid used in hydraulic fracturing process [9], [77]. Besides, during hydrocarbon recovery, some particulate solids,

(mostly sand particles) would come from the production wells of oil and are transported with the liquid, due to well aging [4], [12].

In this research, the experimental study is undertaken with dilute sand-water mixed flow (sand concentration by volume within 4%). One benefit of erosion tests with dilute slurry flow is that low sand concentration would gradually erode Coriolis flowmeters in a slow and controllable manner. Otherwise, if erosion scars or even tiny erosion ripples appear on the Coriolis tubes which are typically difficult to notice promptly, the resulting tube erosion would negatively impact Coriolis flow metering. The effect of tube erosion would be superimposed on the influence of solid-liquid two-phase flow conditions, both of which can degrade the measurement performance of Coriolis flowmeters. With dilute slurry flow, tube erosion would be less likely to occur during the flow measurement tests, so that measurement errors of Coriolis flowmeters can be clearly identified and further correlated with the presence of solids solely, free of the influence of tube erosion.

In order to fulfill the experimental requirements in this study, the essential functions of the slurry flow test rig should include: start-stop batching procedures in a gravimetric system, flow sampling procedures, as well as slurry erosive tests. Flow batching and sampling procedures are employed to examine the measurement errors of Coriolis flowmeters with slurry flow. Erosive tests are conducted so as to investigate the wear problem of Coriolis flowmeters along with the performance of the structural condition monitoring techniques.

3.2.1 **Start-Stop Batching Procedures**

The measurement errors in mass flowrate as well as density of Coriolis flowmeters are typically obtained with respect to the reference (served as the true values). A start-stop gravitational method can be utilized to recognize the measurement errors in mixture mass flowrate of Coriolis flowmeters when solid particles are present in liquid carrier. To assist in start-stop batching operations, an accurate weighing system is required, so as to provide the reference of batch mass. The basic working principle of the start-stop gravitational method is that the exact amount of fluid going through the Coriolis flowmeter will enter the weighing tank. As a result, mass flowrate errors can be evaluated by comparing the reading of total mass flowing through the Coriolis flowmeter under test with the reference value provided by a weighing scale over the period of batching.

By means of a highly accurate weighing scale which can typically deliver much lower (at least 3 times suggested by the manufacturer) measurement uncertainty than Coriolis flowmeters, the gravitational method has the advantage of low uncertainty and high accuracy. Thus, the start-stop gravitational method is commonly used for mass calibration or verification. For example, Coriolis flowmeters are typically calibrated through start-stop batching procedures performed in a gravimetric system in the factory of the manufacturer.

3.2.2 **Flow Sampling Procedures**

Since Coriolis flowmeters offer independent measurement of mass flowrate and density, it is not essential to know the actual flow density during mass batching operation. That means it is reasonable to examine measurement errors in density separately from errors in mass flowrate. A dynamic flow sampling method is chosen for the assessment of density errors. Since sand particles tend to settle in the bottom of pipe under the effect of gravity, the delivered sand concentration can be easily impacted by any changes in flow conditions (e.g. flowrate). Hence, a rapid flow sampling test is utilized and consideration should be given on avoiding disturbances to the current flow conditions during the flow sampling operation.

Through a quick operation of a three-way valve being mounted on a sampling point, a certain amount sample of slurry flow is collected. By separating sand particles from the sample, the actual sand concentration is determined, and thereby the reference mixture density of slurry flow is obtained. Accordingly, density errors are computed with respect to the apparent density reading from Coriolis flowmeters. The benefit of employing flow sampling tests is the easy operation and no need of supplementary apparatus which helps save the cost as well as the installation space. If an additional density meter (e.g. gamma ray densitometer) is utilized for determining sand concentration for reference, the cost would be higher. Nevertheless, the main drawback of using flow sampling method is probably the less accurate results from sampling. Since only limited sample is gathered and the sampling time is short, it may be difficult to reach a steady flow condition during the short sampling period. However, slight compromise on the accuracy of experimental results of density errors is acceptable, because the accuracy requirement of density measurement is less stringent than mass flowrate measurement in Coriolis flowmeters.

3.2.3 **Erosive Tests**

Erosive tests need to be performed under sand-water erosion conditions for the purpose of inspection of wear problems of Coriolis flowmeters. The slurry flow test rig to be built should be able to supply a horizontal closed loop for slurry flow circulation, to generate continuous impingements of moving solid particles on Coriolis tubes for erosion purpose. Recirculation of slurry flow is a cost-effective way for erosion purpose. Nevertheless, flow recirculation would naturally cause the degradation of erodents (sand) during the erosion process. Thus, the erosion rate could probably decrease with erosion time. However, the observation of erosion phenomenon is not the interest of this work. The purpose of erosive tests is to create a slow erosion process for gradually eroding the Coriolis tubes. Through erosive tests, the wear problem of Coriolis flowmeters as well as the structural condition monitoring technique for diagnosing the erosive wear will be investigated experimentally.

3.3 Rig Design and Implementation

3.3.1 **General Requirements**

Generally, this slurry flow test rig should be able to supply the suitable pipe routes along with the facilities to perform the essential tasks as clarified in Section 3.2. In addition, the rig should be capable of achieving control over mass flowrate and sand concentration for creating various flow conditions for experimental tests. The design needs to solve the following problems about 1) how to feed or inject sand particles; 2) how to mix sand particles with liquid; 3) how to change the delivered mass flowrate along with sand concertation; 4) how to filter sand particles occasionally; 4) how to drain the slurry flow if needed.

The design of a slurry flow test rig is challenging which needs rich knowledge and extensive engineering work experience. Some relevant experience and helpful information have been found in the prior publications [78]–[82]. However, these existing studies focus on the slurry erosion test rigs with the intention to investigate the erosion phenomenon while the concerns of flow measurement are rarely involved. In this research, the slurry flow test rig is purposely built to cover both flow measurement tests as well as erosive tests on Coriolis flowmeters. Thus, in addition to the considerations of potential wear problem as well as the rig service life, more attention needs to be paid for lowering uncertainty in experimental tests and offering an appropriate use of Coriolis flowmeters.

A laboratory-scale slurry flow test rig has been designed and constructed in Instrumentation Lab at University of Kent. The schematic of the slurry flow test rig is given in Figure 3.1, along with its photos shown in Figure 3.2. This slurry test rig is a low-pressure rig operated below 3 bar and at ambient temperature (15 °C to 30 °C). It is relatively simple, cost-effective and easy to operate for delivering dilute slurry flows. The details of this test rig will be presented in the following six sub-sections: main circulation loop, selection of valves, flow sampling point, weighing system, installation of flowmeters along with safety precautions.

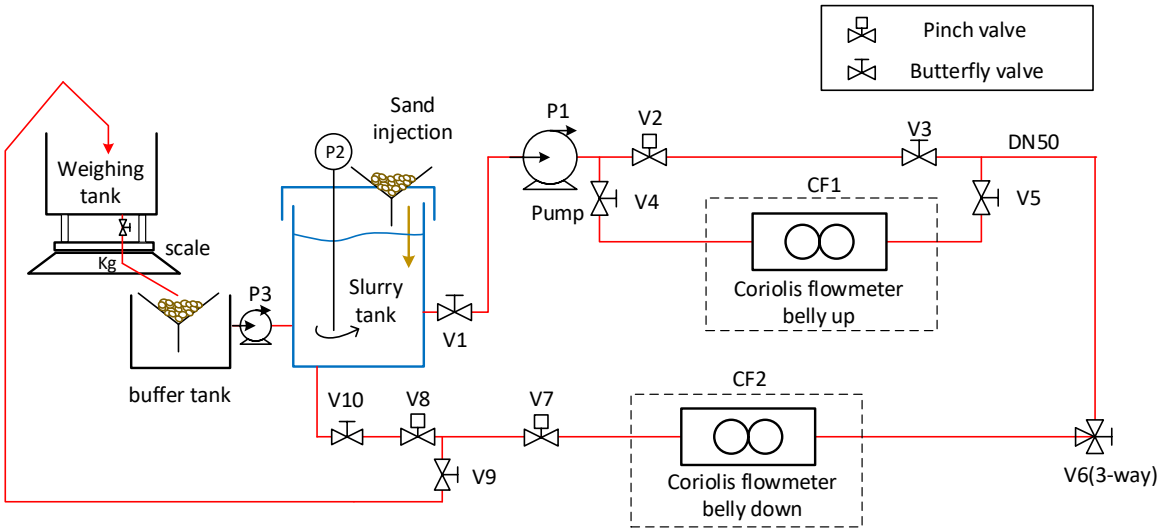

Figure 3.1 Schematic of the slurry flow test rig

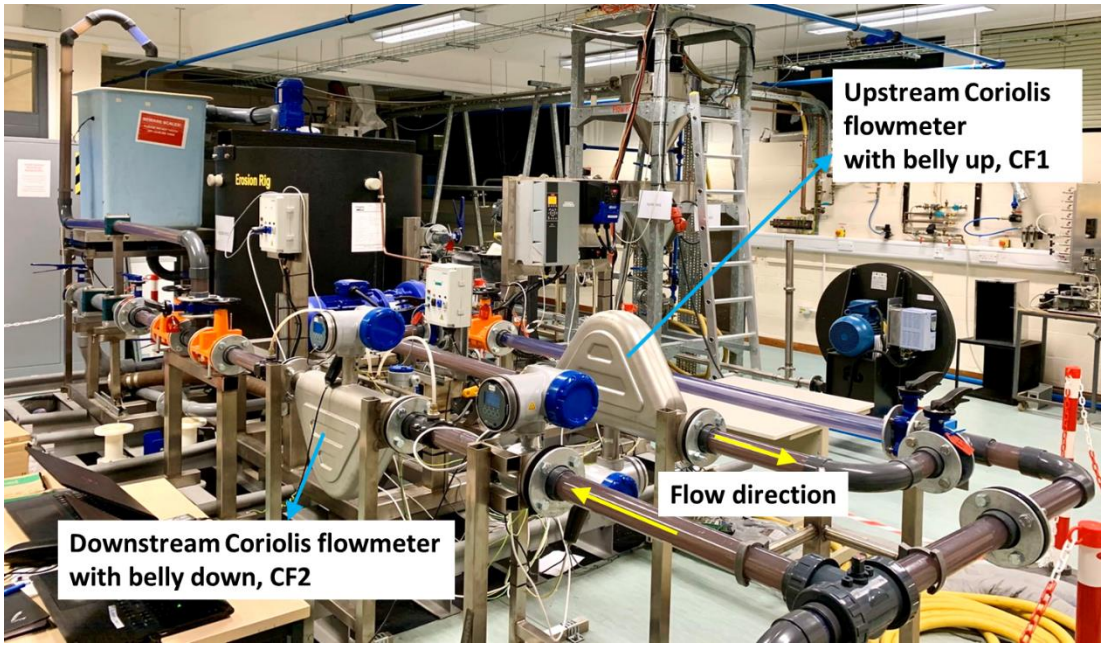

Figure 3.2 Photo of the slurry flow test rig

3.3.2 **Main Circulation Loop**

The main horizonal loop offers the functionality of flow circulation, which primarily consists of a centrifugal pump, a slurry storage tank, an agitator, and a horizontal pipe loop.

It is common to employ a centrifugal pump for mixture flow circulation and occasionally a positive displacement pump can be an alternative choice [78]. However, in this particular case where running the pump dead-headed for a short duration is required for batching operation as well as zeroing of Coriolis flowmeter, a centrifugal pump (KSB Etabloc ETB 100-080-200) is selected over a positive displacement pump as positive displacement pump is not allowed to run dead-headed. In consideration of the cost, a normal type but durable centrifugal pump is used here to deliver dilute slurry flow, rather than a specialized slurry pump. This low-pressure centrifugal pump allows a maximum flowrate of 100 m^3/h and a maximum discharge pressure of 1.5 barg. Being controlled by a connected frequency inverter, this pump can deliver a wide range of mass flowrates for experimental tests. Although the pump is not intentionally designed for slurry applications, it can handle solid spheres up to 10 mm in diameter. Moreover, it has been tested that without significantly reducing the performance, this pump can normally work on fluid that carries around 8% solids by weight. Thus, this pump can fulfill the needs in terms of the allowable sand concentration, the permissible sand particle size as well as the achievable range of flowrate.

To guarantee the solid-liquid two-phase conditions for experimental investigation, it is necessary to avoid the potential sources of gas entrainment as much as possible. The undesired presence of gas bubbles may arise from the slurry storage tank standing in the open air, the joints of pipes as well as of pipe fittings. Due to these concerns, careful consideration has to be given to keep some redundancy in the tank capacity. In the meanwhile, the tank outlet pipe should be properly located so as to maintain a sufficient liquid depth for preventing air from entering into the delivered slurry flow. The tank capacity should exceed the total volume of circulation loop pipeline to allow the pipeline full of liquid and additionally remaining a certain liquid depth from the liquid level in tank to the location of tank outlet. Moreover, the pipes along with fittings need to be closely connected together during rig construction.

In this rig, a large cylindrical tank with the capacity of 1500 litres (see the black tank in Figure 3.3) is connected to the inlet of centrifugal pump, severed as the slurry storage tank.

Being covered by a half-openable lid, this slurry tank is 1500 mm in height and 1200 mm in diameter. Furthermore, the tank is made from polypropylene copolymer (PPC) with the advantage of good durability as well as impact strength.

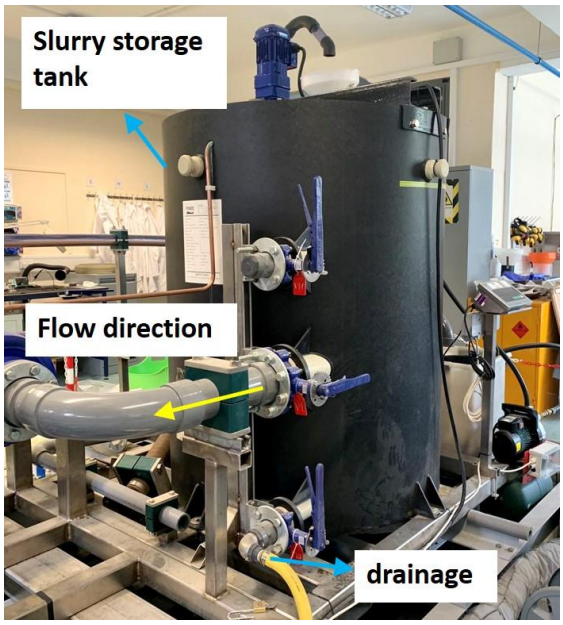

Figure 3.3 Large slurry storage tank

One agitator is utilized to uniformly distribute solids in the liquid medium. The motor of the agitator is seated on the top of the slurry tank. The shaft is long enough to reach the very bottom of the slurry tank and the propeller is attached at the bottom of the shaft. By using a frequency inverter, the rotation speed along with rotation direction of the agitator can be adjusted to supply sand-water mixtures at different concentrations. Photo of the motor control panel of the pump as well as the agitator is shown in Figure 3.4. Therefore, this slurry flow test rig can achieve good control over the delivered mass flowrate via the frequency inverter of pump and the supplied sand concentration through the inverter of agitator.

Figure 3.4 Motor control panel of centrifugal pump and agitator

In terms of loop pipeline, adequate pipe length should be retained for delivering fully developed slurry flow which can reach stable flow conditions. In the meanwhile, wear-resistant pipe material needs to be chosen for reducing the chance of erosion. In this rig, the horizontal loop pipeline has been primarily constructed using transparent polyvinyl chloride (PVC) pipe of 50 mm bore diameter which can give a clear observation of flow regime in the test section. The total length of horizontal pipeline is roughly 10 m. PVC pipe is chosen due to its durable and impact-resistant properties. The allowable working pressure of the PVC pipe in use is rated up to 16 bar although the slurry flow rig is supposed to be operated within 3 bar. The benefit of selecting high pressure pipe is to thicken the pipe wall against the potential erosive wear to ensure safety.

As a demonstration of the operation, first of all, the slurry tank would be filled up with tap water through hose and sand particles can be fed into the tank via a hopper to prepare sand-water mixture. After that, the dilute slurry flow can be pumped from the slurry tank to the 50 mm bore horizonal test section and then transferred back to the tank to finish the flow circulation. By means of the motor control panel of the pump and the agitator, the delivered mass flowrate and sand concentration can be adjusted for the target set in the experiments. After all tests are finished, slurry can be drained away from the tank outlet located fairly low, though some sand-water mixture would inevitably stay in the bottom of the tank as well as the pipeline. The use of the agitator can help clear up the remaining sand particles in the tank. Moreover, the piping system and tank can be flushed by using clean water. After several repeats, the overwhelming majority of sand particles can be

flushed away. Furthermore, the sand particles can also be recovered from the drained slurry by means of sand filters for a reuse of sand.

3.3.3 **Selection of Valves**

Vales are required in a number of places to assist with experimental operations such as zero calibration of Coriolis flowmeters, batching operation as well as flow sampling. Valves should be chosen carefully to offer satisfactory performance as permitting flow transportation, cutting off, or regulating slurry flow. Poor performance or failure of valves can negatively impact the experimental work. For instance, if erosion on valves occurs, the slurry flow probably cannot be completely blocked by closing the valves, which would lead to the potential of flow leakage. As a result, it would affect the zero calibration of the meter thus give rise to a certain level of uncertainties in the flow measurement results. For that reason, it is necessary to select suitable valves and arrange them properly on rig in order to reduce the adverse influence of valves erosion.

Generally, several common factors should be taken into account in the selection of valves for slurry applications, which include the physical and chemical properties of the flow media, the working temperature and pressure, the required type of seal, as well as the cost of the valves. Here the physical properties often refer to the solid composition, solid content and solid grain size whilst the chemical characteristics would decide whether specific requirement should be fulfilled for instance in the corrosive flows (e.g. acids).

There are a variety of valve types commercially available in the market. A detailed discussion on valves for slurry applications can be found in [83]. This section only lists a few typical options which may suit the needs. Since the slurry flow in use is dilute sand-water mixture with fine sand particles, it would be less likely to cause severe erosive damage on the valves in such dilute flow compared with thick slurry. Moreover, there are no special requirements in terms of the working environment. Therefore, in this case, the most important demand is the ability to provide a fairly tight seal or closure at the relevant points in assistance with experimental operations. Otherwise, any small flow leakage from the valve would increase uncertainties in the experimental results.

All valves installed on the slurry flow test rig are manual valves because of the low cost and convenience. Among different types of valves, butterfly or ball valves are typically two common and cost-effective options. Owing to the narrow body, butterfly valves are

often preferred in the applications with limited installation space. The advantage of ball valves is the capability to meet various requirements of flow control by adjusting the geometries correspondingly. However, there might be a risk to damage the disc or seat of a butterfly or ball valve, resulting from the continuous interactions with solids present in flow, although the erosion process is expected to be slow with such dilute slurry. Compared with ball or butterfly valves, pinch valves are less susceptible to be eroded, attributable to the abrasion-resistant characteristics of their elastic rubber sleeve. Therefore, pinch valves are usually beneficial for the cases where completely isolation or nearly 100% tight shut-off of flow is needed. Knife gate valves are especially suitable for handling heavy solid contents, viscous, abrasive as well as corrosive fluids. They can perform well in cutting through the concentrated slurry with heavy solids because of having the sharp metal gates, whereas they are primarily designed for providing on-off services, not recommended for regulating flow.

Based on the above discussions, butterfly and pinch valves are used here for slurry flow test rig construction. Several butterfly valves are utilized to save the spaces because of their dimensional benefit. At the key points to ensure meter calibration and batching operation, a butterfly valve and a pinch valve were installed in series. The idea here is that by taking advantage of employing two different types of valves, it is intended to provide a reliable shut-off as close to 100% as possible.

Two examples are given to illustrate the combination use of butterfly and pinch valves on the test rig, given by Figure 3.5. In order to ensure the same amount of flow transferred from upstream Coriolis flowmeter (CF1) to downstream Coriolis flowmeter (CF2), no flow should be allowed to pass through the by-pass pipe of CF1. As shown below, two valves were installed on the by-pass line, referring to a pinch valve (V2) and a butterfly valve (V3) Similarly, a pinch valve (V8) together with a butterfly valve (V10) are arranged at the point where the flow needs to be fully cut off for the purpose of meters' zero calibration as well as batching. The specifications of all valves on slurry flow test rig are summarized in Appendix 1.

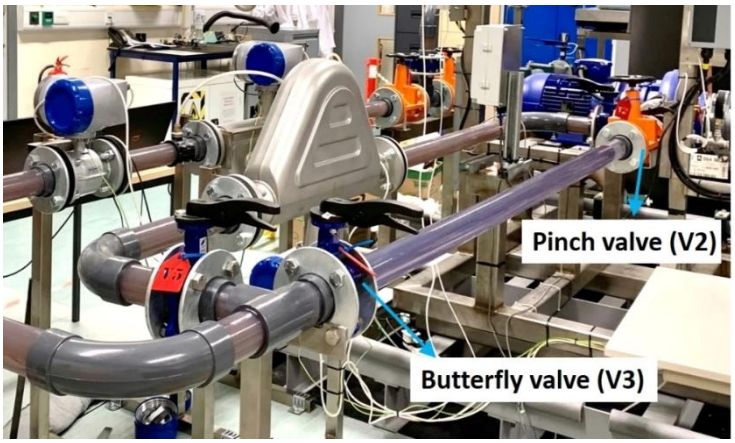

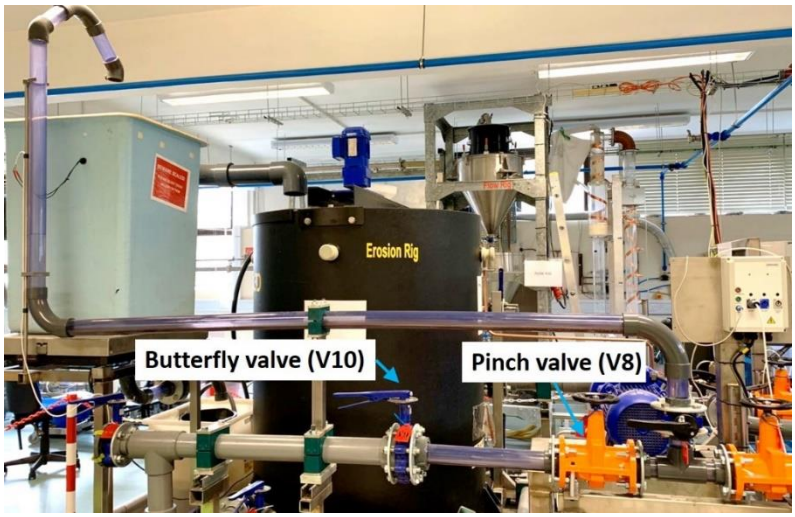

Figure 3.5 Arrangment of a pinch valve along with a butterfly valve

3.3.4 **Flow Sampling Point**

Appropriate flow sampling point needs to be retained for flow sampling. The criteria for the selection of sampling point is that the collected flow samples should be able to represent the slurry passing through the Coriolis flowmeters under test whilst the sampling operation should bring less disturbance to the developed flow conditions.

A 50 mm bore “T” port three-way ball valve (V6) is mounted on the 50 mm test pipe to build up the sampling point, as shown in Figure 3.6. The bore diameter of sampling valve is kept consistent with that of test pipe so as to lower the disruption to the average velocity in test pipe due to the opening of three-way valve. The working position of this three-way ball valve is normally set as “90° diverting” for flow circulation. The position can be changed to “180° straight through” for gathering some slurry sample.

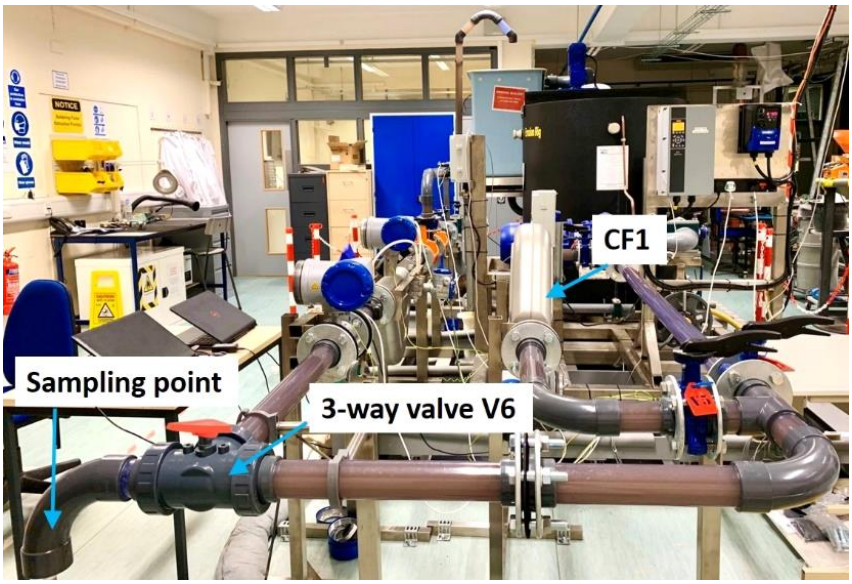

Figure 3.6 Flow sampling point with three-way valve

3.3.5 **Weighing System**

A reliable and high-accurate weighing system plays an important role in assistance with identification of mass flowrate errors. The weighing system should be carefully designed and built so as to lower the uncertainty in flow measurement tests. Here the whole weighing system is assembled by a weighing tank, a weighing scale, a set of batching pipe, a buffer tank along with a small water pump, displayed in Figure 3.7.

Figure 3.7 Setup of whole weighing system

In detail, a weighing scale (Mettler Toledo KCC300) has been served as the reference device for mass flow measurement. The maximum capacity of this scale is 300 kg with the resolution of 2 g, offering the accuracy at 6.67×10^{-6} (better than 0.001%) [84]. Such high accuracy of the scale is 100 times (two orders of magnitude) lower than the claimed measurement accuracy (0.1% for liquids in mass flowrate) of the Coriolis flowmeter under test. Hence it is reasonable to regard the reading of scale as the reference (true values of batch mass). Before any flow measurement tests were carried out, this scale was calibrated in-situ to ensure the reliable functionality. When selecting the scale, proper considerations should be given on both capacity and resolution. The measurement uncertainty of weighing scale should be at least three times lower than the flowmeters under test. Larger capacity of scale can allow a longer duration of batching process, which is favourable to improve the flow stability at a steady flow rate and reduce the batch errors. In the experiments of this work, for example, the batching process can last roughly 40 s when high mass flowrate is at 20000 kg/h. Figure 3.8 displays the weighing tank being seated on the scale.

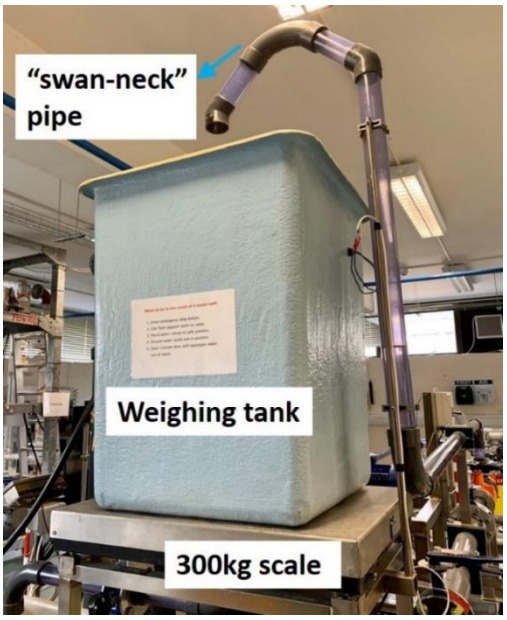

Figure 3.8 Weighing tank seated on the scale

The inlet pipe of the weighing system was designed with a "swan-neck" shape, with the benefit to keep the constant liquid level in the inlet pipe for each batching operation. To reduce the uncertainties in flow measurement results, the pipe has been primed before batching.

With regard to the design of weighing system, two typical designs can be considered, illustrated by Figure 3.9. Design A employs a pump to drain the mixture fluid out of the weighing tank, while design B uses the gravity to discharge the fluid. If the fluid is clean water, both design A and B can work well. However, in the case of sandy water, design B is more suitable. If the pumping method (stated in design A) is applied, the buoyancy of the immersed suction pipe needs to be compensated before the accurate weight of the batch can be obtained. However, this is difficult due to the unknown mixture density over different test conditions. Thus, design B has been chosen in this work.

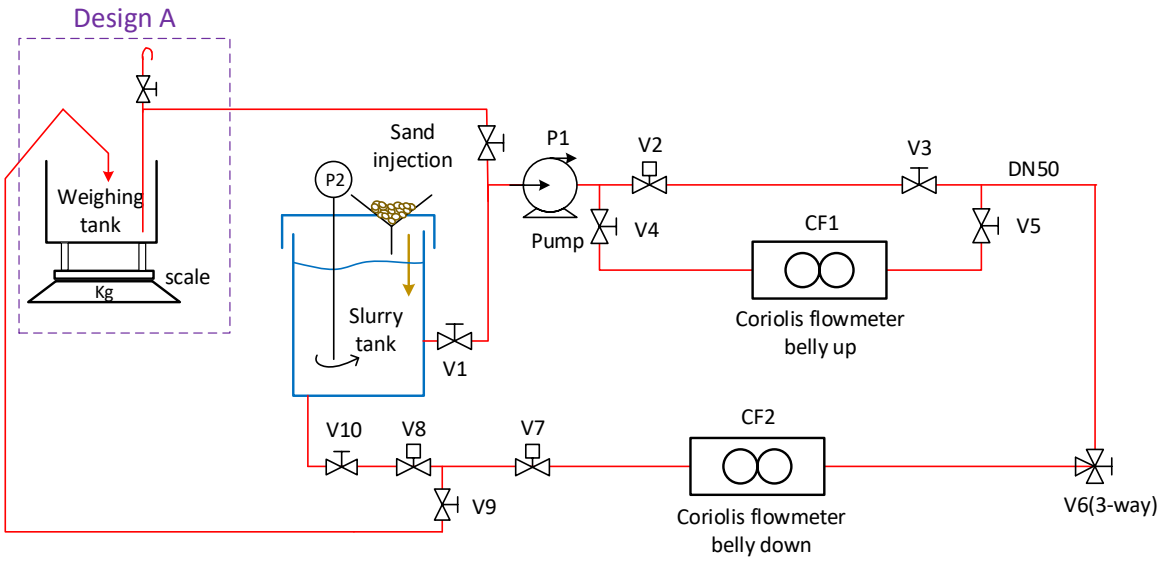

(a) Design A, pumping method

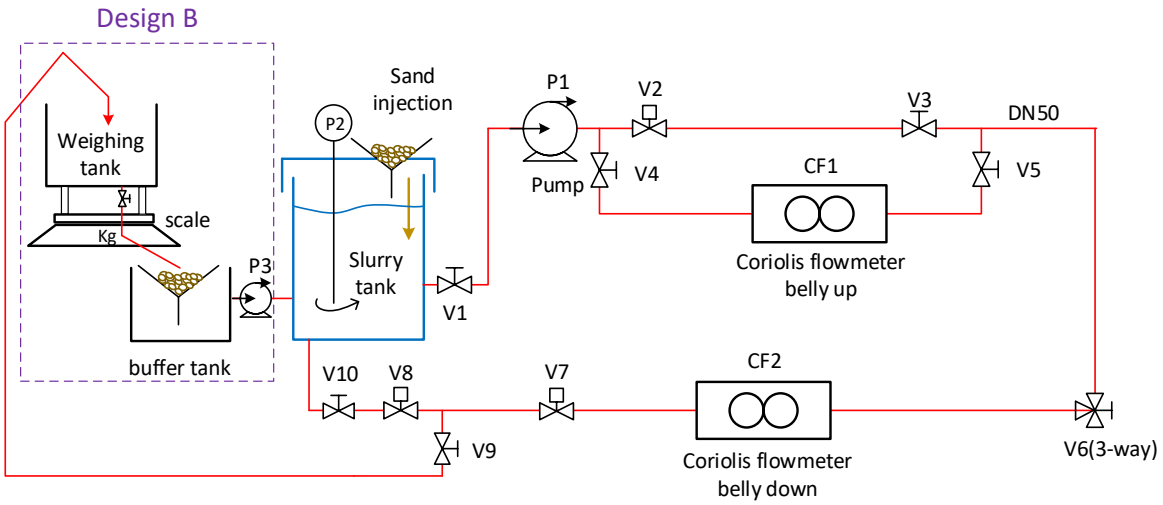

(b) Design B, gravity method

Figure 3.9 Two typical designs of weighing system

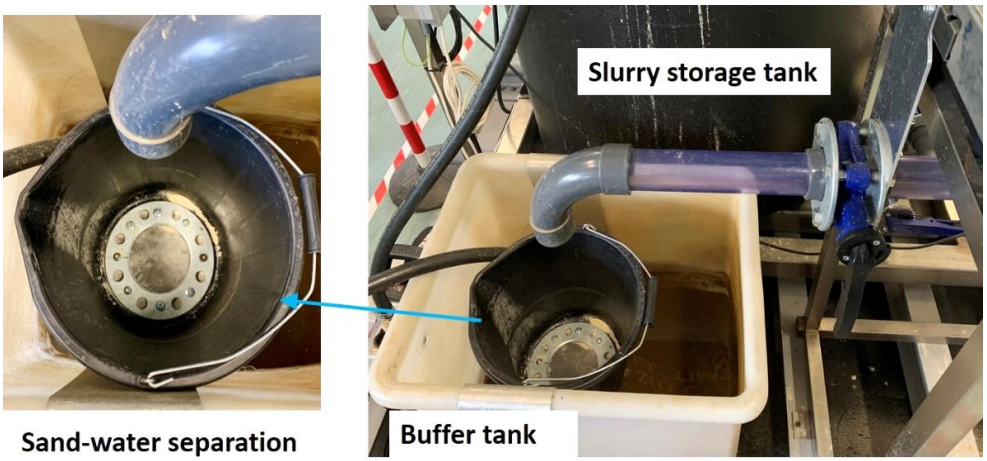

Figure 3.10 Sand-water separation inside buffer tank

Furthermore, since this small pump can only deliver the water without heavy solid contents, a simple sand-water separation facility is employed to assist with the transportation of fluid from buffer tank back to big slurry storage tank, as shown in Figure 3.10. The separation facility is made of a bucket with the sand mesh in 75 μm sieve openings being fitted on the bottom. After separation, that part of sand is fed back to the large slurry tank again.

To summarize, with the assistance of weighing system, the sand-water mixture undergoing batching can be carried into the weighing tank through a "swan-neck" pipe, and then drained to the buffer tank, and finally pumped back to the slurry tank, to complete the whole batching process. Through the correct operations on relevant valves (V7 to V10), the slurry flow can either be pumped directly back to the slurry tank for horizontal flow circulation or into the weighing tank for batching.

3.3.6 **Installation of Flowmeters**

To measure the sand-water mixture flow, two 50 mm bore Coriolis flowmeters have been mounted horizontally in series but with different mounting orientation. The Coriolis flowmeters under test (KROHNE OPTIMASS 6400 S50) are designed with a twin-bent tube configuration, of which nominal flowrate is 35000 kg/h. For single-phase liquid measurement, the measurement uncertainty of mass flowrate is within ±0.1% covering the turndown ratio in the range of 20:1, whilst the measurement uncertainty of density is less than ±1 kg/m^3 [85]. The upstream Coriolis flowmeter is mounted with its measuring tubes (belly) up, named as CF1, while the belly of downstream flowmeter (CF2) is placed downwards, illustrated by Figure 3.11. For entrained solids applications, it is generally

recommended to install a bent-tube Coriolis flowmeter with its belly up in order to prevent solids from settling in the Coriolis tubes. However, no prior research has been carried out for the experimental investigation into the mounting effect on Coriolis flow metering in slurry applications. Hence in this study, two different horizontal mounting orientation, belly up and belly down, are both employed to check whether the mounting of Coriolis flowmeters would affect their behaviours in dilute and non-settling slurry flow, which means there is no sand deposition in the Coriolis tubes.

Additionally, a bypass line was installed which can protect the upstream Coriolis flowmeter (CF1) from erosion when necessary. Both CF1 and CF2 can be tested through batching operation for examining the mass flowrate errors, while flow sampling can only be conducted against the density measurement in CF1. Since CF2 is installed downstream of sampling point, the CF2 density reading is not comparable with flow sampling test results.

(a) (b)

Figure 3.11 Two Coriolis flowmeters under test (a) Upstream Coriolis flowmeter with its belly up, CF1 (b) Downstream Coriolis flowmeter with its belly down, CF2

To deliver the ideal performance, Coriolis flowmeters should be properly installed to meet the requirements as specified by the manufacturer. Sufficiently long pipe length needs to be maintained to help sand-water mixture reaching equilibrium state before entering the Coriolis flowmeter. In terms of upstream straight pipe, approximately 20 *D* (*D* referring to pipe bore diameter, 50 mm) pipe length is kept on test rig, whilst the length of downstream pipe is retained over 6 *D*, both exceeding the required lengths as stated in the user guidance

[85]. Moreover, both meters are well fixed via the rigid frame being bolted on ground against the vibrations from external environment. Although most modern types of Coriolis flowmeters are claimed being capable of tolerating a certain level of external vibrations, this work has found that rigid support is favourable to decrease the potential negative influence from external vibrations on Coriolis flow metering such as zero-drift in meters or degradation of measurement accuracy.

In the loop where CF1 and CF2 are mounted in series, the achievable maximum mass flowrate is up to approximately 28000 kg/h, covering 80% nominal flowrate of the Coriolis flowmeters under test. The drop in the discharge rate of centrifugal pump can be attributable to the pressure loss induced by the Coriolis flowmeters.

3.3.7 **Safety Precautions**

Concerning the safety issues, several precautions have been prepared to manage the potential hazards and risks probably arising from equipment failure, improper or incorrect manual operation, as well as emergencies. Figure 3.12 demonstrates the safety precautions taken in place, including a pressure relief valve, an emergency stop, and an overflow pipe along with a level switch.

A pressure relief valve can rapidly release pressure to avoid over-pressure beyond the safety threshold. Here a pressure relief valve was installed downstream of the main pump, in case of pipe plugging, incorrect closure of valves, or equipment failure. Emergency stop can immediately cut off all electrical contacts once being activated so as to cease or lower the potential or existing hazards to operators, equipment or any work in progress. A level switch along with an overflow pipe are both measures to prevent overflow from the weighing tank which may occur during batching operation. Overflow can be highly dangerous since the water spills may cause electric shock and short circuit. The function of a level switch is to detect the liquid level within the weighing tank. The level switch can be regarded as a type of liquid level sensor, which is connected with the centrifugal pump. If the liquid level in the tank exceeds the mounting position of the level switch, the power supply of pump will be shut down and batching will be suspended. Furthermore, a 4-inch overflow pipe was mounted to efficiently drain the excess liquid from weighing tank in case that the level switch fails to function although extremely unlikely, served as a double security.

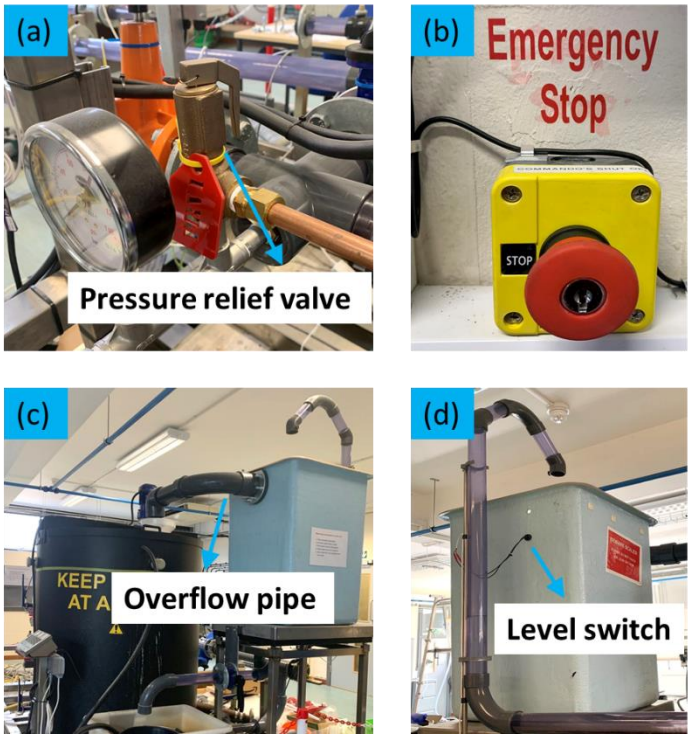

Figure 3.12 Safety precautions

3.4 Data Acquisition

In this research, Coriolis flowmeters under test are operated under two different working modes. One is the normal working mode, under which Coriolis flowmeters are driven at the first vibrating mode by one single drive frequency (resonant frequency). The other is meter diagnostic mode, which offers the information of structural conditions of Coriolis flowmeters with two additional frequencies added into the drive signal (apart from one resonant frequency). Throughout the flow measurement tests (Chapter 4), Coriolis flowmeters under test are set in the normal working mode and flow measurement related data are logged for experimental evaluation of the measurement accuracy of the flowmeters. For collecting the structural condition related data, the meters under test worked in the diagnostic mode during erosive tests (Chapter 4). Normal flow measurement provided by Coriolis flowmeters is not disturbed by the meter diagnostics. Under the diagnostic mode, the structural condition related data are collected whilst the normal flow measurement data are also available.

The data acquisition from Coriolis flowmeters is performed through the tool developed by the R&D department of KROHNE Ltd based on Modbus protocol (see Figure 3.13). The user interface of the flow measurement data logging software (called “xFC Data Logger”)

is shown in Figure 3.14. During data logging of flow measurement data, the host PC requests data from the Coriolis flowmeters every 10.24 ms and the raw data is stored if available from the Coriolis meters. Such data acquisition rate is high enough to meet the needs for data analysis in consideration of varying two-phase flow conditions.

Figure 3.13 Data acquistion tool

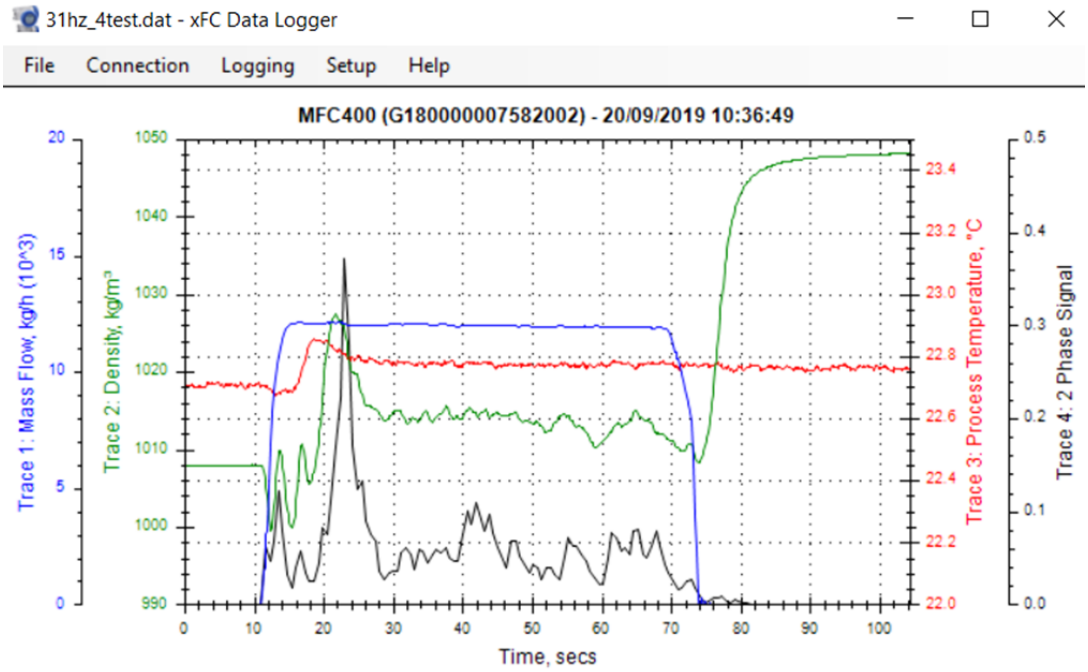

Figure 3.14 User interface when logging flow measurement data

Table 3.1 lists the raw flow measurement data obtained from the Coriolis flowmeters, including apparent mass flowrate, density, drive frequency, fluid temperature, sensor A &

B level, drive level, together with 2-phase signal. The raw data points are stored for further analysis and the details of data post-processing will be presented in Section 4.3.5.

Table 3.1 Raw flow measurement data obtained from the Coriolis flowmeters under test

Term	Symbol (unit)	Description
Apparent mass flowrate	$\dot{m}_{m,app}$	Mixture mass flowrate reading in Coriolis flowmeters
Apparent density	$\rho_{m,app}$	Mixture flow density reading in Coriolis flowmeters
Drive frequency	f_r (Hz)	It refers to the working frequency of Coriolis oscillation system, acquired by tracking the resonance frequency.
Normalized sensor level	S_A, S_B (%)	Sensor level displays the voltage amplitude of sensor signal, being normalized to percentage with respect to the maximum voltage. When the flow direction is forward, the sensor located on outlet side is sensor A.
Normalized drive level	I_{dr}(%)	It provides the current amplitude of input signal allocated into driver, being normalized on maximum current.
Fluid temperature	T_f (°C)	It is measured by a PT500 temperature sensor being attached to one of the tubes. In most cases tube temperature can be assumed equal to process or fluid temperature, which can be applied for temperature compensation on Coriolis flow metering.
2-phase signal	P_{2P}	It is a dimensionless parameter, calculated from the phase variance multiplied by damping indicator (the ratio of drive current to sensor voltage, P_d). Phase variance usually arises from density variation. It is helpful for reporting the presence of a second phase in flow being metered.

Through OPD (Online Parameter Determination) function developed by the R&D department of KROHNE Ltd, Coriolis flowmeters can work at a diagnostic mode and structural condition related data are acquired. A logging software ("MFC400 Condition Monitor Data Logger") is utilized for collecting condition related data from Coriolis flowmeters under test. Raw data are recorded at an interval of 60 s and the logging duration is set as 10 s. Then the time-averaged value of a logging duration of 10 s is stored as the processed data for further analysis. When OPD function is performed, signal processing in Coriolis flowmeters is more complex than normal signal processing of flow measurement, which requires relatively longer time to supply data. Since the condition data is used for indicating the structural health of Coriolis tubes, the data update rate is not a primary consideration, whereas the high accuracy and reliability of data are more beneficial. The relevant contents of structural condition monitoring will be described in detail in Chapter 5.

3.5 Operating Procedures

This section firstly describes the initial examination of the functionality of the slurry flow test rig, before conducting the experimental work. Then the section demonstrates how to perform batching operation as well as flow sampling in detail. The erosive tests can be carried out through the horizontal circulation loop, which is quite simple and straightforward, and hence the operation is not presented.

3.5.1 **Initial Examination of Coriolis Flowmeters and Test Rig**

The purpose of an initial examination of the test rig is to inspect the joints of pipe sections as well as pipe fittings for checking any potential liquid leakage and determine the achievable test matrix. Furthermore, an in-situ calibration of the Coriolis flowmeters under test has been conducted, so as to verify the measurement uncertainty of the Coriolis flowmeters with respect to the reference device.

At the very beginning, the slurry tank was filled up with clean tap water, without any sand fed into the liquid. The purpose of the initial verification of the Coriolis flowmeters is to recognize the measurement uncertainties of CF1 and CF2 under single-phase conditions (clean water), before any tests conducted with slurry flow. Additionally, samples of tap water being used in the experiments are collected and measured in laboratory, for the purpose of determination of actual water density for reference. Then the value of actual

water density is given to CF1 and CF2 for in-situ density calibration. The initial density reading of water in CF1 is set equally to that in CF2, to ensure no difference in their density readings between these two meters under the single-phase condition.

Through batching operation, the relative errors in mass flowrate from CF1 (belly up) and CF2 (belly down) are calculated with respect to the reference from weighing scale. The initial verification is carried out at five flowrates, with three repeats at each flowrate. Figure 3.15 below displays the initial verification results with clean water. Both meters met the manufacturer's specification regarding mass flowrate measurement, within ±0.1%.

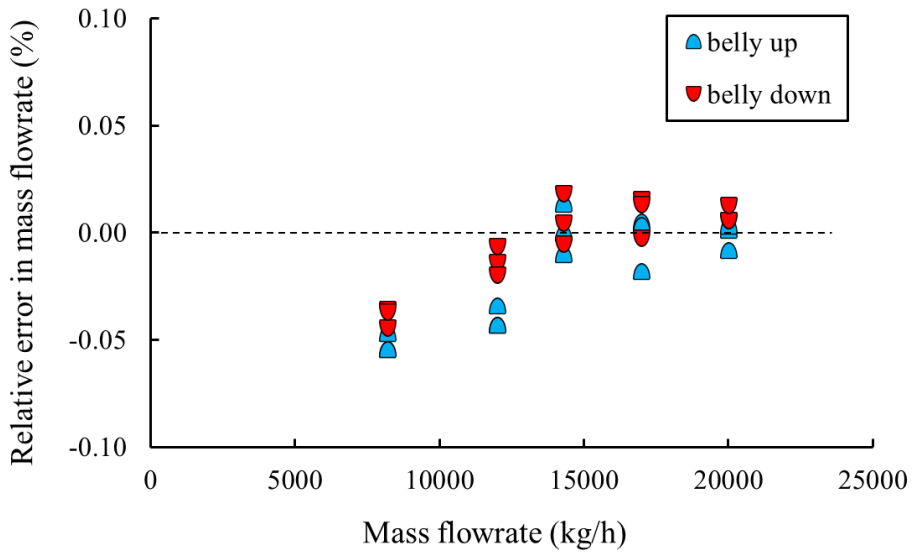

Figure 3.15 Initial verification of mass flowrate measurement with clean water

After the initial run with clean water, sand particles were gradually injected into the slurry tank for determination of the achievable test matrix in terms of mass flowrate and sand concentration. In order to ensure homogenous slurry flow regime or at least non-settling slurry flow, allowable range of sand concentration are identified against the delivered mass flowrate. The test matrix will be given in Section 4.4.2. It should be noted that special attention should be paid to the vertical part of inlet batching pipe to guarantee the transportation of sand particles into the weighing tank by the carrier liquid, in consideration of the counter gravity effect on the sand particles in vertical flow.

3.5.2 **Operating Procedures of Flow Batching**

Generally, the mass flowrate is well-controlled via the variable-speed centrifugal pump whilst the sand concentration can be changed by adjusting the agitator and sand dosing. Since all valves in use are manual valves, the experiments are primarily conducted by manual operations. Automatic operations or control on the pump, valves as well as data logging can be achieved by upgrading this test rig in the future. The detailed operating procedures of batching are given,

1) **Preparing** - Operate on the control panel to start the centrifugal pump (P1) as well as the agitator (P2). Run the slurry flow at target mass flowrate in circulation loop for a while (e.g. three minutes), so as to expel the potential bubbles and stabilize the process conditions (e.g. flow profile, the distribution of fluid temperature). Corresponding operations on valves are as follows: open V1, V4, V5, V7, V8, V10 and V13, while all other switch valves are closed. "T" port three-way valve V6 works as a 90° diverting valve.
2) **Resetting totalizer in Coriolis flowmeters and weighing scale** - Reduce the mass flowrate to the low value (e.g. 5000 kg/h). Shut down V10 and V8, while leave the centrifugal pump running for a short while. Meanwhile, check whether the zero-calibration point of Coriolis flowmeters (CF1, CF2) drift, by comparing with the historical value. If no drift, reset the weighing scale and "totalizer" function on Coriolis flowmeters to zero. If the zero-calibration point drifts (beyond the acceptable range), return to step 1) and repeat the operation.
3) **Starting data logging and batching** - Start logging data from Coriolis flowmeters. Increase the mass flowrate to target value, and then open V9.
4) **Weighing batch and completing data logging** - Observe the reading of batch from the weighing scale. When the reading approaches 220 kg, shut down V9 firstly, subsequently stop the centrifugal pump. Save the data of Coriolis flowmeters during batching and record the reference weight from the scale when the reading becomes stable.
5) **Emptying weighing tank** - Finally, open the valve (V16) beneath the weighing tank, to drain the sandy water out from the weighing tank into the buffer tank. When the sand-water mixture enters the buffer tank, the sand separation can be carried out with the help of the sand mesh in 75 μm sieve openings. After filtration, the gathered sand

on mesh should be injected back to slurry storage tank whilst water is pumped back to the slurry storage tank through hose.

Experimental work has found that although the valves are in closed positions to assist with meters' zero calibration, the running time of the centrifugal pump in step 3) could affect the delivered sand concentration. It is probably because with the longer running time more sand particles would be trapped into the pump chamber. Once the discharge valve is open, these sand particles could be pumped into the fluid stream. Therefore, the pump running time is suggested to be fixed for each test point, to lower the uncertainty in experimental tests.

3.5.3 **Operating Procedures of Flow Sampling**

The operation procedure of sampling is presented below:

1) **Preparing** - Circulate slurry flow at target mass flowrate for a while. The detailed operation can be found in the step 1) in flow batching operation as described above.
2) **Starting data logging and flow sampling** - Change the working position of the three-way valve (V6) from "90° diverting" to "180° straight through", to run off the test slurry from the sampling point to a 40 litres bucket. As soon as V6 is turned to "180° straight through", start data logging from CF1.
3) **Completing data logging and flow sampling** - When the fluid level approaches the set line on the bucket (25 litres), operate V6 back to "90° diverting" position for slurry circulation. Meanwhile, stop data logging from CF1.
4) **Weighing collected sample** - Weigh the fluid sample on a small scale (maximum 50 kg, with resolution 1 g). The total weight of sand-water mixture sample can be recorded as $m_{m,S}$.
5) **Separating sand particles and drying sand** - Subsequently sand particles can be separated from the fluid sample on extremely fine sand mesh with 25 μm sieve openings, shown in Figure 3.16. After separation, the sand particles can be dried by a heating oven (see Figure 3.17). Then the dried sand particles are weighed as $m_{s,S}$.
6) **Computing sand-water mixture density and sand volume fraction** - The reference sand weight fraction ($\beta_{s,R}$) can be acquired by using $m_{s,S}$ over $m_{m,S}$. With known sand density along with water density, reference sand weight fraction ($\beta_{s,R}$) can be further

converted into sand-water mixture density as reference ($\rho_{m,R}$), as well as reference sand volume fraction ($\alpha_{s,R}$).

As stated in step 6), the relevant computations of reference values are expressed,

$$\beta_{s,R} = \frac{m_{s,S}}{m_{m,S}}\ 100\% \tag{3-1}$$

$$\rho_{m,R} = \frac{1}{\frac{\beta_{s,R}}{\rho_s} + \frac{1-\beta_{s,R}}{\rho_w}} \tag{3-2}$$

$$\alpha_{s,R} = \frac{\rho_{m,R}-\rho_w}{\rho_s-\rho_w}\ 100\% \tag{3-3}$$

where ρ_s denotes the "actual sand density" and ρ_w is water density. The relevant calculation of ρ_s and ρ_w in this study will be given in Chapter 4.

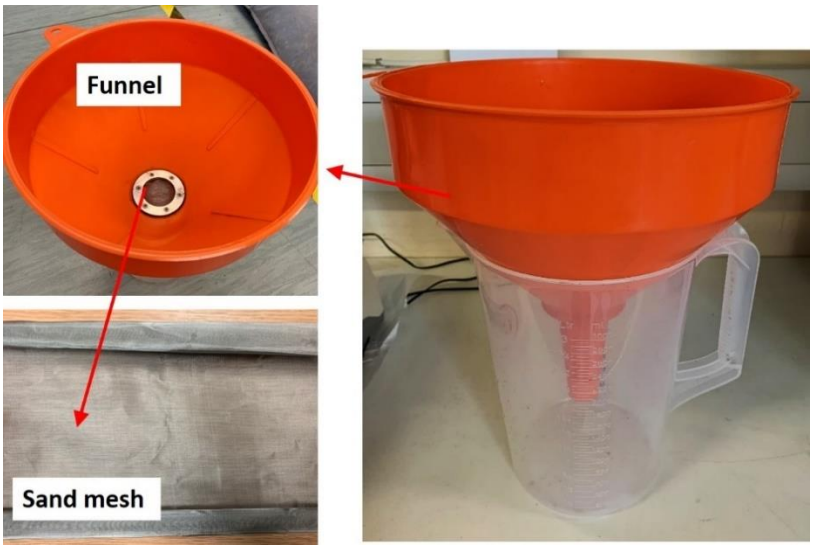

Figure 3.16 Separation of sand particles from the colletced fluid sample

Figure 3.17 Heating oven to dry wet sand

3.6 Advantages and Limitations

In light of the practical experience in rig design, construction as well as operation, the advantages of this slurry flow test rig are summarized as follows,

1) Overall, this slurry flow test rig is relatively simple to construct and easy to operate. The main benefit is that the rig can cover two different functions for performing flow measurement and erosive tests.
2) Transparent PVC pipe has been found as a satisfactory choice, attributable to the advantages from its durable, impact-resistant properties as well as the capability of offering clear observation of flow regime.
3) The characteristics of slurry flow transportation should be taken into account when the flowmeters are installed for slurry flow metering. For example, as illustrated in this work, if a bent-tube Coriolis flowmeter is horizontally mounted on the pipe, it is recommended to place its measuring tube (belly) upwards, preventing from the settlement of heavier sand or even blockage in tube.
4) Valves need to be carefully selected in consideration of the potential erosion. This work provides a good example to make use of two valves from different types at the key points where the fairly tight closure is required and the flow leakage arising from valve erosion is not acceptable.

5) In terms of design of weighing system, the gravity method is more suitable than the pumping method to lower the uncertainty in experimental tests, as illustrated in Figure 3.9.
6) Appropriate safety precautions are suggested to be held in place in cases of equipment failure, emergencies, improper or incorrect manual operation, as demonstrated in Section 3.3.7.

In the meantime, the limitations of this slurry flow test rig are pointed out,

1) The main shortcoming is the difficulty in controlling the delivered sand concentration. There are two possible causes. The first reason is that it is difficult to fully mix the sand-water mixtures in the large slurry tank. The second problem is the lack of an appropriate sand dosing system by which the sand particles can be continuously injected into the fluid stream at a desired flowrate.

The performance of the current agitator in use may not function quite well for supplying fairly uniform and well-mixed slurry flow, probably attributable to the relatively small size of stirrer propeller compared with the capacity of large tank, as well as the limited length of the rotating shaft resulting in some distance to reach the very bottom layer of sand.

In the study of gas-liquid flow metering, it is common to see the separate transportation of pure gas and pure liquid flow before mixing together, and beneficially it allows to apply the accurate reference system for the single-phase flow metering as well as the control of the portions of the two phases. Nevertheless, the separate transportation of solid and liquid cannot be implemented in this case due to the fact that solid materials cannot flow like liquid or gas. The transportation of solids is typically performed by a hydraulic or pneumatic system. However, additional introduction of gas must be avoided since the presence of gas is a leading error source in Coriolis flow metering. The same problem exists when a vibrating sand feeder is utilized. Therefore, the pneumatic conveying of solids is not applicable for this case, which brings the challenge to source a proper sand dosing system.

2) The sand degradation has been found in the experiments, likely attributable to two reasons. The dominant reason could be the centrifugal pump may grind the sand particles into smaller segments or more spherical shape, whilst the flow recirculation would also give rise to sand degradation.

3.7 Summary

A cost-effective and easily operable 50 mm bore slurry flow test rig has been designed and built for undertaking experimental investigation in this research. This chapter mainly describes the design and construction of the slurry flow test rig, with the particular emphasis on providing accurate references to the Coriolis flowmeters under test.

Detailed descriptions of the slurry flow test rig along with the operating procedures have been presented. Practical considerations as well as experience in the rig design and construction have been provided. The advantages and limitations of this slurry flow test rig have been briefly discussed, which can offer practically useful information to future improvements in rig design and construction.

Flow measurement tests and erosive tests have been conducted on the test rig with dilute sand-water slurry flow. Through a series of flow measurement tests, the influence of entrained solid particles on Coriolis flow metering is evaluated quantitatively and the experimental results are given in Chapter 4. Through erosive tests, the wear problem of Coriolis flowmeters is investigated and the performance of the condition monitoring technique for examining the structural health of Coriolis tubes is assessed in Chapter 5.

Chapter 4

Mass Flow Measurement of Dilute Slurry Using Coriolis Flowmeters

4.1 Introduction

This chapter mainly describes a novel methodology for slurry flow measurement using Coriolis flowmeters incorporating a semi-empirical analytical model, concerning the degradation of measurement accuracy of Coriolis flowmeters owing to the presence of solid particles in the liquid.

Firstly, this chapter presents a theoretical analysis of the influence of the entrained solids on Coriolis flow metering, in light of existing theory of decoupling effect and compressibility effect. The theoretical analysis provides the fundamentals of an analytical modelling approach for predicting and further correcting the measurement errors of Coriolis flowmeters under solid-liquid two-phase flow conditions. Then, the chapter describes the experimental work conducted on the slurry flow test rig for examining the measurement errors of Coriolis flowmeters handling dilute sand-water slurry flow. A series of flow measurement tests were carried out with five different mass flowrates and SVF (solid volume fraction) ranging from 0 to 4% whilst two Coriolis flowmeters under test were horizontally installed with two different orientations (belly up and belly down). Thirdly, the chapter presents the experimental results, providing the original measurement errors of the Coriolis flowmeters under test as well as the basic regression analysis of the original errors. Lastly, a basic analytical model is derived from the existing decoupling theory and then utilized for compensating the decoupling effect on Coriolis flow metering. The outcomes from model prediction are compared with the actual experimental results so as to evaluate the performance of the model. Moreover, in order to lower the differences between modelling outcomes and experimental results, a correction term is introduced into the basic analytical model for yielding better prediction. After correction, a semi-empirical analytical model is established which can extend the application of Coriolis flow metering technology from single-phase flow to slurry flow.

4.2 Theoretical Analysis

In this section, the existing theory reporting the underlying physics causing measurement errors of Coriolis flowmeters under two-phase flow conditions is applied into the case of solid-liquid flow. Theoretical investigation into the impact of entrained solids not only illustrates the physical mechanisms leading to measurement errors of Coriolis flowmeters with slurry flow but also explains the theoretical basis of analytical modelling for error prediction and compensation in Coriolis flowmeters.

Prior research work has revealed the typical causes of measurement errors of Coriolis flowmeters due to the interactions between two phases [31], [57], [58], [63], [69], [86]. Two major error sources are phase decoupling error and compressibility error [58]. In order to demonstrate decoupling error as well as compressibility error, two typical examples of two-phase cases are used, representing solid-liquid and gas-liquid two-phase conditions respectively. Although this work focuses on slurry flow, it is beneficial to put these two cases together for a comparison, which can give a better understanding of the underlying physics resulting in measurement errors of Coriolis flowmeters for two-phase flow metering. Furthermore, other error sources (asymmetry and imbalance error) which may bring additional measurement errors, are also briefly discussed at a qualitative level.

4.2.1 **Phase Decoupling Error**

4.2.1.1 **Overview**

As stated in Section 2.3.7, a Coriolis flowmeter offers mass flow measurement based on the resulting inertia force from the interactions between the moving fluid and its conveying tube. Accurate Coriolis flow metering is based on a fundamental assumption, that the centre of the vibrating mass in the Coriolis oscillation system is fixed on the axial direction of the conveying tube [58]. However, when there is a second phase, the centre of mass is likely disturbed by the relative motions between two different phases. As a result, errors arise in mass flowrate along with density measurement.

The term, phase decoupling, describes the phenomenon when Coriolis flowmeters handle two-phase flows, the second phase (e.g. solid particles or gas bubbles entrained in liquid) cannot exactly follow the Coriolis oscillation. For two-phase mixed flow, the differences in phase density result in different accelerations along the Coriolis oscillation direction, and

consequently the induced vibration amplitudes of two phases become different. As a result, the phase decoupling effect would cause some part of the mass or inertia not sensed by the Coriolis measuring tubes, and thereby lead to the under-estimation of mixture mass flowrate as well as mixture density.

In the case of slurry flow, since the solid phase is typically heavier than the liquid, the solids would experience less acceleration and move less distance in the Coriolis oscillation direction. Accordingly, less part of solid particles can be sensed by Coriolis tubes, whereas, more liquid portion can be "felt". In other words, the phase decoupling effect would cause an under-reading of the dense phase (solid phase here) but an over-reading of the light phase (liquid phase). Overall, Coriolis flowmeters would provide an under-reading of the mixture mass flowrate.

4.2.1.2 **Decoupling Effect in Inviscid Fluid**

This theoretical analysis starts with the decoupling effect in inviscid fluid and particles. Assumptions are stated as follows to simplify the computation [69]:

The fluid and entrained particles are both assumed to be incompressible. The entrained solid particles or gas bubbles are spherical in shape and uniformly distributed along the tube. In addition, the tube is excited in a sinusoidal wave whilst it is sufficiently spacious to accommodate the motions of the spheres, meaning the spheres can move freely within the tube. Moreover, the spheres are assumed to experience rectilinear motion along the Coriolis oscillation direction and no contacts with neither the adjacent spheres nor the tube wall.

First of all, basic terms for analytical modelling are defined. The movements of the tube (X_t) and entrained spheres (X_s) are expressed below,

$$X_t = U_t \ sin(\omega_r t) \tag{4-1}$$

$$X_s = U_s \ sin(\omega_r t + \theta) \tag{4-2}$$

where the subscript "s" denotes entrained spheres which can be solid particles or gas bubbles, the subscript "t" refers to the Coriolis tube, U is the vibration amplitude, ω_r is angular frequency of Coriolis oscillation, t is time and θ is the phase shift of the entrained spheres.

To quantify phase decoupling effect, the ratio of the vibration amplitude of the entrained sphere (U_s) to that of tube (U_t) is expressed below, called as decoupling ratio (F),

$$F = \frac{U_s}{U_t} \tag{4-3}$$

The velocities (u) can be obtained from the derivative of displacement expressions,

$$u_t = \omega_r \, U_t \, cos(\omega_r t) \tag{4-4}$$

$$u_s = \omega_r \, U_s \, cos(\omega_r t + \theta) \tag{4-5}$$

Then, based on the above assumptions, force analysis can be applied to solve the motions of the tube as well as the entrained particles. In the scenario of inviscid fluid and particle, there are two force terms acted on the particles, including buoyancy-like force and added mass force [31], [69], [86].

$$F_T = F_B + F_A \tag{4-6}$$

$$F_A = -m_I \, \frac{d(u_s - u_t)}{dt} \tag{4-7}$$

$$m_I = \frac{V_s}{2} \, \rho_s \tag{4-8}$$

$$F_B = \rho_l \, V_s \, \frac{du_t}{dt} \tag{4-9}$$

$$F_T = \rho_s \, V_s \, \frac{du_s}{dt} \tag{4-10}$$

where F_T means the total force, F_B denotes the buoyancy-like force, F_A is the added mass force, m_I is the induced mass related to F_A; the subscript "s" denotes the entrained sphere again, the subscript "t" refers to the Coriolis tube; m is mass, ρ is density, u refers to the absolute velocities, and V_s denotes the volume of an entrained sphere.

The buoyancy-like force (F_B) arises from the pressure difference induced by the acceleration of the surrounding liquid. Driven by the Coriolis oscillation, when a solid particle enters the tube, the solid particle would experience less acceleration than the liquid since solids are typically heavier. For example, if the tube is driven upwards, the solid particles would move downwards with respect of the liquid, which is similar to the fall of solid particles under the effect of gravity.

When the entrained object constantly pushes the surrounding liquid away, the added mass force (F_A) is generated from the substituted liquid, which tends to impede the relative motions. The induced mass (m_I) is dependent on the shape of the entrained object. In the situation of a spherical shape, the induced mass can be regarded as half of the mass of the substituted liquid as illustrated in equation (4-8).

By combining the force terms together, equation (4-6) becomes,

$$\rho_s V_s \frac{du_s}{dt} = -\frac{V_s}{2} \rho_s \frac{d(u_s-u_t)}{dt} + \rho_l V_s \frac{du_t}{dt} \tag{4-11}$$

Finally, the velocities of entrained spheres and Coriolis tubes are solved,

$$\frac{u_s}{u_t} = \frac{3\rho_l}{\rho_l+2\rho_s} \tag{4-12}$$

The decoupling ratio (F) can be written as,

$$F = \frac{3\rho_l}{\rho_l+2\rho_s} \tag{4-13}$$

It is clear that when $\rho_s < \rho_l$ (gas-liquid two-phase flow), $F > 1$; while $\rho_s > \rho_l$ (solid-liquid two-phase flow), $F < 1$. To visualize the phase decoupling effect, two examples are given by using scenarios of solid-liquid and gas-liquid mixtures. Solid phase is commonly heavier than liquid phase while gas is lighter, which makes the opposite contribution to the relative motions between two phases.

In the case of solid-liquid mixtures, water density is set as 998 kg/m^3 whilst 2680 kg/m^3 is used as solid density which is the measured sand density obtained from the tests in this work (see Section 4.3.2.2). According to equation (4-13), the decoupling ratio (F) equals to 0.47. As shown in Figure 4.1, the black dashed line is tracing the motion of a Coriolis tube whilst the blue dash-dot line depicts the motion of a solid particle. As solid is denser than liquid, the solid object experiences less acceleration as shown in the blue dash-dot line. The decoupling phenomenon can be illustrated by the slightly lower amplitude of trace of centre-of-mass location (red solid line), compared with the trace of a Coriolis vibrating tube (black dashed line). It can be observed that the centre of mass travels less, which would result in under-reading in mass flowrate and density of the mixed flow.

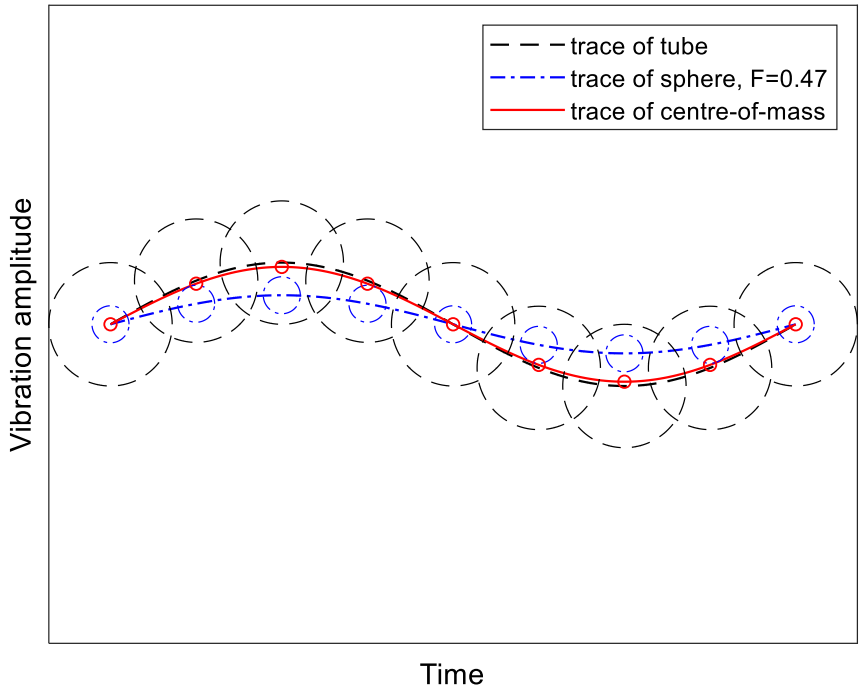

Figure 4.1 Decoupling effect under solid-liquid two-phase conditions

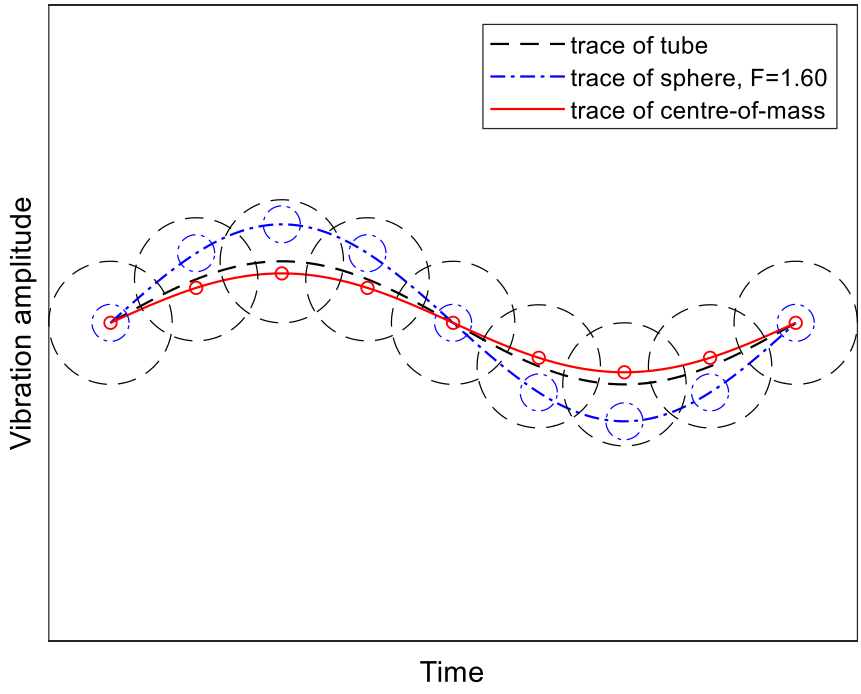

Figure 4.2 Decoupling effect under gas-liquid two-phase conditions

Figure 4.2 displays the decoupling effect in gas-liquid mixtures, where F is 1.60. In contrast to solid-liquid flow, if the entrained object (e.g. gas bubbles) is lighter than liquid, the gas bubbles can move farther than the surrounding liquid (see the blue dash-dot line). As a result, a negative decoupling error can be produced, indicated by the lower amplitude of trace of centre-of-mass (red solid line) compared with that of tube (black dashed line).

To conclude, due to phase decoupling effect, Coriolis flowmeters tend to over-read the light phase but under-read the heavy phase. Overall, under-estimation of the mixture mass flowrate along with mixture density can occur. Therefore, decoupling effect always lead to negative measurement errors of Coriolis flowmeters, under both solid-liquid and gas-liquid two-phase conditions.

4.2.1.3 **Decoupling Effect on Coriolis Flow Metering**

Without decoupled motions between different phases, the actual (correct) mass flowing through the Coriolis flowmeters should be,

$$m_a = \rho_l \, A_t \, (1 - \alpha_s) + \rho_s \, A_t \, \alpha_s \tag{4-14}$$

Attributable to decupling effect, the apparent (observed) mass "felt" by Coriolis flowmeters can be expressed as,

$$m_d = \rho_l \, A_t \, (1 - F \, \alpha_s) + \rho_s \, A_t \, F \, \alpha_s \tag{4-15}$$

where m_a denotes the actual mass as reference, m_d refers to the apparent mass reading due to decoupling effect; α_s denotes the volume fraction of entrained spheres, A_t is the cross-sectional area of the Coriolis tube.

The decoupling error in mass flowrate ($E_{d,\dot{m}}$) is calculated by,

$$E_{d,\,\dot{m}} = \frac{m_d - m_a}{m_a} \, 100\% \tag{4-16}$$

By combining equations (4-14) to (4-16) together, decoupling error can be written as,

$$E_{d,\,\dot{m}} = \frac{\rho_l \, \alpha_s \, (1-F) + \rho_s \, \alpha_s \, (F-1)}{\rho_l \, (1-\alpha_s) + \rho_s \, \alpha_s} = \frac{(\rho_s - \rho_l) \, \alpha_s \, (F-1)}{\rho_l \, (1-\alpha_s) + \rho_s \, \alpha_s} \, 100\% \tag{4-17}$$

By substituting F given by equation (4-13) into (4-17), decoupling error becomes,

$$E_{d,\dot{m}} = \frac{-2(\rho_s-\rho_l)^2\,\alpha_s}{[\rho_l\,(1-\alpha_s)+\rho_s\,\alpha_s]\,(\rho_l+2\rho_s)}\,100\% \tag{4-18}$$

It can be seen that decoupling error is a function of SVF (solid volume fraction) as well as solid density. Additionally, equation (4-18) mathematically proves that decoupling error is a negative error term. Moreover, the decoupling error in density ($E_{d,\rho}$) is supposed to equal to the error in mass flowrate ($E_{d,\dot{m}}$), not repeated again. These two error terms ($E_{d,\dot{m}}$, $E_{d,\rho}$) are collectively called as decoupling error in this study.

$$E_{d,\rho} = E_{d,\dot{m}} \tag{4-19}$$

It is worth mentioning that the above analytical modelling on decoupling effect could deviate from actual errors in the real-world applications of Coriolis flowmeters, due to a series of assumptions as stated in 4.2.1.2. Large deviations are expected with the increasing concentration of entrained spheres because all interactions between spheres as well as to the tube wall are neglected in the assumptions. Thus, as reported in previous work, the error estimation from decoupling model is very likely only accurate when the volume fraction of entrained spheres is less than 10% [58].

4.2.1.4 **Comparison between Solid-Liquid and Gas-Liquid Flows**

This section provides a comparison between two typical cases (solid-liquid and gas-liquid flows) regarding decoupling error. In consideration of the restrictions of decoupling model, the range of volume fraction of the second phase is limited within 10% representing dilute two-phase flows. As depicted in Figure 4.3, it is obvious that decoupling error (absolute value) grows with the fraction of the second phase. When the volume fraction of entrained solids or gas reaches 10%, decoupling error with sand-water mixtures approximately approaches −7.6%, while a greater error (−22.1%) occurs in gas-liquid mixtures. It suggests that decoupling error in slurry is roughly less than 1/3 of that in gas-liquid flow. It can be deduced that measurement errors encountered in slurry flow would be smaller, as the density difference between solid and liquid is less significant. Nevertheless, since gas (e.g. air) density is extremely small compared with water density, such great density difference can give rise to large decoupling error in the case of gas-liquid mixed flow.

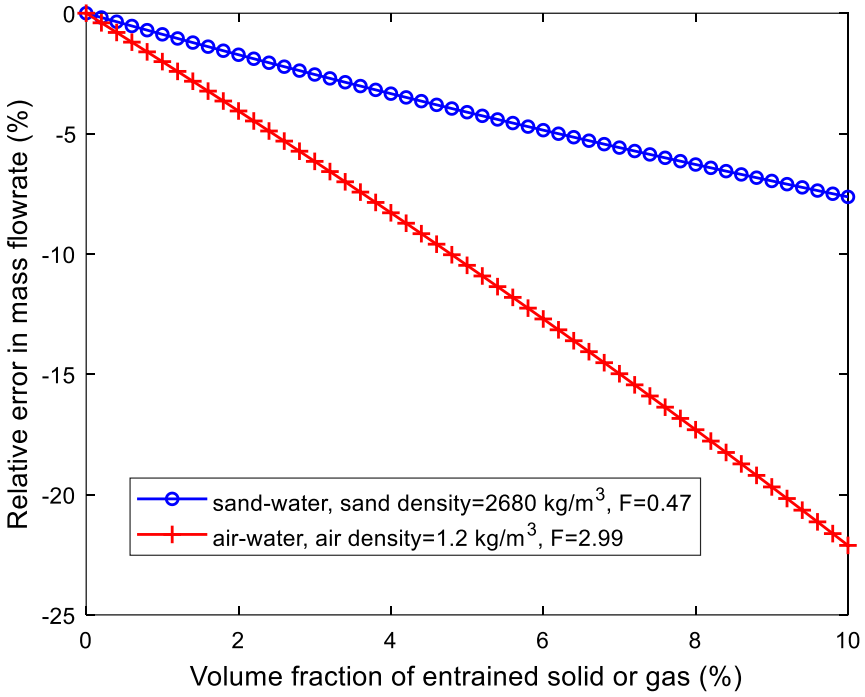

Figure 4.3 Comparion between decoupling error in sand-water and air-water cases (SVF from 0 to 10%)

4.2.1.5 **Decoupling Error Resulting from Different Sand Densities**

Generally, the term "sand" is a broad description which could include a relatively wide category of materials. Sand density is dependent on the composition, the source, even the batch of production. In most cases, it is difficult to determine sand density very accurately, here referring to actual sand density (ρ_s), rather than sand bulk density. Since sand density is always a measured or estimated value, different measurement methods may yield different results. The information of sand density is quite essential to perform analytical modelling of decoupling effect. As illustrated by equations (4-13) and (4-18), ρ_s is directly linked with decoupling ratio and thus decoupling error. Hence, the measurement uncertainty of sand density can be regarded as an important error source which can impact the results of analytical modelling.

This section evaluates the resulting decoupling errors from different sand densities. A common range of sand densities varying from 2000 kg/m^3 to 3000 kg/m^3 is considered. Figure 4.4 plots decoupling error against SVF ranging from 0 to 10% with six different sand densities. The relationships between sand density and SVF and the decoupling error are illustrated by Figure 4.5. It can be observed that with the same SVF, higher sand

density (ρ_s) results in smaller decoupling ratio (F) moving farther with respect to unity (without decoupling issues). Consequently, greater decoupling error (absolute value) appears in larger sand density. In addition, it suggests when slurry flow becomes denser, the same level of measurement uncertainty in sand density could produce greater impact on the analytical modelling results.

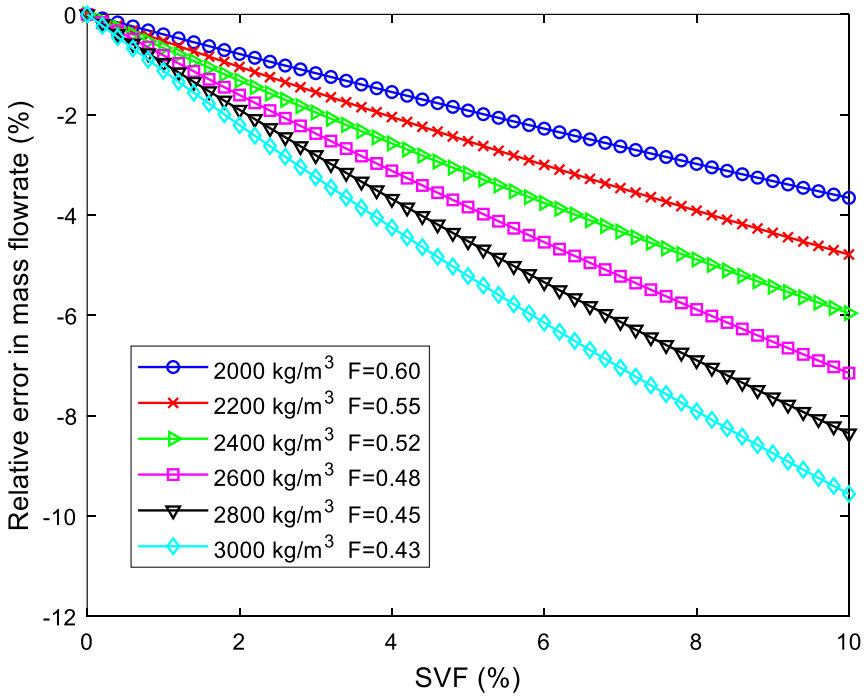

Figure 4.4 Decoupling error resulting from different sand densities

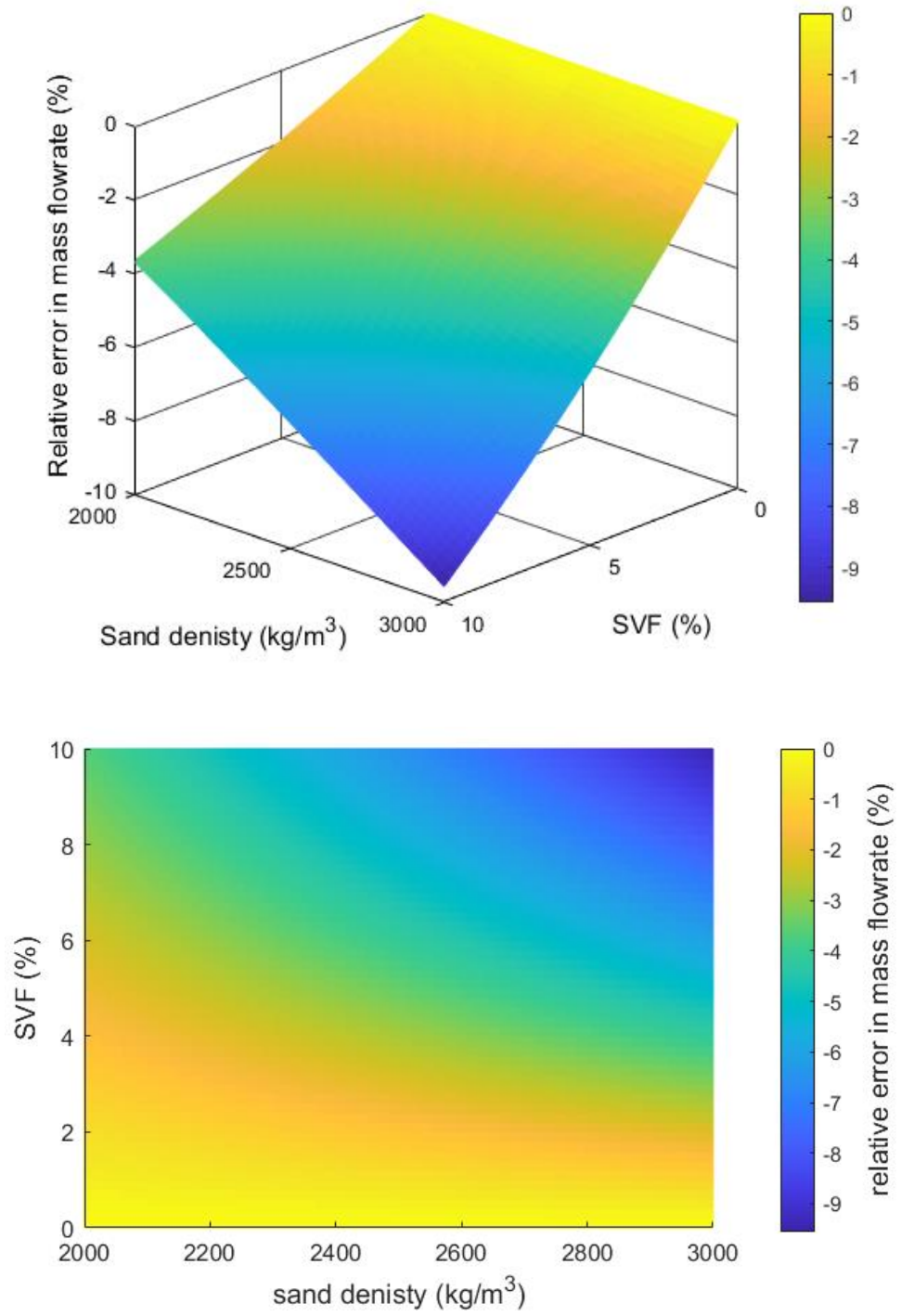

Figure 4.5 Relationships between decoupling error and sand density and SVF

4.2.2 **Compressibility Error**

Apart from decoupling error, compressibility error has been well identified as the other leading error source. Earlier research has supplied the detailed explanation of compressibility effect, or interpreted as moving resonance effect, which can lead to positive measurement errors of Coriolis flowmeters in gas-liquid two-phase flows [31],

[57], [69]. In this section, the basic theory of compressibility error is briefly described and then applied for theoretically investigating compressibility effect in slurry flow.

4.2.2.1 **Overview**

Under the influence of the second phase, the physical properties of two-phase mixtures are changed from those of each single phase [69]. For instance, the presence of gas in liquid not only simply affects the mixture density, but also impacts on the mixture compressibility. Compressibility characterizes the ability of the two-phase mixtures to deform inside the Coriolis measuring tubes [31]. When the mixture fluid (e.g. gas-liquid mixture) passes through Coriolis tubes, it may generate an additional motion (e.g. compression or expansion) besides fluid-tube oscillation and consequently, it could yield an extra force on the tubes. It can be regarded as the existence of a second spring acting in the Coriolis oscillation system, illustrated by Figure 4.6. As a result, Coriolis drive frequency would deviate from the desired resonance frequency when the second spring exists in the vibrating system [31], [57]. Because of the drift in Coriolis drive frequency, measurement errors could occur in apparent density and mass flowrate readings, particularly in the situation wherein the resonance frequency of the second spring-mass-damper system approaches the original drive frequency of Coriolis flowmeters. Due to the presence of the second spring, a part of fluid (two-phase mixtures) would vibrate in the opposite direction to tube oscillation (e.g. compression or expansion of gas-water mixtures), resulting in higher reaction force sensed by the Coriolis tube. As a result, compressibility effect would lead to over-estimation in density as well as mass flowrate, contrary to the negative errors arising from phase decoupling effect as explained above.

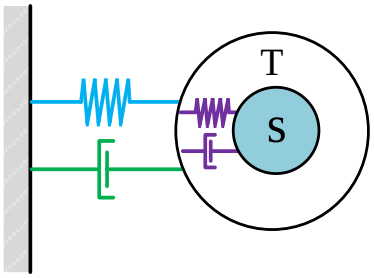

Figure 4.6 Second-order mass-spring-damper model representing compressibility effect

4.2.2.2 **Compressibility Effect on Coriolis Flow Metering**

As presented above, the change in physical properties of mixture fluid is closely linked with compressibility effect. To quantify compressibility effect on Coriolis flow metering, the calculation of mixture compressibility along with the speed of sound traveling in mixture fluid is introduced. The mixture compressibility, β_m (m^2/N), can be defined and calculated below [69],

$$\beta_m = \frac{1}{\rho_m c_m^2} = \frac{1-\alpha_s}{\rho_l c_l^2} + \frac{\alpha_s}{\rho_s c_s^2} \tag{4-20}$$

The speed of sound traveling in mixture fluid (c_m) is solved,

$$c_m = \sqrt{\frac{1}{\rho_m}\left(\frac{\rho_l c_l^2 \rho_s c_s^2}{\rho_s c_s^2 (1-\alpha_s) + \rho_l c_l^2 \alpha_s}\right)} \tag{4-21}$$

where β is the compressibility, c denotes the speed of sound, ρ is the density, and α_s is the volume fraction of entrained solid or gas.

The compressibility error in mass flowrate ($E_{c,\dot{m}}$) and density ($E_{c,\rho}$) have been derived in [57], which is dependent on the speed of sound in two-phase mixtures,

$$E_{c,\dot{m}} = \frac{1}{2}\left(\frac{\omega_r}{c_m} r_t\right)^2 \tag{4-22}$$

$$E_{c,\rho} = \frac{1}{2} E_{c,\dot{m}} = \frac{1}{4}\left(\frac{\omega_r}{c_m} r_t\right)^2 \tag{4-23}$$

where ω_r is the Coriolis drive frequency and r_t is the inner radius of the Coriolis tube.

As revealed in equations (4-22) and (4-23), the compressibility error is always positive, which means Coriolis flowmeters over-estimate the mass flowrate and density of the mixture flow due to compressibility effect.

4.2.2.3 **Comparison between Solid-Liquid and Gas-Liquid Flows**

Here two situations are considered, wherein the liquid is mixed with air and sand particles, respectively. The changes in the mixture compressibility and the speed of sound travelling in the mixtures are computed from equations (4-20) and (4-21). The sound speed of pure air, water and sand are quoted from the Table 2 in an earlier study [58]. The parameters of

Coriolis drive frequency as well as tube inner radius are set based on the data from the Coriolis flowmeters (KROHNE OPTIMASS 6400 S50) used in experiments. To simplify the calculation, the drive frequency is assumed as a fixed value, independent of the portion of entrained solid or gas. The relevant parameters used in the calculation are listed in Table 4.1.

Table 4.1 Source of parameters used for analysis of compressibility error

Ambient temperature **Atmospheric pressure**	air	water	sand
ρ (kg/m^3)	1.2	998	2680
c (m/s)	343	1481	5968
Coriolis flowmeter	KROHNE OPTIMASS 6400 S50		
Drive frequency (Hz)	240		
Coriolis tube inner radius (mm)	11.05		

Figure 4.7 displays the variations in mixture compressibility with the growth of volume fraction of solid or gas from 0 up to 100%. It can be clearly seen that the absolute change in compressibility of sand-water mixtures is much smaller than that of air-water mixtures. Similarly, the speed of sound travelling in sand-water flow increases fairly slowly while a small amount of gas entrained into water can lead to a dramatic drop in the speed of sound in air-water flow, as shown in Figure 4.8.

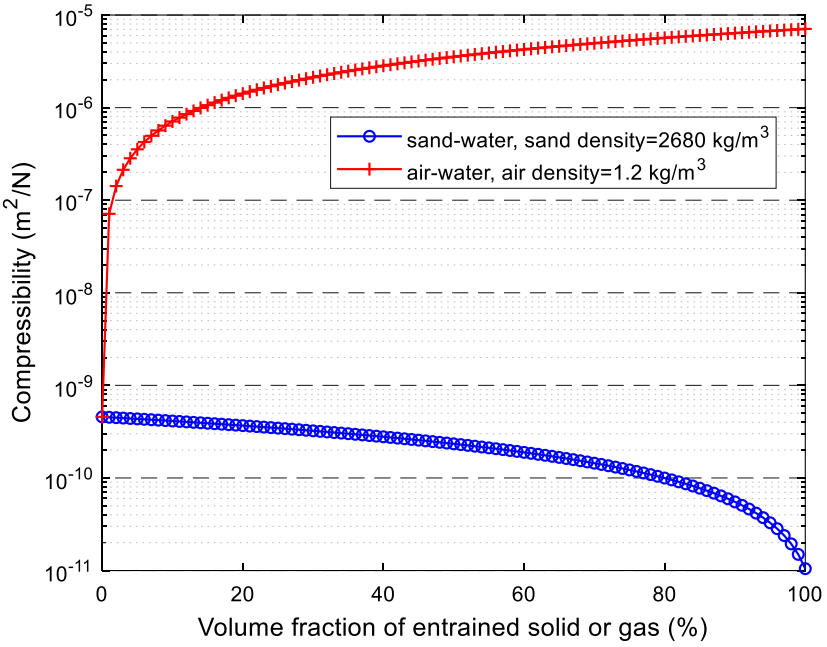

Figure 4.7 Compressibility of sand-water and air-water flow

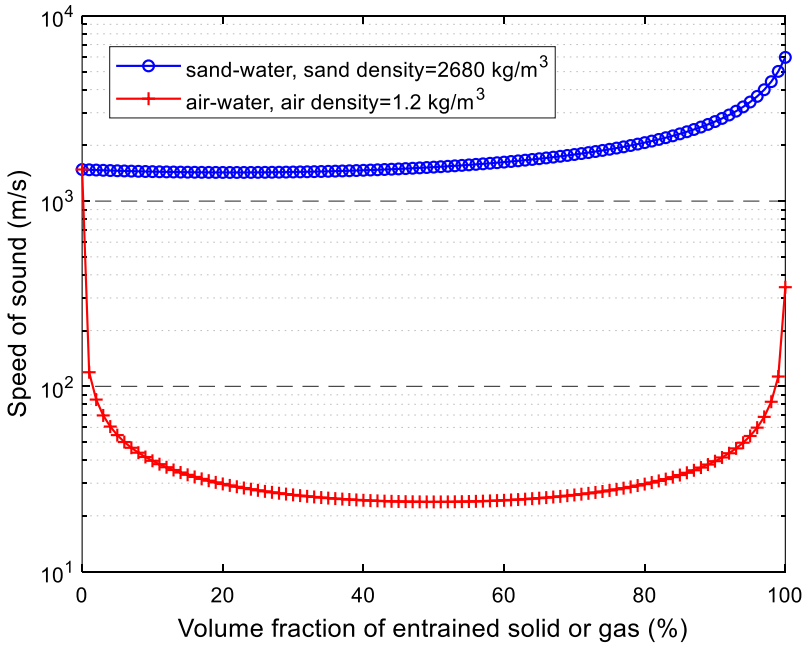

Figure 4.8 Speed of sound in sand-water and air-water flow

In consideration of the complexity of flow conditions and assumptions for modelling, the compressible model is suggested only applicable to dilute two-phase flows (e.g. volume fraction of gas less than 15%) [31]. Here the compressibility error in air-water and sand-water flow are plotted against volume fraction ranging from 0 to 15%, given by Figure 4.9.

It suggests that compressibility error encountered in dilute slurry is negligibly small. The underlying physical reason is that both solid and liquid phases are relatively incompressible. Through the comparison with air-water flow, it can be evidently concluded that compressibility effect leads to considerably small impact on Coriolis flow metering in slurry flow, whereas a small amount of gas can cause noticeable compressibility error owing to the significant increase in the mixture compressibility.

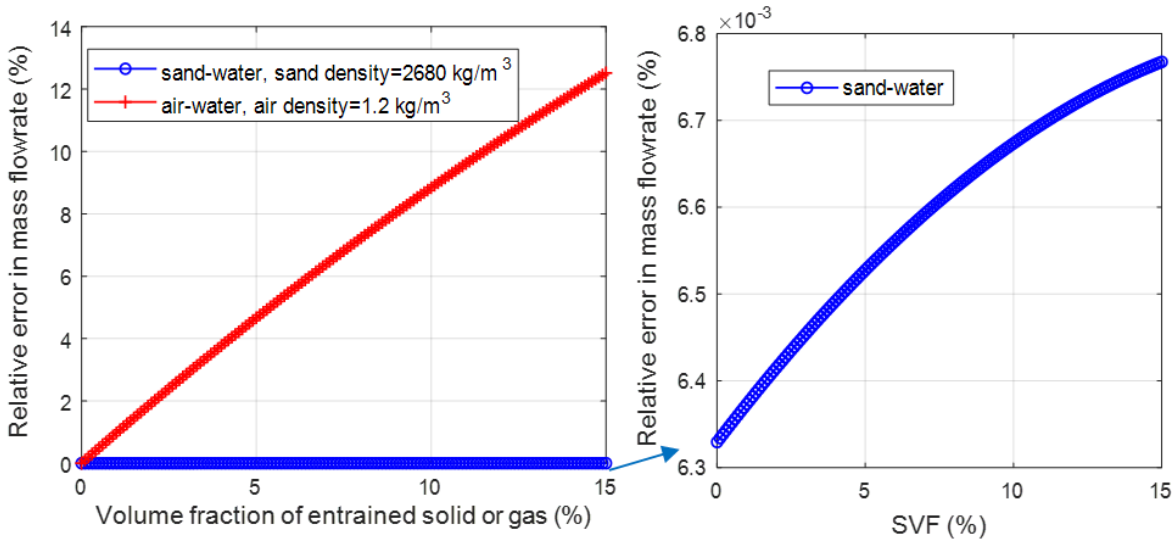

Figure 4.9 Comparion between compressibility error in sand-water and air-water flow (SVF from 0 to 15%)

As a conclusion of the theoretical analysis above, in the case of dilute slurry flow, the decoupling error would dominate the measurement errors whilst the compressibility error is negligibly small. It suggests that the errors arising in Coriolis flowmeters for slurry flow metering are primarily attributable to the decoupled motions between solid and liquid phases, while the compressibility effect can be reasonably neglected. Therefore, the existing decoupling theory will be implemented into analytical modelling for error prediction and compensation in Section 4.5.1. Besides, theoretical analysis illustrates that the entrained solids could cause less problems than entrained gas, which is favourable to apply Coriolis flowmeters for slurry flow metering.

4.2.3 **Asymmetry and Imbalance Error**

Besides the two leading error sources (decoupling error and compressibility error), there are a few other errors sources which may degrade the measurement accuracy of Coriolis flowmeters, as reported in [87]–[89]. Asymmetry and imbalance error are the primary

interest in consideration of the uneven distribution of solid phase along Coriolis tubes, while slip ratio error resulting from slipping movement along the axial direction of Coriolis tube is often involved in gas-liquid flow, not discussed here.

A Coriolis flowmeter is a delicately designed vibrating system. The excellent symmetry and perfect balance are vital to delivering accurate flow measurement by a Coriolis flowmeter. However, under two-phase conditions, the second phase (e.g. solid particles or gas bubbles) typically appears as a non-continuous phase, which is usually dispersed or not uniformly distributed in the fluid, giving rise to the asymmetries along the Coriolis tube. Concerning a Coriolis flowmeter with twin or quad tubes, the mixture flow may not be equally split into each measuring tube, resulting in imbalance. Once flowmeters are not well symmetric and balanced, the sensor signal is likely to be distorted by the external influences such as pump vibration, and accordingly Coriolis flow measurement errors can occur. Particularly, when the flow velocity becomes low, the shift in flow regime and the gravity effect on particles distribution would bring the extra asymmetry as well as imbalance errors of Coriolis flow metering.

These two terms, asymmetry and imbalance, are some sort of errors related to the geometry of Coriolis tubes. For that reason, asymmetry and imbalance errors would vary from the different products or different types from different manufacturers. Although it is difficult to quantify such errors, a basic qualitative analysis is performed here for developing an understanding of the underlying physics.

For a bent-tube Coriolis flowmeter being horizontally installed on the pipe, asymmetry errors would possibly drift to negative or positive directions, which depends on its installation orientation and whether the entrained spheres are heavier or lighter than the carrier liquid. For example, in the case of gas-liquid flow, gas bubbles always tend to pile up on the side of tube where the mixture flow begins to move downward, arising from the buoyancy effect on gas. Accordingly, if the measuring tube (belly) is placed down, the inlet would hold more gas bubbles and hence, positive asymmetry error is produced from the added damping on inlet side [86], while negative asymmetry error appears if the belly is up. On the contrary, asymmetry would have an opposite impact on Coriolis flow metering under solid-liquid flow due to the gravity effect on solid. Since solid phase is heavier than liquid carrier, it can be inferred that solid particles can be accumulated when the mixture flow starts to go upward. That suggests if the meter belly is mounted down,

more solid particles would be gathered in the outlet. As a result, the damping of outlet side gets increased and negative asymmetry error is expected, whereas extra over-reading can happen if the belly is up.

Furthermore, it is worth clarifying that the gravity effect and flow regime are not the direct causes which can degrade the measurement accuracy of Coriolis flowmeter as explained in [86]. However, the additional error sources, for instance the asymmetry error associated with the gravity effect, the slip ratio error associated with the flow regime, would adversely impact Coriolis flow metering. Therefore, it can be observed that the factors including mass flowrate, the flow regime, pipe orientation, the installation of flowmeters as well as the geometry of the Coriolis tube could affect the behaviour of Coriolis flowmeters under two-phase conditions.

4.3 Experimental Tests with Dilute Slurry Flow

Experimental tests were conducted with dilute sand-water flow (SVF within 4%), aiming to experimentally investigate the influence of solid-liquid two-phase conditions on Coriolis flow metering. This section firstly describes the definitions of key terms. Then the section presents properties of sand used in the experiments. In addition, the experimental conditions as well as data processing are given.

4.3.1 **Definitions of Key Terms**

- Relative mass flowrate error, relative density error

First of all, it is worth noting that the measurement errors discussed here refer to the measurement of sand-water mixture (slurry) flow, instead of individual phase (liquid phase, solid phase), due to the fact that Coriolis flow metering offers the measurement of mixture flow. With respect to the reference, the relative error in mixture mass flowrate and mixture density are calculated as follows,

$$E_{\dot{m}} = \frac{m_{m,app} - m_R}{m_R}\ 100\% \tag{4-24}$$

$$E_{\rho} = \frac{\rho_{m,app} - \rho_R}{\rho_R}\ 100\% \tag{4-25}$$

where $E_{\dot{m}}$ and E_{ρ} are the relative error in mass flowrate measurement and density measurement, respectively; m is mass, $\dot{m}$ denotes mass flowrate, ρ is density; the subscript "app" denotes the apparent (observed) readings in Coriolis flowmeters, and the subscript "R" represents the reference.

- Apparent mass flowrate, apparent density

Apparent mass flowrate refers to the mass flowrate readings observed from Coriolis flowmeters, denoted as $\dot{m}_{m,app}$. Similarly, apparent density is the density readings from Coriolis flowmeters, denoted as $\rho_{m,app}$.

- Solid volume fraction (SVF), solid weight fraction (SWF)

Solid volume fraction (α_s), abbreviated as "SVF", represents the volume fraction of solid phase in slurry flow, which is defined as the ratio of the solid volumetric flowrate to the solid-liquid mixture volumetric flowrate, expressed in percentage. Similarly, solid weight fraction (β_s), abbreviated as "SWF", is the weight fraction of solid phase in the solid-liquid mixtures.

Since both solid and liquid phases can be assumed as incompressible, the density of sand-water mixture (ρ_m) can be derived from SVF or SWF,

$$\rho_s\,\alpha_s + \rho_w\,(1-\alpha_s) = \rho_m \tag{4-26}$$

$$\frac{1}{\frac{\beta_s}{\rho_s}+\frac{1-\beta_s}{\rho_w}} = \rho_m \tag{4-27}$$

where α is volume fraction, β is weight fraction; the subscript "s" denotes sand particles (solid phase), the subscript "w" represents water (liquid phase), the subscript "m" denotes two-phase mixtures.

Accordingly, the conversion between SVF and SWF is obtained,

$$\beta_s = \frac{\alpha_s\,\rho_s}{\alpha_s\,\rho_s+(1-\alpha_s)\,\rho_w} \tag{4-28}$$

- Apparent SVF

Apparent solid volume fraction ($\alpha_{s,app}$), abbreviated as "apparent SVF", is derived from apparent density reading from Coriolis flowmeters, similar to equation (4-26),

$$\rho_s \, \alpha_{s,app} + \rho_w \left(1 - \alpha_{s,app}\right) = \rho_{m,app} \tag{4-29}$$

By rearranging the equation, $\alpha_{s,app}$ is written as,

$$\alpha_{s,app} = \frac{\rho_{m,app} - \rho_w}{\rho_s - \rho_w} \, 100\% \tag{4-30}$$

There is a similar term to "apparent (observed) density drop" ($\Delta\rho_{app}$), which is commonly used in previous work reporting the problems of Coriolis flow metering with gas-liquid flow [22], [23], [61]. To distinguish these two terms, the term "observed or apparent density drop" ($\Delta\rho_{app}$) is calculated from apparent readings of mixture density ($\rho_{m,app}$) with respect to that of pure water ($\rho_{w,app}$) from Coriolis flowmeters, employed as an indicator of gas volume fraction (GVF),

$$\Delta\rho_{app} = \frac{\rho_{m,app} - \rho_{w,app}}{\rho_{w,app}} \, 100\% \tag{4-31}$$

In the situation of gas-liquid flow, gas density can be neglected compared with that of liquid, so essentially the "observed density drop" almost equals to apparent GVF. However, sand density cannot be ignored in the case of slurry flow. Therefore, apparent SVF is more suitable than the term of "observed density rise" for the presentation of the sand portion in slurry flow.

- Reference SVF, reference SWF, reference slurry density

Reference solid volume fraction (SVF), reference solid weight fraction (SWF) as well as reference slurry density are acquired or calculated from the flow sampling tests. The detailed computation has been demonstrated in Section 3.5.3 according to equations (3-1) to (3-3).

- Water density, sand density

The reference density of pure water is computed according to a common industrial method (IAPWS R7-97 [90]) which can offer the estimation of pure water density at current process pressure and temperature. The reference density of tap water being employed in

the experiments can be further corrected by adding a constant offset term into the calculated pure water density from IAPWS R7-97 method. This density offset is pre-set according to the measurement of actual density of tap water sample using a densimeter in the laboratory.

The value of actual sand density is determined based on the water displacement method which will be stated in Section 4.3.2.2, using a constant of 2680 kg/m^3 in this study. The influences of process pressure as well as temperature on sand density are both neglected.

4.3.2 **Properties of Solid Particles**

4.3.2.1 **Selection of Sand**

The physical properties of entrained solids (e.g. size, shape, solid density) are considered to be factors which can most likely affect the performance of Coriolis flowmeters in slurry flow, inferred from the relevant existing research [31], [69], [86]. Thus, when selecting the solid particles utilized in the experiments, considerations should be given on the grain size, shape, solid density together with the hardness for erosion purpose. Although the ideal experimental material is expected to own uniform size and spherical shape for correlating experimental outcomes with theoretical analysis, natural silica sand is chosen over artificial or manufactured sand in this work, for the purpose of simulating the slurry transportation as it often occurs in real-world slurry applications.

To represent the solids typically involved in the petroleum industry, for example sand coming from production wells of oil and gas, a kind of beach dune sand particles (BS 1881-131:1998 Fraction D) in size ranging from 150 μm to 300 μm (size similar to table salt) is chosen. The sand used here is a type of natural, uncrushed, but washed, dried and graded silica sand. It is clean and dust free, with bulk density in range from 1310 kg/m^3 to 1510 kg/m^3 (provided by the sand supplier). The shape of sand particles is rounded to sub-rounded, in pale silver to light brown colour.

4.3.2.2 **Determination of Sand Density**

Among sand properties, sand density is one of the most important parameters to this research. Quite often sand suppliers provide a coarse estimation of sand density for their products, for instance loose or compacted sand bulk density. However, instead of bulk density, the “actual sand density” is the interested parameter for the purpose of calculation

of sand-water mixture density. Here the "actual sand density (ρ_s)" can be understood as a sort of sand density as sand particles are mixed with liquid. A dimensionless number, often known as relative density or specific gravity, can be employed to quantify the "actual sand density". As shown in equation (4-32), relative density (N_{Rd}) is defined as the ratio of density of a substance (sand) to density of water under its densest condition (at 4 °C and under atmospheric pressure, nearly 1000 kg/m^3).

$$N_{Rd} = \frac{\rho_s}{\rho_w} \tag{4-32}$$

According to the datasheet provided by the sand supplier, the value of N_{Rd} is claimed as 2.65. To verify if this value is accurate, a simple test based on water displacement method was carried out, with the intention of measuring the "actual sand density" with respect to water, illustrated by Figure 4.10.

Figure 4.10 Sand density measurement based on water displacement method

The detailed procedures are described as follows,

1) Firstly, prepare a certain weight of sand ($m_{s,D}$) whilst fill up a beaker using tap water. The beaker needs to be fixed at a certain angle to ensure a constant liquid level within the beaker.
2) Then the sand particles are slowly poured into the beaker. In the meantime, use one container to pick up the displaced water from the beaker until all sand particles fully sink into the water.
3) Finally, the weight of the displaced water can be determined by a very accurate small scale (maximum 8 kg, with resolution 0.01 g), recorded as $m_{w,D}$.

The weight of the displaced water ($m_{w,D}$) can be directly converted into the volume of the displaced water ($V_{w,D}$) based on water density (ρ_w), and ρ_w is calculated as described in Section 4.3.1. $V_{w,D}$ is assumed to equal to the volume of entrained sand particles ($V_{s,D}$). Finally, $V_{s,D}$ can be estimated and hence the "actual sand density (ρ_s)" can be inferred accordingly.

$$\begin{cases} V_{w,D} = \frac{m_{w,D}}{\rho_w} \\ V_{s,D} = V_{w,D} \\ \rho_s = \frac{m_{s,D}}{V_{s,D}} \end{cases} \tag{4-33}$$

After six repeated tests, the averaged value of ρ_s works out at 2.713 g/cm^3, which is found close to the given specific gravity (2.65) in the sand datasheet. According to the given specific gravity (2.65) and measured sand density (2.713 g/cm^3), the mean value (2.680 g/cm^3) is finally determined as the "actual sand density" (ρ_s) throughout this research. The consideration here is that although the test on basis of water displaced method can provide more accurate measurement of sand density but may be less representative for covering all sandbags coming from different batches.

4.3.3 **Experimental Conditions**

In the experimental work, a series of flow measurement tests were carried out with flowrate varying from 8200 kg/h to 20000 kg/h and SVF between 0 and 4%. Flow measurement tests comprise two parts, batching procedures to quantify relative error in mass flowrate, as well as flow sampling tests to identify relative error in density. During batching, two Coriolis flowmeters (CF1 and CF2) are both under test, while density error is only examined on the upstream Coriolis flowmeter (CF1) since CF2 is not usable for flow sampling.

4.3.3.1 **Batching for Assessment of Mass Flowrate Error**

After initial verification using clean water as described in Section 3.5.1, sand particles were gradually fed into the large slurry tank to create slurry flow. There are two common factors which can typically affect the performance of Coriolis flow metering under two-phase conditions, identified in previous research [23], [55], [63]. One factor is the portion of the second phase (SVF in this case), and the other is mass flowrate. By adjusting the rotation speed of the centrifugal pump, the desired mass flowrates are achieved. The

mixture mass flowrate is measured by CF1 quantitatively, named as apparent mixture mass flowrate ($\dot{m}_{mix,app}$). Five flowrates are tested, roughly 8200, 12000, 14300, 17000, 20000 kg/h from low to high, covering nearly 20% to 60% nominal flowrate of Coriolis flowmeters under test. Additionally, SVF is derived from the mixture density readings from CF1, named as apparent SVF ($\alpha_{s,app}$), demonstrated by equation (4-30).

In terms of SVF, there is one misunderstanding that SVF of slurry can be simply calculated from the amount of sand added into the tank. However, the fact is that the sand concentration is dependent on a range of factors, for instance, the position of the tank outlet, pipe dimension of test section, mass flowrate, and sand properties. Therefore, the amount of injected sand can only be employed for a very rough estimation of sand concentration, instead of quantification. In the slurry flow test rig, the sand concentration can be changed by regulating the weight of sand dosing as well as the rotation of the agitator. However, it is found practically difficult to control the delivered sand concentration to reach the target, attributable to the limitations of the slurry flow test rig, as described in Section 3.6.

In the experiments, sand concentration is created from low to high and exactly the same weight of sand is injected for each sand dosing. After each sand dosing, five flowrates are tested from high to low, with three repeats under each test condition (the identical sand dosing and mass flowrate). In total, five flowrates and seven different levels of sand concentrations have been tested, resulting in 105 test points as shown in Figure 4.11.

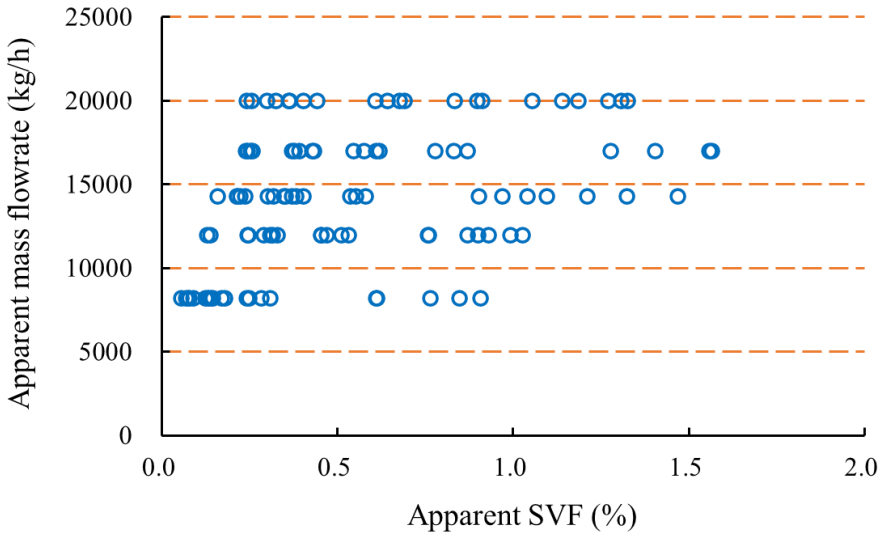

Figure 4.11 Test matrix of mass batching against apparent SVF

Figure 4.11 reveals two problems regarding rig stability control. Firstly, the test points are not uniformly distributed throughout the designed range of SVF, although the same increment of sand is injected into tank to raise SVF. It verifies that SVF cannot be simply estimated by the weight of sand dosing as presented above. The repeatability condition of test points is difficult to implement or control well. Ideally, with the identical settings of the repeated test points, the delivered SVF is expected to be distributed very close to each other. However, even for some repeated test points, they are scattered as shown in Figure 4.11. The reason here is that the sand transportation can be affected by many related process conditions. In batching operation, the variables which can be managed on the slurry flow test rig have been well controlled, including the speed of centrifugal pump, sand dosing, the ration of agitator as well as the opening of valves, but still several factors are out of the regulation. Secondly, mass flowrates also affect SVF, resulting in different range of SVF with different mass flowrates, as revealed in Figure 4.11. Generally, with the rise of mass flowrate, SVF would go up and the range of SVF could be extended. It can be interpreted that higher velocity tends to carry more sand particles moving with water. Nevertheless, for example, the case of the highest mass flowrate (20000 kg/h) is an exception. The reason here probably is that under high flowrate, the agitator could not meet the demand of creating the high-concentrated slurry flow, and consequently the centrifugal pump has to deliver more water into test section in order to reach the target mass flowrate.

Furthermore, due to the consideration that the flow regime could also affect Coriolis flow metering with two-phase flows as suggested in the prior research [60], [62], [86], homogenous slurry flow or at least non-settling flow is maintained throughout the flow measurement tests. The benefit of keeping homogenous slurry flow is to avoid uneven sand distribution, sliding sand dunes, or even sand sediment, which could adversely affect the behaviours of Coriolis flowmeters. For that reason, the range of SVF is limited by the achievable maximum flow rate.

4.3.3.2 **Flow Sampling for Assessment of Density Error**

Flow sampling tests were conducted to evaluate measurement error of mixture density of Coriolis flowmeters. Similar to batching, a set of sampling tests were carried out at different mass flowrates and SVF. An ideal scenario is to create the identical test matrix as that in batching, for the purpose of comparing mass flowrate error and density error under the identical test conditions. However, it is practically difficult to reproduce exactly the

same test conditions, because of the difference in pipe routes as well as the practical difficulty in rig stability control. Again, five mass flowrates are tested, while the medium-high (17000 kg/h in batching) as well as high flowrates (20000kg/h in batching) are adjusted to slightly lower values (16000 kg/h and 18000 kg/h in sampling), respectively. It is due to the limitation of the maximum volume of fluid sample. By reducing the flowrates slightly, the sampling duration can last over 5 s at high flowrate, which can help improve the flow stability in sampling tests. Otherwise, if flowrate is too high, the high flow velocity would cause sandy water splashing out of the bucket, giving rise to the measurement uncertainty.

As shown in Figure 4.12, the test matrix consists of 90 test points in total. Five different flowrates are tested whilst 18 sampling tests are arranged with different sand concentrations at each flowrate. In addition, since reference SVF became available from the flow sampling results, instead of using apparent SVF from CF1, the test matrix is also plotted against reference SVF, given by Figure 4.13. It can be noticed that apparent SVF is obviously lower than reference SVF, and this difference is owing to the negative decoupling errors of Coriolis flowmeters when applied into two-phase flow metering.

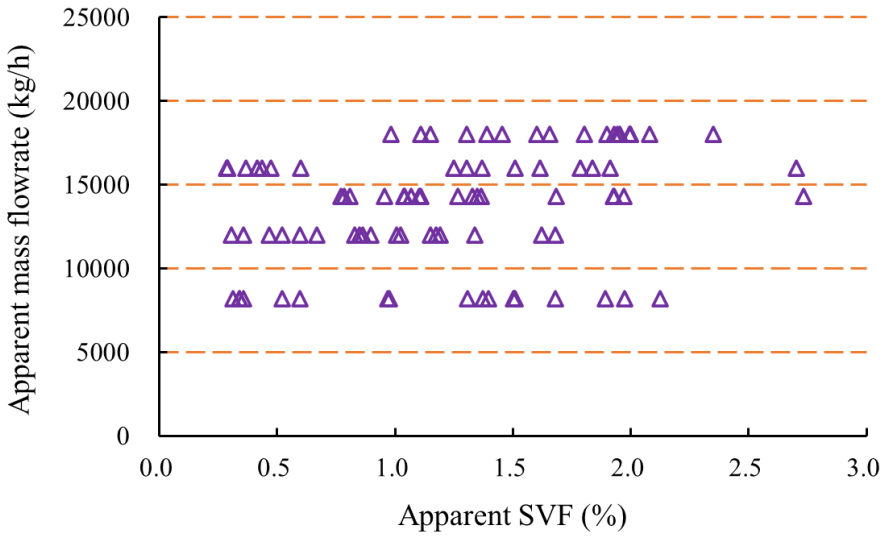

Figure 4.12 Test matrix of flow sampling against apparent SVF

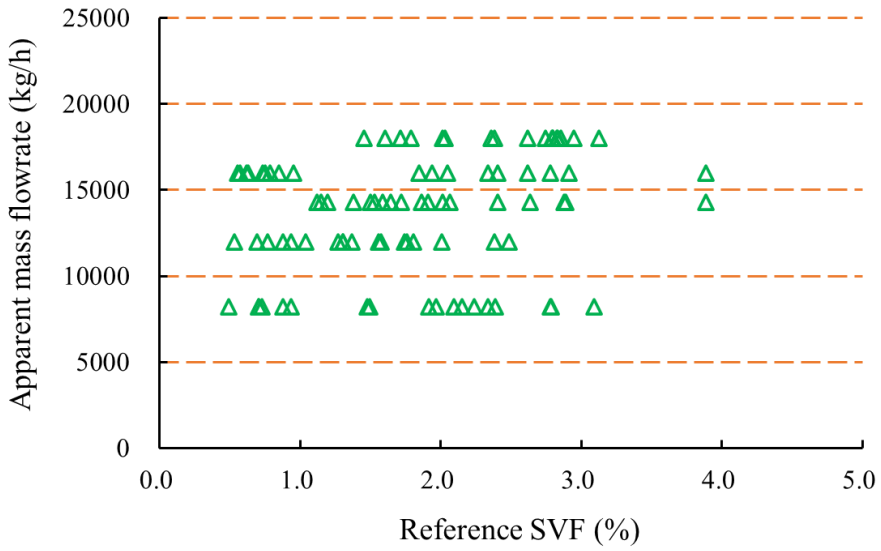

Figure 4.13 Test matrix of flow sampling against reference SVF

4.3.4 **Meter Reverification with Clean Water**

After the completion of flow measurement tests with dilute slurry, the measurement uncertainties of CF1 and CF2 are reverified by using clean water. The purpose is to examine the structural integrity of the Coriolis flowmeters under test, judging whether CF1 or CF2 has been eroded during the flow measurement tests. Repeating the same test matrix as that in initial verification (see Section 3.5.1), the performance of Coriolis flowmeters after flow measurement tests is depicted in Figure 4.14. It can be seen that the relative error in mass flowrate from two meters is within its claimed specification (±0.1%), which means both meters are still in good status and free of erosive wear on the tubes. This reverification test validates the reliability and confidence of the experimental data acquired from the above flow measurement tests.

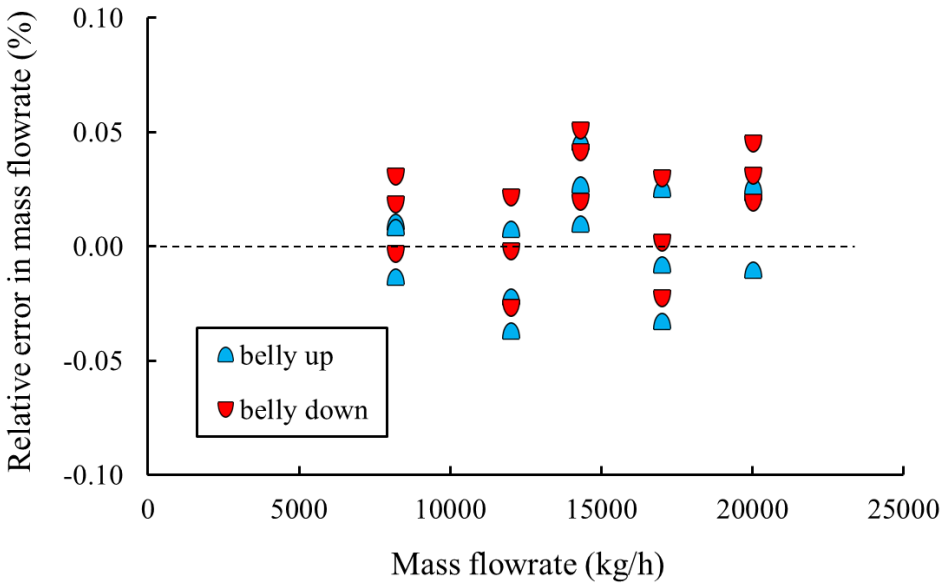

Figure 4.14 Reverification of mass flowrate measurement with clean water

4.3.5 **Data Acquisition and Processing**

In the flow measurement tests, the flow measurement related data (as listed in Table 3.1) are logged from Coriolis flowmeters under test at a requisition rate of 10.24 ms per data point. Typically, the mass flowrate easily becomes steady while density fluctuates with the variations or sudden changes in flow velocity, especially at the time of opening or shutting off valves. To lower the effect of fluctuations, the data logging from very beginning or final stage of batching is not used for further analysis. Instead of covering the whole batching process, the batching duration is defined and trimmed when the mass flowrate stabilises at the set target. The readings of mass flowrate and density are averaged within the batching duration for the further analysis. Table 4.2 illustrates the processing of internal parameters obtained from Coriolis flowmeters in this study. Flow sampling data are processed in a similar way, not repeated.

Table 4.2 Processing of internal parameters from Coriolis flowmeters

Symbol (unit)	Description	Processing
$\bar{\dot{m}}_{m,app}$	Apparent mass flowrate	Time-averaged
$\bar{\rho}_{m,app}$	Apparent density	Time-averaged
$\bar{T}_f$(°C)	Fluid temperature	Time-averaged
$\alpha_{s,app}$ (%)	Apparent SVF	Calculated from equation (4-30) based on $\bar{\rho}_{m,app}$
$\bar{S}_A$, $\bar{S}_B$(%)	Sensor A & B level	Time-averaged
$\bar{I}_{dr}$(%)	Drive level	Time-averaged
P_{2P} (%)	2-phase signal level	2-phase signal is further normalized to percentage with respect to the maximum value (1000)
ASY_N	Normalized asymmetry It characterizes the asymmetry between inlet and outlet of the tube. Normalization is performed by subtracting the initial value acquired under single-phase condition (clean water).	$ASY = \frac{S_B}{S_A}$ $ASY_0 = \frac{S_{B_0}}{S_{A_0}}$ $ASY_N = ASY - ASY_0$
P_{dN}	Normalized damping indicator Damping indicator is the ratio of drive current to sensor voltage. It can be normalized by subtracting the initial value under single-phase condition.	$P_d = \frac{I_{dr}}{(S_A + S_B)/2}$ $P_{d0} = \frac{I_{dr_0}}{(S_{A_0} + S_{B_0})/2}$ $P_{dN} = P_d - P_{d0}$

An example of batching at 12000 kg/h is given by Figure 4.15 and Figure 4.16 which display the typical curves of several key parameters logged from CF1 and CF2, respectively, including the mass flowrate, fluid temperature, density, drive level, 2-phase level. From the curve of mass flowrate, the batching duration can be explicitly recognized

corresponding to the stabilization period at the target. On one hand, several similarities are discovered from the two figures. Firstly, it can be seen that at the beginning of batching, when the valves are suddenly open, an obvious local peak arises in density, indicating a relatively large amount of sand particles being picked up and carried with water, illustrated in Figure 4.15 (a) and Figure 4.16 (a). Then a similar trend is found in the curve of fluid temperature along with the presence of sand, shown in Figure 4.15 (b) and Figure 4.16 (b). The small peak in temperature is believed to be induced from pump heating up as well as the intense and successive collisions between the solids and the Coriolis tube. In the meanwhile, drive frequency responds to the fluctuations in density accordingly. It is clear that drive frequency drops owing to the rise in density, given by Figures 4.15 (c) and 4.16 (c). In terms of drive level, it is a dimensionless parameter, being expressed in percentage. When solid particles or gas bubbles are entrained into the liquid, quite often more energy is required to maintain the Coriolis oscillation, which implies more current would be allocated into the drive, and consequently a higher drive level can be noticed than that under single-phase condition. Moreover, 2-phase level is closely linked with the two-phase or multiphase conditions of the flow being measured, which can help report the presence of a second phase. Thus, the similar trends of drive level as well as 2-phase level are observed from (d) and (e) in Figures 4.15 and 4.16, which can be interpreted from the variations in density.

On the other hand, it is interesting to see the different mounting orientations can yield some differences in the curves. The primary distinction comes from the density reading, shown in Figures 4.15 (a) and 4.16 (a). When the Coriolis flowmeter is installed with belly down (CF2), the sand could be trapped within the tube in the moments before and after batching. Before batching operation, when the flowmeters are checked for the zero-calibration point and reset for mass totalizer, a certain amount of sand would be delivered into the flowmeters since the centrifugal pump is still running at low flowrate while the downstream valve of CF2 is closed. As a result, some sand particles would settle in the tube of CF2, leading to the higher density reading, while the density from CF1 is much lower, close to density of “clean” water attributable to the benefit of belly up installation. When batching is completed, the valves are suddenly shut off and the pump is stopped. The density reading in CF1 (belly up) significantly drops down to nearly “clean” water density, whereas a dramatic density rise is noted in CF2 (belly down), which indicates a relatively heavy sand load within its tubes. In addition, the sand deposition in tubes would

consume more energy, and thereby a higher drive level is observed in CF2 after batching, through comparison between Figures 4.15 (e) and 4.16 (e). However, the constant sand sediment would not induce noticeable 2-phase level as long as the required drive current is still within the permissible limitation and the flowmeters can work normally, shown in Figure 4.16 (d). The reason is that the constant sand staying in tubes cannot produce density or phase fluctuations which dominate the computation of 2-phase level.

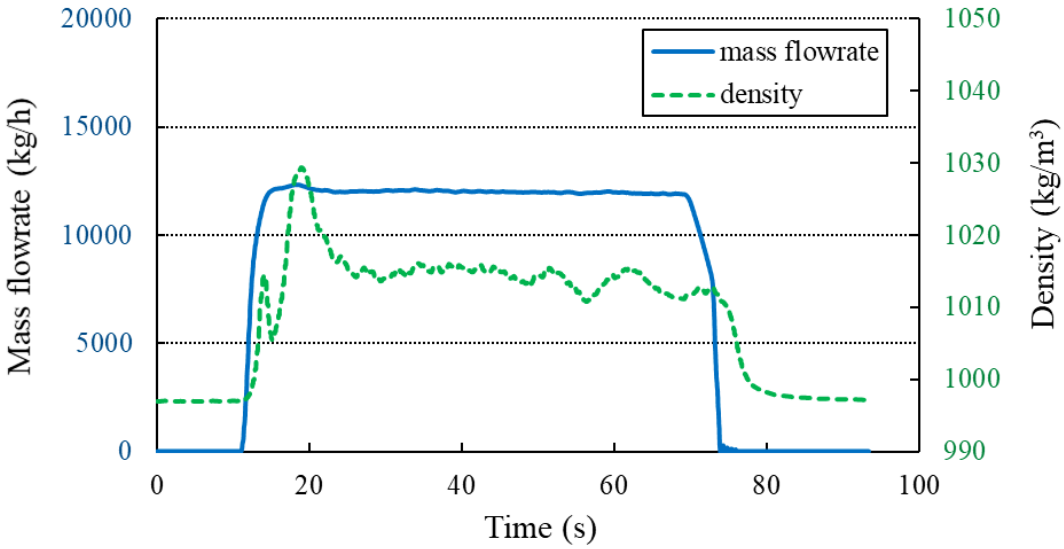

(a) Density and mass flowrate

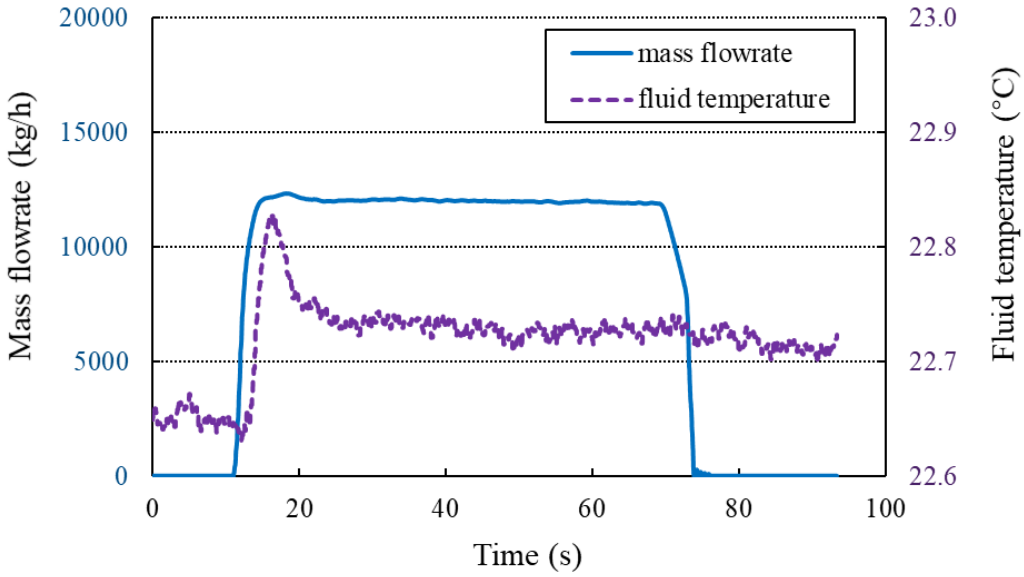

(b) Fluid temperature and mass flowrate

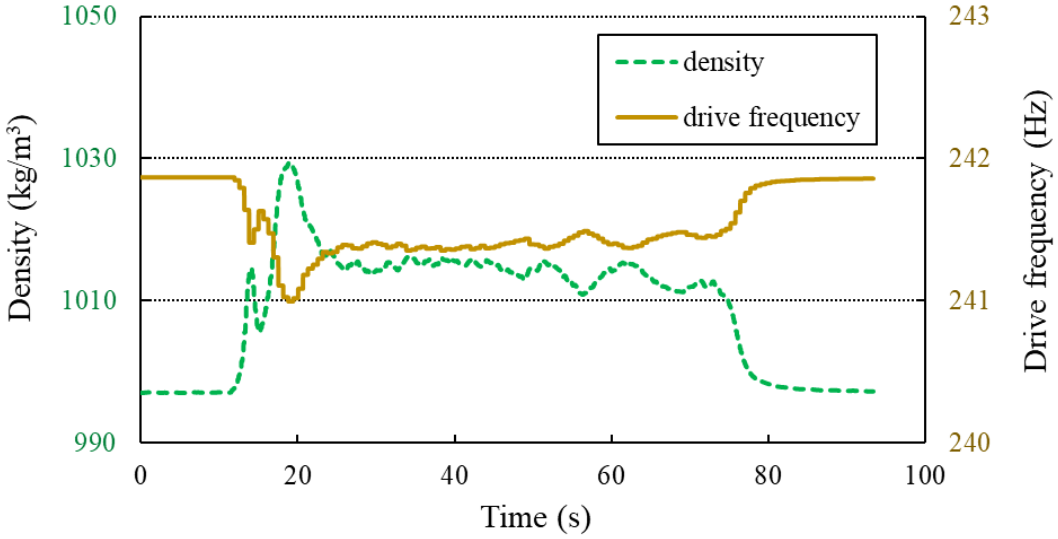

(c) Drive frequncy and density

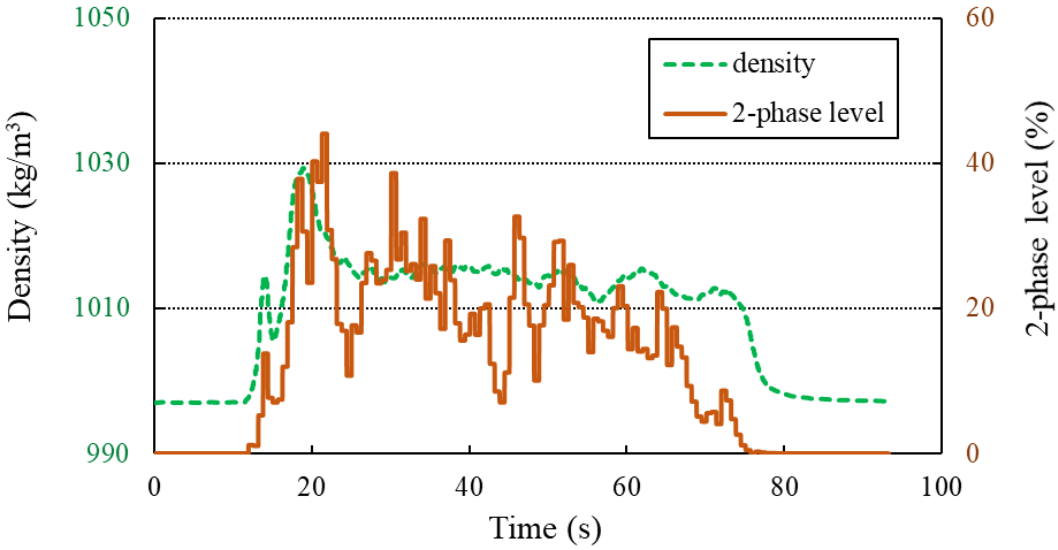

(d) 2-phase level and density

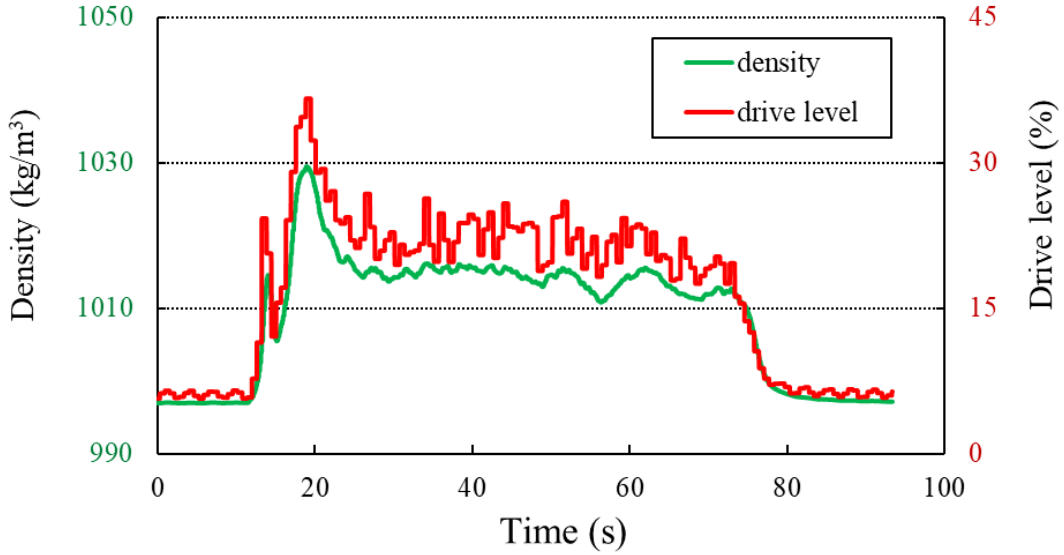

(e) Drive level and density

Figure 4.15 Typical curves of key parameters from CF1 (belly up) during batching at 12000 kg/h

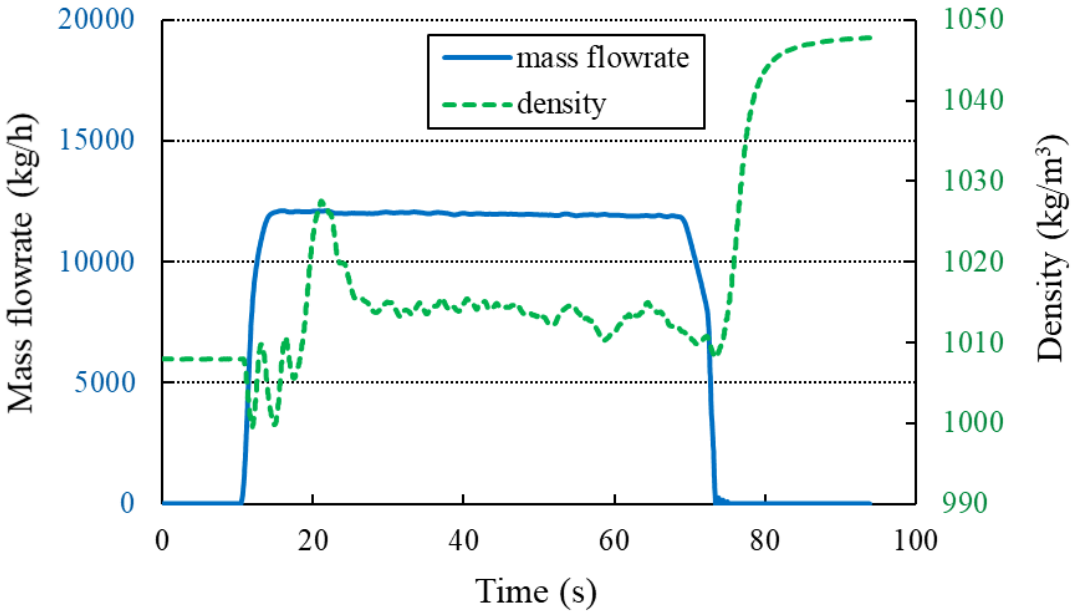

(a) Density and mass flowrate

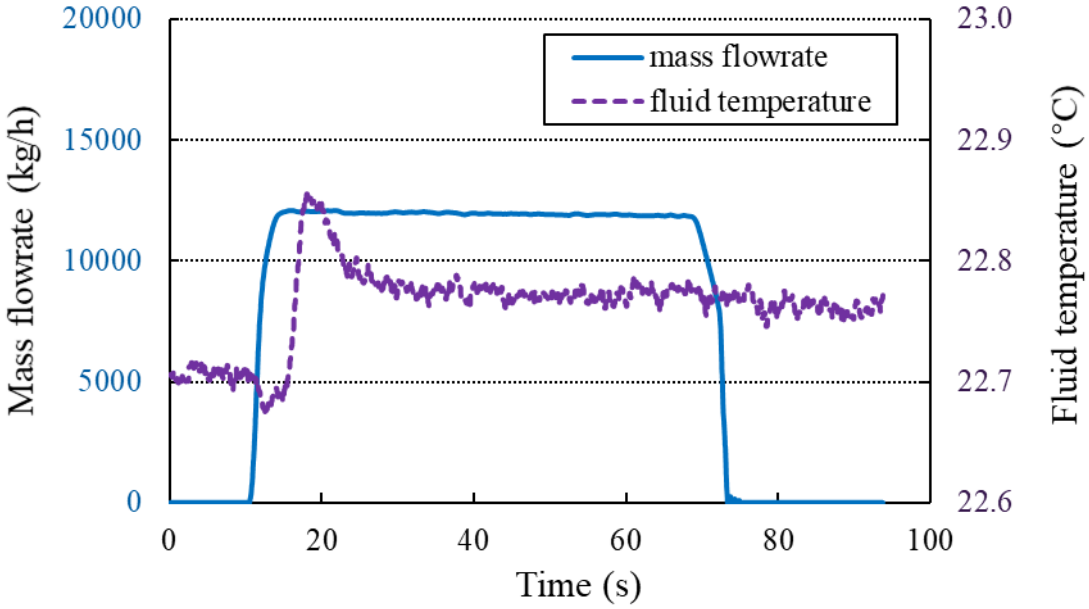

(b) Fluid temperature and mass flowrate

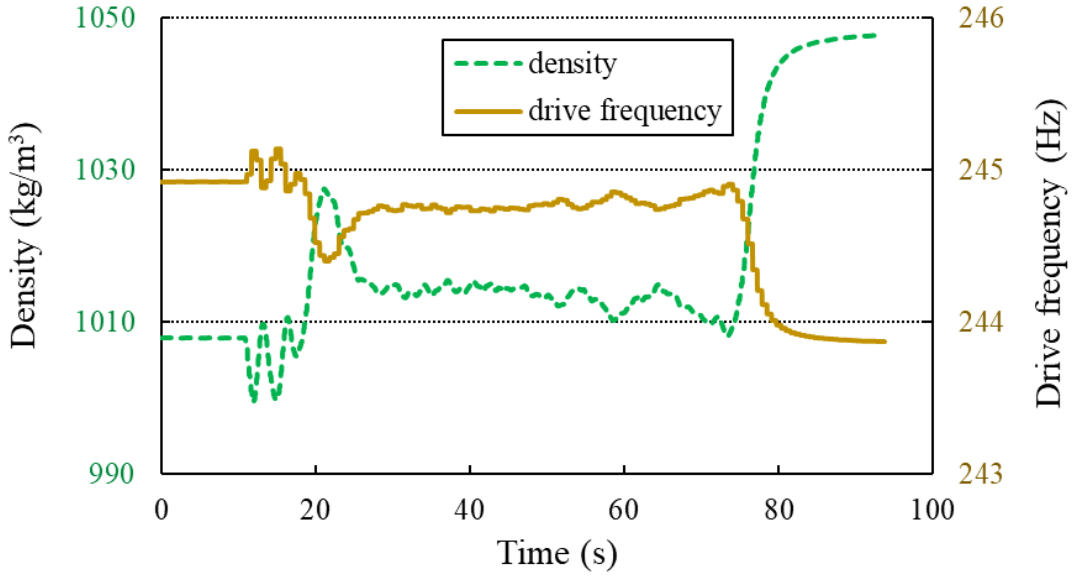

(c) Drive frequncy and density

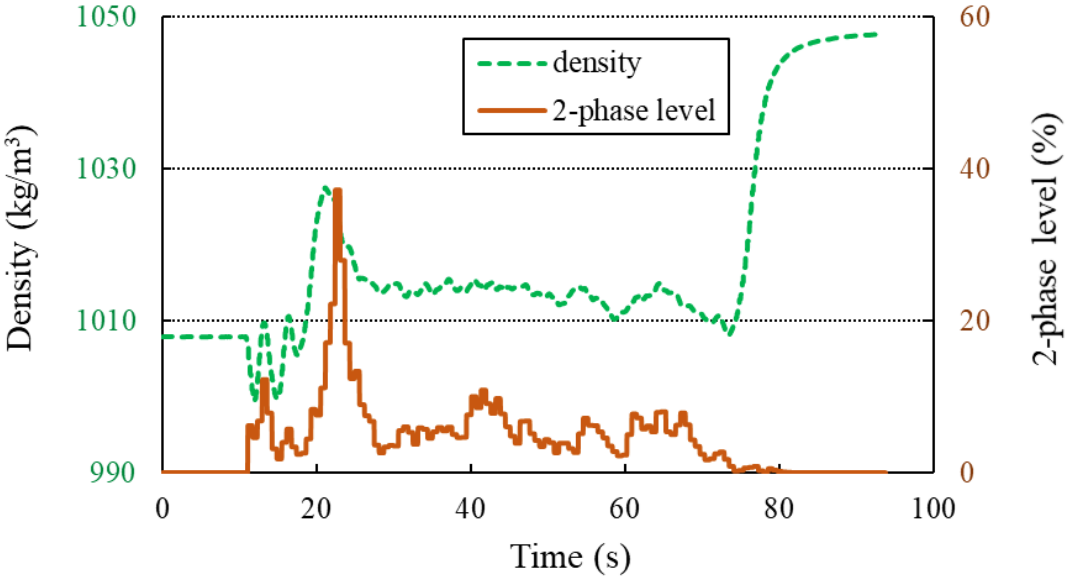

(d) 2-phase level and density

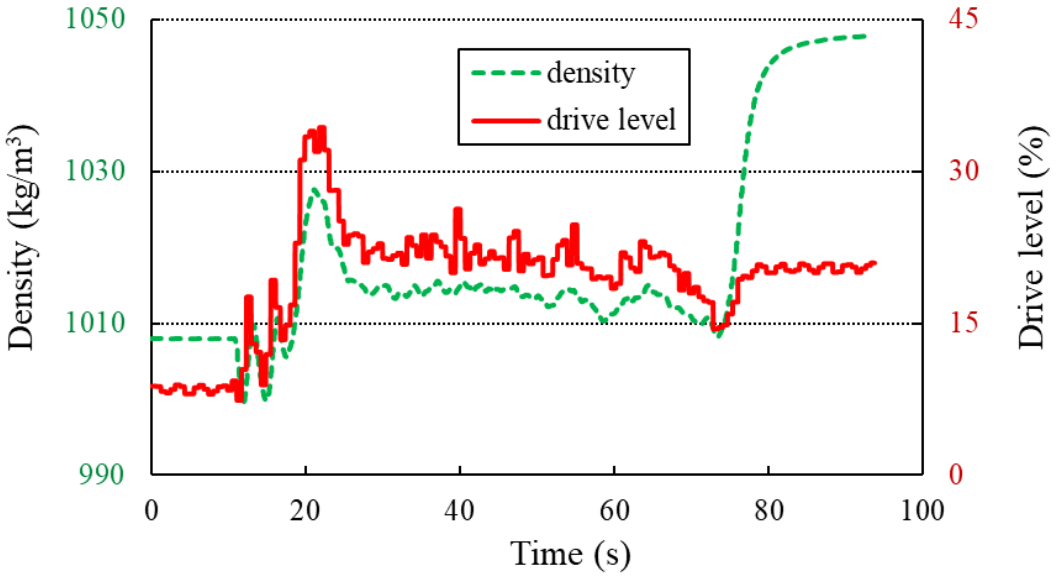

(e) Drive level and density

Figure 4.16 Typical curves of key parameters from CF2 (belly down) during batching at 12000 kg/h

4.4 Analysis of Original Errors

This section firstly presents the typical original error trends of Coriolis flowmeters with dilute slurry as the experimental results and then describes the basic regression analysis of the error trends.

4.4.1 Error Trends of Mass Flowrate

According to the experimental results from batching, the original mass flowrate error of the Coriolis flowmeters under test with dilute slurry are presented here. The mass flowrate errors ($E_{\dot{m}}$) of CF1 and CF2 are plotted against apparent SVF which is calculated from apparent density reading, as demonstrated in Figure 4.17 and Figure 4.18, respectively. Firstly, it illustrates that error trends of mass flowrate go into a negative direction, which agree with the theoretical analysis of the negative errors arising from decoupling effect. With more solids present in the liquid, the resulting errors become more noticeable. Secondly, the error trends show good linearity with the low and narrow range of SVF (within 4%). Thirdly, it can be identified that the mass flowrates slightly affect the behaviour of Coriolis flowmeters with slurry flow.

Generally, higher mass flowrate would produce less errors, which is consistent with the previous studies conducted on air-water two-phase flows [31]. Figure 4.18 (belly down) illustrates such influence of mass flowrate on measurement errors very well, whereas there is one exception to this rule in Figure 4.17 (belly up), in the situation of the lowest mass flowrate at 8200 kg/h. This exception would be attributable to the effect of other factors, such as the asymmetry errors associated with uneven sand distribution along the Coriolis tubes or the slight shift in flow regime when the flowrate becomes low, which can typically affect Coriolis flow metering under two-phase conditions.

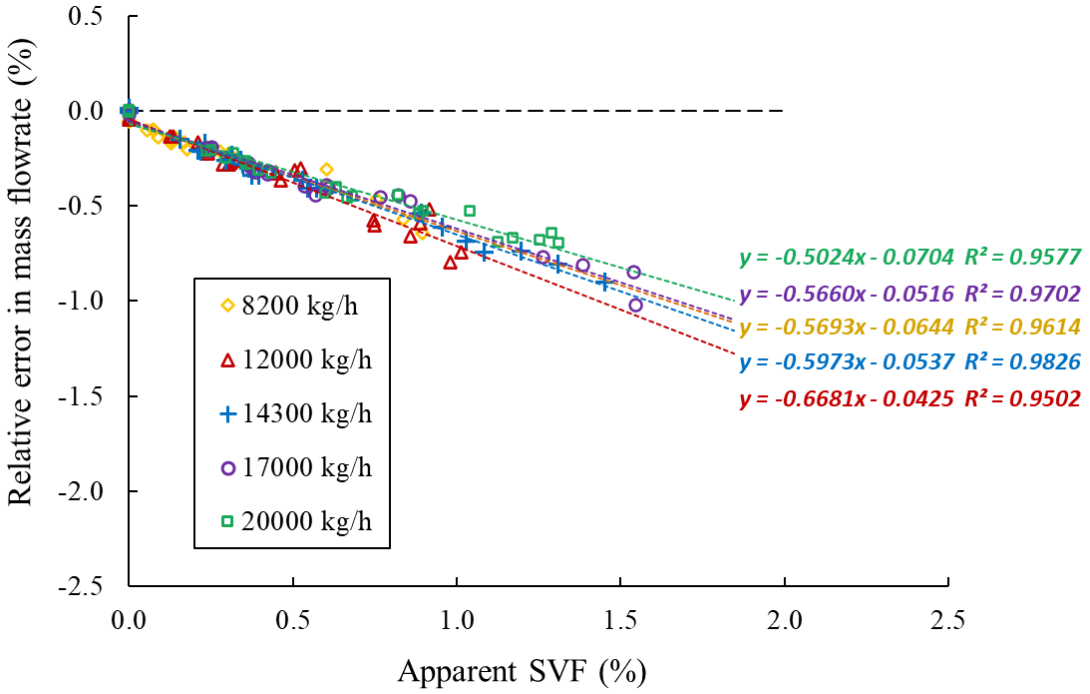

Figure 4.17 Original errors in mass flowrate against apparent SVF (with belly up, CF1)

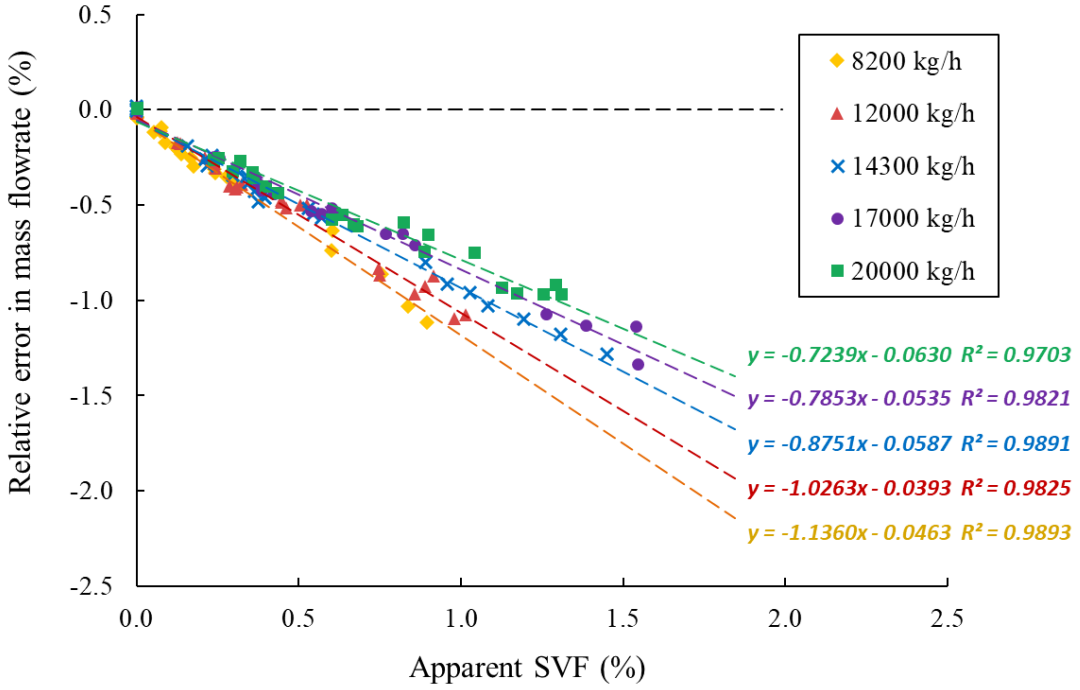

Figure 4.18 Original errors in mass flowrate against apparent SVF (with belly down, CF2)

The measurement performances of CF1 (belly up) and CF2 (belly down) are plotted together as shown in Figure 4.19, for a comparison of the installation effect. It can be found the errors with belly up are smaller than that with belly down, which suggests the

installation of belly up outperforms the belly down with dilute slurry flow. It is probably due to the resulting asymmetries from the uneven distribution of sand particles along the measuring tubes, which depends on the mounting orientation. The detailed explanation is as follows: if a Coriolis flowmeter is installed horizontally with its belly up, more sand tends to settle in the inlet due to the gravity effect, which would add extra damping on the inlet side, and consequently it causes additional positive errors in mass flowrate [86]. In contrast, the installation of belly down would create the accumulation of sand in the outlet, resulting in more damping imposed on the outlet as well as extra negative errors. As a result, when the belly is up, the additional positive errors due to asymmetry can cancel out a part of negative errors from decoupling effect, while placing belly down would lead to extra asymmetry negative errors. Therefore, the belly-up installation would produce smaller errors, compared with belly-down installation. Furthermore, in most cases such asymmetry errors would become more noticeable by lowering the mass flowrate wherein the slurry flow is less homogeneous.

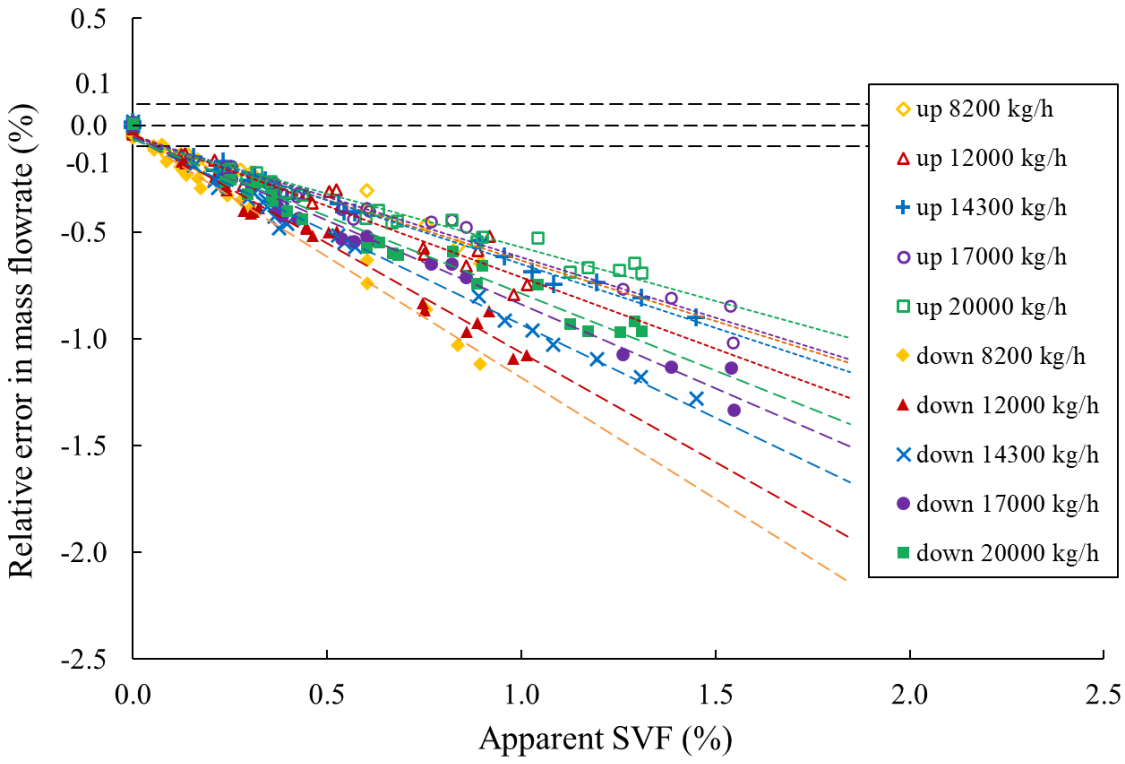

Figure 4.19 Original errors in mass flowrate against apparent SVF, belly up versus belly down

4.4.2 **Error Trends of Density**

Based on flow sampling results, the original density error (E_ρ) of CF1 with dilute slurry flow is plotted against apparent SVF ($\alpha_{s,app}$), as shown in Figure 4.20. If using reference SVF acquired from flow sampling over apparent SVF, the relationship of E_ρ and $\alpha_{s,ref}$ is displayed in Figure 4.21.

Firstly, negative error trends are clearly depicted in Figure 4.20 and Figure 4.21, from which it can be observed that the errors (absolute value) grow larger when more sand particles get entrained into the liquid. It can be concluded that it is the entrained solid particles that leads to the measurement errors in Coriolis flowmeters, and the errors are always negative under dilute slurry flow, attributable to decoupling effect.

Secondly, through comparison between Figure 4.17 and Figure 4.20, both of which are conducted on the same flowmeter (CF1), the density error trend is found close to the mass flowrate error trend. The experimental results agree with the theoretical analysis of phase decoupling effect suggesting that density error is equivalent to mass flowrate error.

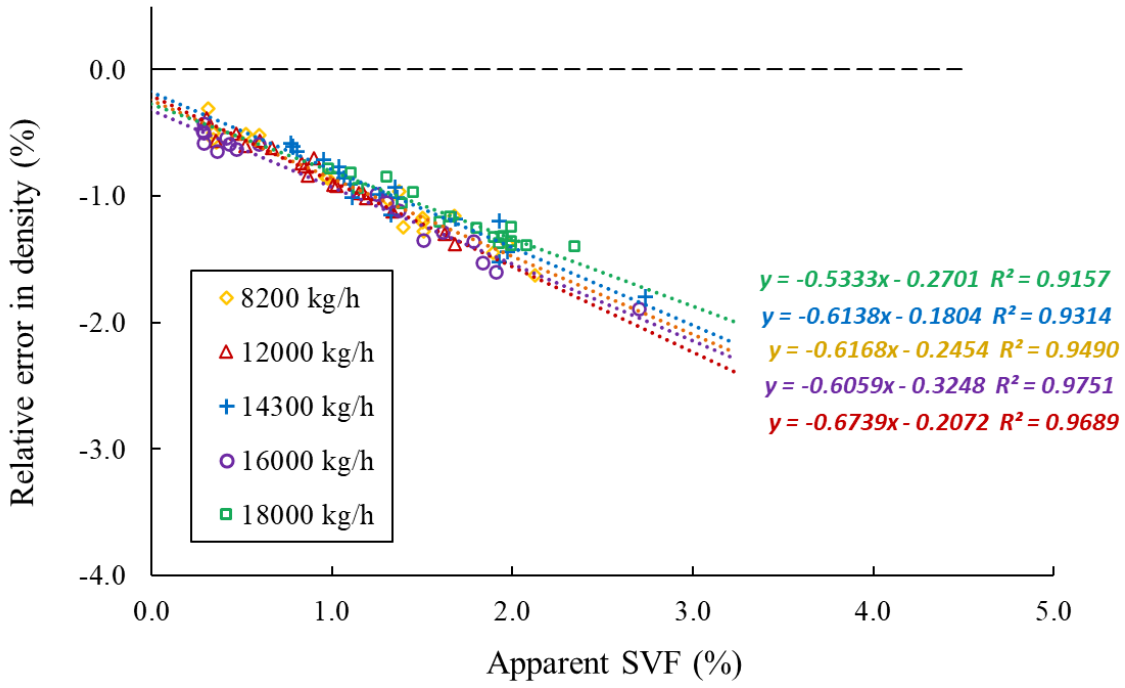

Figure 4.20 Original errors in density against apparent SVF (with belly up, CF1)

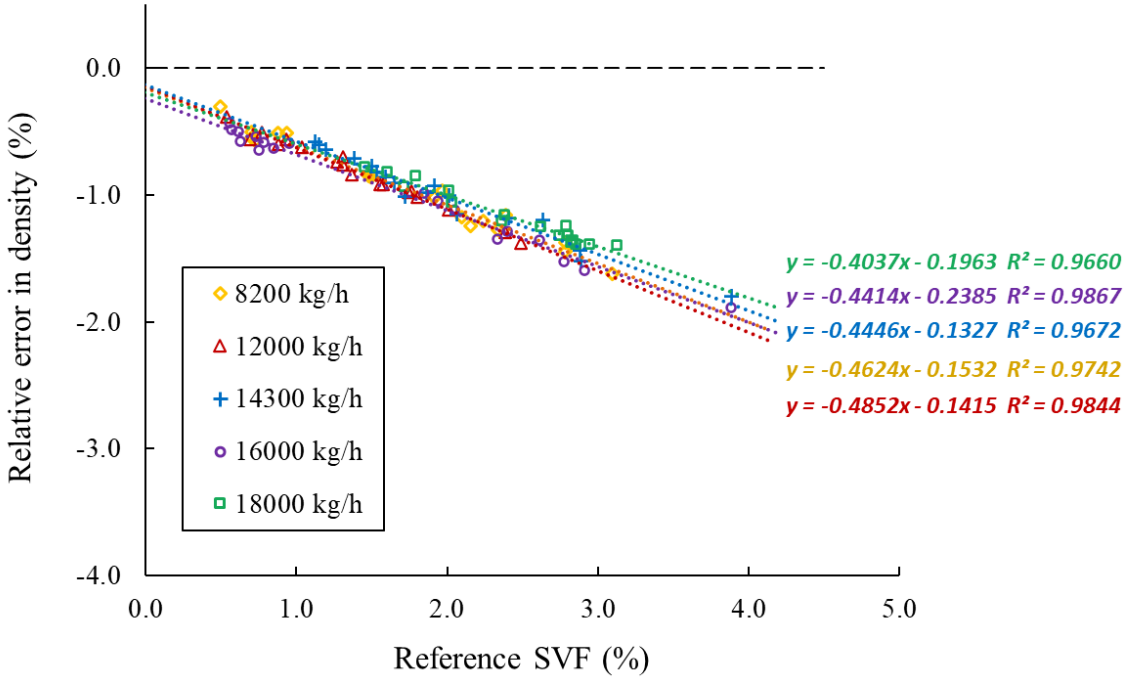

Figure 4.21 Original errors in density against reference SVF (with belly up, CF1)

4.4.3 **Regression Analysis of Original Errors**

In light of the original errors presented above, error trends of both mass flowrate and density demonstrate good linearity. For that reason, it is possible to correct the measurement errors of Coriolis meters occurred in dilute slurry flow using regression model. Linear least squares approach is applied to fit the experimental data. The linear relationship is written in a "slope-intercept" form with slope (K_1) together with vertical intercept (K_0), expressed in equation (4-34). Commonly R^2 is used to evaluate the goodness-of-fit.

$$Y = K_1 X + K_0 \tag{4-34}$$

Table 4.3 summarizes the relevant regression analysis results. Regarding mass flowrate errors, the regression lines drift slightly negatively from the initial zero point (0, 0), indicated by the small negative values of K_0. Through comparison between the slopes K_1 at different mass flowrates, it can be recognized that in most cases the curves usually become steeper by reducing mass flowrate, which means lower flowrates would tend to produce greater errors. In terms of density errors, K_0 drifts farther from zero point whilst R^2 decreases slightly compared with the outcomes from mass flowrate error, which suggests

fitting results in density are a bit worse than that in mass flowrate. It is believed that the limited volume of sand-water sample adversely affects the accuracy of flow sampling method. Over 200 kg slurry flow is batched for evaluation of mass flowrate errors while only 25 litres sample is collected for identification of density errors. For that reason, data fitting of mass flowrate errors is superior to that of density, and a small difference exists in the corresponding regression analysis results.

Table 4.3 Regression analysis results derived from mass flowrate and density errors

Meter under test	Mass flowrate (kg/h)	Y	X	K_1	K_0	R^2
CF1	8200	$E_{\dot{m}}$	$\alpha_{s,app}$	−0.5693	−0.0644	0.9614
CF1	12000	$E_{\dot{m}}$	$\alpha_{s,app}$	−0.6681	−0.0425	0.9502
CF1	14300	$E_{\dot{m}}$	$\alpha_{s,app}$	−0.5973	−0.0537	0.9826
CF1	17000	$E_{\dot{m}}$	$\alpha_{s,app}$	−0.5660	−0.0516	0.9702
CF1	20000	$E_{\dot{m}}$	$\alpha_{s,app}$	−0.5024	−0.0704	0.9577
CF2	8200	$E_{\dot{m}}$	$\alpha_{s,app}$	−1.1360	−0.0463	0.9893
CF2	12000	$E_{\dot{m}}$	$\alpha_{s,app}$	−1.0263	−0.0393	0.9825
CF2	14300	$E_{\dot{m}}$	$\alpha_{s,app}$	−0.8751	−0.0587	0.9891
CF2	17000	$E_{\dot{m}}$	$\alpha_{s,app}$	−0.7853	−0.0535	0.9821
CF2	20000	$E_{\dot{m}}$	$\alpha_{s,app}$	−0.7239	−0.0630	0.9703
CF1	8200	E_{ρ}	$\alpha_{s,app}$	−0.6168	−0.2454	0.9490
CF1	12000	E_{ρ}	$\alpha_{s,app}$	−0.6739	−0.2072	0.9689
CF1	14300	E_{ρ}	$\alpha_{s,app}$	−0.6138	−0.1804	0.9314
CF1	16000	E_{ρ}	$\alpha_{s,app}$	−0.6059	−0.3248	0.9751
CF1	18000	E_{ρ}	$\alpha_{s,app}$	−0.5333	−0.2701	0.9157
CF1	8200	E_{ρ}	$\alpha_{s,ref}$	−0.4624	−0.1532	0.9742
CF1	12000	E_{ρ}	$\alpha_{s,ref}$	−0.4852	−0.1415	0.9844
CF1	14300	E_{ρ}	$\alpha_{s,ref}$	−0.4446	−0.1327	0.9672
CF1	16000	E_{ρ}	$\alpha_{s,ref}$	−0.4414	−0.2385	0.9867
CF1	18000	E_{ρ}	$\alpha_{s,ref}$	−0.4037	−0.1963	0.9660

According to the results given by Table 4.3, regression model is established to predict and correct the original errors of Coriolis flowmeters. The predicted results from regression model are compared with the actual experimental data for evaluating the performance of

regression model. After the corrections on the original errors (presented in Figures 4.17, 4.18, 4.20 and 4.21), the differences between original errors and corrected outcomes are displayed in Figure 4.22 to Figure 4.25, respectively. In terms of mass flowrate, 98% corrections on mass flowrate errors fall within ±0.1% error (difference) range as shown in Figures 4.22 and 4.23, which can meet the claimed measurement accuracy of the Coriolis flowmeters under test again. The compensation on density errors behaves slightly worse. If using reference SVF, 96% corrected data drop within the range of ±0.1% (as illustrated in Figure 4.25), while only 82% data can be compensated down to ±0.1% on the basis of apparent SVF (see Figure 4.24). It can be interpreted that two terms involved in the corrections in Figure 4.24, including apparent density and apparent SVF, are both suffered from decoupling effect as well as uncertainty in flow sampling tests, which yields the worst performance among all error corrections.

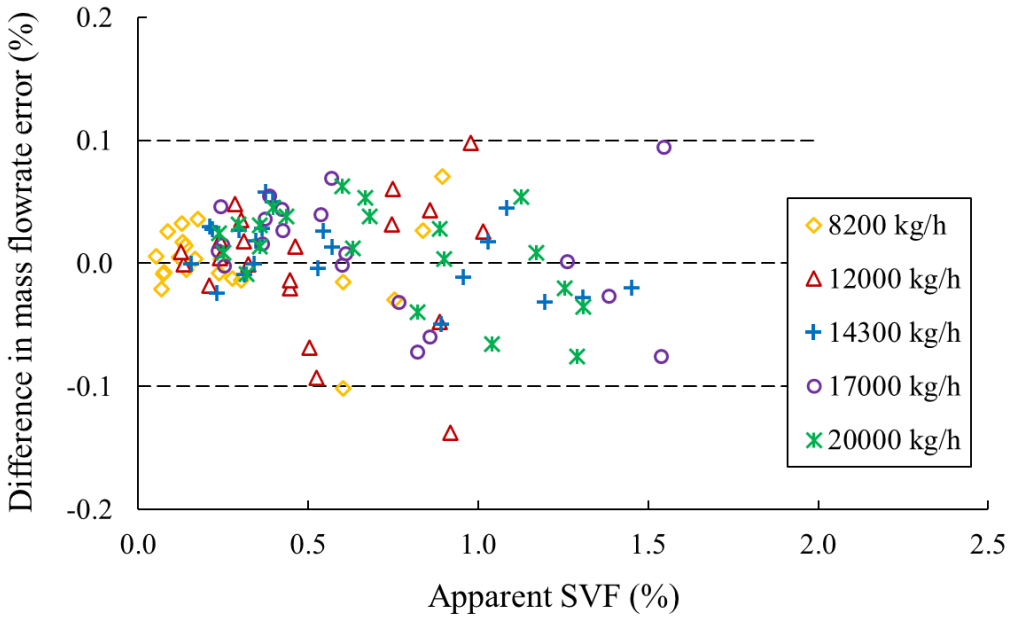

Figure 4.22 Differences in mass flowrate errors based on apparent SVF from regression model (with belly up, CF1)

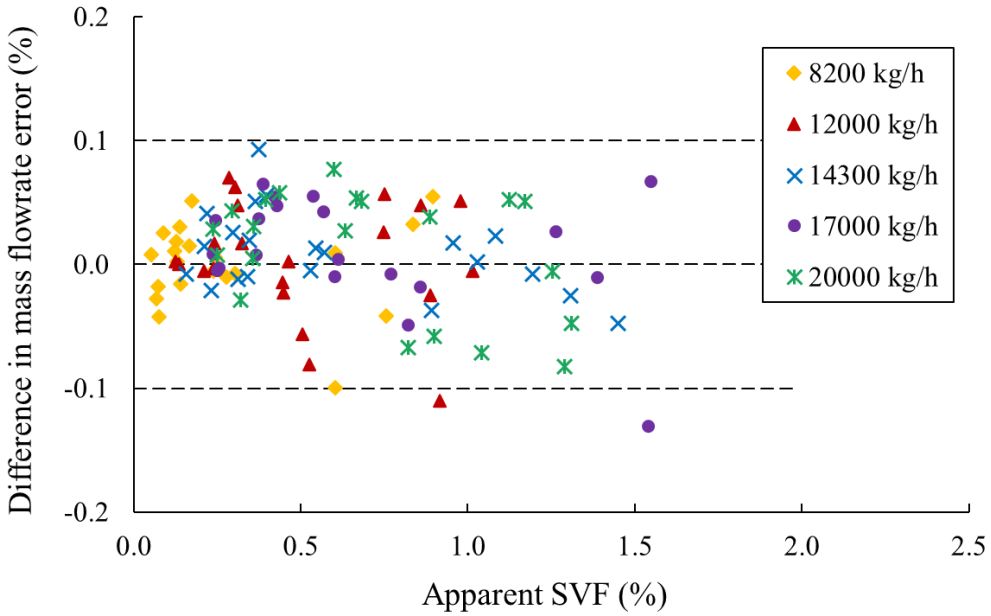

Figure 4.23 Differences in mass flowrate errors based on apparent SVF from regression model (with belly down, CF2)

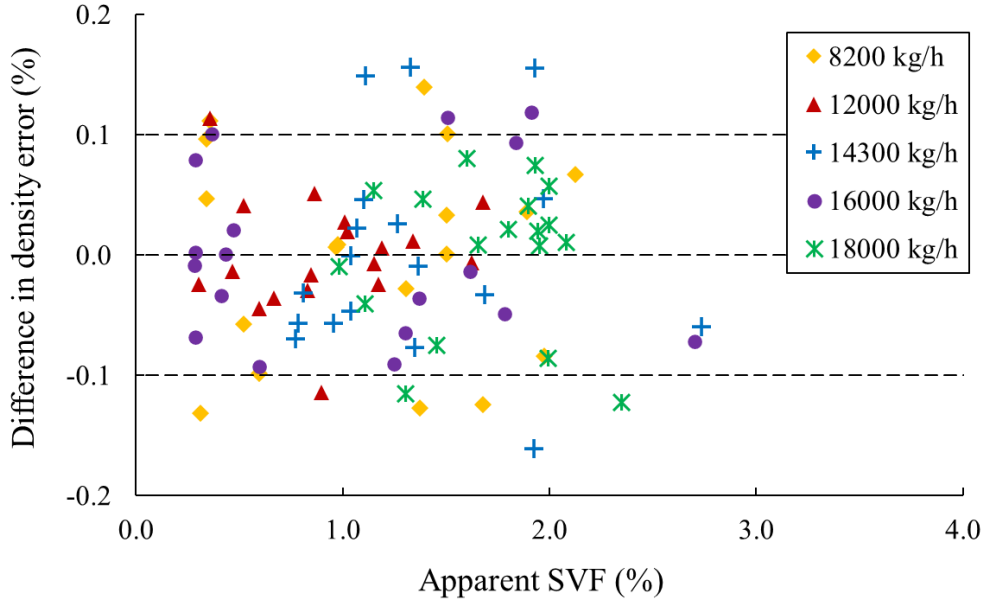

Figure 4.24 Differences in density errors based on apparent SVF from regression model (with belly up, CF1)

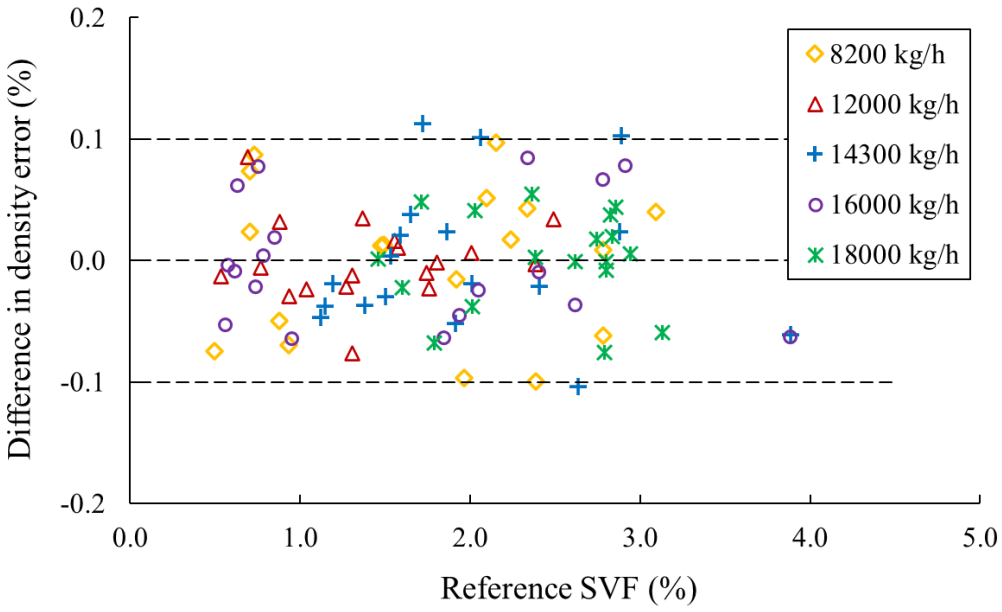

Figure 4.25 Differences in density errors based on reference SVF from regression model (with belly up, CF1)

To conclude, the results have illustrated that the typical errors trends of Coriolis flow metering can be well fitted by the regression analysis with satisfactory R^2 value. It suggests the excellent potential of modelling to predict and compensate the decoupling effect on Coriolis flow metering with dilute slurry flow.

4.5 Error Compensation by Analytical Modelling

4.5.1 **Compensation of Decoupling Effect**

Section 4.4.3 illustrates the good potential to compensate decoupling effect by using established regression model. However, it is impractical to carry out experiments covering all test conditions in terms of different mass flowrates and sand concentrations. In other words, owing to the limitations as well as costs in collecting massive experimental data for establishing regression models, the analytical model would be a practical and promising tool for compensating the measurement errors of Coriolis flowmeters with slurry flow on the basis of the underlying physical mechanisms.

According to the theoretical analysis in Section 4.2, decoupling effect is the major error source degrading the measurement accuracy of Coriolis flowmeters with slurry applications, while the compressibility effect can be neglected. Thus, the existing

decoupling theory is adopted for analytical modelling of Coriolis flow metering with slurry flow. For sand-water mixtures, sand particles and water can be both regarded as inviscid phases. Hence, the basic decoupling theory in inviscid fluid is applicable for this case (Section 4.2.1.2). As illustrated in equation (4-18), estimation of decoupling error requires three parameters, including water density, sand density, and actual (reference) SVF. Liquid density as well as solid density can be considered as constants under certain process conditions, which can be typically obtained through sampling. The changes of water and sand densities can be compensated when fluid temperature and pressure deviate from the initial (reference) conditions during sampling. Nevertheless, it is always practically difficult to obtain actual SVF as reference in situ. Supplementary apparatus (e.g. densimeter) or a second technique (e.g. ultrasonic attenuation) is typically required so as to get the information of actual SVF, which increases the cost, complexity as well as installation space. Due to the fact that apparent density reading from Coriolis flowmeters is always available, it will be practically beneficial if decoupling errors can be compensated based on apparent SVF which is directly derived from apparent density, instead of actual SVF, making it more accessible to the end users when employing Coriolis flowmeters in real-world slurry applications.

In light of the decoupling theory, apparent density reading provided by Coriolis flowmeters is,

$$\rho_{m,app} = \rho_l\,(1 - F\,\alpha_s) + \rho_s\,F\,\alpha_s = \rho_l + (\rho_s - \rho_l)\,F\,\alpha_s \tag{4-35}$$

The relationship between $\rho_{m,app}$ and α_s can be derived from the above equation,

$$\alpha_s = \frac{\rho_{m,app} - \rho_w}{(\rho_s - \rho_w)\,F}\,100\% \tag{4-36}$$

According to equations (4-30) and (4-36), it is straightforward that

$$\alpha_s = \frac{\alpha_{s,app}}{F} \tag{4-37}$$

The equation above illustrates a direct link between actual SVF (α_s) and apparent SVF ($\alpha_{s,app}$) through decoupling ratio (F). It is practically useful for inferring actual SVF from apparent density reading (internal parameter) from Coriolis flowmeters.

By substituting equation (4-37) into the original formula of estimation of decoupling error given by equation (4-17), the decoupling error ($E_{d,\dot{m}}$) can be expressed against apparent SVF ($\alpha_{s,app}$).

$$E_{d,\dot{m}} = \frac{\rho_l \frac{\alpha_{s,app}}{F}(1-F)+\rho_s \frac{\alpha_{s,app}}{F}(F-1)}{\rho_l\left(1-\frac{\alpha_{s,app}}{F}\right)+\rho_s \frac{\alpha_{s,app}}{F}} = \frac{(\rho_s-\rho_l)\,\alpha_{s,app}\,(F-1)}{\rho_l\,(F-\alpha_{s,app})+\rho_s\,\alpha_{s,app}}\ 100\% \qquad (4\text{-}38)$$

As illustrated by equation (4-38), the measurement errors of Coriolis flowmeters can be predicted and compensated according to its apparent readings (internal parameters) along with other known constants (ρ_s, ρ_w), without requiring the information of reference (e.g. actual SVF). The advantage of the error compensation method is that without supplementary device or apparatus, Coriolis flowmeters are able to provide accurate mass flow metering with slurry flow by using a simple analytical model.

Since the density error ($E_{d,\rho}$) is supposed to be equivalent to the mass flowrate error term ($E_{d,\dot{m}}$), the analysis of density error is not repeated again. Figure 4.26 depicts how decoupling error changes with apparent SVF. Due to the consideration of the applicable range of SVF of decoupling theory, the theoretical decoupling error is plotted against apparent SVF increasing from 0 to 10% shown in Figure 4.26 (a), whilst Figure 4.26 (b) depicts a closer look of decoupling error against a narrow range within 3%, which is the maximum level of apparent SVF in the experiments of this study. In addition, curve fitting is performed on the decoupling error trends against apparent SVF.

It can be observed that curve fitting performs outstandingly well, indicated by the high value of R^2 very close to 1 (see Figure 4.26). The results suggest that when apparent SVF range is limited within 3%, the relationship between decoupling error and apparent SVF can be assumed as linear, as shown in Figure 4.26 (b). The linear fitting results yield a slope (k_1) at −1.7084 and an intercept (k_0) at −0.0879 which is a tiny value drifted slightly negatively from the initial point (0,0). Comparison with the regression results listed in Table 4.3, the basic analytical model produces steeper error curves than actual experimental results, which suggests the existing decoupling theory would over-estimate decoupling errors than true values.

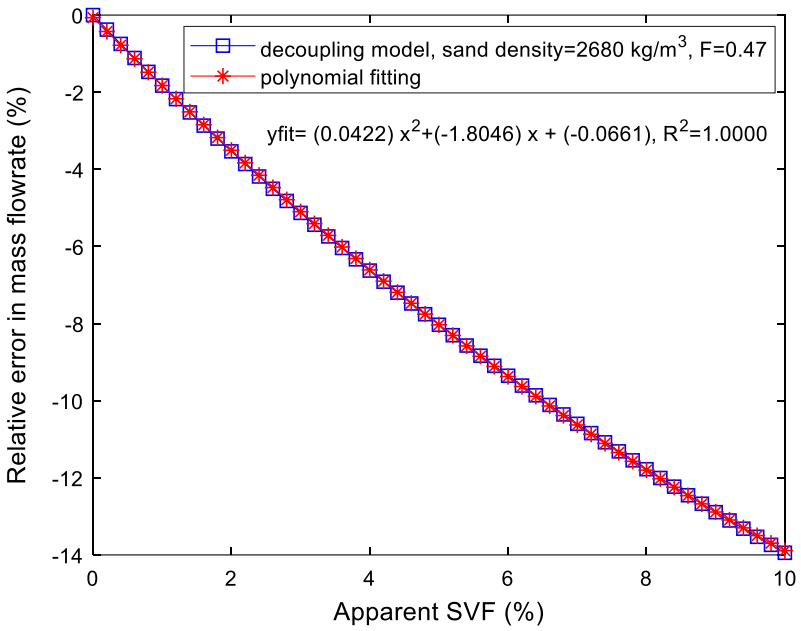

(a) Decoupling error against apparent SVF from 0 to 10%

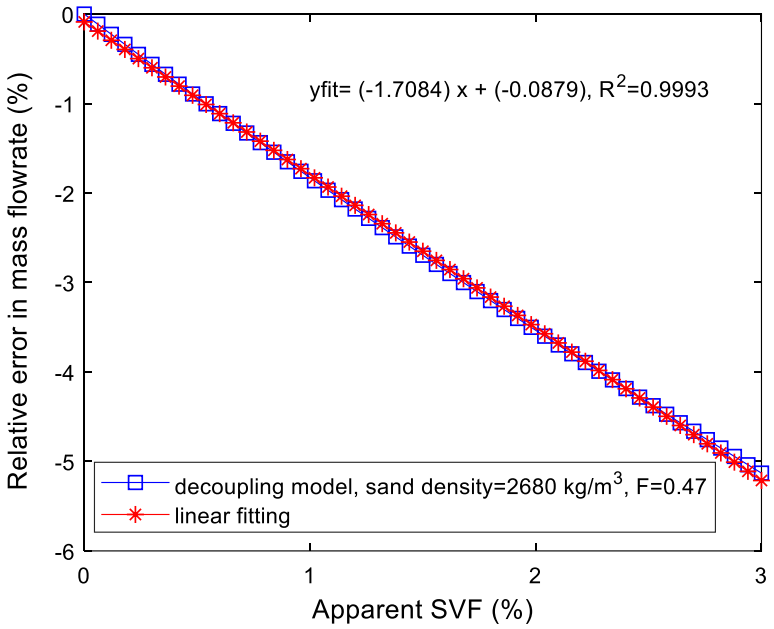

(b) Decoupling error against apparent SVF from 0 to 3%

Figure 4.26 Decoupling error against apparent SVF from basic analytical model

4.5.2 **Comparisons between Model Prediction and Experimental Results**

The performance of the basic analytical model derived from existing decoupling theory is evaluated in this section. The comparisons between experimental results and model

prediction are displayed in Figure 4.27 to Figure 4.29. It can be discovered that the basic analytical model cannot accurately predict the measurement performance of Coriolis flowmeters with slurry flow. The actual errors (absolute values) are less than the model prediction, in terms of both mass flowrate and density measurement. And the deviations between the outcomes from modelling and experiments become more noticeable with the increasing SVF.

The over-estimation from decoupling theory can be attributable to the assumptions for modelling wherein the entrained particles are assumed to be non-interacting, far away from the tube and in ideal spherical shapes. However, in reality, the solid particles cannot move freely within the Coriolis tubes. The movements of particles would be inevitably hindered by the contacts with adjacent particles and restricted by the container. As the solid-liquid decoupled motions cannot be fully developed, it causes the actual measurement errors (referring to the absolute values) smaller than predicted errors from modelling. When the content of solid particles is growing, the particle-particle and particle-tube interactions would become more intensive and frequent. As a result, such over-estimation from decoupling theory would be greater with higher SVF.

Moreover, through comparison between Figure 4.27 and Figure 4.28 concerning the effect of installation orientation, it can be noticed that the experimental data under the scenario of belly down (Figure 4.28) is relatively closer to the model prediction. The reason is that the installation of belly down would bring additional negative asymmetry errors, superimposed on the phase decoupling effect, which leads to greater negative measurement errors of CF2. Furthermore, although mass flowrate would affect the measurement errors under slurry flow, the resulting differences are relatively small in the experiment results. It is probably because that there is no significant change in solid phase distribution or flow pattern throughout the experiments, owing to the low and narrow range of SVF retained during tests. Hence, the influence of mass flowrate can be neglected in the following improvements on the basic analytical model.

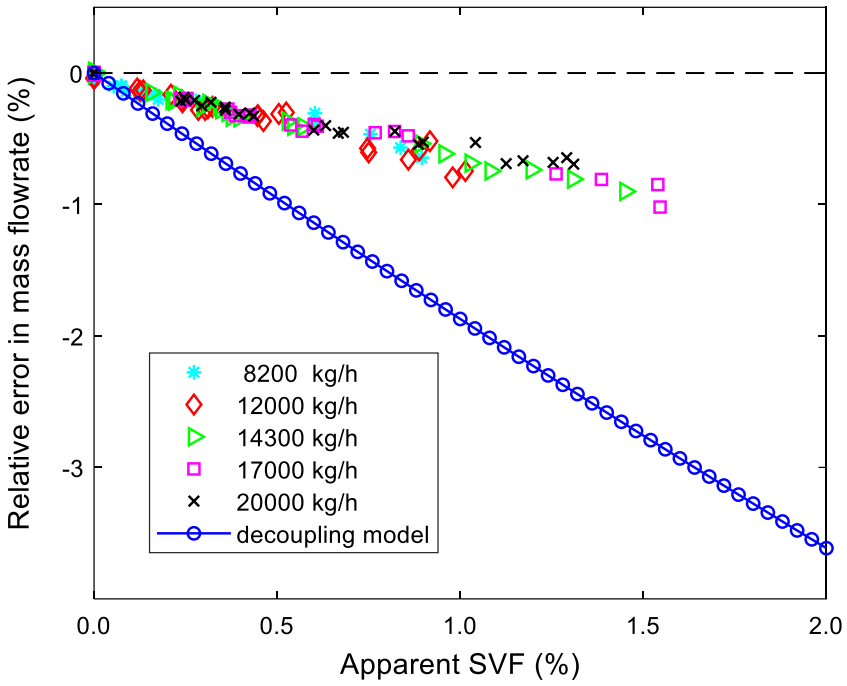

Figure 4.27 Comparison between actual error in mass flowrate and prediction from basic analytical model (with belly up, CF1)

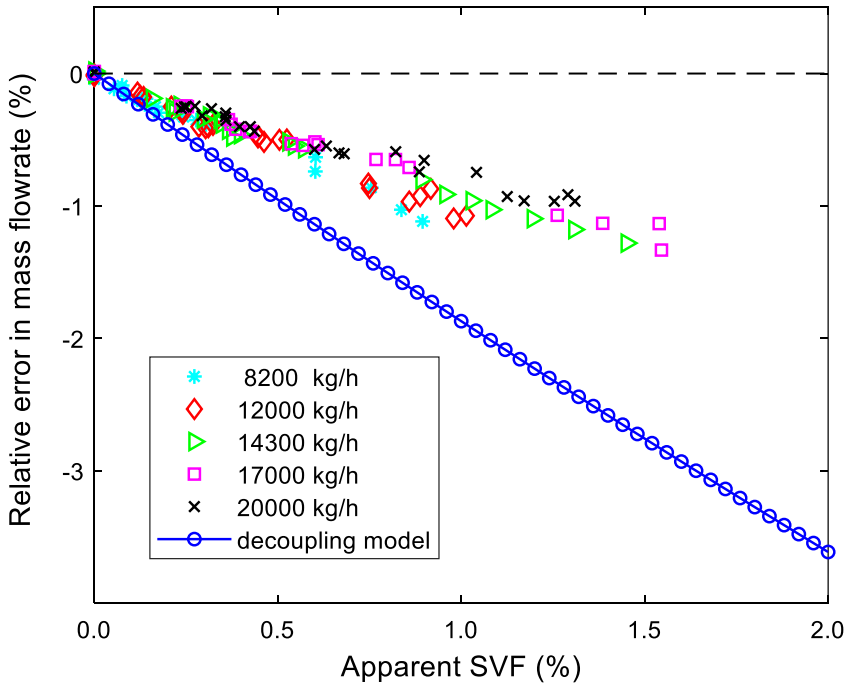

Figure 4.28 Comparison between actual error in mass flowrate and prediction from basic analytical model (with belly down, CF2)

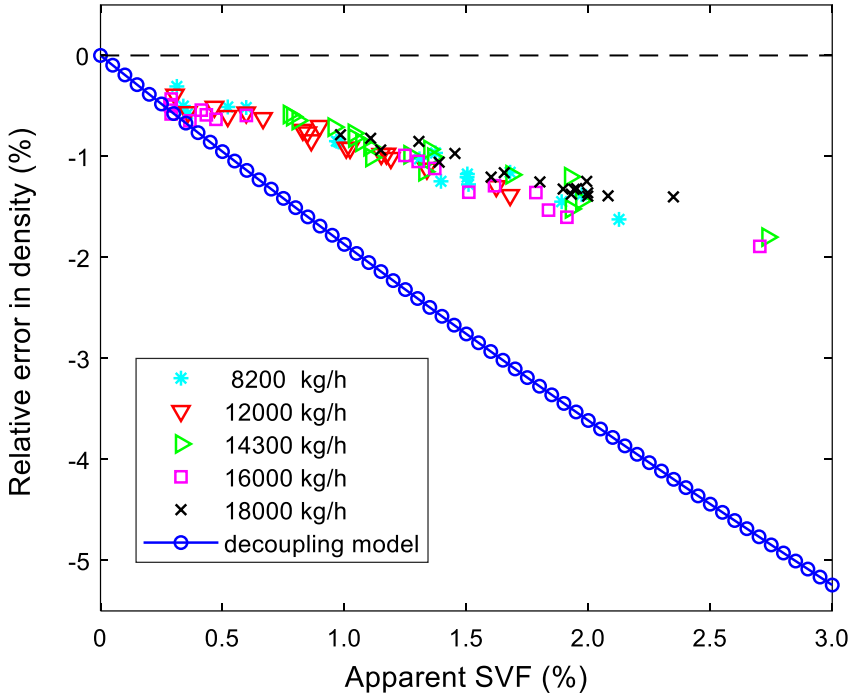

Figure 4.29 Comparison between actual error in density
and prediction from basic analytical model (with belly up, CF1)

4.5.3 **Improvement on the Basic Analytical Model**

Since the existing decoupling theory is not good enough to predict the actual measurement errors of Coriolis flowmeters with dilute slurry flow, appropriate compensation should be given in order to seek improvements. As presented above, the deviations between the experimental results and model prediction are primarily owing to the neglected particle-particle and particle-tube interactions in modelling. The phase interactions can be affected by a range of factors, including the properties of solids (e.g. grain size and shape), liquid characteristics (e.g. liquid viscosity), two-phase flow conditions (e.g. flowrate, flow regime and solid concentration) and the relevant features of Coriolis flowmeters (e.g. tube geometry, meter size, Coriolis drive frequency, meter installation).

It is practically difficult to develop a full compensation on decoupling effect covering all the relevant factors, which needs massive experimental data under various test conditions. Among these factors, three factors have been involved in the experimental work of this study, including SVF (solid volume fraction), mass flowrate along with two different installation orientations of meters (horizontally belly up and belly down). According to the

experimental results, SVF can be identified as one of the most dominant and common factors. Besides, the influence of meter installation is also found quite important. Hence, in this section, the improvements are conducted on two scenarios, belly up and belly down, separately. As the differences between the original measurement errors at different mass flowrates are negligible small, the effect of mass flowrate is not considered in the following compensation of the decoupling effect on Coriolis flow metering.

Essentially the decoupling ratio is the key to predict the decoupling error of Coriolis flowmeters under two-phase flow conditions. As stated in equation (4-13), the decoupling ratio (F) in the basic inviscid case is a function of the phase densities (solid density and liquid density). However, under real-world process conditions, the actual decoupling ratio also depends on a series of factors, affected by the solid-liquid interactions. Here a semi-empirical formula is proposed by introducing a correction term (F'),

$$F' = C_F\, F \tag{4-39}$$

where F' refers to the corrected decoupling ratio, F is the original decoupling ratio, C_F is an empirical coefficient which can be determined from the differences between modelling prediction and actual experimental results.

The corrected F' is used to replace the original F in equation (4-17), and then the estimation of decoupling error can be modified accordingly,

$$E_{d,\dot{m}} = \frac{(\rho_s - \rho_l)\,\alpha_s\,(F'-1)}{\rho_l\,(1-\alpha_s)+\rho_s\,\alpha_s}\ 100\% \tag{4-40}$$

$$F < F' < 1 \tag{4-41}$$

Since the decoupling theory would over-estimate the actual measurement errors (referring to the absolute values), a positive correction term should be introduced. The criteria here is that after correction, F' should be larger than F (moving closer to unity "1"). Through iterative calculation, the empirical constant C_F is estimated to be 1.5182 in the situation of belly up and 1.3743 with belly down. Thus, a semi-empirical analytical model is established so as to compensate the impact of the particle-particle and particle-tube interactions being ignored in the original model.

To validate the proposed semi-empirical analytical model, the prediction results from the improved model are plotted against the actual experimental data, shown in Figure 4.30 and Figure 4.31, corresponding to the scenarios of belly up and belly down, respectively. Accordingly, the differences between model prediction and experimental data are displayed in Figure 4.32 and Figure 4.33. These differences can be regarded as the remaining errors after the compensation using the improved analytical model.

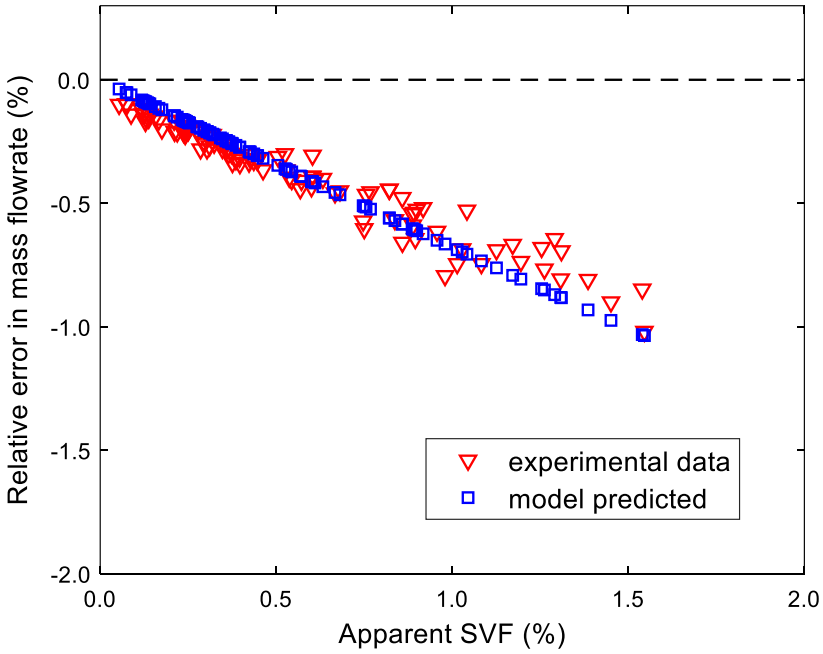

Figure 4.30 Comparison between actual error in mass flowrate and prediction from improved analytical model (with belly up, CF1)

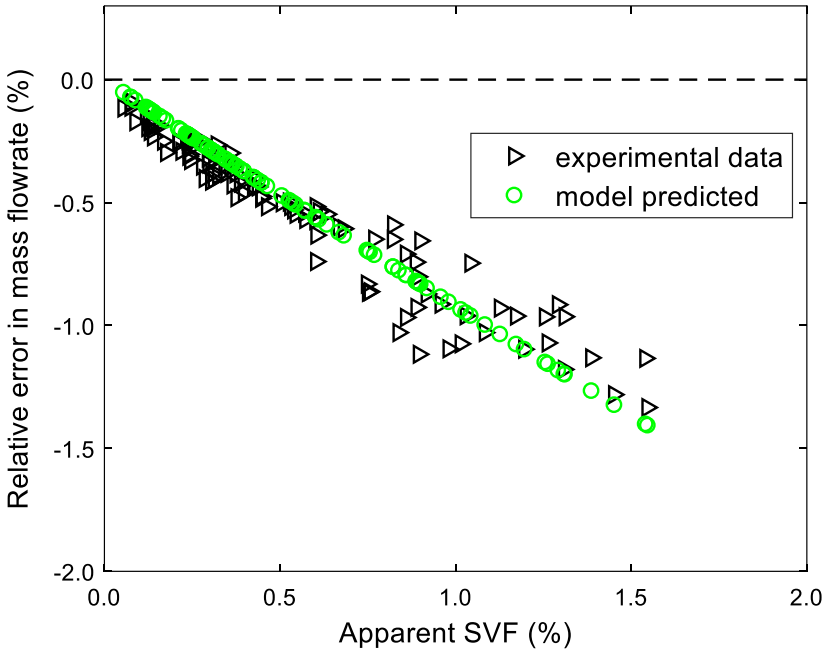

Figure 4.31 Comparison between actual error in mass flowrate and prediction from improved analytical model (with belly down, CF2)

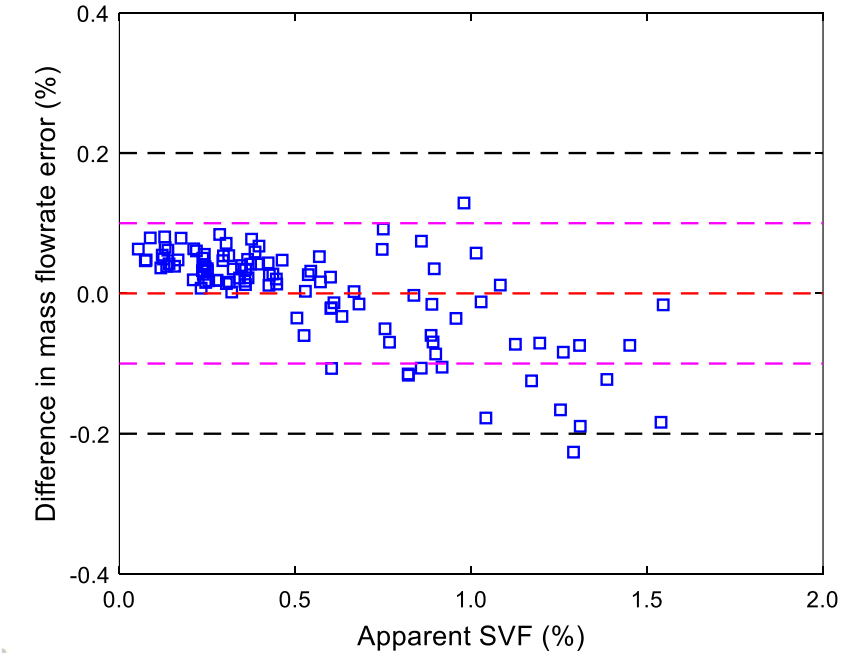

Figure 4.32 Differences in mass flowrate errors based on apparent SVF from improved analytical model (with belly up, CF1)

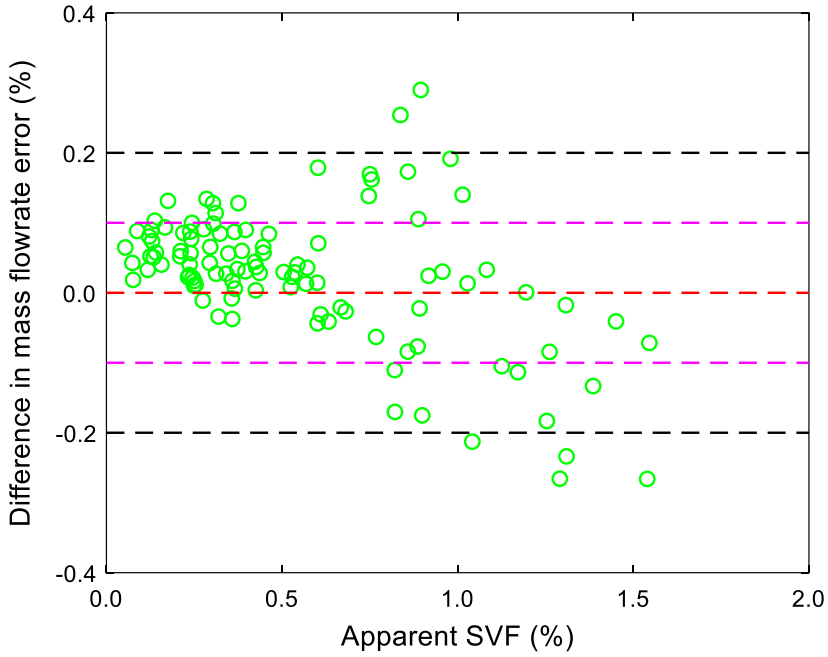

Figure 4.33 Differences in mass flowrate errors based on apparent SVF from improved analytical model (with belly down, CF2)

Regarding the mass flowrate errors collected with belly up installation (shown in Figure 4.32), the improved analytical model yields less than ±0.1% difference for 88% outcomes, and 99% prediction fall within ±0.2% deviation range. In the case of belly down, given in Figure 4.33, 81% correction can achieve less than ±0.1% deviation range, and 94% outcomes are below ±0.2%. The satisfactory outcomes indicate the feasibility of applying Coriolis flowmeters incorporating a semi-empirical analytical model for dilute slurry flow metering. Although limited factors are considered for compensating solid-liquid interactions being ignored in the decoupling theory, this work can provide a general methodology so as to determine a semi-empirical model for predicting and compensating errors of Coriolis flowmeters for two-phase flow metering.

Besides, regarding density measurement, the same methodology as described above is adopted to establish an improved model based on the actual experimental data of density errors. According to the differences between the prediction from the basic analytical model and the experimental results from flow sampling with CF1 (belly up), the empirical constant C_F is estimated to be 1.4555. The performance of the improved analytical model for density measurement is further evaluated, as depicted in Figure 4.34 and Figure 4.35. After correction, the improved analytical model yields less than ±0.2% difference for 82%

outcomes, and all prediction fall within ±0.4% deviation range. Compared with the results from model prediction for mass flowrate measurement (Figure 4.32 and Figure 4.33), the remaining measurement errors in density are a bit larger (Figure 4.35). In other words, the semi-empirical model performs slightly worse in errors compensation in density than that in mass flowrate. The reason is believed to be the less accurate experimental data in density which are acquired from the flow sampling tests. As explained above, since the measurement errors in mass flowrate and density are identified by using two different methods, the experimental data in mass flowrate are found more accurate than density data. Apart from the influence of different experimental methods, another possible cause can be the variation of density during each test run. Furthermore, regarding the generality of the analytical model presented in this study, it should be noted that the corrections of measurement errors in mass flowrate and density are sharing the same principle which is based on the decoupling effect theory. The empirical coefficient C_F is obtained from the experimental data of the original measurement errors of Coriolis flowmeters. Thus C_F would vary with a range of factors, such as the flow conditions (including mass flowrate, SVF, solid particle size, solid particle density, solid particle shape, liquid carrier density, liquid viscosity), pipe orientation, Coriolis tube geometry (shape, size) as well as the installation of Coriolis flowmeters.

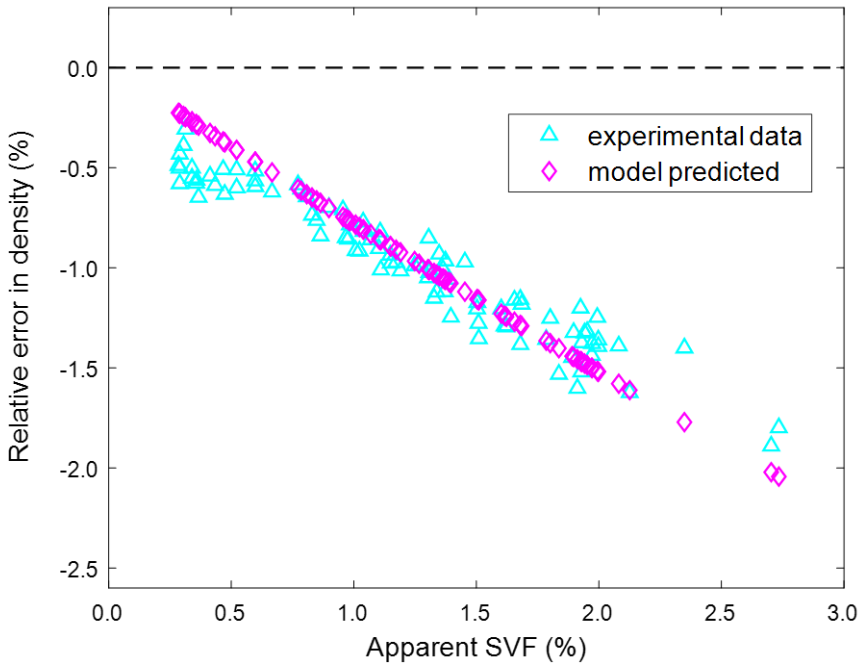

Figure 4.34 Comparison between actual error in density and prediction from improved analytical model (with belly down, CF1)

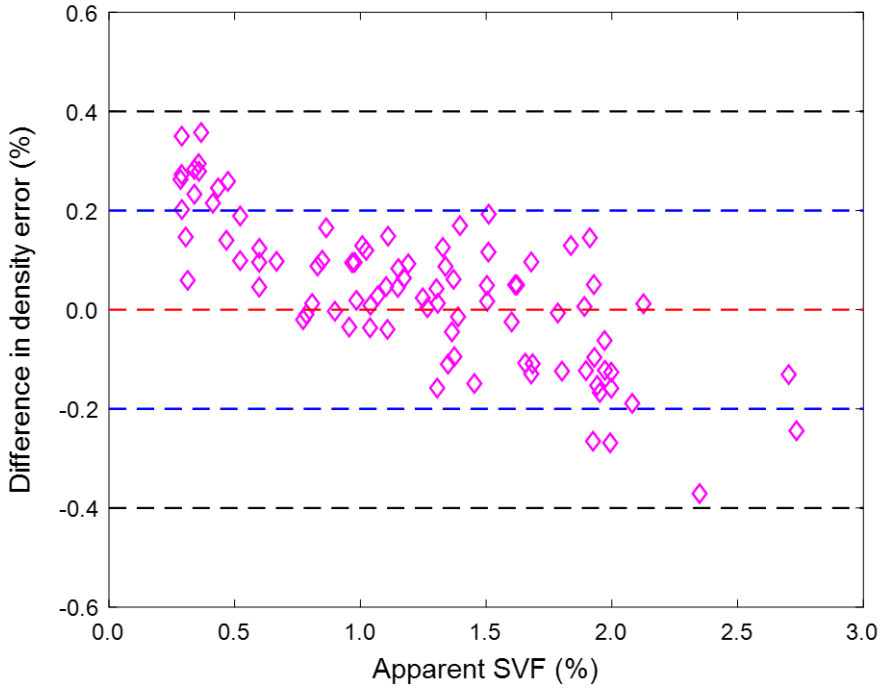

Figure 4.35 Differences in density errors based on apparent SVF from improved analytical model (with belly up, CF1)

4.5.4 **Discussion on the Influences of Process Conditions**

This section primary discusses the influences of three process conditions, including the fluid viscosity, particle size, along with Coriolis drive frequency, on Coriolis flow metering at a qualitative level for the purpose of extending this study on sand-water mixtures to a wider range of slurry applications (e.g. sand-oil flow). As presented above, the density difference of two phases dominates the decoupling effect, while there are a range of other factors which can influence thus the behaviours of Coriolis flowmeters under slurry flow. The relevant factors can be classified into four categories, including the physical properties of carrier liquid, the characteristics of particulate solids, the characteristics of two-phase flow, the features along with installation of the Coriolis flowmeters. The operating conditions can also make an impact on decoupling effect, due to the connections between the fluid properties (e.g. fluid density, viscosity) and the operating conditions (e.g. temperature, pressure).

Due to the difficulties in creating various test conditions, it is impractical to go through each condition to check its influence on Coriolis flow metering by experimental investigation. In this study, the experimental investigation covers two test conditions,

different mass flowrate along with the meters' installation orientation. This section briefly presents the viscous decoupling model for the purpose of extending this study on sand-water mixture to a wider range of slurry applications (e.g. sand-oil flows). Three typical factors involved in viscous model, including particle size, fluid viscosity as well as Coriolis drive frequency, and their influences are discussed on a qualitative level by means of theoretical analysis of decoupling effect in viscous fluid.

The first consideration is how to modify the decoupling model from the inviscid fluid to the viscous fluid, which is quite important to the investigations into flow metering for the viscous cases, such as sand-oil flows typically involved in petroleum industry. As discovered in prior research [31], [58], [68], [86], the basic inviscid decoupling model can be modified to the viscous model by introducing two new forces terms, including the Stokes drag force and the history force. The detailed descriptions of force analysis can be found in [86], not repeated here. Simply speaking, the addition of fluid viscosity limits the decoupled motions between different phase, and thus the decoupling effect is reduced in viscous model.

Inverse Stokes number or also called as penetration depth (δ_N) is a considerably important non-dimensional parameter for the estimation of the motion of a particle entrained into viscous flow field under Coriolis oscillation.

$$\delta_N = \sqrt{\frac{2\,v_l}{r_s^2\,\omega_r}} \tag{4-42}$$

where

$$v_l = \frac{\mu_l}{\rho_l} \tag{4-43}$$

where δ_N represents the normalized inverse Stokes number or called as penetration depth, r_s denotes the radius of the entrained object (here sand particles), ω_r is drive frequency of Coriolis flowmeters, and v_l is the kinetic viscosity of liquid which is computed using dynamic viscosity of liquid (μ_l) divided by liquid density (ρ_l).

As shown in equation (4-42), it reveals the ratio of the Coriolis oscillation time scale with respect to the diffusion time scale of the surrounding vorticity of an oscillating object into the viscous medium [86]. Inverse Stokes number (δ_N) is dependent on fluid kinetic viscosity, the size of entrained object, as well as Coriolis oscillation frequency. This dimensionless parameter measures the required distance between two oscillating objects so

as to get rid of the disturbance from each other. For instance, a large inverse Stokes number indicates that the oscillating motion of an entrained particle is more likely to be affected by the adjacent particles and thereby the decoupling motion with respect to liquid phase would be restricted. As a result, the decoupling effect would be less noticeable than that in inviscid fluid.

With the help of inverse Stokes number, the influences of fluid viscosity, the size of entrained object, as well as Coriolis oscillation frequency on decoupling effect can be inferred. Concerning fluid viscosity, the higher fluid dynamic viscosity would increase the drag force, which hinders the solid-liquid relative motion, and thus reduces the decoupling effect. It suggests that if Coriolis flowmeters encounter with sand-oil flows, a lower level decoupling error would be expected due to the high viscosity of oil, compared with Coriolis measurement errors under sand-water flows. In terms of particle size and Coriolis drive frequency, as illustrated by equation (4-42), a smaller size particle or lower drive frequency would produce larger inverse Stokes number, implying less decoupling error occurring in Coriolis flowmeters. To conclude, larger fluid viscosity or smaller particle size or lower oscillation frequency would resist the decoupled motion. Consequently, the decoupling ratio would be closer to 1, and less decoupling error would happen.

Furthermore, it should be clarified that in light of decoupling theory, the changes in flow regime or different cross-sectional distributions of solid phase associated with different tube geometries or meters' installations would not impact the decoupling phenomenon directly. Their indirect influences on Coriolis flow metering should be attributable to other error sources, including slip ratio, asymmetry and imbalance errors, as described in Section 4.2.3. The effect of installation orientation has been clearly identified in this research. With regard to different types of Coriolis flowmeters, for example, comparison between bent-tube and straight-tube types, it can be deduced that particles are trapped in certain locations of the bent-tube type (as demonstrated in this work) while it may less likely happen in straight type of tube.

4.6 Summary

This chapter primarily proposes a practical useful methodology for slurry flow measurement using Coriolis flowmeters incorporating a simple semi-empirical analytical

model. Three major tasks for investigating the measurement errors of Coriolis flowmeters handling dilute slurry are described.

Firstly, the existing theory reporting the underlying physics causing the measurement errors of Coriolis flowmeters under two-phase flow conditions has been applied for undertaking a theoretical study on the impact of entrained solids on Coriolis flow metering. According to the theoretical analysis, decoupling effect has been identified as the dominant error source, while compressibility effect can be neglected for slurry flow measurement using Coriolis flowmeters.

Secondly, a series of flow measurement tests were conducted to examine the original measurement errors of Coriolis flowmeters occurred in dilute sand-water flow (SVF within 4%). Based on the experimental data, basic regression analysis of the error trends has been performed for predicting and further correcting the measurement errors of Coriolis flowmeters. The results have demonstrated that through the established regression model, mass flowrate errors of Coriolis flowmeters are corrected to within ±0.1% for 98% outcomes, which illustrates the outstanding potential of curve fitting for compensating errors with slurry flow, owing to the relatively simple solid-liquid decoupled motions without compressibility effect.

Thirdly, with an adoption of the existing decoupling effect theory, a basic analytical model has been determined for compensating the effect of entrained solids on Coriolis flow metering. Through comparison between model prediction and experimental results, the performance of the basic decoupling model has been evaluated, whereas noticeable deviations have been found. Thus, a simple correction of the basic analytical model has been further introduced to lower the differences between the model prediction and actual experimental data. After correction, the improved semi-empirical analytical model is able to yield less than ±0.1% deviation for over 81% outcomes, and at least 94% compensation fall within ±0.2% deviation range for mass flowrate measurement. In terms of density measurement, the original measurement errors of Coriolis flowmeter are successfully reduced to ±0.4% error range whilst 82% correction are within ±0.2%. The results have indicated the feasibility of applying Coriolis flow metering technology into dilute slurry flow measurement with a semi-empirical analytical model.

Chapter 5
Structural Condition Monitoring of Coriolis Flowmeters

5.1 Introduction

This chapter mainly investigates a special issue in using Coriolis flowmeters for slurry flow metering. The potential wear problem of Coriolis flowmeters can adversely affect the measurement performance and excessive erosion can even lead to facility failure. In order to examine the structural health of Coriolis flowmeters, an efficient condition monitoring technique is required.

This chapter firstly presents the basics and the working principle of an in-situ structural condition monitoring technique through on-line stiffness diagnostics. A stiffness related diagnostic parameter (SRDP) is used to track the potential structural changes in Coriolis measuring tubes. By adding additional frequencies into the Coriolis drive signal, SRDP data are acquired through the analysis of frequency response. Then, both theoretical and experimental investigations are undertaken for exploring the factors which affect the performance of stiffness determination under complex process conditions. By using a spring-mass-damper model representing the Coriolis vibrating tube, computational simulation is conducted to examine the outcomes of stiffness determination when the modal parameters (damping, degrees of freedom) change and experimental validation is performed to offer the experimental evidence. Thirdly, the chapter discusses the influence of temperature variations on stiffness determination and proposes a compensation method for reducing the temperature effect, which can improve the measurement accuracy. Lastly, erosive tests were carried out with slurry flow, in order to experimentally evaluate the feasibility and sensitivity of the condition monitoring technique. Furthermore, as-found tests were conducted for meter recalibration with clean water, so as to assess the measurement performance of the meter under test potentially affected by tube erosion.

5.2 Structural Condition Monitoring Through Stiffness Diagnostics

5.2.1 Coriolis Tube Stiffness and Meter Calibration

First of all, this section explains the concept of Coriolis tube stiffness as well as the close link between tube stiffness and FCF (flow calibration factor) of a Coriolis flowmeter. For a Coriolis flowmeter, the reading of mass flowrate ($\dot{m}$) is directly proportional to the time shift (Δt) between sensor signals of the inlet and outlet sensors. A Coriolis flowmeter is normally calibrated in the factory by the manufacturer under a reference condition.

$$\dot{m} = C_{FCF}\,\Delta t \tag{5-1}$$

where C_{FCF} denotes FCF of a Coriolis flowmeter. This calibration coefficient (C_{FCF}) is typically determined through a standard calibration process (e.g. start-stop batching procedure in a gravimetric system) and then stored in the transmitter.

The physical meaning of FCF is illustrated through dimensional analysis, which suggests that FCF has the units of stiffness ($\frac{force}{displacement}$) [76].

$$(C_{FCF})_{units} = \frac{mass}{time^2} = \frac{\frac{force}{acceleration}}{time^2} = \frac{\frac{force}{\left(\frac{displacement}{time^2}\right)}}{time^2} = \left(\frac{force}{displacement}\right)_{units}$$

$$k = \frac{F_1}{\Delta x_1} \tag{5-2}$$

The physical stiffness parameter is generally defined as equation (5-2). With an external force (F_1) imposed on an object or a structure, stiffness (k) is the ratio of this force to the resulting displacement (Δx_1).

$$k \propto C_{FCF} \tag{5-3}$$

The analysis above demonstrates tube stiffness (k) is the essence of FCF of a Coriolis flowmeter. Due to this reason, tube stiffness can be regarded as a quite important parameter strongly linked with the performance of a Coriolis flowmeter. Any changes in tube stiffness would affect FCF and consequently degrade the measurement accuracy.

In a Coriolis oscillating system, the measuring tubes are typically excited at one of its resonant frequencies, commonly the first fundamental vibration mode [91]. Vibrating at

the resonant frequency, a Coriolis flowmeter is also capable of providing an independent measurement of fluid density resulting from the effective vibrating mass. The expression of angular drive frequency of a tube working in its first vibration mode is,

$$\omega_{r1} = \sqrt{\frac{k_1}{m_1}} \tag{5-4}$$

where m_1 denotes the effective vibrating mass, k_1 is the tube physical stiffness, and ω_{r1} is the angular resonant (drive) frequency of the first vibration mode.

Here the effective vibrating mass (m_1) comprises the mass of the empty tube (m_t) along with the mass of the conveying fluid. The mass of fluid can be expressed using the fluid density (ρ_f) and the tube internal volume (V_t).

$$m_1 = m_t + \rho_f \, V_t \tag{5-5}$$

For simplification, the lumped mass (m_1) is simply expressed as the sum of the empty tube mass (m_t) and the conveying fluid mass ($\rho_f V_t$), although these mass terms should be the effective vibrating mass which requires some corrections.

$$\rho_f = \frac{k_1}{\omega_{r1}^2 \, V_t} - \frac{m_t}{V_t} \tag{5-6}$$

Derived from equations (5-4) and (5-5), the fluid density can be determined as illustrated by equation (5-6) which demonstrates that tube stiffness is also closely related to density measurement.

Tube stiffness is a parameter related to the structural characteristics of the tube, dependent on the tube dimensions and material properties [75]. The changes in tube geometry, dimensions as well as degradation of tube material can affect the value of tube stiffness. From the analysis above, it can be concluded that unchanged values of FCF (C_{FCF}) and tube stiffness (k) are extremely important for delivering accurate mass flow measurement from factory calibration to the real-world applications. However, over the service life of a Coriolis flowmeter, tube stiffness may shift to a different value. For example, in corrosive (e.g. acids) or abrasive (e.g. slurry flow) industrial processes, there is a potential risk to erode the measuring tubes. If tube erosion occurs, the structural properties of Coriolis tubes would change, consequently giving rise to incorrect FCF together with measurement errors encountered in an eroded Coriolis flowmeter.

Erosion can be generally observed from erosion scars or ripples on the tube internal surfaces or welds. Nevertheless, regular visual inspection of tubes (e.g. image inspection of the internal surfaces) are impractical to implement, always requiring the operator to stop the ongoing flow transportation. Therefore, it will be very helpful if the structural conditions of measuring tubes can be monitored in situ during the meter's service life. In this work, an in-situ condition monitoring technique is employed through online stiffness determination. A stiffness related diagnostic parameter (SRDP) is used to examine structural health and report potential structural changes, which can assist Coriolis flowmeters in delivering accurate mass flow measurement.

5.2.2 **Model of a Coriolis Vibrating Tube**

In this section, tube stiffness parameter is explained by means of analytical modelling. A Coriolis vibrating tube can be characterized by a simple spring-mass-damper model according to the working principle of Coriolis flowmeters. Under the assumption that all the components in the vibrating system are coupling together so can follow the same motion, a single measuring tube can be simplified by a basic SDOF (single-degree-of-freedom) spring-mass-damper model, as shown in Figure 5.1.

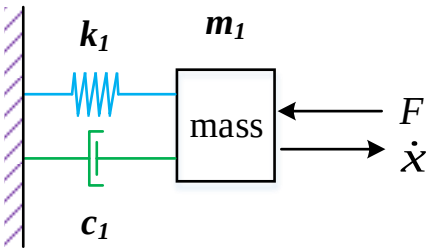

Figure 5.1 SDOF spring-mass-damper model of a Coriolis tube

In the SDOF model, the lumped mass (m_1) is composed of the effective mass of the tube together with the fluid. The vibrating tube acts as the spring which can described by its physical stiffness (k_1). The energy loss, resulting from the interactions between the vibrating tube and surrounding environment as well as other sources, can be quantified by viscous damping coefficient (c_1). The transfer function ($\dot{H}$) of this oscillating system can be written as,

$$\dot{H}(s) = \frac{\dot{x}(s)}{F(s)} = \frac{s}{m_1 s^2 + c_1 s + k_1} \tag{5-7}$$

where F denotes the exerted force; x means the displacement of this lumped mass so $\dot{x}$ is the resulting velocity.

By converting equation (5-7) to frequency domain, FRF (frequency response function) of an oscillating system is expressed as,

$$FRF_P = \dot{H}(\omega) = \frac{\dot{x}(\omega)}{F(\omega)} = \frac{j\omega}{-m_1\omega^2 + jc_1\omega + k_1} \tag{5-8}$$

A dimensionless parameter, Q factor, is always used to describe the resonance behaviour of an oscillator. High Q factor indicates the oscillating system has a noticeable and narrow peak with great amplitude at the resonant frequency, being less damped. Normally the Coriolis oscillating system has a considerably large value of Q factor for delivering accurate mass flow measurement (e.g. under single-phase condition) and Q factor can reach 10000 [55]. The calculation of Q factor is shown below,

$$Q = \frac{\omega_{r1} m_1}{c_1} \tag{5-9}$$

A typical FRF of a Coriolis oscillating system working in its first vibration mode can be given by Figure 5.2 where the resonant frequency is 240 Hz and Q factor is 10000. As illustrated, the resonant peak is narrow and evident whilst the phase transition from +90° to -90° is steep owing to high Q factor.

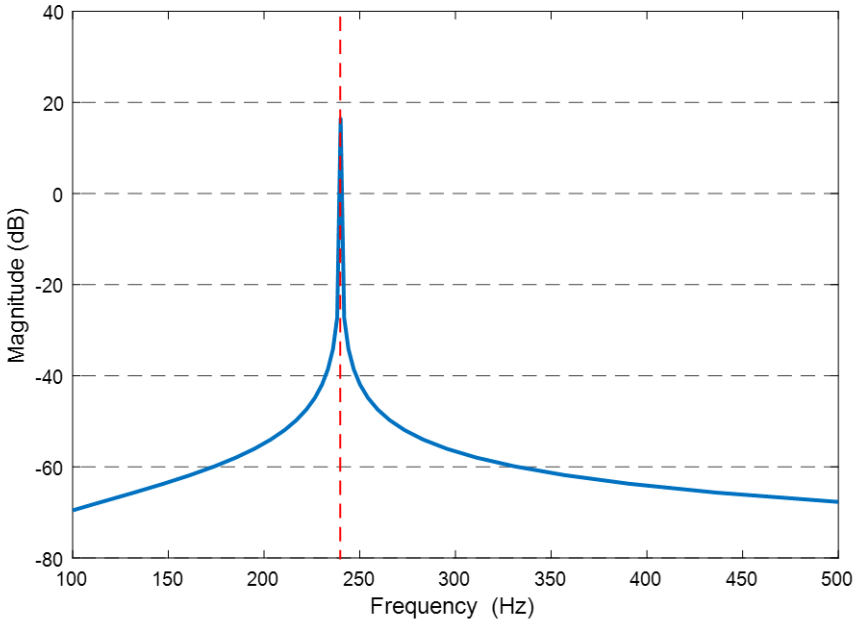

(a) Magnitude

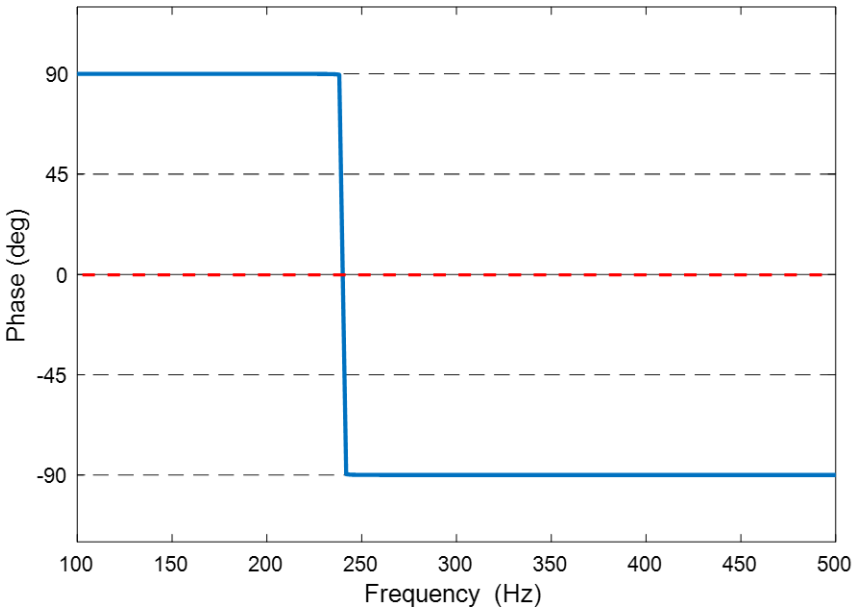

(b) Phase

Figure 5.2 Bode plot of typical FRF of a Coriolis vibtrating tube

5.2.3 **Extraction of Stiffness Related Diagnostic Parameter**

It is worth noting that FRF or transfer function of an oscillating system is generated from the real physical parameters (i.e. force and velocity). However, it is not convenient to measure these physical parameters directly. For a Coriolis flowmeter, the drive and sensor signals are closely related to the physical parameters of force and velocity. The added drive current (I) is proportional to the force (F_C) whilst the sensor voltage (ε) is proportional to the velocity ($\dot{x}$), illustrated by the relevant electromagnetic equations,

$$F_C = I\, L_{dr}\, B \tag{5-10}$$

$$\varepsilon = \dot{x}\, L_{sr}\, B \tag{5-11}$$

where B denotes the flux density of the MF (magnetic field) which is created by the magnet being attached on Coriolis tubes; F_C is the actuation force generated by drive current (I); L_{dr} is the effective length of drive coil which can be simply understood as an geometry factor of drive coil; ε represents the sensor voltage induced by the tube motion at velocity $\dot{x}$; L_{sr} is the geometry factor related to motion sensors.

The terms F_C, I, ε, $\dot{x}$, B are vectors, but only the magnitude parts are considered for simplification. Moreover, the induced MF strength around drive coil and sensors is assumed to be the same. To distinguish the real physical FRF of an oscillating system and measured FRF from a Coriolis sensing unit, these two terms are named as FRF_P and FRF_C, respectively. FRF_P data is linked with the oscillation of a Coriolis tube, while is FRF_C is obtained from the electrical signals (drive and sensor signals) of a Coriolis meter.

In the light of the electromagnetic equations above, the measured FRF (FRF_C) from a Coriolis flowmeter can be expressed as,

$$FRF_C = \frac{\varepsilon}{I} = \frac{(BL_{sr}\, BL_{dr})\, \dot{x}}{F} \tag{5-12}$$

By comparing equations (5-8) and (5-12), it is clear that the physical FRF data (FRF_P) is directly proportional to the measured FRF data (FRF_C) via a scale factor (C_{SF}).

$$FRF_C = C_{SF}\, FRF_P \tag{5-13}$$

This scale factor (C_{SF}) is dependent on the created MF strength,

$$C_{SF} = BL_{sr}\, BL_{dr} \tag{5-14}$$

By introducing C_{SF} into the transfer function given by equation (5-8), FRF_C can be written as,

$$FRF_C = \dot{H}_C(\omega) = C_{SF}\, \dot{H}(\omega) = \frac{j\, C_{SF}\, \omega}{-m_1\omega^2 + jc_1\omega + k_1} \tag{5-15}$$

Accordingly, it is not convenient to measure the real physical tube stiffness directly. Instead of measuring the real tube stiffness, a stiffness related diagnostic parameter ("diagnostic tube stiffness"), abbreviated as SRDP, is used here. SRDP can be determined by means of the onboard electronics (drive coil and motion sensors) in a Coriolis flowmeter. Equation (5-15) can be split up into the real and imaginary parts so as to calculate the "diagnostic tube stiffness" (SRDP),

$$\begin{cases} Re\left\{\dot{H}_C(\omega)\right\} = \frac{C_{SF}\, c_1\, \omega^2}{(k_1 - m_1\omega^2)^2 + (c_1\omega)^2} \\ Im\left\{\dot{H}_C(\omega)\right\} = \frac{C_{SF}\, (k_1 - m_1\omega^2)\, \omega}{(k_1 - m_1\omega^2)^2 + (c_1\omega)^2} \end{cases} \tag{5-16}$$

It is well-known that a Coriolis flowmeter tracks the resonant frequency through phase-locking loop control. The Coriolis drive frequency is actually the undamped resonant frequency [91], as shown in equation (5-4). In order to determine "diagnostic tube stiffness", at least one additional off-resonant frequency (f_{or}) is required to apply into the drive signal besides the resonant frequency (f_r) to yield a second equation. With the complementary response excited by f_{or}, the diagnostic parameters related to tube stiffness, damping as well as lumped mass can be finally derived from equations (5-4) and (5-16),

$$k_C = \frac{k_1}{C_{SF}} = \frac{\omega_r^2\, \omega_{or}\, Im\{\dot{H}_C(\omega_{or})\}}{(\omega_r^2 - \omega_{or}^2)\, |\dot{H}_C(\omega_{or})|^2} \tag{5-17}$$

$$c_C = \frac{c_1}{C_{SF}} = \frac{Re\{\dot{H}_C(\omega_{or})\}}{|\dot{H}_C(\omega_{or})|^2} \tag{5-18}$$

$$m_C = \frac{m_1}{C_{SF}} = \frac{k_1}{\omega_r^2\, C_{SF}} = \frac{\omega_{or}\, Im\{\dot{H}_C(\omega_{or})\}}{(\omega_r^2 - \omega_{or}^2)\, |\dot{H}_C(\omega_{or})|^2} \tag{5-19}$$

where ω_r denotes the resonant (angular) frequency, ω_{or} is the off-resonant frequency. k_C, c_C, m_C are the diagnostic parameters related to tube stiffness, damping and lumped mass, respectively.

By using one off-resonant frequency, SRDP (k_C) can be determined by equation (5-17). If more than one off-resonant frequencies are applied into the drive signal, it can yield more diagnostic outcomes. It can be regarded as an over-determined solution for measuring k_C, which may be useful to improve the measurement accuracy or verify the correctness of diagnostic results.

Furthermore, it can be deduced that too heavy damping added into Coriolis oscillation would probably limit the application of this stiffness determination approach. In other words, Q factor is expected to be a large value so that FRF can exhibit a high and narrow resonant peak. More importantly, for the high-Q oscillation, the damped resonant frequency would not shift too much with respect to the undamped resonant frequency, otherwise likely the accuracy of stiffness determination would be adversely affected. The influence of damping will be presented later in Section 5.3.

5.2.4 **Stiffness Diagnostics of Coriolis flowmeters**

When the end user conducts in-situ structural health diagnostics of a Coriolis flowmeter, the relative change in SRDP (Δk_C) which contains the information of structural changes is more useful than the absolute value of SRDP. Δk_C can be computed with respect to the factory baseline,

$$\Delta k_C = \frac{k_{CI} - k_{C0}}{k_{C0}}\ 100\% \tag{5-20}$$

where k_{CI} refers to SRDP data acquired by the end user in situ, and k_{C0} denotes the initial value of SRDP obtained under a reference condition in factory.

The factory baseline is established under a reference condition. Appropriate limit of permissible change in "tube stiffness" can be preset by the manufacturer. If Δk_C is within the limit, it indicates the measuring tubes have maintained their good structural integrity. Conversely, if Δk_C exceeds the limit, it suggests the underlying change in the structural conditions of tubes.

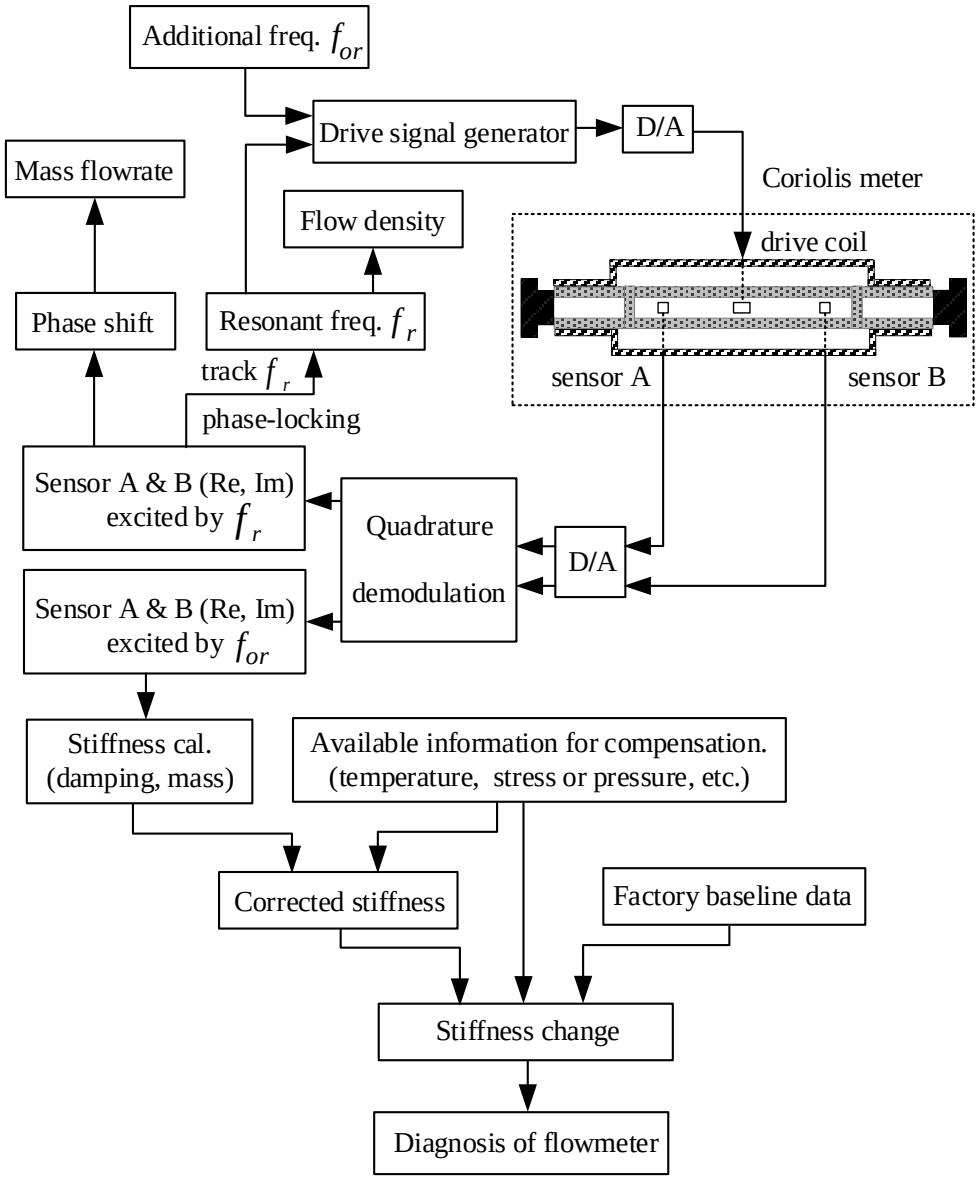

Figure 5.3 Flowchart of stiffness diagnostics of a Coriolis flowmeter

Figure 5.3 depicts how to conduct stiffness diagnostics of a Coriolis flowmeter. The resonant frequency (f_r) is determined by phase-locking closed-loop control. To perform stiffness diagnostics, firstly, one or more additional off-resonant frequencies (f_{or}) are added into the drive signal, apart from f_r. Secondly, the frequency responses of the vibrating tubes which are induced by f_r and f_{or}, are collected from the sensor signal. Thirdly, by means of quadrature demodulation, the raw sensor signal can be decomposed into several individual components in terms of frequencies. These separated components are picked out to acquire FRF data (complex number). Then the measured FRF can be further split into real and imaginary parts. Next, SRDP (k_C) can be calculated from equation (5-17). Finally, compared with the reference (factory baseline data), the relative

change in SRDP (Δk_C) can be determined. According to the permissible relative change, further diagnostic results can be provided to the end user regarding the current structural condition of the Coriolis flowmeters in use.

It is still an open question concerning the proper limit or allowable change in SRDP, which determines the achievable sensitivity of meter diagnostics. On one hand, in order to promptly report the structural change (e.g. erosion or coating) at an early stage, the allowable change should not be set as a high threshold or a wide range because any drift in "tube stiffness" can directly degrade the measurement accuracy. For example, if SRDP data has shown a 4% change, 4% measurement error would be expected in mass flowrate, according to equation (5-1), which is beyond the typical claimed uncertainty (±0.1%) of a Coriolis flowmeter. It also should be noted that the real case could be more complex than the simple theoretical analysis, in consideration of the additional asymmetry errors resulting from the uneven decrease in the thickness of tube wall. On the other hand, if the limit is set too low, the chance of false alarms may rise which would confuse the end user.

The technical challenge here is that the uncertainty or accuracy of stiffness determination has not been fully determined. The accuracy is dependent on a range of factors, such as the performance of stiffness determination method, the behaviour of signal processing unit, the functionality of onboard electronics as well as the influences of various process or operating conditions. For instance, when the in-situ process or operating condition greatly deviates from the reference condition, the accuracy of stiffness determination would strongly depend on whether proper compensations are given for reducing the influence of changes in process condition. In terms of signal processing procedures, different manufacturers may employ different measurement methods (e.g. different additional frequencies) as well as various signal processing methods (e.g. different designs of low-pass filters), thus the achieved sensitivity of structural health diagnostics could differ. For example, one manufacturer has released a diagnostic feature called "Smart Meter Verification" and specified the limit of stiffness uncertainty at ±4% by employing four additional frequencies [75].

5.3 Identification of Factors Affecting Stiffness Determination

This section investigates the potential factors which can affect the outcomes of stiffness determination. Computational simulation based on spring-mass-damper vibration models

has been conducted for two purposes. One purpose is to validate the feasibility of this measurement method with a SDOF model. The second purpose is to explore the influences of other modal parameters (damping, degrees of freedom) on stiffness extraction with a 3DOF (three-degree-of-freedom) model, which can help to understand the potential causes resulting in false alarms during structural condition monitoring of Coriolis flowmeters. Besides, experimental work is carried out to validate the simulation results.

5.3.1 **Computational Simulation Based on Spring-Mass-Damper Model**

5.3.1.1 **Description of Simulation System**

As presented in Section 5.2.2, a measuring tube can be simply characterized by a SDOF spring-mass-damper model which is described by four modal parameters including degrees of freedom, lumped mass, stiffness, and damping level. In consideration of the complexity of real-world process conditions, different mass-spring-damper models have been tested using Simulink. This simulation work begins with a basic SDOF model, as illustrated by Figure 5.4. And then it is extended to a 3DOF (three-degree-of-freedom) case so as to evaluate the effect of degrees of freedom on stiffness extraction.

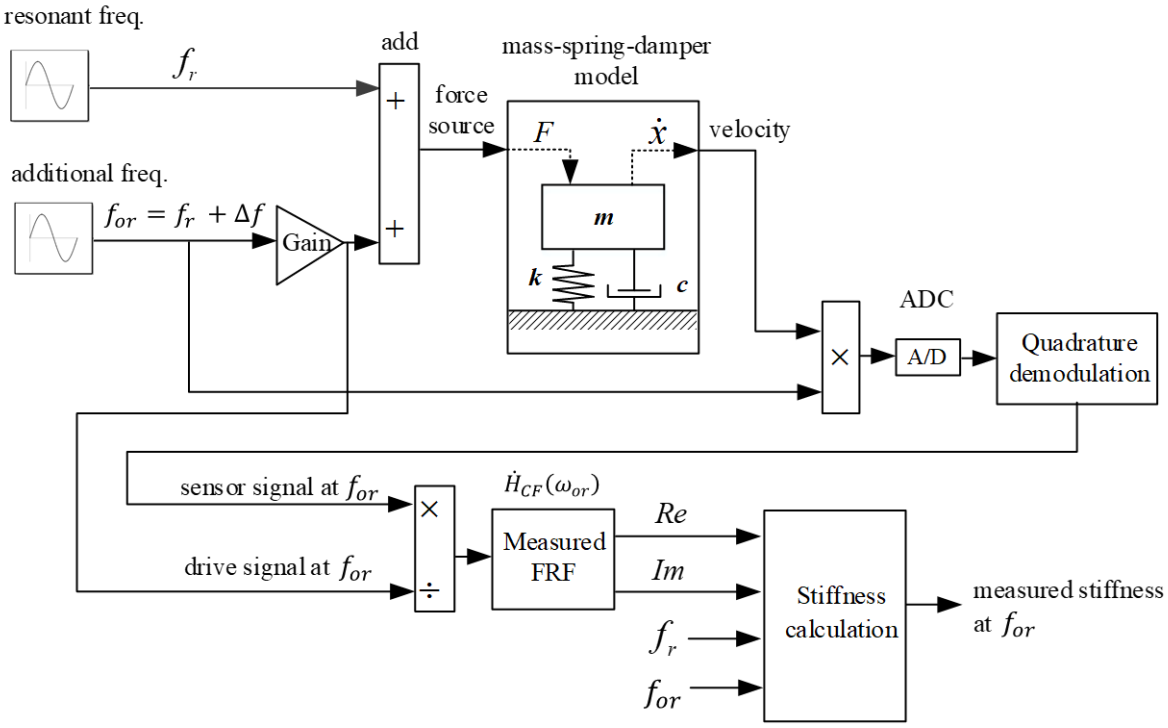

Figure 5.4 Schematic of simulation based on a SDOF model

The value of stiffness is set according to a basic estimation shown below. Here the numerical substitutions of ω_{Ar}, ω_{Wr}, A_t, and L_t are undertaken based on actual data of the Coriolis flowmeters (KROHNE OPTIMASS 6400 S50) under test at room temperature in this work. Since air is much lighter than water, m_A is neglected to simplify the calculation.

$$\begin{cases} \omega_{rA} = \sqrt{\frac{k_1}{m_t+m_A}} = \sqrt{\frac{k_1}{m_t}} \\ \omega_{rW} = \sqrt{\frac{k_1}{m_t+m_W}} = \sqrt{\frac{k_1}{m_t+\rho_w A_t L_t}} \end{cases} \tag{5-21}$$

where the subscript "A" means air, "W" denotes water; ω_{rA}, ω_{rW} represent the resonant frequencies when pure air and water flow through the tube, respectively; m_t again is the mass of empty tube, m_A and m_W denote the mass of flow medium (air and water); m_W is determined by water density (ρ_w) and the internal volume of tube; the tube internal volume is estimated from the known dimension data using tube cross sectional area (A_t) along with tube length (L_t).

The unknown k_1 and m_t can be solved from equation (5-21). The value of k_1 is roughly $2.4 \times 10^6\ N/m$ later used in the simulation. In terms of the low-pass filter for signal demodulation, a Butterworth IIR filter is employed with cut-off frequency at 1.5 Hz. All numeric variables are stored in 64-bit floating-point values for a high computation precision.

5.3.1.2 **Simulation Results Based on a SDOF Model**

The relevant parameters for modelling are described as follows: the undamped resonant frequency (f_r) is assumed as 240 Hz, according to the first working frequency of the Coriolis flowmeter under test as mentioned above; The spring stiffness is $2.4 \times 10^6\ N/m$, regarded as the reference (k_R); Based on equation (5-4), the lumped mass term (m_1) is estimated at 1.0554 kg; Different damping levels are added into this model so as to explore the effect of damping on stiffness determination. Here the dimensionless Q factor is given to characterize the damping levels. In the lightly damped case in this simulation, Q factor is calculated as 1592 and later it is decreased to 159 for creating the heavily damped case. Such damping level is exaggerated in order to identify the effect of high damping on the resonance behaviour of Coriolis oscillation, which can help examine the applicability of

this stiffness determination method into a heavily damped scenario (e.g. caused by entrained gas).

Single additional off-resonant frequency (f_{or}) at different frequency locations is fed into the drive signal one at a time, with frequency offset $\Delta f = f_{or} - f_r = -10, -9, \dots, -3, +3, \dots, +10$ in Hz. The minimum frequency offset ($|\Delta f|$) is set at 3 Hz and maximum offset is 10 Hz. In this way, 16 stiffness outcomes are collected corresponding to 16 different frequency locations, which is used to investigate the influence of frequency locations. To assess the stiffness diagnostic results, the absolute value of relative difference (z_i) between the simulation outcomes (k_S) and the reference stiffness (k_R) is computed as follows,

$$z_i = \left|\frac{k_{S(i)} - k_R}{k_R}\right| 100\% \quad (i = 1, 2, \dots, 16) \tag{5-22}$$

In the meanwhile, according to 16 stiffness diagnostic data, the mean value of absolute relative difference ($\bar{z}_{Avg}$) is calculated to evaluate the accuracy, whilst the standard deviation (σ) is computed to check the repeatability. The simulation results based on a SDOF model are given by Figure 5.5 which displays the averaged absolute value of the relative difference ($\bar{z}_{Avg}$) with error bars of standard deviation (σ). It can be seen that relative differences between the outcomes from simulation and the reference value are negligibly small (much lower than 0.01%), although heavy damping can lead to slightly higher errors as well as uncertainties indicated by the larger $\bar{z}_{Avg}$ and σ. Theoretically speaking, the simulation results are expected to fully agree with the given reference. This quite small difference can be attributable to the errors from signal processing, such as the influence of applied low-pass filter. From the simulation results, it can be concluded that this stiffness determination method is feasible with excellent accuracy and repeatability, although a quite small difference (error or uncertainty) could arise from the implementation of signal processing.

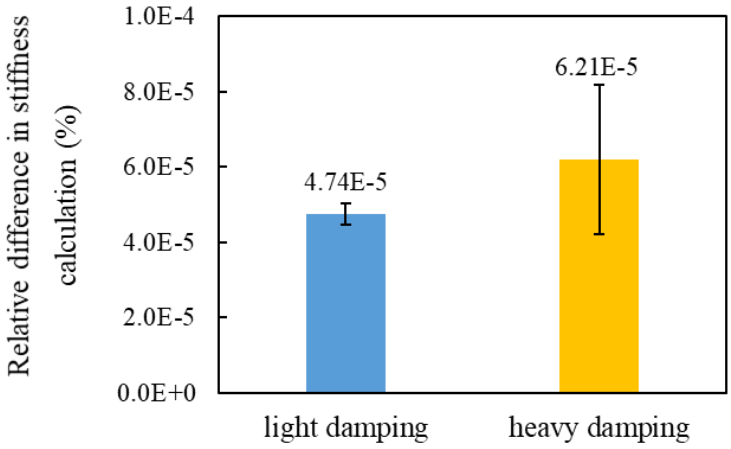

Figure 5.5 Simulation results based on a SDOF model

5.3.1.3 **Simulation Results Based on a 3DOF Model**

A Coriolis oscillating tube usually contains more than one degree of freedom in reality. From the view of its sensing unit, a Coriolis measuring tube can be divided into three concentrated elements. Among them, one element is assigned at the central location of drive coil with the lumped mass including the mass of substitute part of empty tube together with the conveying flow. The other two elements are located near the inlet sensor (sensor B) and outlet sensor (sensor A), respectively. Based on these substitutions, a tube can be assumed as a 3DOF system, as shown in Figure 5.6.

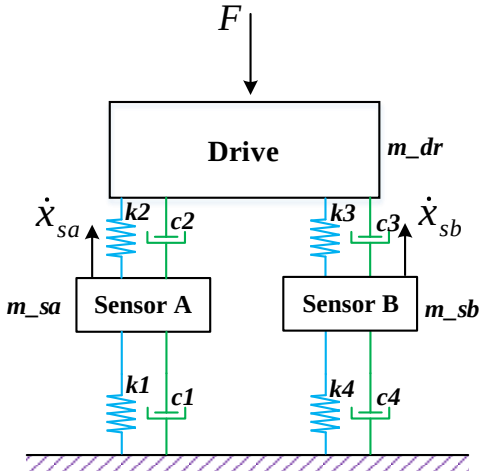

Figure 5.6 3DOF model of a Coriolis tube

The simulation system is modified by using a 3DOF model. Drive signal is exerted upon the drive element, whilst two sensor signals are picked up from sensor A & B, respectively.

In this 3DOF model, the values of mass and spring stiffness are set symmetrically with respect to the drive element. The related modal parameters are given,

$$m_{dr} = 1.1\ kg, m_{sa} = m_{sb} = 0.355\ kg,$$

$$k1 = k4 = 6.95 \times 10^6\ N/m, k2 = k3 = 1.45 \times 10^6\ N/m.$$

Through theoretical calculation, the undamped stiffness of the first oscillation mode can be solved as reference (k_{R_sa} and k_{R_sb}). In the same way as mention above, 16 different frequencies are added into the drive signal with offset $|\Delta f|$ from 3 to 10 Hz, yielding 16 pairs stiffness outcomes (k_{S_sa} and k_{S_sb}) from sensor A & B, respectively. The values of k_{S_sa} and k_{S_sb} are averaged for a final outcome. Different damping levels are introduced in the 3DOF model to create the lightly damped and heavily damped cases. The resonant frequency (f_r) is determined using frequency sweep at an increment of 0.001 Hz by means of phase-locking.

Figure 5.7 summarizes the simulation results on the basis of a symmetric 3DOF model. The results demonstrate the possibility of large relative errors (above 1%) as heavy viscous damping are added. It suggests fairly heavy damping can give rise to uncertainty in stiffness determination, especially in a MDOF (multi-degree-of-freedom) vibrating system. It can be deduced that for a non-ideal scenario wherein the degrees of freedom are varying with the process conditions (e.g. two-phase or multiphase flows) and the oscillation is seriously damped (e.g. Q factor below 1000), a certain level of errors or uncertainties in stiffness determination may appear. The underlying reason is that in such complex situations, the measured FRF data could become less accurate, owing to the influence of adjacent vibration modes along with the low magnitude of off-resonant response which becomes difficult to detect.

Furthermore, the performance of stiffness extraction can be slightly affected by the locations of additional frequencies (f_{or}), demonstrated by the standard deviation (σ) in Figure 5.7. The effect of frequency locations could be understood as a sort of measurement error or uncertainty associated with signal processing, particularly in a MDOF case where the vibration modes are close to each other. Therefore, careful considerations should be given on the selection of appropriate frequency offset. When f_{or} is employed far from f_r, the induced off-resonant response could be too small to measure. Nevertheless, very near

location to f_r would bring difficult in signal filtering as well as extra cost of processing time.

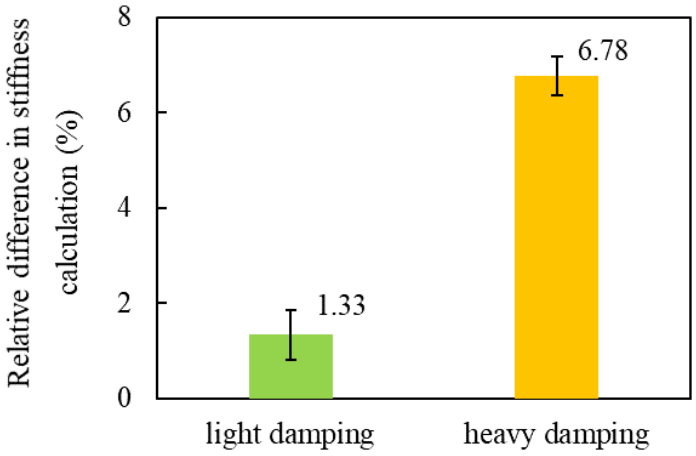

Figure 5.7 Simulation results based on a 3DOF model

A comparison between the simulation results presented in Figure 5.5 and Figure 5.7 indicates that this stiffness determination method is capable of determining stiffness with quite high accuracy (relative differences much less than 0.01%) in the ideal case of SDOF model (Figure 5.5), whereas the accuracy can be negatively impacted by the influence of other modal variables (degrees of freedom and damping) yielding differences greater than 1% in some complex or undesirable occasions (Figure 5.7). For example, when damping level is extremely high, it would be difficult to obtain the response of off-resonant frequency. When the oscillating system has multiple vibration modes but hard to distinguish which usually happens in a seriously damped MDOF case, the impact of nearby modes would become more noticeable [92] and thus, very likely the measured FRF data is less accurate. As a result, these factors can bring some errors and uncertainties in stiffness determination, which may trigger false alarms in the real-world process conditions.

The simulation results suggest that in order to offer accurate and reliable stiffness determination, it is recommended to retain the process conditions stable and consistent with the reference condition in the factory of the manufacturer, which can help reduce the chance of false alarms of tube erosion. Besides, this simulation work has identified that the restrictions of this stiffness determination method generally arise when the single-mode assumption cannot be applicable. For a MDOF situation with well-separated vibration

modes, the contribution of adjacent modes is typically a small amount and it hence can be regarded as a sort of "single mode", likely causing less problems.

5.3.2 **Experimental Validation of Factors Affecting Stiffness Determination**

Experimental assessment is carried out for seeking experimental support to the simulation results presented above. Here the meter under test is CF2 which is horizontally installed with its belly down. In consideration of the applicability of the integrated signal processing unit in the meter's transmitter, two additional off-resonant frequencies (f_{or}) are employed into the drive signal with frequency offset (Δf) at ±20 Hz. Through OPD (Online Parameter Determination) function, structural condition related data are collected at an interval of 60 s and the raw data are averaged within a duration of 10 s for yielding one processed outcome used in later analysis, described in Section 3.4. As explained in Section 5.2.3, one additional frequency can yield one diagnostic outcome. Generated from two additional frequencies, two groups of SRDP data are acquired, named as SRDP2 and SRDP3. The mean value of SRDP2 and SRDP3 is computed, called SRDP1. Accordingly, there are three types of SRDP data used in this work, including SRDP1, SRDP2 & SRDP3.

5.3.2.1 **Tests with Clean Water**

Firstly, in order to validate this stiffness determination method, initial tests were conducted with clean tap water at room temperature (around 18°C) and four different mass flowrates (9000, 18000, 24000, 32000 kg/h). SRDP1 data are continuously recorded for 10 mins. To evaluate the repeatability of stiffness determination results, relative change in SRDP (Δk_C) is calculated with respect to the factory baseline. This baseline is pre-determined under a reference condition in the factory. As displayed by Figure 5.8, relative change in SRDP1 is less than ±0.15%, showing the feasibility as well as good repeatability of this method under single-phase flow condition (tap water).

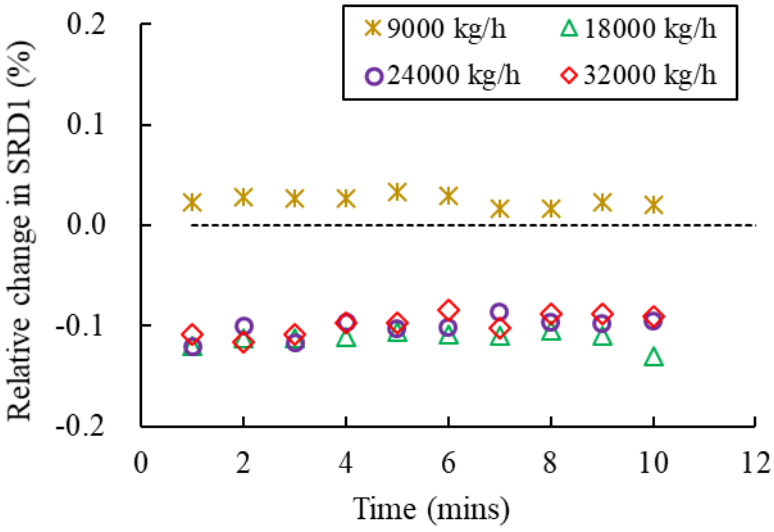

Figure 5.8 Relative change in SRDP1 with clean water

5.3.2.2 **Tests with Two-Phase Flow**

For the purpose of experimental investigation into the effect of two-phase conditions, two situations of two-phase (sand-water and air-water) flows are utilized to test this stiffness determination method. Apparent density rise ($\Delta\rho_{app}$) is calculated in percentage to indicate the portion of sand particles, given again for convenience,

$$\Delta\rho_{app} = \frac{\rho_{m,app} - \rho_{w,app}}{\rho_{w,app}} 100\% \tag{5-23}$$

where $\rho_{m,app}$ denotes the apparent readings of sand-water mixture density from Coriolis flowmeters and $\rho_{w,app}$ is the apparent density reading of pure water.

Figure 5.9 depicts the experimental results with dilute homogenous sand-water flow. From Figure 5.9 (a), it can be found that generally this stiffness determination method can still behave well (Δk_C less than ±0.5%) under dilute solid-liquid two-phase conditions ($\Delta\rho$ below 2%). The entrained solids can cause some small disturbances to the diagnostic results indicated by the scattered SRDP data around zero line. Large content of solids or sudden change in flow conditions would contribute to a certain level of fluctuations in SRDP data. The reason is that the presence and movement of solids can bring some flow noises but could not change the degrees of freedom of Coriolis oscillation. It can be concluded that as long as a Coriolis flowmeter can work normally which means its oscillation is not heavily damped, the effect of entrained solids on stiffness determination

should be small. Figure 5.9 (b) displays the normalized 2-phase signal level in percentage, which is used to imply the presence of second phase. It suggests that the induced 2-phase signal is weak under solid-liquid conditions, which is consistent with the small impact of sand particles as found in SRDP outcomes.

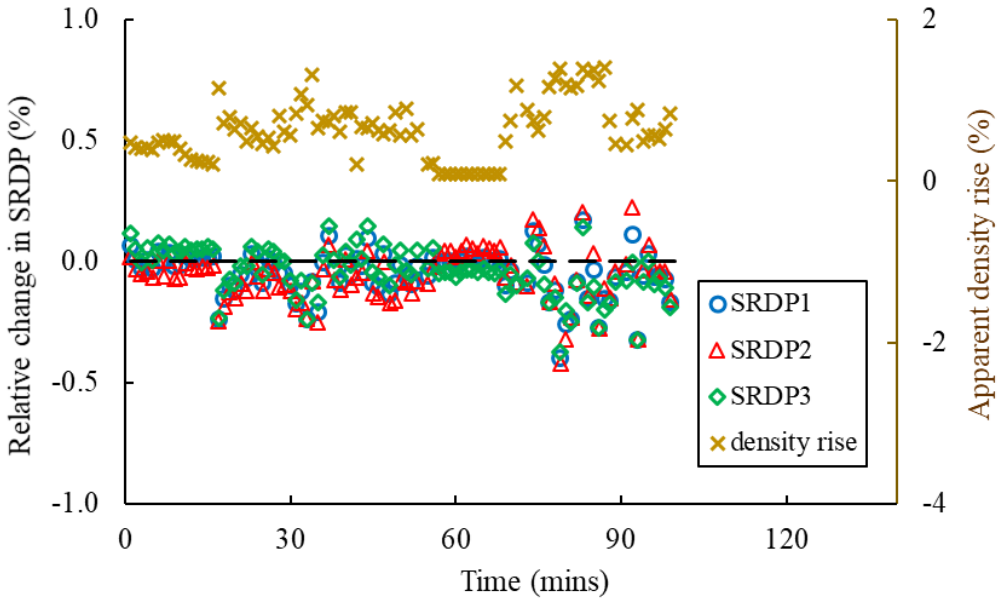

(a) SRDP1, SRDP2, SRDP3 and apparent density rise

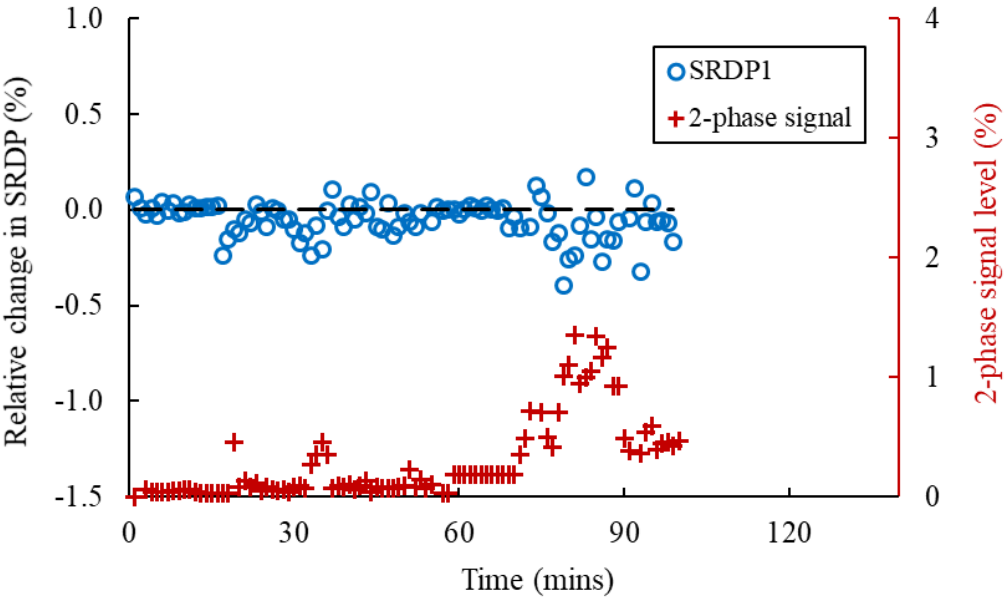

(b) SRDP1 and 2-phase signal level

Figure 5.9 Relative change in SRDP with sand-water mixtures

When gas bubbles are entrained into pure water, the experimental results with bubbly two-phase flow are illustrated by Figure 5.10. Similarly, apparent density drop ($\Delta\rho_{app}$) is given for estimating the gas content. The results clearly demonstrate the noticeable impact of entrained gas on stiffness determination. When (absolute) $\Delta\rho_{app}$ is below 2%, the resulting Δk_C can go up to more than ±10%. Greater deviations as well as fluctuations can be noticed when more gas bubbles are present in the flowstream. The unsteady flow conditions such as uneven distribution of gas bubbles along the tube can give rise to the large differences between SRDP2 and SRDP3. Moreover, evident 2-phase signal appears associated with the entrainment of gas bubbles as shown in Figure 5.10 (b), implying the significant influence of gas-liquid two-phase conditions on the resonance behaviour of a Coriolis flowmeter.

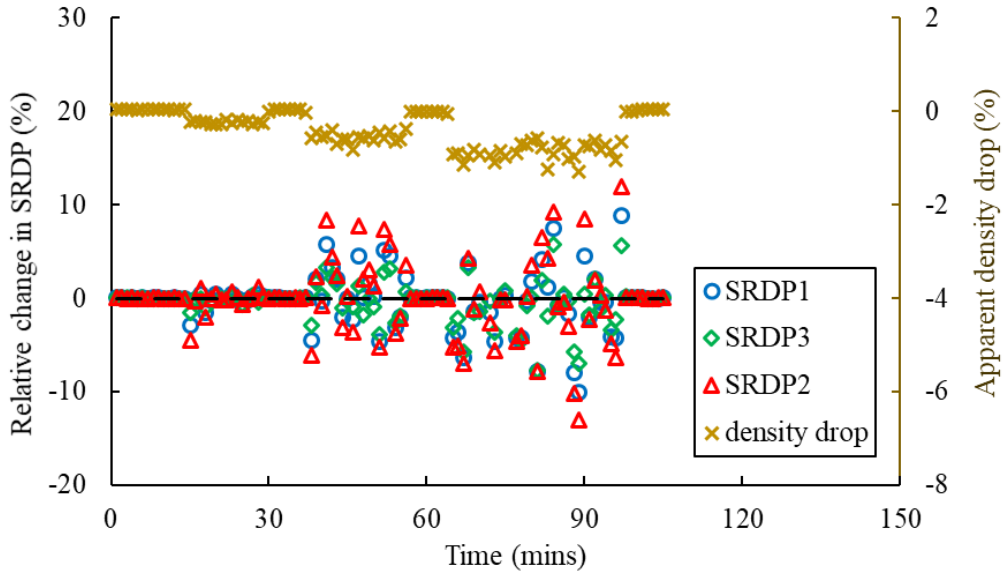

(a) SRDP1, SRDP2, SRDP3 and apparent density drop

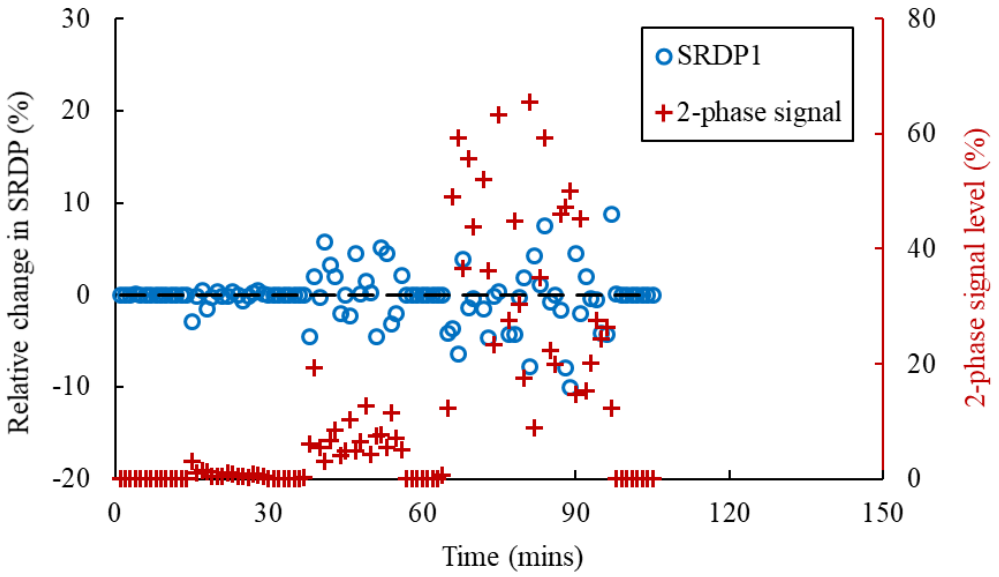

(b) SRDP1 and 2-phase signal level

Figure 5.10 Relative change in SRDP with air-water mixtures

Comparison between experimental results with sand-water and air-water mixtures, it well demonstrates the much greater impact of entrained gas on stiffness determination, whereas SRDP outcomes are relatively less affected by solids. The noticeable influence of gas-water two-phase conditions is believed to be caused by the compressibility effect due to the gas-liquid interactions. As described in Section 4.2.2, the compressibility effect can be simply understood as the presence of a second spring imposed on the original Coriolis vibrating system. The experimental findings agree with the simulation results above, showing that the change in degrees of freedom is a dominant cause which can adversely affect the performance of this stiffness determination method. To conclude, this method is able to deliver accurate stiffness determination when a Coriolis flowmeter is normally operated. under single-phase condition. A careful consideration should be given if a Coriolis flowmeter exhibits poor resonance behaviour, likely because of the complex operating conditions for instance heavy damping or disturbances from gas entrainment (giving additional degrees of freedom), or the failure of electronics.

Moreover, experimental results have suggested the good potential of using the 2-phase signal as extra information of process conditions which can help judge whether the tube is really eroded. For example, if Δk_C exceeds the preset limit but the 2-phase signal level is significantly high, it is very likely that SRDP outcomes are experiencing strong effect of

two-phase conditions, instead of true shift in tube stiffness. Similarly, the damping related diagnostic data and further calculation of Q factor (or damping ratio) could help to give a comprehensive conclusion regarding the structural condition of the tube apart from SRDP data. Furthermore, since the two-phase flow conditions are always unstable and varying over time, it should be advantageous to repeat the diagnostic tests several times in order to ensure the reliability of diagnostic results.

5.4 Compensation of Temperature Effect on Stiffness Determination

This section firstly discusses the effects of temperature variations on stiffness determination. Then it provides a method to compensate the temperature effect in order to improve the accuracy of stiffness determination for different applications (e.g. high-temperature application). Lastly, the performance of the proposed compensation method is verified by experimental work.

5.4.1 **Theoretical Analysis**

5.4.1.1 **Influence of Fluid temperature**

First of all, theoretical analysis is given concerning the influence of changes in fluid temperature (alternatively called process or operating temperature by other researchers) on SRDP outcomes. As explained by prior research [93], the behaviour of a bent-tube Coriolis flowmeter is usually less influenced by variations in fluid temperature, compared with a straight-tube type. The reason is that for a bent-tube design, the axial stress generated by temperature fluctuations is negligibly small while a rapid change in temperature can lead to a large stress in a straight tube. In this study, the meter under test is a bent-tube Coriolis flowmeter, so the stress induced by temperature changes can be reasonably ignored in the following analysis.

A simplified equation of mass flowrate measurement in a Coriolis flowmeter working in its first vibration mode is given below [93], [94],

$$\dot{m} = \frac{C\, E_t\, I_t}{Y\left(\frac{G_{SR}}{L_t}\right) L_t^3}\, \Delta t \tag{5-24}$$

where

$$I_t = \frac{\pi}{64}(D_t^4 - d_t^4) \tag{5-25}$$

where C is a constant number; E_t is Young's modulus (or known as elastic modulus) of the tube material; I_t denotes the tube's moment of inertia, computed by the tube's outer diameter (D_t) along with the inner diameter (d_t); Δt is the created time shift by conveying flow; the tube length is L_t; G_{sr} represents the location of motion sensors arranged on the tube; $Y\left(\frac{G_{sr}}{L_t}\right)$ is a function of sensors' location along the tube, as a factor related to the arrangement of sensors for different model types of Coriolis flowmeters.

According to equations (5-1), (5-3) and (5-24), it can be found that essentially the physical tube stiffness is a term dependent on tube material properties as well as tube geometry, as shown below,

$$k \propto \frac{E_t\, I_t}{Y\left(\frac{G_{sr}}{L_t}\right) L_t^3} \tag{5-26}$$

When the fluid temperature (T_f) changes, the tube temperature can vary. Accordingly, it can affect Young's modulus (E_t), the moment of inertia (I_t) together with the tube geometry (G_{sr}, L_t) resulting from thermal expansion. Hence, physical tube stiffness can be regarded as a function of fluid temperature.

As presented above, structural diagnostics of a Coriolis flowmeter is implemented by tracing the relative change in SRDP. The initial value of reference SRDP (k_{C0}) is normally obtained from calibration procedure at the reference condition in factory. However, the in-situ operating or process condition can most likely deviate from the reference condition. For instance, if in-situ temperature differs from the reference temperature, this temperature shift would impact on physical tube stiffness as well as SRDP results. It means physical tube stiffness as well as SRDP are closely related to fluid temperature, rather than fixed values.

The compensation of changes in fluid temperature can refer to the existing study which has demonstrated how to deliver accurate mass flow measurement at cryogenic temperatures using Coriolis flowmeters [93], [95]. The compensation should consider two factors connected with temperature dependence of Young's modulus (E_t) along with thermal expansion. In terms of Young's modulus, a thermal change ratio (C_E) can be defined to characterize the temperature dependence,

$$C_E = \frac{(E_t/E_{t_0}-1)}{T_f-T_{f0}} = \frac{(E_t/E_{t_0}-1)}{\Delta T_f} \tag{5-27}$$

where E_{t_0} is Young's modulus at the reference fluid temperature T_{f0}; $\Delta T_f = T_f - T_{f0}$, denotes the temperature deviation from the reference temperature.

Similarly, a linear thermal expansion coefficient (α_e) can be expressed as,

$$\alpha_e = \frac{(D_t/D_{t0}-1)}{T_f-T_{f0}} = \frac{(d_t/d_{t0}-1)}{T_f-T_{f0}} = \frac{(L_t/L_{t0}-1)}{T_f-T_{f0}} \tag{5-28}$$

where D_{t0} denotes the tube outer diameter, d_{t0} is the tube inner diameter and L_{t0} is the tube length at the reference fluid temperature T_{f0}.

A simple correction term can be further derived from equations (5-26) to (5-28), for compensating the effects of changes in fluid temperature,

$$k_f = \left(1 + C_E\, \Delta T_f\right)\left(1 + \alpha_e\, \Delta T_f\right) k_{f0} \tag{5-29}$$

where k_f represents the corrected physical stiffness of tube, k_{f0} is the initial value of tube stiffness at reference temperature and ΔT_f is the temperature deviation from the reference.

The second-order term is extremely small which can be neglected as suggested by [93]. Hence, equation (5-29) can be further simplified as a linear expression by using a first-order correction factor (C_f),

$$k_f = \left[1 + (C_E + \alpha_e)\Delta T_f\right] k_{f0} = \left(1 + C_f\, \Delta T_f\right) k_{f0} \tag{5-30}$$

To compensate the fluid temperature effect, there are two terms involved in equation (5-30), including the correction factor (C_f) as well as the temperature shift (ΔT_f). For the stainless steel 316 tube which is used in this work, the factor (C_f) can be theoretically calculated based on values of C_E and α_e. The values of C_E and α_e at various temperatures are quoted from Table A.1 in [93]. The temperature correction factor (C_f) is finally estimated as -4.06×10^{-4}, according to the given material data at 20°C. Fluid temperature (T_f) generally refers to the temperature of carrying fluid, being assumed as equivalent to tube temperature. T_f can be measured by RTD (resistance temperature detector) attached on the Coriolis tube. The underlying assumption here is that RTD can supply representative measurement of tube temperature which requires temperature is

equally distributed along the tube and reaches at a stable condition. According to the real-time reading of RTD, the temperature deviation from reference (ΔT_f) can be obtained.

Furthermore, similar to fluid temperature, pressure would also affect the physical tube stiffness by changing Young's modulus (E_t) as well as the tube geometry [91], [96], [97]. Cunningham [98] reported an over-pressurized case which leads to noticeable rise in tube stiffness along with negative mass flowrate error. Since the high-pressure experimental conditions are not available in this work, the study on pressure effect in not included.

5.4.1.2 **Influence of Electromagnetic coil temperature**

As presented above, the working principle of stiffness diagnostics is to trace the relative change in SRDP between the factory baseline data (reference) and the real-time SRDP outcomes. It should be noted that this stiffness determination method offers a measure of stiffness related parameter (SRDP), rather than real physical tube stiffness. SRDP is directly proportional to physical tube stiffness via a scale factor (C_{SF}) while this factor is dominated by the strength of induced MF field (B) surrounding the drive coil and motion sensors, as illustrated by equation (5-14). Therefore, it is necessary to correct C_{SF} concerning the potential changes in MF strength. Since the induced MF strength can vary with electromagnetic coil temperature (T_{EMC}), coil temperature is another potential source which can affect SRDP outcomes, besides fluid temperature (T_f).

Electromagnetic coil temperature (T_{EMC}) refers to the temperature of created magnetic field around drive coil and sensors (copper coils), which cannot be measured directly but can be inferred by DCR (drive coil resistance). The measuring principle is that DCR is a value of temperature-dependent electrical resistance. Therefore, DCR can be used to provide an indirect measure of coil temperature owing to the temperature dependence of resistance for metal materials, as presented in [94], [99]. The fundamental assumption is that electromagnetic coil temperature around drive coil equal to that around sensors and so coil temperature can be well inferred by DCR.

Firstly, in order to characterize the temperature dependence of drive coil (copper coil), the temperature coefficient (α_{dr}) can be defined as,

$$\alpha_{dr} = \frac{(R_{dr}/R_{dr_0} - 1)}{T_{EMC} - T_{EMC0}} \tag{5-31}$$

where R_{dr} denotes the real-time drive coil resistance (DCR) at coil temperature T_{EMC}, R_{dr0} is the initial value of DCR at reference coil temperature T_{EMC0} stored in factory baseline.

The temperature coefficient (α_{dr}) can be understood as the resulting change in resistance per degree Celsius of temperature change. The value can be estimated from the thermal slope of resistance against temperature. With the known α_{dr} and real-time reading of DCR, the change in coil temperature from the reference can be calculated,

$$\Delta T_{EMC} = T_{EMC} - T_{EMC0} = \frac{(R_{drv}/R_{drv_0} - 1)}{\alpha_{dr}} \tag{5-32}$$

In this study, a thermal test was carried out to determine how DCR changes against ambient temperature (increasing from 0 to 100°C) by using a laboratory oven. To guarantee the accuracy of test results, the drive copper coil is taken from the same type of the Coriolis flowmeter (OPTIMASS 6400 S50) under test. Ten different temperature points (0, 10, 15, 20, 25, 30, 40, 60, 80, 100°C) have been tested individually. Actual temperature is measured by a temperature probe which can provides a resolution of 0.001°C. 20°C is selected as the reference temperature (T_{EMC0}). The value of coil resistance is measured using a multimeter with resolution of 0.1 ohms. Three repeats have been performed and recorded for each temperature point. The value of DCR is normalized with respect to the value at reference temperature (20°C). Figure 5.11 depicts how the normalized DCR changes against the temperature deviation (ΔT_{EMC}) from the reference. It clearly shows the linear temperature-dependence of copper coil resistance. According to the slope, the temperature coefficient (α_{dr}) of DCR can be finally determined as 3.896×10^{-3}. This measured value of α_{dr} is found fairly close to the common temperature coefficient of copper material given in [100], which verifies the correctness of this value. The very small difference is likely caused by the material variations as well as the geometry of copper coil.

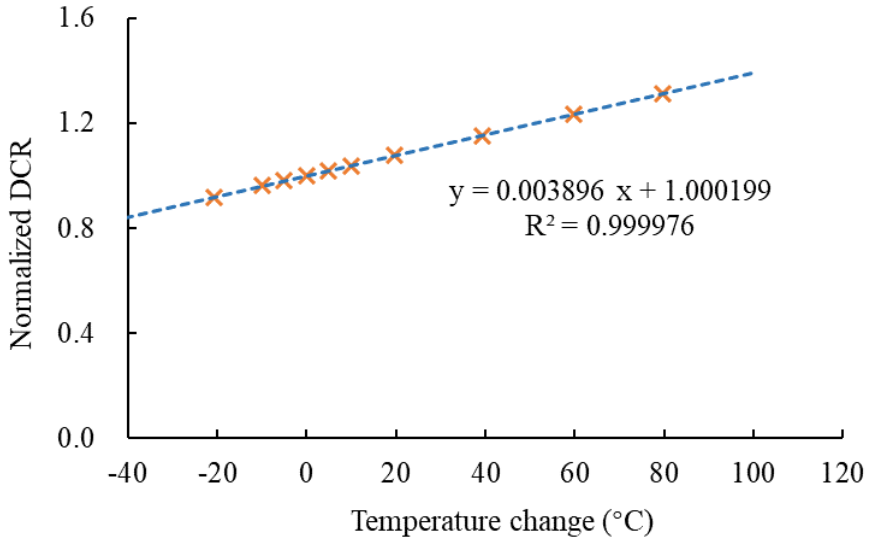

Figure 5.11 Trend of DCR against temperature change in thermal test

In addition, MF strength (B) can be generally regarded as a linear function of coil temperature (T_{EMC}) with a first-order coefficient (C_{MF}). In the light of equation (5-14), the compensation of the scale factor (C_{SF}) can be finally established below, using a squared correction term of $(1 + C_{MF}\,\Delta T_{EMC})$,

$$C_{SF} = (1 + C_{MF}\,\Delta T_{EMC})^2\, C_{SF0} \tag{5-33}$$

where C_{SF} denotes the corrected scale factor according to the current MF strength; C_{SF0} is the initial value of scale factor acquired at reference condition T_{EMC0}; ΔT_{EMC} can be obtained from equation (5-32); MF strength related the first-order correction factor C_{MF} is -3.5×10^{-4}.

5.4.2 **Compensation Scheme**

According to the analysis above, it has been clearly identified that there are two temperature sources which can affect stiffness diagnostic results (SRDP), including fluid temperature along with electromagnetic coil temperature. Fluid temperature (T_f) can be directly obtained by RTD whilst coil temperature (T_{EMC}) can be inferred from DCR. Accordingly, the whole compensation of temperature effect can be organized as two parts:

1) One part is to compensate the influence of coil temperature deviation (ΔT_{EMC}) by using equation (5-33). The change in coil temperature (ΔT_{EMC}) can be inferred from the real-time measurement of DCR, as illustrated in equation (5-32).

2) The other part is to compensate the effect of fluid temperature change (ΔT_f) by equation (5-30). The change in fluid (tube) temperature (ΔT_f) is measured by the real-time reading of RTD.

Figure 5.12 demonstrates the proposed compensation scheme for reducing the influences of temperature changes on stiffness determination. According to the current T_{EMC} inferred from DCR, raw SRDP data can be corrected with respect to the coil temperature effect. The real-time reading of RTD provides the current T_f and the factory baseline data of reference SRDP at T_{f0} is determined. The relative change between corrected SRDP and reference SRDP is obtained by examining the relative change in tube stiffness. By adding proper compensation, the accuracy of stiffness determination can be improved, which helps to achieve good sensitivity of erosion warning and reduce the chance of false alarms.

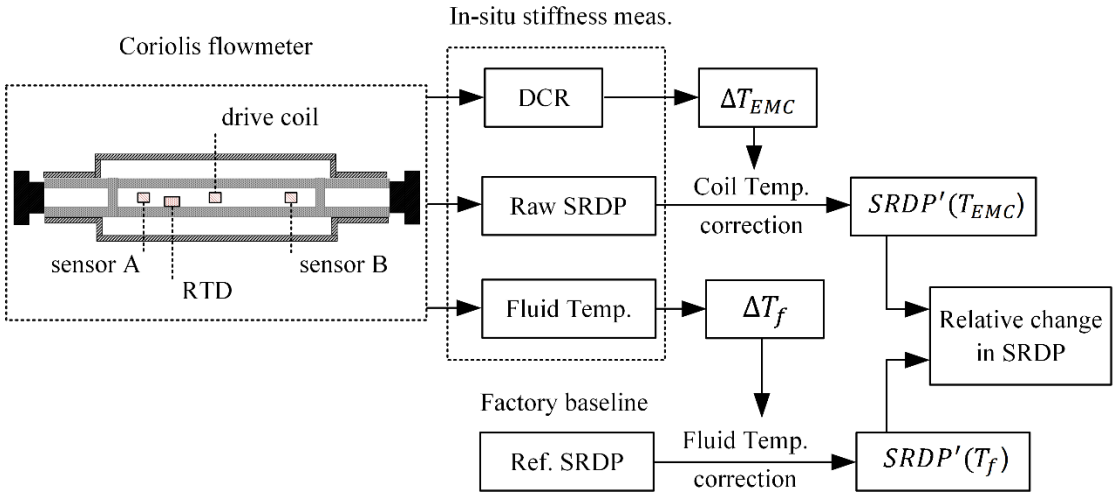

Figure 5.12 Schematic of temperature compensation for SRDP outcomes

5.4.3 **Experimental Validation of Temperature Effect**

In order to evaluate the performance of the compensation scheme for reducing the effect of temperature changes, the stiffness determination method is tested at various fluid temperatures (roughly between 18°C to 70°C) but a fixed mass flowrate (22000 kg/h). The flowmeter under test is CF2 (downstream meter on slurry rig) which is horizontally installed with belly down, as shown in Figure 5.13. The experiment was conducted on the standard calibration rig in the factory of the manufacturer, as illustrated by Figure 5.14. The varying temperature test conditions are achieved by choosing cold, warm and hot water supply tank. It covers a complete process of heating up from low temperature to high

temperature and then cooling down to cold setting. The reference temperature is selected as around 18.4°C. Accordingly, the reference value refers to the value acquired at reference condition (18.4°C). A set of data including normal measurement data (e.g. mass flowrate, density, drive frequency, fluid temperature) as well as structural condition related diagnostic data (e.g. SRDP) are continuously collected from the meter under test.

Figure 5.13 Photo of the Coriolis flowmeter under test (CF2) with belly down

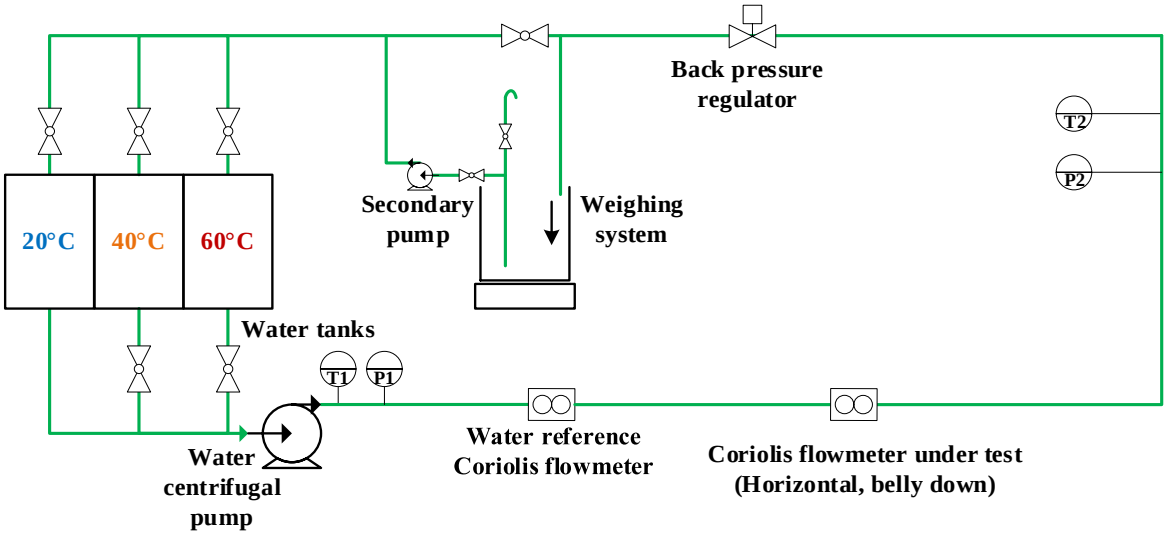

Figure 5.14 Schematic of the standard gravimetric calibration rig

Figure 5.15 displays the experimental conditions of this varying-temperature process. Transition points in which the test conditions are distinctly unsteady are excluded. Figure 5.15 demonstrates the resulting change in DCR from varying fluid temperatures. It

suggests that electromagnetic coil temperature could need longer time to become stable than tube temperature, under the influence of varying fluid temperatures.

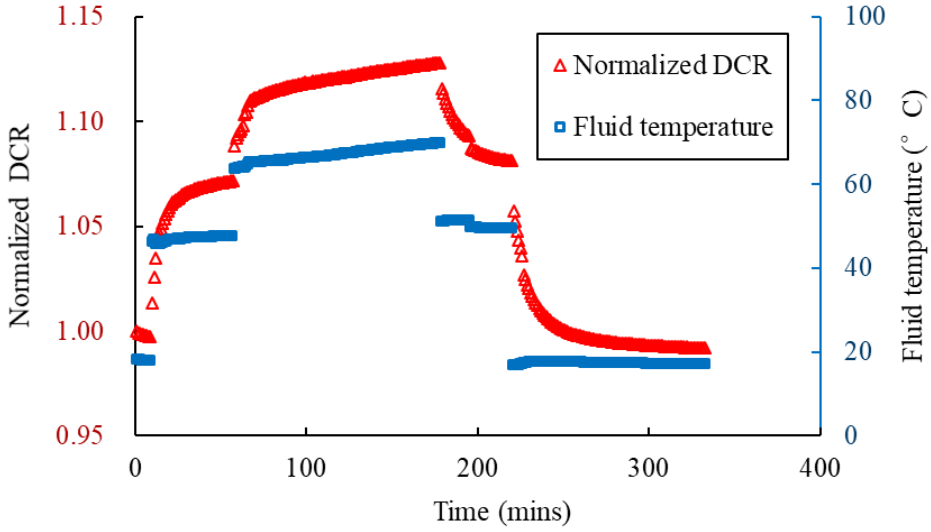

Figure 5.15 Trend of normalized DCR under varying temperature conditions

The raw SRDP data (no corrections) is normalized with respect to the reference and the outcomes are shown in Figure 5.16 (a). Without correction of MF strength, the raw data of SRDP is distributed without an observable temperature-dependent relationship. Then the compensation of MF strength is added into the raw data. The corrected SRDP results are given by Figure 5.16 (b). After compensation, the correct SRDP outcomes exhibit a linear declining tendency with the increasing fluid temperature, which agrees with the thermal properties (negative temperature-dependence) of tube material (stainless steel). According to the curve fitting result as shown in Figure 5.16 (b), the first-order correction factor can be solved as -3.59×10^{-4}. Compared with the estimation from theoretical analysis given in Section 5.4.1, this curve fitting result is close to the theoretical estimation (-4.06×10^{-4}). The small difference between experimental outcome and theoretical estimation is likely attributable to the material variations arising from the manufacturing processes, which can also be found in earlier research [93]. It is believed that the actual experimental results can be more accurate than the theoretical estimation based on material data. Therefore, the temperature correction factor (C_f) is eventually set as -3.59×10^{-4}, which is used for compensating the effect of fluid temperature in this study.

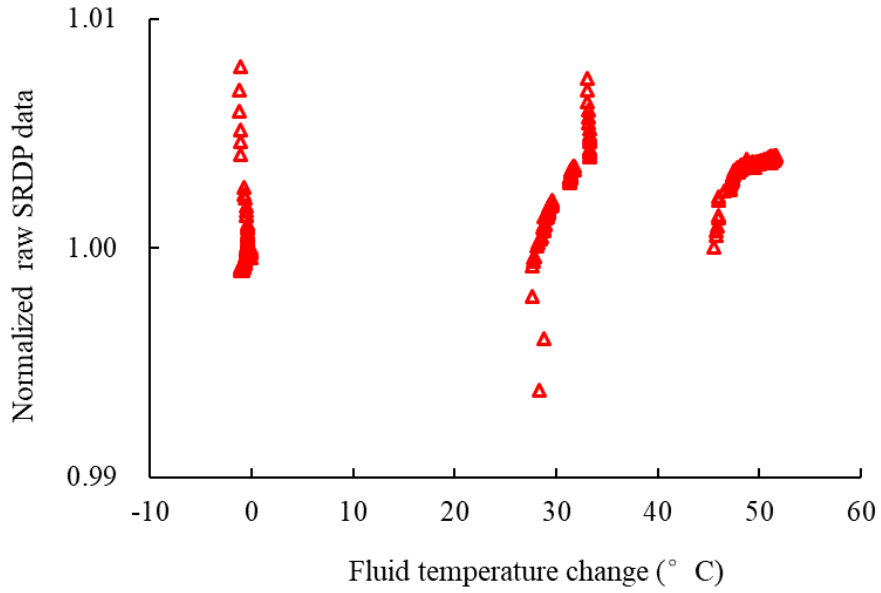

(a) Raw SRDP data against fluid temperature change

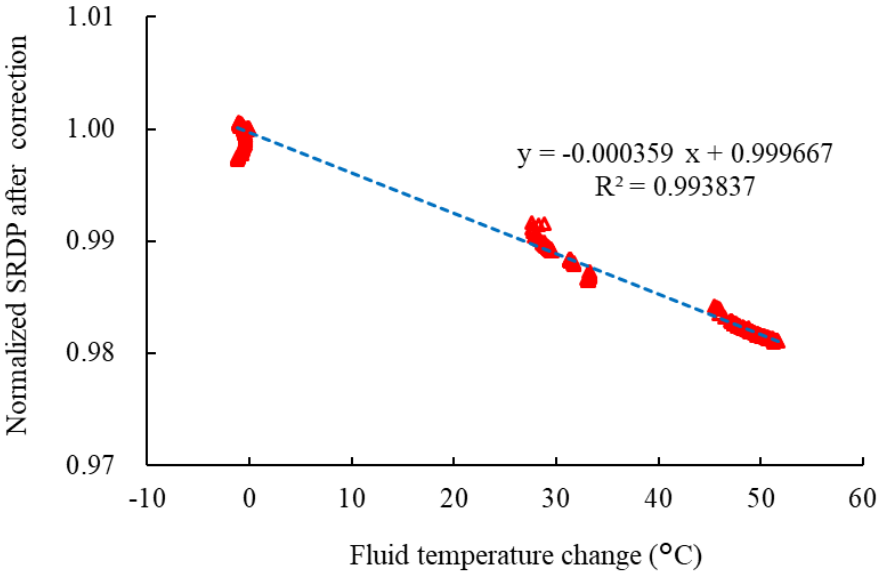

(b) Corrected SRDP data against fluid temperature change

Figure 5.16 Normalized SRDP outcomes before and after correction of MF strength at various fluid temperatures

Then, according to the raw data, the relative changes in SRDP outcomes are calculated with respect to the reference value at reference temperature. The purpose is to examine the influence of temperature changes on stiffness determination results. Without any corrections, large relative changes (up to ±0.8%) can be observed due to the variations in

temperature, as shown in Figure 5.17. Such noticeable effect of temperature would directly lead to the errors in stiffness determination. Therefore, it is necessary to compensate the effect of temperature, which is particularly beneficial for high-temperature processes or cryogenic applications.

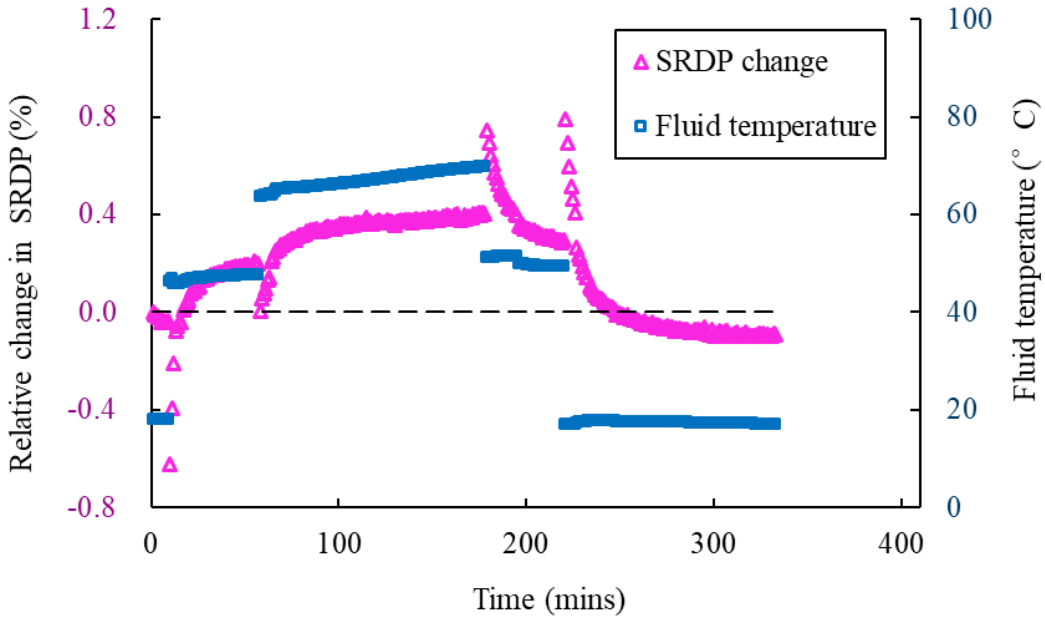

Figure 5.17 Relative change in SRDP outcomes without correction at various fluid temperatures

The compensation scheme is further tested according to the experimental data at various temperatures. The purpose is to examine whether this compensation method can successfully correct SRDP results at different temperatures. The actual experimental data can be served as the reference. According to the real-time data of fluid temperature and DCR, the raw data of SRDP are corrected following the method as demonstrated by Figure 5.12. The relative errors (differences) between compensated results and actual experimental data are calculated. As depicted by Figure 5.18, firstly, the compensation results prove the satisfactory performance of this compensation method. The relative differences are within around ±0.3% error range. Improvements can be clearly seen by comparing the results in Figure 5.17 and Figure 5.18. Secondly, it can be observed that greater errors always occur at the transition periods (e.g. the early time of heating up or cooling down). In addition, the errors can get closer to zero line over time, which means when process time is long enough the errors can drop down to a very small level. It suggests the large errors are primarily induced by the instability of external environment,

instead of this compensation method. The underlying reason is likely that a sudden change in process conditions (e.g. temperature) could lead to a certain delay in the responses of measured data (e.g. DCR, temperature reading from RTD) in a Coriolis flowmeter. Therefore, it can be concluded that this compensation method is able to successfully compensate the effects caused by changes in temperature when the process conditions become stable.

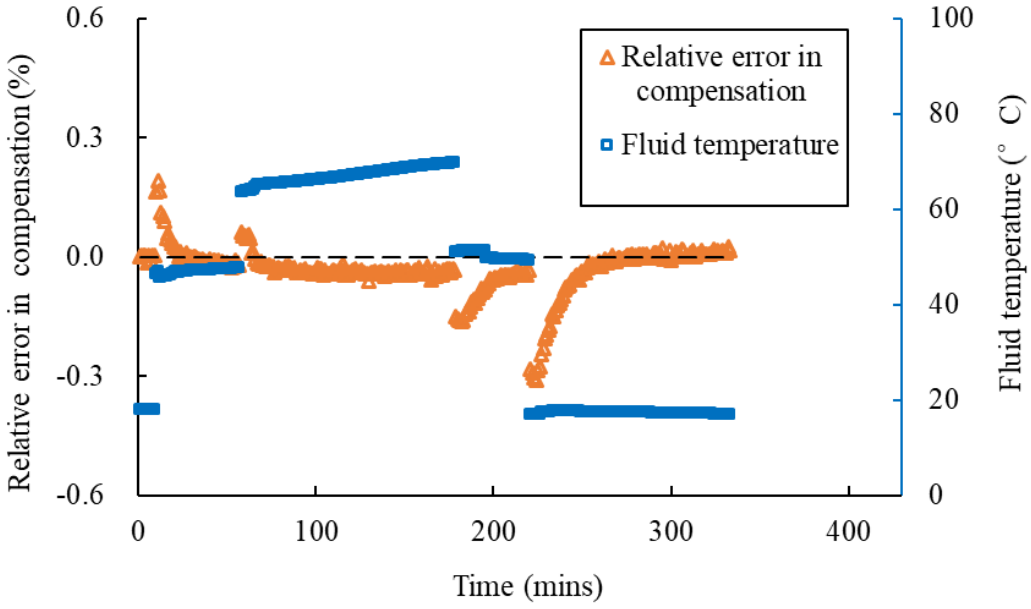

Figure 5.18 Relative error between compensated data and experimental data at various fluid temperatures

5.5 Erosive Tests and Results

5.5.1 **Description of Erosive Tests**

There are two primary purposes of performing the erosive tests. One purpose is to verify the feasibility of this stiffness diagnostic approach for monitoring the structural condition of a Coriolis flowmeter in an abrasive application. The second purpose is to identify the achievable sensitivity of stiffness diagnostics to report tube erosion at an early time. As mentioned above, the proper limit of allowable change in SRDP is still a remaining question. The limit should be set as low as possible in order to give early warning of tube erosion while too low limit may increase the chance of false alarms in consideration of the influences of process conditions. This study is aiming to reduce the uncertainty of stiffness determination (indirect measurement) within ±1%. In other words, by monitoring and

tracking the relative change in SRDP, the aim is to achieve a sensitivity of stiffness diagnostics at 1%.

Erosive tests were conducted on slurry flow test rig with dilute slurry (sand-water mixture) flow. Erosion rate is generally dependent on a range of variables including properties of solid particles (e.g. size, shape, hardness), flow conditions (e.g. flow velocity, flow density, flow viscosity, solid concentration, impact angle and velocity of solid particles) as well as characteristics of target material (mechanical and endurance properties) [81], [101]. Among these factors, the impact velocity of solid particles has been identified as a leading factor of erosion rate [102]–[104]. Hence, in the erosive tests, effective control should be given on mass flowrate as well as sand concentration of slurry flow while the delivered flow velocity is estimated as a key parameter. The reason of using dilute slurry is to simulate the natural erosion process so that the Coriolis flowmeters can be eroded at a slow manner which can help recognize the sensitivity of this stiffness diagnostic method.

Erosive tests were performed by selecting the horizontal circulation loop at mass flowrate around 20000 kg/h and ambient temperature ranging from 18°C to 28°C. The average flow velocity in DN50 test section is estimated roughly 2.82 m/s and the flow velocity in the Coriolis tube is about 7.20 m/s. The sand concentration of slurry flow is approximately 4% by weight (around 1.5% by volume). The sand in use comes from the same source of natural quartz sand as utilized in the flow measurement test presented in Section 4.3.2, but with a larger grain size in range of 300 μm to 600 μm so as to slightly speed up the erosion process. During the flow recirculation, it has been noticed that the centrifugal pump would grind the sand particles into smaller segments or more spherical shape so that the erosion rate would decrease over the running time. The Coriolis flowmeters under test are CF1 and CF2 which are installed with their belly up and belly down, respectively. In order to keep consistent with the experimental assessment above (Sections 5.3.2 and 5.4.3), the experimental results of CF2 are presented in detail. The experimental findings of CF1 are very close to that of CF2, giving a similar conclusion regarding stiffness diagnostics and meter recalibration, not repeated here. The results derived from CF1 is attached in Appendix 3.

Before erosive tests, the measurement uncertainty of the meters under test has been verified, as described in Section 4.3.4. The relative error in mass flowrate is within the claimed specification (±0.1%), which means the meter under test can deliver accurate flow

measurement. After that, a certain amount of sand was fed into the liquid storage tank to create the dilute slurry flow for erosion purpose. Normal flow measurement data (including mass flowrate, flow density, drive frequency, fluid temperature, DCR) and structural condition related diagnostic data (including SRDP1, SRDP2, SRDP3) are recorded periodically throughout the erosive tests. Before data logging, the slurry flow is circulated at least 30 mins for providing stable test conditions. Diagnostic data are collected at a low mass flowrate (nearly 5000 kg/h) with quite low sand concentration, by adjusting the rotation speed of pump and turning off the agitator. When the agitator is off, most sand particles would settle in the slurry storage tank, and only a small quantity of sand could enter into the test section. In this case, the fluid becomes very dilute slurry flow, which can be assumed as close to "clean water". The purpose is to reduce flow noises for stiffness diagnostics in consideration of the disturbances of sand movements.

The reference of diagnostic parameters (SRDP1, SRDP2, SRDP3) are established by using factory baseline data. The relative change in SRDP (Δk_C) is tracked throughout the erosive tests. According to the value of Δk_C, the erosive tests were interrupted for performing as-found tests which can help examine the potential erosion through standard calibration producers with clean water. The first time of as-found test was carried out when Δk_C reached nearly −0.6%. And the second as-found test was conducted for Δk_C observed at around −1%. Correspondingly, the erosive tests are divided into two stages, Stage 1 (Δk_C at about −0.6%) and Stage 2 (Δk_C at roughly −1%).

5.5.2 **Results of Stiffness Diagnostics**

As described in Section 5.3.2, structural condition related diagnostic data (SRDP1, SRDP2, SRDP3) are recorded at an interval of 60 s. In erosive tests, 60 data points (1-hour duration) are collected at each time of data acquisition. In order to deliver accurate results of stiffness determination, the raw data of SRDP outcomes are further corrected for reducing the effect of temperature changes. The detail of the compensation method has been presented in Section 5.4. The erosion hours are roughly estimated as the additional information for recording the erosion process. The reference of diagnostic parameters is established by using factory baseline data. Figure 5.19 displays the trend of relative change in SRDP1, SRDP2, SRDP3 against the erosion time, after temperature correction. The data points are averaged within the logging duration of 60 mins and the mean values are also shown in Figure 5.19.

Firstly, relative changes in SRDP (Δk_C) are all negative values. It means SRDP outcomes (diagnostic "tube stiffness") drift negatively from the factory baseline, which agree with the expected reduction in tube thickness associated with erosion. The declining tendency of Δk_C can be evidently observed during the erosive tests, suggesting the meter under test has been gradually eroded due to the impingement of solids. Secondly, the resulting wear in Stage 1 is small and the diagnostic outcomes exhibit some fluctuations, while the diagnostic results become more stable in Stage 2. Thirdly, there are some small differences between results of SRDP1, SRDP2 and SRDP3. As mention above, SRDP2 and SRDP3 are computed from the frequency response induced by different frequency locations. The differences between SRDP2 and SRDP3 can be attributable to the different locations of the additional frequencies added into the drive signal. The underlying reason of such differences is the deviation in the measured FRF data from the true FRF data. SRDP1 is the mean value of SRDP2 and SRDP3. By averaging SRDP2 and SRDP3, it is believed to help lower the measurement uncertainty resulting from different frequency locations.

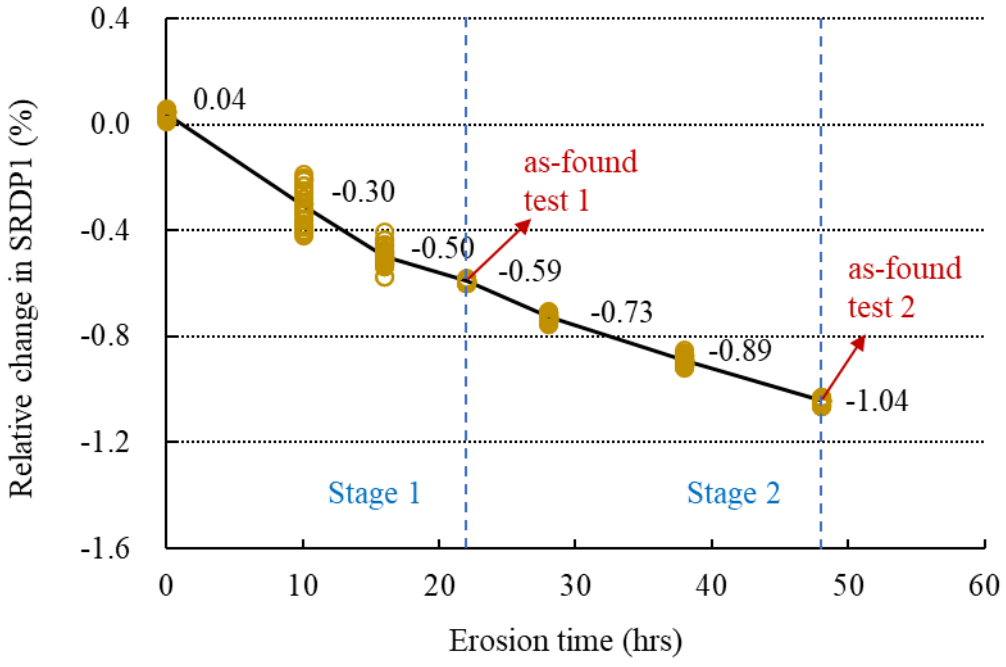

(a) Relative changes in SRDP1 with erosion time

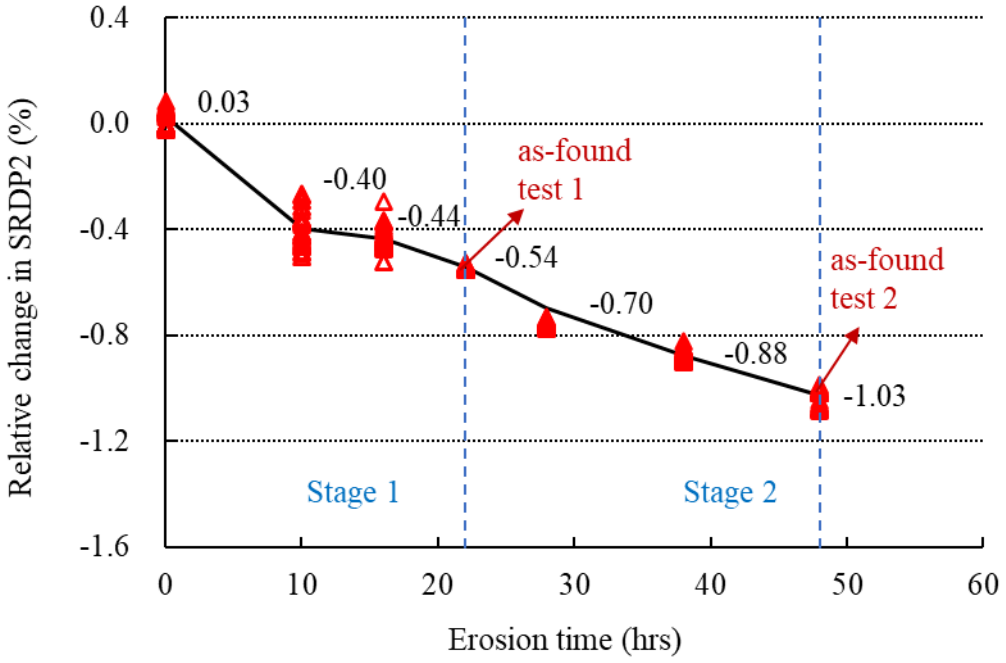

(b) Relative changes in SRDP2 with erosion time

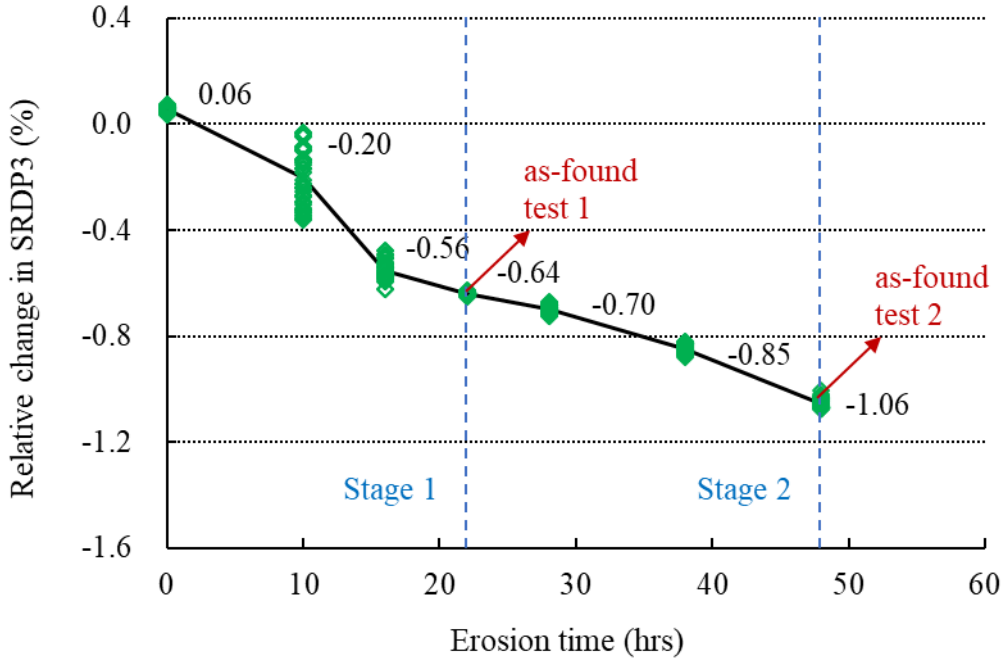

(c) Relative changes in SRDP3 with erosion time

Figure 5.19 Trend of relative changes in SRDP during erosive tests on CF2

To further investigate the asymmetry of tube, the signal amplitude of sensor A and sensor B are compared by using the logged data of sensor level. The relative change in asymmetry can be calculated below,

$$\Delta ASY = \frac{S_B/S_A - S_{B0}/S_{A0}}{S_{B0}/S_{A0}}\ 100\% \tag{5-34}$$

where S_B denotes the sensor level of sensor B, S_A is the sensor level of sensor A; S_{B0}, S_{A0} are the initial values under a reference condition; ΔASY is the relative change as a measure of asymmetry.

As presented earlier, when the flow direction is forward, the sensor located on outlet side is sensor A while sensor B is on the inlet side. For a normally working Coriolis flowmeter free of structural damage, the difference between sensor level of sensor A & B is always negligible. Figure 5.20 depicts how asymmetry changes during the erosive tests. The results well prove the resulting asymmetry from erosive damage on tube. The upward tendency in the positive direction implies the asymmetry is increasing with the erosion time. In addition, the positive values illustrate that the sensor level of sensor B is higher than that of sensor A. In other words, the signal amplitude of inlet sensor is greater than that of outlet, which also agrees with the experimental finding reported in an earlier publication [11]. The reason is probably the outlet side may experience more severe erosive damage than the inlet side, as suggested by the visual inspection after sectioning the eroded tube in [11] as well as the numerical simulation results in a relevant study [104].

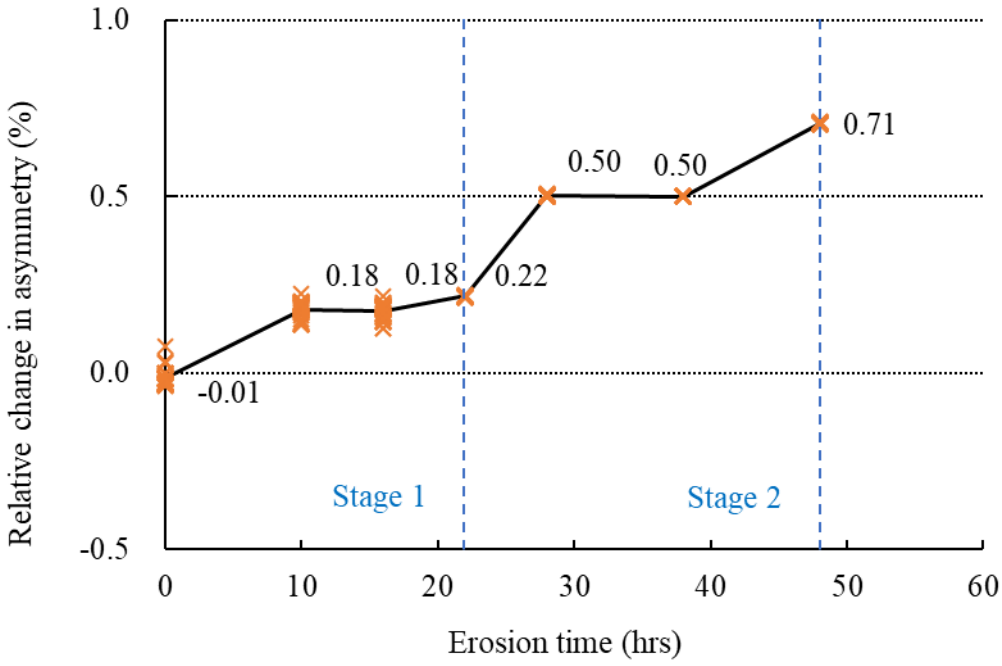

Figure 5.20 Trend of relative changes in asymmetry during erosive tests on CF2

5.5.3 **Meter Recalibration with Clean Water**

As-found tests were performed on the meter under test (CF2) to evaluate the performance in terms of mass flowrate and density measurement. Relative error in mass flowrate is identified by means of start-stop gravitational method. Density error is calculated with respect to the reading of a reference flowmeter sharing the same type and meter size. As-found tests were carried out on the standard calibration test rig in the manufacturer' factory. The flowmeter under test is horizontally installed with its belly down. Calibrations were conducted by using the standard gravimetric calibration rig as given by Figure 5.14. Cold water supply tank is utilized to provide clean water at temperature in range of 16°C to 18°C. Three different mass flowrates are tested with five repeats at each mass flowrate.

The results of as-found tests are shown in Figure 5.21. According to the results from as-found test 1, mass flowrate measurement drifts positively to around 0.45% while there is a negative deviation about −0.67% in density reading, beyond the claimed measurement uncertainty. In as-found test 2, the meter under test is found to over-read mass flowrate with relative error roughly 1.99% whilst the meter under-estimate density with −2.75% error.

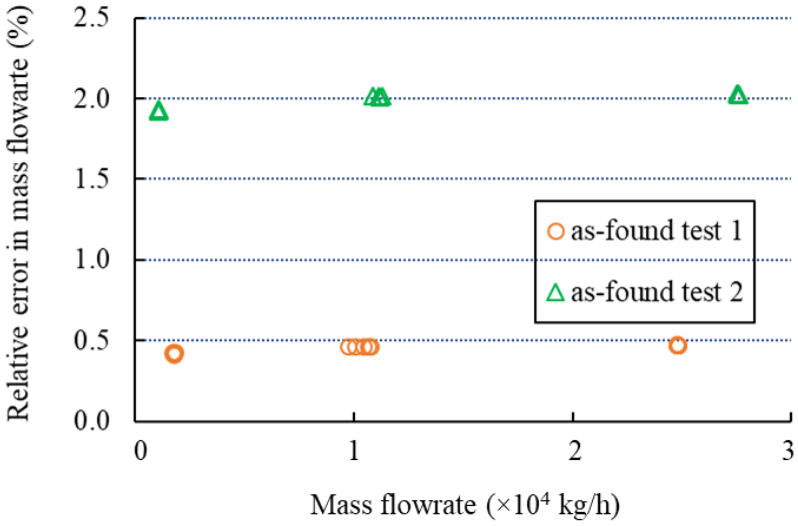

(a) Relative errors in mass flowrate due to erosion

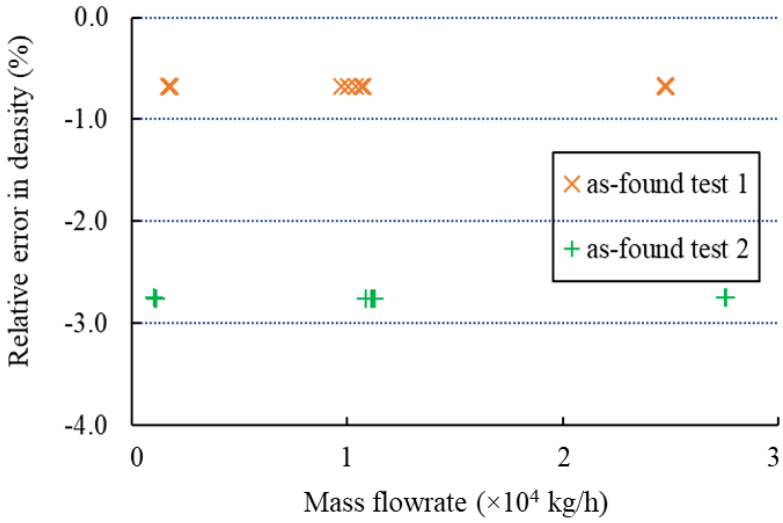

(b) Relative errors in density due to erosion

Figure 5.21 As-found results of CF2

Table 5.1 summarizes the results obtained from erosive tests and as-found tests, listing the averaged relative change in SRDP1, SRDP2, SRDP3, along with the averaged relative error in mass flowrate as well as density. It can be concluded that linked with tube erosion, the Coriolis flowmeter under test offers over-reading in mass flowrate and under-reading in density. The drift in the delivered measurement results well demonstrates the erosive damage occurring on the tubes.

Table 5.1 Resulting change in SDRP data and the measurement performance of CF2

Average (%) / Test	Relative change in SRDP1	Relative change in SRDP2	Relative change in SRDP3	Relative error in mass flowrate	Relative error in density
As-found test 1	−0.59	−0.54	−0.64	0.45	−0.67
As-found test 2	−1.04	−1.03	−1.06	1.99	−2.75

Erosion can cause a thinner tube wall and accordingly a reduction in tube stiffness. When the tube becomes less stiff, the induced time-shift is larger than the correct value and consequently the Coriolis flowmeters can over-read the mass flowrate. This over-estimation in mass flowrate can be alternatively explained by equation (5-1). As presented above, tube stiffness is directly linked with C_{FCF} (flow calibration factor). Because of the decrease in tube stiffness, C_{FCF} would drift negatively from the original value stored in the transmitter. If the meter still uses the original (incorrect) value of C_{FCF}, positive error in mass flowrate can be produced, as shown in Table 5.1.

The density error can be illustrated by the measuring principle as given in equation (5-4) or (5-6). There are two terms which would affect density measurement, including tube stiffness (k_1) and the lumped mass (m_1) which is composed of the effective mass of empty tube together with the conveying flow. As erosion happens, both terms (k_1 and m_1) become smaller owing to the loss of tube material. Nevertheless, these two factors can lead to the opposite effect on density reading. Decrease in k_1 can cause over-reading of density while smaller m_1 results in under-estimation of density. Thus, the overall influence on density measurement depends on which factor is more dominant. In this study, density measurement is governed by the negative impact of mass loss so under-estimation occurs in the meter under test. It should be noted that the density error of an eroded meter can be positive or negative, differing from various types of the measuring tubes from different

manufacturers. For example, the previous investigation [11] identified the positive density errors in one meter under test but negative density deviations in the other meter under test from another manufacturer.

As a short summary, due to tube erosion, an eroded Coriolis flowmeter can over-read mass flowrate whilst it may under-read or over-read flow density depending on the types of tube. Moreover, additional measurement errors can be caused by asymmetry associated with uneven loss in tube thickness. Numerical simulation may help to further investigate into the location of erosion scars as well as the asymmetry errors, which is beyond the topic of this work.

In this work, the measured 1% change in SDRP is also correlated with the physical wear of the tube. A small inspection camera is utilized to observe the potential erosive damage on the inside surface of tube wall, as shown in Figure 5.22. Several erosion scars appeared on the bends of tube and Figure 5.23 gives the examples of observed erosion. Relatively larger erosion scars can be found on the outer radius of the outlet bend, which is consistent with the experimental findings in the existing study [11]. Different meter installations can affect the locations of the erosion scars on the Coriolis tubes, resulting from the gravity effect on solids. Noticeable erosion scars are discovered on the outer radius of the outlet bend from CF2 with its belly down (Figure 5.23 (a)). For CF1 with its belly up (Figure 5.23 (b)), some erosion scars on the inner radius of the inlet bend become observable.

Figure 5.22 Photo of visual inspection of the meter under test (CF2)

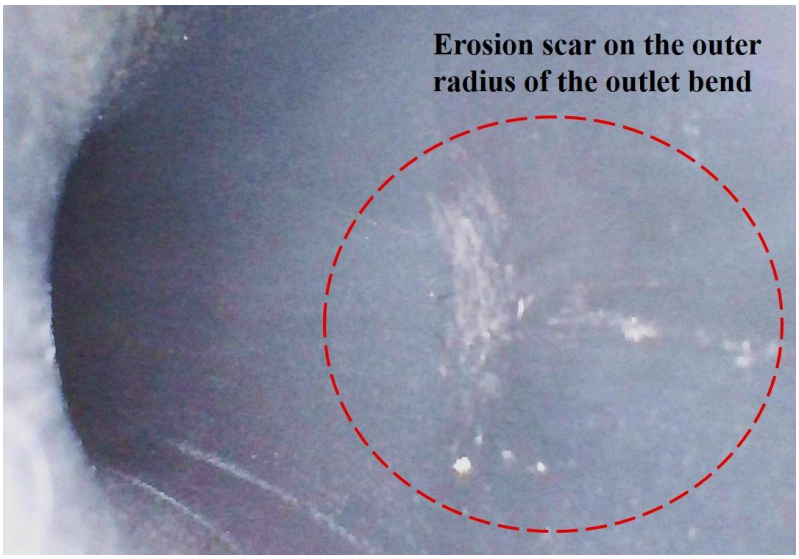

(a) Erosion scars observed from CF2 with belly down

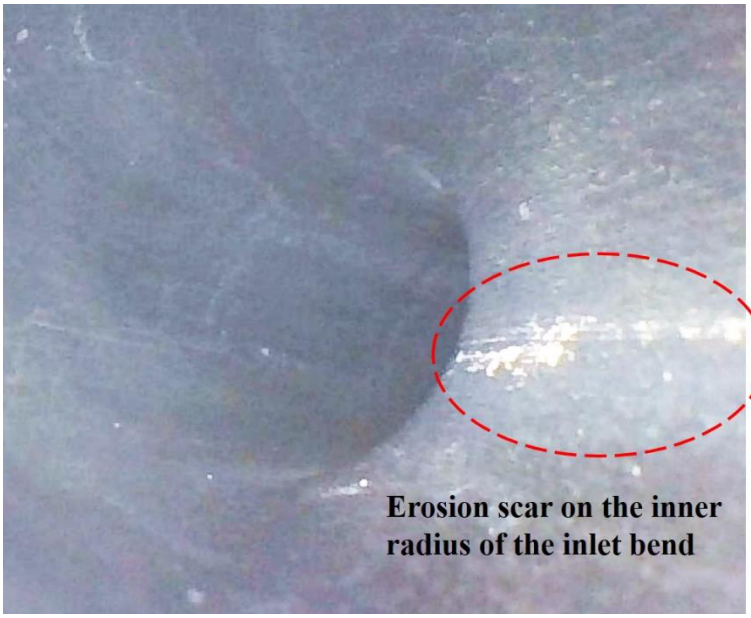

(b) Erosion scars observed from CF1with belly up

Figure 5.23 Photos of observed erosion scars

To conclude, such hardly noticeable erosion scars by visual inspection (Figure 5.23) on Coriolis tubes can result in severe measurement error (1.99%) in mass flowrate. The capability of erosion identification for the in-situ examination of tube structural conditions on a real time basis highlights the significance as well as benefits of the condition monitoring methodology based on on-line stiffness determination as illustrated in this thesis. According to the results from erosive tests with dilute slurry, the sensitivity of the

stiffness diagnostics reaches 1%, being able to provide the end user with sufficient early warning of tube erosion.

5.6 Summary

This chapter has described an in-situ structural condition monitoring technique through stiffness diagnostics. The chapter covers the detailed explanation of methodology of stiffness determination (indirect measurement of stiffness), identification of potential factors affecting the accuracy of stiffness determination, along with erosive tests and results served as experimental validation.

The Coriolis oscillation system is simply represented by a spring-mass-damper model, and the influence of modal parameters (degrees of freedom, damping level) on the extraction of stiffness has been investigated. Through computational simulation, it has been identified that changes in degrees of freedom as well as heavy damping bring errors in stiffness determination. Experimental results have demonstrated the excellent performance of stiffness determination under single-phase flow condition (measurement uncertainty less than ±0.15%), and found noticeable uncertainty encountered in some complex cases, (±10% measurement uncertainty arising from the air-water mixed flow). The results have suggested that in order to deliver accurate and reliable stiffness determination, it is recommended to retain the process conditions stable and consistent with the reference condition in the factory, which can help reduce the chance of false alarms of tube erosion.

In addition, the influence of temperature changes on stiffness determination has been investigated by theoretical analysis and examined by experimental tests under varying temperature conditions. Fluid temperature as well as electromagnetic coil temperature has been identified as two factors which can affect the outcomes of stiffness determination. In order to improve the measurement accuracy, compensation scheme of temperature effect is proposed. The performance of this compensation method has been further tested by using experimental data acquired at various fluid temperatures. The results have illustrated the satisfactory performance of this compensation method which can yield corrections within around ±0.3% error range, suggesting the compensation scheme can favorably reduce the effect of temperature variations.

Erosive tests were carried out with sand-water mixed flow to evaluate the performance of the condition monitoring technique. As-found tests were performed with clean water so as

to examine the measurement performance of the Coriolis flowmeter under test due to the consideration of potential tube erosion. The experimental assessment has clearly illustrated when the relative change in SRDP reaches −1%, the condition monitoring technique successfully gives the warning of tube erosion with confidence. Furthermore, as-found tests have reported that the eroded flowmeters over-read the mass flowrate due to the reduction in tube stiffness while density errors can be positive or negative depending on different types of measuring tubes.

Chapter 6
Conclusions and Recommendations for Future Work

6.1 Introduction

The research work presented in this thesis is concerned with the measurement of solid-liquid two-phase flow using Coriolis flowmeters incorporating error compensation and structural condition monitoring techniques. Two primary technical issues in slurry flow metering using Coriolis flowmeters have been investigated. One issue arises from the influence of entrained solid particles on Coriolis flow metering and the other issue results from the potential erosive damage on the measuring tubes of Coriolis flowmeters.

A laboratory-scale slurry flow test rig has been designed and constructed in Instrumentation Lab at University of Kent to provide the experimental platform for investigating the two technical issues. Experimental investigations confirm the negative measurement errors of Coriolis flowmeters with dilute sand-water flow (SVF within 4%), which agree with the theoretical study based on the existing theory of phase decoupling effect. A basic analytical model is derived from the decoupling effect theory, for predicting and correcting measurement errors of Coriolis flowmeters under solid-liquid two-phase flow conditions. According to the actual experimental data, the basic analytical model is further improved to yield better model prediction. As a result, a semi-empirical analytical model is proposed for compensating the negative impact of entrained solid particles on Coriolis flow metering.

Concerning the second issue, an in-situ structural condition monitoring technique based on tube stiffness determination is employed to examine the structural health of Coriolis measuring tubes. The factors which affect stiffness determination (e.g. damping level, two-phase flow conditions) as well as the effect of variations in temperature (including fluid temperature and electromagnetic coil temperature) on stiffness determination are identified and investigated, both theoretically and experimentally. Moreover, a compensation scheme is proposed to reduce the temperature effect on stiffness determination. Furthermore, erosive

tests have been conducted under sand-water erosion conditions to evaluate the effectiveness and sensitivity of the condition monitoring technique whilst the behaviours of eroded meters are assessed with clean water.

This chapter presents the conclusions that have been drawn from the research programme conducted and makes recommendations for future work in the field.

6.2 Conclusions

6.2.1 **Design and Construction of the Slurry Flow Test Rig**

A cost-effective and easily operable slurry flow test rig has been designed and constructed. According to the experimental work in this research, the essential functions of the slurry flow test rig are required to cover three major tasks: conducting start-stop batching procedures in a gravimetric system for identifying mass flowrate errors, flow sampling for examining density errors as well as erosive tests for evaluating the performance of the structural condition monitoring technique used for the verification of the structural health of Coriolis flowmeters. Practical considerations and experience in the design and construction of the laboratory-scale slurry flow test rig are provided. The primary focus of the rig design and construction is to offer accurate references to the Coriolis flowmeters under test. The full details are explained from the following aspects: main circulation loop, selection of valves, flow sampling point, weighing system, installation of flowmeters as well as safety precautions. The advantages and limitations of this slurry flow test rig are discussed, which can offer practically useful information to future improvements in rig design and construction.

6.2.2 **Measurement Errors of Coriolis Flowmeters with Slurry Flow**

In light of existing theory of phase decoupling effect and compressibility effect, theoretical analysis of the influence of entrained solid particles on Coriolis flow metering is provided. Theoretical analysis illustrates that the leading contribution to the measurement errors with slurry flow is from the phase decoupling effect, whereas the impact of compressibility changes is negligibly small, since both solid and liquid phases can be regarded as relatively incompressible.

Experimental tests of two DN50 bent-tube Coriolis flowmeters (KROHNE OPTIMASS 6400 S50) were conducted with dilute sand-water slurry (SVF below 4%). Two Coriolis flowmeters were installed on the horizontal test section of the slurry flow test rig with two different orientations (belly up and belly down) for the purpose of comparison. Through experimental work, the influence of the solid phase on Coriolis flow metering is envaulted and analysed. Negative errors (ranging from 0 to −2%) are recognized in both mixture mass flowrate and density readings with solid fraction up to 4% in volume, which agree with the theoretical analysis of decoupled motions between solid and liquid phases.

According to the theoretical study, a basic analytical model is established to compensate the decoupling effect. Through comparisons between the results from analytical modelling and experimental tests, a certain level of deviations is observed. As can be found from the comparisons, analytical modelling over-estimates the measurement errors (absolute values), mainly attributable to the underlying assumptions in modelling. Accordingly, a correction term is introduced into the basic analytical model to reduce the differences between model prediction and actual experimental data. After correction, the original errors in mass flowrate measurement are reduced to mostly within ±0.2% and errors in density measurement are down to ±0.4% error range.

In terms of the influence of installation orientations, experimental results show that the installation with the belly up is superior to mounting the belly down. Greater errors (the absolute value) are observed from the meter with its belly down. The underlying reason is believed to be the opposite effect of asymmetry errors which is superimposed on the negative decoupling errors.

This proposed methodology for slurry flow measurement using Coriolis flowmeters is simple for the manufacturers or users to implement the derived semi-empirical analytical model to compensate the measurement errors of Coriolis flowmeters due to decoupling effect. The benefit of using analytical modelling approach is that the measurement errors can be corrected based on the apparent mass flowrate and density readings (internal parameters) from Coriolis flowmeters along with other prior information (e.g. liquid density, solid density), without using other supplementary instrumentation for providing reference (e.g. actual SVF).

6.2.3 **Structural Condition Monitoring of Coriolis Flowmeters**

An in-situ structural condition monitoring technique through stiffness diagnostics (indirect measurement of stiffness) is reported for examining the structural health of Coriolis flowmeters when handling abrasive or corrosive applications. By adding additional frequencies into the drive signal of Coriolis flowmeters, FRF (frequency response function) data are collected and processed for analysing the resonance behaviour of Coriolis flowmeters. A stiffness related diagnostic parameter (SRDP) is obtained from FRF and used to track the potential structural changes in the Coriolis measuring tubes.

In order to identify the potential factors affecting the extraction of stiffness, computational simulation is conducted based on a spring-mass-damper vibration model, so as to examine the outcomes of stiffness determination when the modal parameters (e.g. damping, degrees of freedom of the oscillating system) change from the original values (typically acquired under a reference condition in the factory). Simulation outcomes illustrate that varying degrees of freedom as well as heavy damping associated with variable process conditions can bring errors in stiffness determination. Experimental results demonstrate the reliable performance of stiffness determination under single-phase flow condition (measurement uncertainty below ±0.15%,) and show the noticeable uncertainty encountered in some complex cases, (e.g. ±10% uncertainty arising from the entrained air). The results suggest that, in order to deliver accurate and reliable stiffness determination, it is recommended to retain the process conditions stable and consistent with the reference process condition in the factory of the manufacturer, which can help reduce the chance of false alarms of tube erosion.

In addition, the influence of temperature changes on stiffness determination is investigated through theoretical analysis and experimental tests. Fluid temperature and electromagnetic coil temperature are identified as two factors which affect stiffness determination. In order to improve the accuracy of stiffness determination, a compensation scheme is proposed with respect to the temperature effect. Experimental outcomes validate the effectiveness of this compensation method which can yield corrections within ±0.3% error range.

Erosive tests were carried out with sand-water mixture flow to evaluate the feasibility and the achievable sensitivity of the condition monitoring technique. Besides, as-found tests were performed with clean water so as to examine the behaviour of Coriolis flowmeters

potentially affected by tube erosion. The experimental results clearly illustrate the sensitivity of stiffness diagnostics is able to reach 1% for warning tube erosion with confidence. Furthermore, as-found tests report that because of the decrease in tube stiffness, the mass flow rate reading from the eroded flowmeters is higher than the true value, while density measurement can be over-reading or under-reading, depending on different tube types.

The benefit of the structural condition monitoring technique is that it utilizes the onboard electronics and internal parameters to examine the structural health of a Coriolis flowmeter without the requirement of additional sensors or devices.

6.3 Recommendations for Future Research

The work presented in the thesis has demonstrated the usefulness and potential of the outcomes of the research programme. However, an error compensation scheme based on the semi-empirical analytical model and a structural condition monitoring technique based on stiffness determination to apply Coriolis flowmeters for slurry flow metering are still in their development state. A number of areas require further research and development in the near future, which have been identified as follows:

5) With regard to the limitations of the slurry flow test rig, mainly referring to the present difficulty in achieving target sand concentration for experimental tests, for example, the future improvements can be made by employing two separate tanks rather than using one big slurry mixing tank. One tank can act as a sand-water mixer tank with a smaller volume storing relatively dense sand-water mixtures, whilst the other tank can merely serve as the clean water supplier. In addition, conical tank should be a better choice than the cylindrical geometry, which can help drain sand-water mixtures out.

6) Experimental tests in this study were conducted with dilute sand-water flow and only one type of commercial Coriolis flowmeters was tested. Extensive experimental tests should be performed under a wider range of conditions, so as to further evaluate the proposed methodology for slurry flow measurement. Several suggestions are summarized as follows: slurry flow should be further extended to a higher level of solid concentration, distribution of different grain size of solids, sand-oil mixtures for simulating the real-world processes of high viscosity oil in the petroleum industry. In addition, slurry transportation in vertical or inclined pipeline have not been included in

this study. The cases of different pipe orientations also need to be considered in future work for exploring the gravity effect on slurry flow metering. Moreover, different types of Coriolis flowmeters should be utilized for further investigations into the influences of tube geometry as well as meter size.

7) For monitoring the structural conditions of a Coriolis flowmeter, stiffness determination in this work is performed by adding two additional off-resonant frequencies into the drive signal. The present study should be further extended by employing and comparing different methods for determining tube stiffness, for example using curve fitting method as well as different additional frequencies with different numbers and locations. Moreover, in order to implement the structural condition monitoring technique for various applications, future work is required to identify the effects of operating pressure along with different tube geometry (straight tube and bent tube) on the behaviour of stiffness determination.

8) In consideration of the influences of various process conditions, it will be beneficial to provide a comprehensive assessment of structural health in order to reduce the chance of false alarms. Instead of delivering a conclusion solely according to the change in "tube stiffness", advanced diagnostic technique needs to be performed on the basis of further analysis of the resonance behaviour of a Coriolis flowmeter. Available internal parameters such as 2-phase signal or drive gain, along with other diagnostic parameters related to Q factor or damping ratio could assist in the structural condition monitoring of a Coriolis flowmeter in situ.

References

[1] R. Durand and E. Condolios, “Experimental study of the hydraulic transport of coal and solid material in pipes”, in Proceeding of Colloquium on the Hydraulic Transport of Coal, National Coal Board, London, UK, Nov 1952.

[2] API (American Petroleum Institute), “API RP 19C, Recommended practice for measurement of proppants used in hydraulic fracturing and gravel-packing operations”, Washington D.C, 2008.

[3] D. Mader, Hydraulic Proppant Fracturing and Gravel Packing, Elsevier, 1989.

[4] M. Dehghani, “Oil well sand production control”, in Proceeding of 1st International Applied Geological Congress, Mashad Branch, Iran, Apr 2010.

[5] K. J. Albion, L. Briens, C. Briens, and F. Berruti, “Multiphase flow measurement techniques for slurry transport”, International Journal of Chemical Reactor Engineering, vol. 9, pp.18-19, 2011.

[6] C. A. Shook and M. C. Roco, Slurry Flow: Principles and Practice, Elsevier, 2015.

[7] F. Liang et. al, “Overview of existing proppant technologies and challenges”, in Proceeding of SPE Middle East Oil & Gas Show and Conference, Society of Petroleum Engineers, Mar 2015.

[8] K. M. A. S. Bandara, P. G. Ranjith, and T. D. Rathnaweera, “Improved understanding of proppant embedment behavior under reservoir conditions: A review study”, Powder Technology, vol. 352, pp. 170-192, 2019.

[9] E. J. Esswein, M. Breitenstein, J. Snawder, M. Kiefer, and W. K. Sieber, “Occupational exposures to respirable crystalline silica during hydraulic fracturing”, Journal of occupational and environmental hygiene, vol. 10, pp. 347-356, 2013.

[10] C. A. Meese, M. E. Mullen and R. D. Barree, “Offshore hydraulic fracturing technique”, Journal of Petroleum Technology, vol. 46, pp. 226-229, 1994.

[11] T. Boussouara and J. P. Couput, “Assessment of erosion in flowmeters using

performance and diagnostic data", in 32nd International North Sea Flow Measurement Workshop, St Andrews, UK, Oct 2014.

[12] V. Fattahpour, M. Moosavi, and M. Mehranpour, "An experimental investigation on the effect of grain size on oil-well sand production", Petroleum Science, vol. 9, pp. 343-353, 2012.

[13] R. C. Worster and D. F. Denny, "Hydraulic transport of solid material in pipes", in Proceedings of the Institution of Mechanical Engineers, vol. 169, pp. 563-586,1955.

[14] D. G. Thomas, "Transport characteristics of suspensions: Part VI. Minimum transport velocity for large particle size suspensions in round horizontal pipes", AIChE Journal, vol. 8, pp. 373-378, 1962.

[15] G. Sommer, "The state of the art in the measurement of slurries", in IFAC Proceedings, vol. 20, pp. 131-140, 1987.

[16] C. V. O'Keefe et al, "Non-invasive passive array technology for improved flow measurements of slurries and entrained air", in 4th International Platinum Conference: Platinum in transition 'Boom or Bust', pp. 21-30, 2010.

[17] F. Yuan and R. Pal, "Measurement of solids concentration in aqueous slurries using a microwave technique", Chemical engineering science, vol. 50, no. 22, pp. 3525-3533, 1995.

[18] T. Wang and R. Baker, "Coriolis flowmeters: A review of developments over the past 20 years, and an assessment of the state of the art and likely future directions", Flow Measurement and Instrumentation, vol. 40, pp. 99-123, 2014.

[19] H. Zhu, A. Rieder and Y. Lin, "An innovative technology for coriolis metering under entrained gas condition", in Conference Proceeding of FLOMEKO 2016, Sydney, AU 2016.

[20] "Entrained gas management in Coriolis flowmeters", KROHNE, Available on: https://academy-online.krohne.com/elearning/en/courses/entrained-gas-management-coriolis-flowmeters/, Accessed: 27-Sep-2020.

[21] "Multiphase flow in Coriolis mass flow meters-Identifying multiphase conditions and remediating errors", Micro Motion White Paper (2018), [Online]. Available:

https://www.emerson.com/documents/automation/white-paper-multiphase-flow-in-coriolis-mass-flow-meters-identifying-multiphase-conditions-remediating-errors-micro-motion-en-4236516.pdf, Accessed: 27-Sep-2020.

[22] O. L. Ibryaeva, V. V. Barabanov, M. P. Henry, M. Tombs, and F. Zhou, "A benchmark data set for two-phase Coriolis metering," Flow Measurement and Instrumentation, vol. 72, pp. 101721, 2020.

[23] L. Wang, J. Liu, Y. Yan, X. Wang, and T. Wang, "Gas-liquid two-phase flow measurement using Coriolis flowmeters incorporating artificial neural network, support vector machine, and genetic programming algorithms", IEEE Transactions on Instrumentation and Measurement, vol. 66, no. 5, pp. 852-868, 2017.

[24] R. Thorn, G. A. Johansen, and B. T. Hjertaker, "Three-phase flow measurement in the petroleum industry", Measurement Science and Technology, vol. 24, pp. 12003-12020, 2013.

[25] E. Michaelides, C. T. Crowe, and J. D. Schwarzkopf, Multiphase flow handbook (2nd Edition), CRC Press, 2016.

[26] P. Doron and D. Barnea, "Pressure drop and limit deposit velocity for solid-liquid flow in pipes," Chemical Engineering Science, vol. 50, pp. 1595-1604, 1995.

[27] S. M. Peker and S. S. Helvaci, Solid-Liquid Two Phase Flow (Chapter 6: Flow of Settling Slurries), Elsevier, 2011.

[28] P. Doron and D. Barnea, "Flow pattern maps for solid-liquid flow in pipes," International journal of multiphase flow, vol. 22, pp. 273-283, 1996.

[29] M. L. Nayyar et al, Piping handbook, Mcgraw-hill New York, 1992.

[30] Y. Yan, L. Wang, T. Wang, X. Wang, Y. Hu, and Q. Duan, "Application of soft computing techniques to multiphase flow measurement: A review," Flow Measurement and Instrumentation, vol. 60, pp. 30-43, 2017.

[31] J. Liu, "Gas-Liquid Two-Phase Flow Metering Using Coriolis Flowmeters," Ph.D. dissertation, University of Kent, Canterbury, 2018.

[32] S. K. Lahiri and K. C. Ghanta, "Support vector regression with parameter tuning

assisted by differential evolution technique: Study on pressure drop of slurry flow in pipeline," Korean Journal of Chemical Engineering, vol. 26, pp. 1175-1185, 2009.

[33] S. K. Lahiri and K. C. Ghanta, "Artificial neural network model with parameter tuning assisted by genetic algorithm technique: study of critical velocity of slurry flow in pipeline," Asia-Pacific Journal of Chemical Engineering, vol. 5, pp. 763-777, 2010.

[34] H. M. Azamathulla and Z. Ahmad, "Estimation of critical velocity for slurry transport through pipeline using adaptive neuro-fuzzy interference system and gene-expression programming," Journal of Pipeline Systems Engineering and Practice, vol. 4, pp. 131-137, 2013.

[35] R. C. Baker, Flow Measurement Handbook: Industrial Designs, Operating Principles, Performance, and Applications (2nd Edition). Cambridge University Press, 2016.

[36] C. A. Shook, R. G. Gillies, and R. S. S. Sanders, "Pipeline hydrotransport: With applications in the oil sand industry," SRC Publication No. 11508-1E02, SRC Pipe Flow Technology Centre, May, 2002.

[37] C. A. Shook and J. H. Masliyah, "Flow of a slurry through a venturi meter," The Canadian Journal of Chemical Engineering, vol. 52, pp. 228-233, 1974.

[38] O. A. El Masry and K. El Shobaky, "Pulsating slurry flow in pipelines," Experiments in fluids, vol. 7, pp. 481-486, 1989.

[39] L. P. Liang et al, "Statistical modeling and signal reconstruction processing method of EMF for slurry flow measurement," Measurement: Journal of the International Measurement Confederation, vol. 54, pp. 1-13, 2014.

[40] C. A. Peters, J, and Shook, "Electromagnetic sensing of slurry concentration," The Canadian Journal of Chemical Engineering, vol. 59, pp.430-437,1981.

[41] K. Xu and X. Wang, "Signal modeling of electromagnetic flowmeter under sine wave excitation using two-stage fitting method," Sensors and Actuators, A: Physical, vol. 136, pp. 137-143, 2007.

[42] T. Okada, T. Nishijima, Y. Kuroki, and K. Kuromori, "Advanced technology in

electromagnetic flowmeters," in Proceedings of ISA Conference, 1990.

[43] E. Eryurek, R. Gao and L. H. Tsoukalas, High accuracy signal processing for magnetic flowmeters, Patent US 6505517B1, 2003.

[44] M. Mahmud, Y. Faraj, and M. Wang, "Visualisation and metering of two phase counter-gravity slurry flow using ERT," Procedia Engineering, vol. 102, pp. 930-935, 2015.

[45] J. Y. Xu, Y. X. Wu and Z. C. Zheng, "Measurement of solid slurry flow via correlation of Electromagnetic Flow Meter, electrical resistance tomography and mechanistic modelling," Journal of Hydrodynamics, vol. 21, pp. 557-563, 2009.

[46] T. Dyakowski, L. F. C. Jeanmeure, and A. J. Jaworski, "Applications of electrical tomography for gas-solids and liquid-solids flows-A review," Powder Technology, vol. 112, pp. 174-192, 2000.

[47] Y. Faraj and M. Wang, "ERT investigation on horizontal and vertical counter-gravity slurry flow in pipelines," Procedia Engineering, vol. 42, pp. 588-606, 2012.

[48] S. A. Hashemi, A. Sadighian, S. I. A. Shah, and R. S. Sanders, "Solid velocity and concentration fluctuations in highly concentrated liquid-solid (slurry) pipe flows," International Journal of Multiphase Flow, vol. 66, pp. 46-61, 2014.

[49] Y. Zhao, M. Wang, and J. Yao, "Electrical impedance tomography spectroscopy method for characterising particles in solid-liquid phase," in Proceedings of AIP Conference, Apr 2014.

[50] U. Datta, T. Dyakowski, and S. Mylvaganam, "Estimation of particulate velocity components in pneumatic transport using pixel based correlation with dual plane ECT," Chemical Engineering Journal, vol. 130, pp. 87-99, 2007.

[51] J. A. Bamberger and M. S. Greenwood, "Measuring fluid and slurry density and solids concentration non-invasively," Ultrasonics, vol. 42, pp. 563-567, 2004.

[52] J. A. Bamberger and M. S. Greenwood, "Using ultrasonic attenuation to monitor slurry mixing in real time," Ultrasonics, vol. 42, pp. 145-148, 2004.

[53] J. M. Furlan et al, "Development of A-scan ultrasound technique for measuring

local particle concentration in slurry flows," Powder Technology, vol. 215-216, pp. 174-184, 2012.

[54] C. V. O'Keefe et al, "Non-invasive passive array technology for improved flow measurements of slurries and entrained air," in Proceedings of the 4th International Platinum Conference: Platinum in transition 'Boom or Bust', The Southern African Institute of Mining and Metallurgy, 2010.

[55] J. W. Kunze, R. Storm, and T. Wang, "Coriolis Mass Flow Measurement with Entrained Gas," in Proceedings of the 17th Sensors and Measuring Systems, Nuremberg, Germany, Jun 2014.

[56] M. Anklin, W. Drahm, and A. Rieder, "Coriolis mass flowmeters: Overview of the current state of the art and latest research," Flow Measurement and Instrumentation, vol. 17, pp. 317-323, 2006.

[57] J. Hemp and J. Kutin, "Theory of errors in Coriolis flowmeter readings due to compressibility of the fluid being metered," Flow Measurement and Instrumentation, vol. 17, pp. 359-369, 2006.

[58] N. T. Basse, "A review of the theory of Coriolis flowmeter measurement errors due to entrained particles," Flow Measurement and Instrumentation, vol. 37, pp. 107-118, 2014.

[59] A. Rieder, H. Zhu, and W. Drahm, "Coriolis mass flowmeters: On measurement errors in two-phase conditions," in Proceedings of the 13th International Flow Measurement Conference FLOMEKO, 2005.

[60] D. L. Gysling, "An aeroelastic model of Coriolis mass and density meters operating on aerated mixtures," Flow Measurement and Instrumentation, vol. 18, pp. 69-77, 2007.

[61] L. Wang, Y. Yan, X. Wang, T. Wang, Q. Duan, and W. Zhang, "Mass flow measurement of gas-liquid two-phase CO2 in CCS transportation pipelines using Coriolis flowmeters", International Journal of Greenhouse Gas Control, vol. 68, pp. 269-275, 2018.

[62] J. Liu, T. Wang, Y. Yan, X. Wang, and L. Wang, 'Investigations into the behaviours

of Coriolis flowmeters under air-water two-phase flow conditions on an optimized experimental platform', in Proceedings of 2018 IEEE International Instrumentation and Measurement Technology Conference (I2MTC), Houston Texas, USA, May 2018.

[63] J. A. Weinstein, D. R. Kassoy, and M. J. Bell, "Experimental study of oscillatory motion of particles and bubbles with applications to Coriolis flow meters," Physics of Fluids, vol. 20, pp.103306, 2008.

[64] M. Tombs, F. Zhou, and M. Henry, "Two-phase Coriolis mass flow metering with high viscosity oil," Flow Measurement and Instrumentation, vol. 59, pp. 23-27, 2017.

[65] M. Li, M. Henry, F. Zhou, and M. Tombs, "Two-phase flow experiments with Coriolis Mass Flow Metering using complex signal processing," Flow Measurement and Instrumentation, vol. 69, pp. 101613, 2019.

[66] M. Henry et al., "Two-phase flow metering of heavy oil using a Coriolis mass flow meter: A case study," Flow Measurement and Instrumentation, vol. 17, pp. 399-413, 2006.

[67] M. Henry, M. Tombs, M. Zamora, and F. Zhou, "Coriolis mass flow metering for three-phase flow: A case study," Flow Measurement and Instrumentation, vol. 30, pp. 112-122, 2013.

[68] N. T. Basse, "Coriolis flowmeter damping for two-phase flow due to decoupling," Flow Measurement and Instrumentation, vol. 52, pp. 40-52, 2016.

[69] H. Zhu, "Application of Coriolis mass flowmeters in bubbly or particulate two-phase flows," Ph.D. dissertation, University of Erlangen-Nuremberg, Erlangen, 2008.

[70] F. Ahmadi, M. Ebrahimian, R. S. Sanders, and S. Ghaemi, "Particle image and tracking velocimetry of solid-liquid turbulence in a horizontal channel flow," International Journal of Multiphase Flow, vol. 112, pp. 83-99, 2019.

[71] "OPTIMASS Supplementary Instructions: Corrosion and abrasion guide". [Online]. Available: https://cdn.krohne.com/dlc/AD_OPTIMASS_Corrosion-Abrasion-

Guide_en_160518_4004917302_R02.pdf, Accessed: 27-Sep-2020.

[72] M. J. Rensing, A. T. Patten, T. J. Cunningham, and M. J. Bell, Meter Electronics and Methods for Verification Diagnostics for a Flow Meter, Patent US 8280651B2, 2012.

[73] A. Rieder, W. Drahm, H. Zhu, M. Braun, "Method for Determining Measuring Tube Wall Thickness of a Coriolis Flow Measuring Device," Pantent US 8515691B2, 2013.

[74] R. Baker, T. Wang, Y. Hussain and J. Woodhouse, Method for Testing a Mass Flow Rate Meter, Pantent US 7603885B2, 2009.

[75] T. J. Cunningham, "Using Structural Integrity Meter Verification to Track Corrosion in Coriolis Flowmeters," Micro Motion White Paper (2009), [Online]. Available: https://www.emerson.com/documents/automation/white-paper-using-structural-integrity-meter-verification-to-track-corrosion-in-coriolis-flowmeters-micro-motion-en-66236.pdf, Accessed: 27-Sep-2020.

[76] T. J. Cunningham and T. O'Banion, "Allow Smart Meter Verification to Reduce your Proving and Proof-Test Costs," in Proceedings of the 8th International Symposium on Fluid Flow Measurement (ISFFM), Micro Motion, 2012.

[77] A.A. Daneshy, "Numerical solution of sand transport in hydraulic fracturing", Journal of Petroleum Technology, vol. 30, pp. 132-140, 1978.

[78] N. P. Brown and N. I. Heywood, Slurry Handling: Design of solid-liquid systems, Springer Science & Business Media, 1991.

[79] A. Abouel-Kasem et al, "Design and performance of slurry erosion tester", Journal of Tribology, vol. 132, pp. 1-10, 2010.

[80] P. J. Zu, I. Hutchings and G. Burstein, "Design of a slurry erosion test rig", Wear, vol. 140, pp. 331-344, 1990.

[81] M. Buszko and A. Krella, "Slurry erosion–design of test devices", Advances in Materials Science, vol. 17, pp. 5-17, 2017.

[82] G. Towler and R. Sinnott, Chemical engineering design - chemical engineering

design principles, practice and economics of plant and process design (2nd Edition), Chapter 18 - Specification and Design of Solids-Handling Equipment, Butterworth-Heinemann Press, 2013.

[83] N. J. Alderman, “The design , selection and application of valves for slurry”, BHR group conference series publication, vol. 20, pp. 673-698, 1996.

[84] “Mettler Toledo K-Line datasheet”. [Online]. Available: https:// https://www.mt.com/dam/ind/MTA/Platforms/DataSheet/BR_K_Line_en_120625.pdf, Accessed: 27-Sep-2020.

[85] “OPTIMASS 6000 (with MFC 400) handbook”. [Online]. Available: https://cdn.krohne.com/dlc/MA_OPTIMASS6000_en_180927_4001894006_R06.pdf, Accessed: 27-Sep-2020.

[86] J. A. Weinstein, ‘The motion of bubbles and particles in oscillating liquids with applications to multiphase flow in Coriolis meters’, Ph.D. dissertation, University of Colorado, Boulder, 2008.

[87] S. Enz, J. J. Thomsen and S. Neumeyer, “Experimental investigation of zero phase shift effects for Coriolis flowmeters due to pipe imperfections,” Flow Measurement and Instrumentation, vol. 22, pp. 1-9, 2011.

[88] J. J. Thomsen and J. Dahl, “Analytical predictions for vibration phase shifts along fluid-conveying pipes due to Coriolis forces and imperfections,” Journal of Sound and Vibration, vol. 329, pp. 3065-3081, 2010.

[89] J. Kutin, G. Bobovnik, J. Hemp, and I. Bajsi, “Velocity profile effects in Coriolis mass flowmeters : Recent findings and open questions,” Flow Measurement and Instrumentation, vol. 17, pp. 349-358, 2006.

[90] “IAPWS R7-97(2012): IAPWS-IF97 Industrial Formulation for Thermodynamic Properties of Water and Steam”. [Online]. Available: http://www.iapws.org/relguide/IF97-Rev.html, Accessed: 27-Sep-2020.

[91] T. Wang and Y. Hussain, “Pressure effects on Coriolis mass flowmeters,” Flow Measurement and Instrumentation, vol. 21, pp. 504-510, 2010.

[92] D. J. Ewins, Modal Testing: Theory and Practice (2nd edition), John Wiley & Sons

Ltd, 2009.

[93] T. Wang and Y. Hussain, “Coriolis mass flow measurement at cryogenic temperatures,” Flow Measurement and Instrumentation, vol. 20, pp. 110-115, 2009.

[94] T. Wang and Y. Hussain, Method for installing and operating a mass flowmeter and mass flowmeter, US Patent 20100326204 A1, 2010.

[95] A. T. Pattern, Method and apparatus for operating coriolis flowmeters at cryogenic temperatures, US Patent 6512987 B1, 2003.

[96] C. Mills, “Calibrating and operating Coriolis flow meters with respect to process effects,” Flow Measurement and Instrumentation, vol. 71, pp. 101649, 2020.

[97] K. Kolahi, T. Schröder, and H. Röck, “Model-Based Density Measurement With Coriolis Flowmeter,” IEEE Transactions on Instrumentation and Measurement, vol. 55, pp. 1258-1262, 2006.

[98] T. J. Cunningham, “Verification of Coriolis flowmeter calibration: Theory and Practice, Including Lab and Field Results,” Micro Motion White Paper (2015), [Online]. Available: https://www.emerson.com/documents/automation/white-paper-verification-of-coriolis-flow-meter-calibration-2015-0164-micro-motion-en-66688.pdf, Accessed: 27-Sep-2020.

[99] T. Wang, Device for determining temperature as well as measuring arrangement for determining flow, US Patent 9921088 B2, 2018.

[100] J. Dellinger, “The temperature coefficient of resistance of copper,” Journal of the Franklin Institute, vol. 170, (3), pp. 213-216, 1910.

[101] R. Wood et al., “The performance of marine coatings and pipe materials under fluid-borne sand erosion,” Wear, vol. 219, pp. 46-59, 1998.

[102] Q. B. Nguyen et al., “Slurry erosion characteristics and erosion mechanisms of stainless steel,” Tribology International, vol. 79, pp. 1-7, 2014.

[103] K. Haugen, O. Kvernvold, A. Ronold, and R. Sandberg, “Sand erosion of wear-resistant materials: Erosion in choke valves,” Wear, vol. 186-187, pp. 179-188, 1995.

[104] M. J. Bell and M. Macleod, “Assessment of particle erosion in Coriolis meters,” in 30th International North Sea Flow Measurement Workshop, St Andrews, UK, Oct 2012.

Appendices

Appendix 1 Specification of the Slurry Flow Test Rig

Table A.1 Specification of the slurry flow test rig

Item	Specification
Test section	DN50 bore
Pressure range	Below 3 bar
Temperature range	Ambient temperature (15 °C to 30 °C)
Flowrate range	3 to 30 m^3/h
Phase	Single phase water /Sand-water two-phase

Table A.2 Main components on the slurry flow test rig

Item	Description	Size & Rating
Tank	PP Copolymer	1500 litres
Main pump P1	Low-pressure centrifugal pump	5.5 kW, capacity 100 m^3/h, maximum discharge pressure 1.5 barg, suction PN16 & DN100, discharge DN80 & PN16
Main pump Inverter	Centrifugal pump Inverter	400V/3ph/50Hz
Second pump P2	Agitator	0.37 kW
Second pump Inverter	Agitator inverter	400V/3ph/50Hz
Pipe	clear PVC pipe	PN16, DN50
CF1	Upstream Coriolis flowmeter (KROHNE OPTIMASS 6400 S50), with bypass pipe	PN40, DN50, nominal flowrate 35000 kg/h, measurement accuracy ±0.1% for mass flowrate in single-phase liquid
CF2	Downstream Coriolis flowmeter (KROHNE OPTIMASS 6400 S50)	The same as CF1
EMF	Electromagnetic flowmeter, (KROHNE OPTIFLUX 4300 S50)	PN40, DN50, measuring range within ±12 m/s (around 80 m^3/h), accuracy down to ±0.2%, allowable solid content below 70% by volume

Table A.3 Valves on the slurry flow test rig

Label	Description	Size & Rating
V1	Switch valve	4” butterfly valve
V2	Switch valve	2” pinch valve
V3	Switch valve	2” butterfly valve
V4	Switch valve	2” butterfly valve
V5	Switch valve	2” butterfly valve
V6	Three-way valve	2” three-way ball valve
V7	Switch/regulating valve	2” pinch valve, also can be used to regulate back pressure
V8	Switch valve	2” pinch valve
V9	Switch valve	2” butterfly valve
V10	Switch valve	3” butterfly valve
V11	Switch valve	2” butterfly valve
V12	Switch valve	2” butterfly valve
V13	Switch valve	2” butterfly valve
V14	Switch valve	2” butterfly valve
V15	Switch valve	2” butterfly valve
V16	Switch valve	2” butterfly valve
PRV1	Pressure relief valve	1/2” safety valve

Table A.4 Details of the experimental conditions

Test type	Mass batching test	Flow sampling test	Erosive test
Mass flowrate (kg/h)	8200, 12000, 14300, 17000, 20000	8200, 12000, 14300, 16000, 18000	20000
Estimated SVF	0 to 4%	0 to 4%	1.5%
Sand size (μm)	150 to 300	150 to 300	300 to 600
Average velocity in S50 Coriolis tubes (m/s) (estimated)	2.95 to 7.20	2.95 to 6.48	7.20
Average velocity in DN50 test pipe (m/s) (estimated)	1.15 to 2.82	1.15 to 2.53	2.82
Flowmeters under test	CF1, CF2	CF1	CF1, CF2

Appendix 2 Design Sketches of the Slurry Flow Test Rig

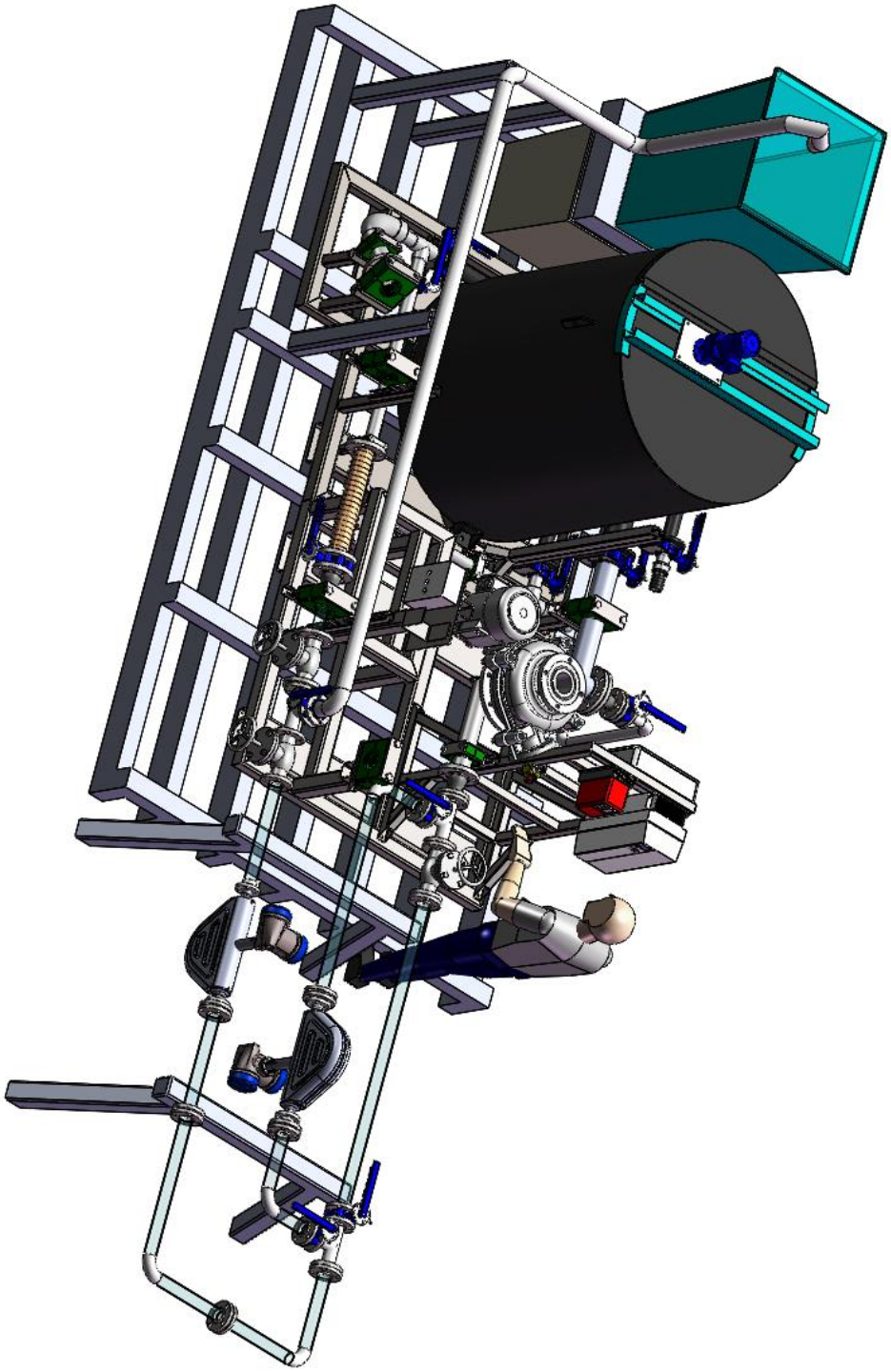

Figure A.0.1 3D drawing of the slurry flow test rig

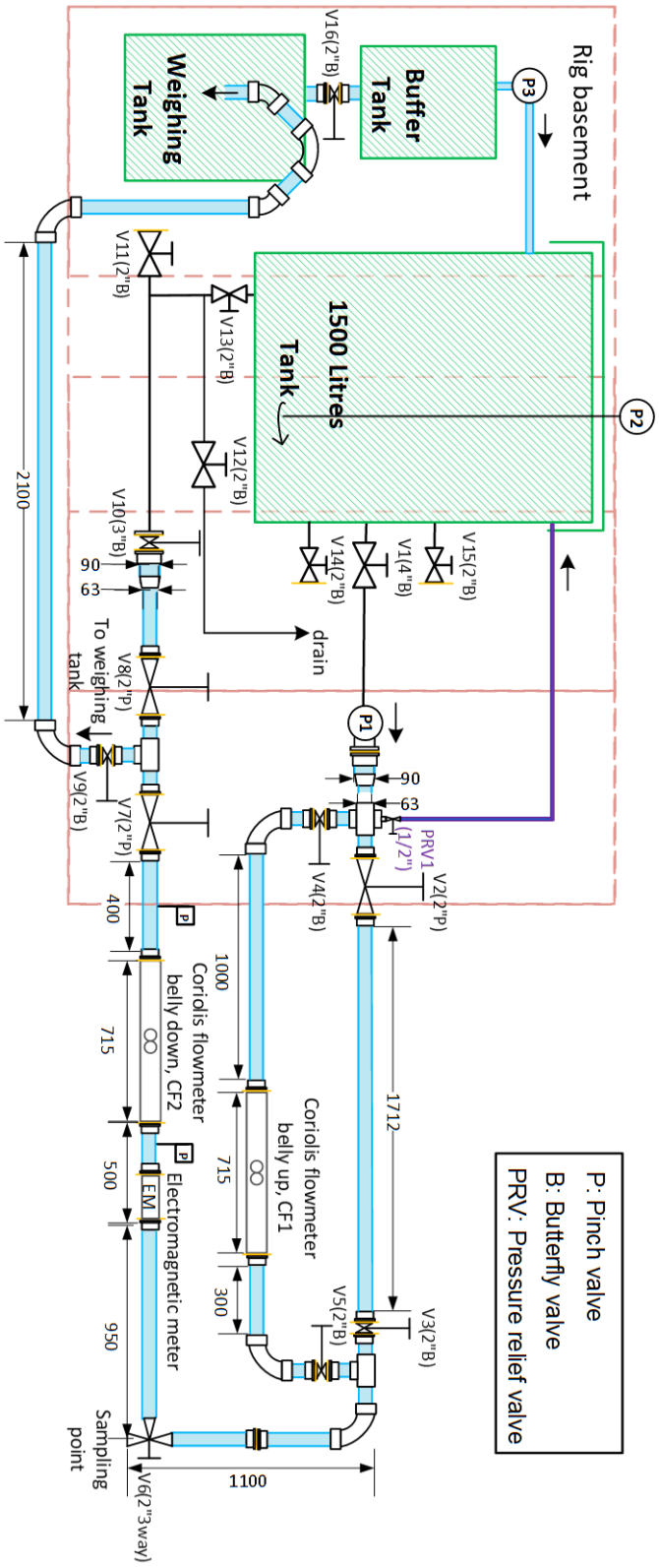

Figure A.0.2 Layout of the slurry flow test rig

Appendix 3 Results of Erosive Tests on the Upstream Coriolis flowmeter (CF1)

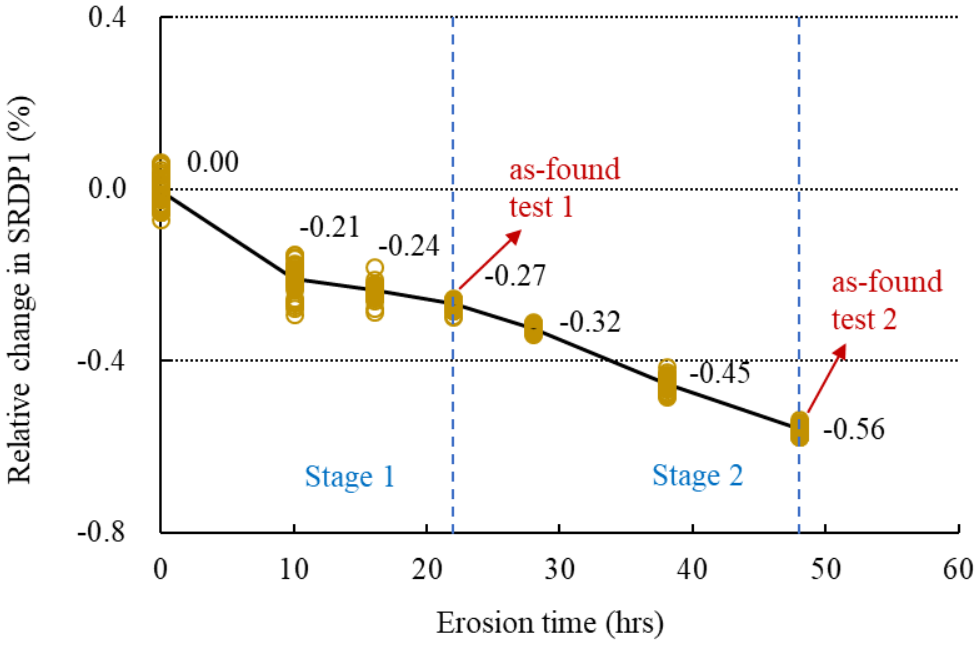

(a) Relative changes in SRDP1 with erosion time

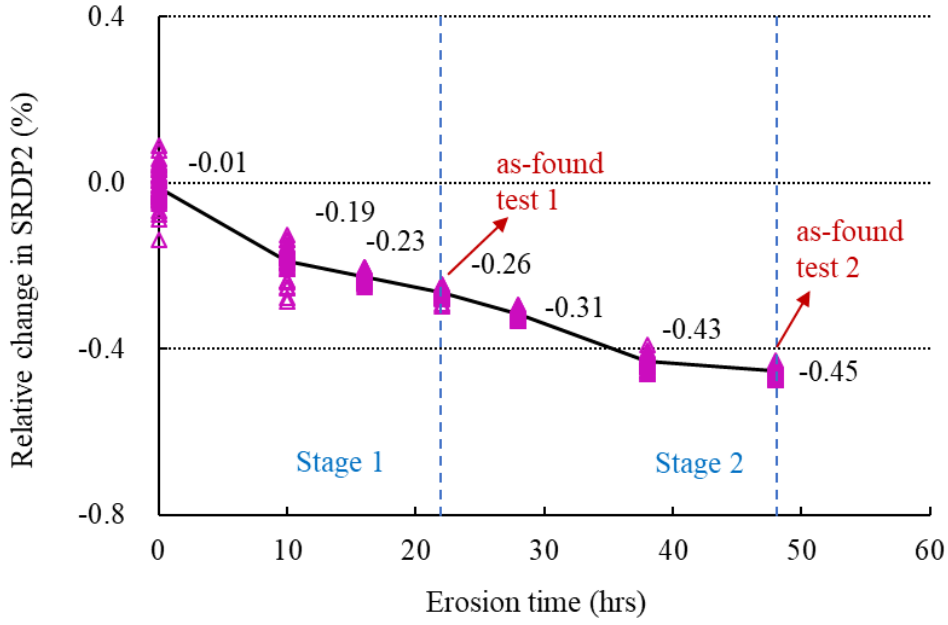

(b) Relative changes in SRDP2 with erosion time

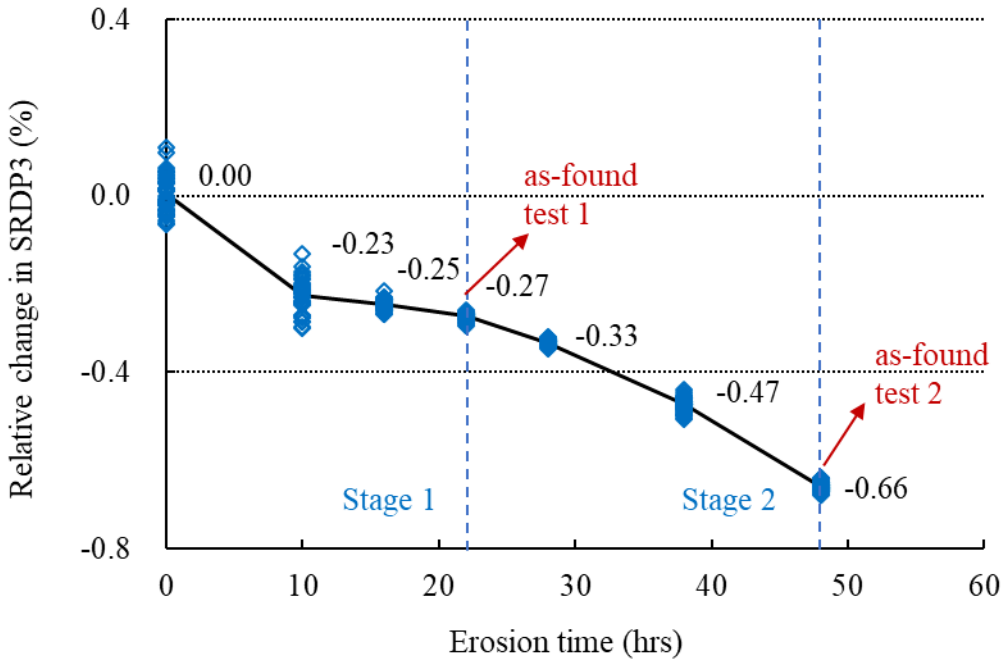

(c) Relative changes in SRDP3 with erosion time

Figure A.0.3 Trend of relative changes in SRDP during erosive tests on CF1

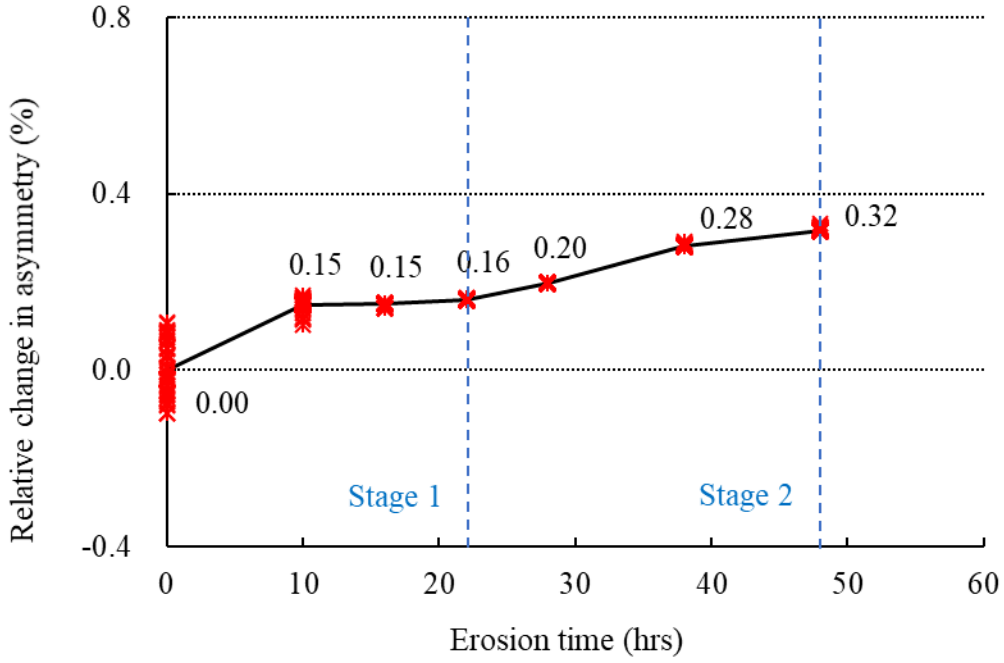

Figure A.0.4 Trend of relative changes in asymmetry during erosive tests on CF1

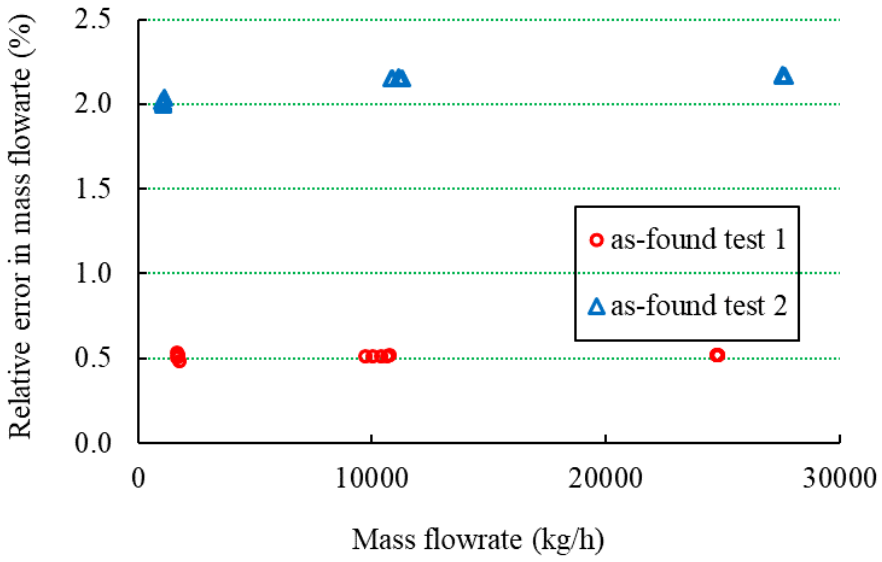

(a) Relative errors in mass flowrate due to erosion

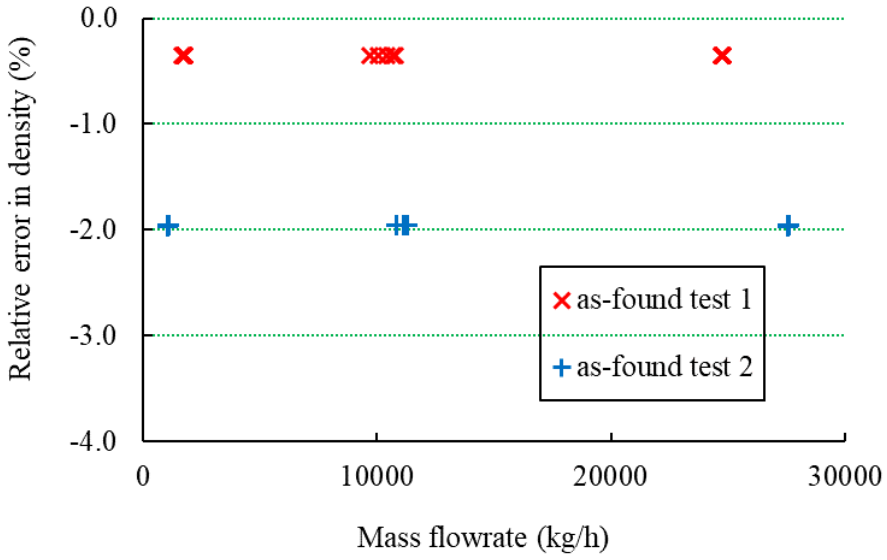

(b) Relative errors in density due to erosion

Figure A.0.5 As-found results of CF1

Table A.5 Resulting change in SDRP data and the measurement performance of CF1

Test \ Average (%)	Relative change in SRDP1	Relative change in SRDP2	Relative change in SRDP3	Relative error in mass flowrate	Relative error in density
As-found test 1	−0.27	−0.26	−0.27	0.51	−0.35
As-found test 2	−0.56	−0.45	−0.66	2.11	−1.96

Publications and Dissemination

1. **J. Zhang**, J. Liu, Y. Yan, E. Jukes, "Application of Coriolis flowmeters to the condition monitoring of liquid-solid two-phase flow," The 6th School Research Conference, University of Kent, UK, 8 January 2020.

2. **J. Zhang**, T. Wang, J. Liu, Y. Yan, E. Jukes, "Structural condition monitoring of Coriolis flowmeters through stiffness measurement," The 18th International Flow Measurement Conference (FLOMEKO), Lisbon, Portugal, 26-28 June 2019.

3. **J. Zhang**, T. Wang, Y. Yan, " Measurement and condition monitoring of solid-liquid flow through multi-sensor integration and dynamic signal processing," The 5th School Research Conference, University of Kent, UK, 12 January 2018.